Unravelling the role of RBOHD in Hypoxia-mediated regulation of plant immune responses

Pablo García González de Heredia

Maynooth University
National University of Ireland Maynooth

This Thesis is submitted to Maynooth University of Ireland for the Degree of Doctor of Philosophy

October 2025

Department of Biology

Supervisor
Dr. Emmanuelle Graciet

Head of Department
Prof. Paul Moynagh

Acknoledgements

I wish to extend my gratitude to everyone who has supported me during my PhD project. First, I would like to express my sincere gratitude to Dr. Emmanuelle Graciet for her unconditional support throughout my PhD, from that online interview to these last weeks of writing, it has been a pleasure to work with you for these four years. Her guidance, patience, and encouragement were essential at every stage of this work and have set the standards for how science should be conducted.

I would like to thank my colleagues in the Plant Biochemistry Lab, Dr. Catherine Doorly, Dr. Ailbhe Brazel, Dr. Shreenivas Singh and Gabin Dajoux, for all the countless favours we did for one another and the support throughout my PhD. I would like to thank my PhD committee members, Dr. Jackie Nugent, Dr. Diarmuid Maoileidigh and Dr. Rebecca Owens for their feedback and suggestions on my work. I also would like to acknowledge the many external collaborators who contributed to this project, including Prof. Rafael de Andrade Moral, Dr. Rachel Wells and Dr. Emmanuel Solomon for their help and expertise, their contributions greatly strengthened the quality and scope of this work. I would also like to thank the football and badminton people for providing a much-needed outlet outside the lab. I also would like to acknowledge the Irish Research Council for funding this work.

To my familiy, Javier, Elena, Pedro y Juan, always providing a welcoming home to return to after months abroad, for the long calls that I always remembered to make, for all the pickups from the airports and the plans on holidays together, for the long talks at the table and for never doubting me in these years. To Dean, for all the gym sessions, jokes, injuries and potatoes shared in these four years. To Sofia, Dafne and Omar, for these long lunch breaks, karaoke nights, worldbuilding ted-talks and memes shared. To Fred, Dan and Osvaldo for endless Carcassone games and chicken dinners, and help with moving and finding places to stay. To Jay, for these therapist coffees in Dublin. To Candela, Margas and Sara, for the chit talks in the gym and all the parties together.

To Esther, this PhD is as mine as yours, for coming to this country to live with me, for supporting me, for picking me up from the lab, for the cranberry juice with the Guinness, for the haircuts, for the trips through Ireland, the dances to Jazz (Te has escapado de un libro...), and more importantly, for your extreme patience. I love you pupi.

Publications and Presentations

Research Publications

[R1] Mooney, B. C.*, Doorly, C. M.*, Mantz, M., García, P., Huesgen, P. F., & Graciet, E. (2024). Hypoxia represses pattern-triggered immune responses in Arabidopsis. *Plant Physiology*. https://doi.org/10.1093/plphys/kiae432

*** Indicates co-autorship**

Review Publications

[R1] García, P.*, Singh, S.*, & Graciet, E. (2024). New Insights into the Connections between Flooding/Hypoxia Response and Plant Defenses against Pathogens. In *Plants* (Vol. 13, Issue 16). Multidisciplinary Digital Publishing Institute (MDPI). https://doi.org/10.3390/plants13162176

*** Indicates co-autorship**

Conference Presentations

[C1] Plant Molecular Mechanisms Ireland 2024 Programme; Pablo Garcia (Maynooth University) "Future-proofing our crops by increasing their resilience to flooding (hypoxia) and pathogens". Maynooth, Ireland, 2024. Oral presentation.

[C2] Irish Plant Scientists' Association Meeting (IPSAM); "Repression of pattern-triggered immunity in plants". Galway, Ireland, 2025. Oral presentation.

[C3] Redox Regulation of Plant Stress and Development (IPG2023). Columbia, Missouri, USA, 2023. Conference Attendance.

Table of Contents

Abstract

Plants in the field rarely face an individual stress, but rather a combination of stresses at the same time. For example, flooding or waterlogging limit oxygen in plant cells (hypoxia) and creates optimal conditions that favour pathogen attack. This thesis investigates how low O_2 regulates plant immune and defence responses. Using *Arabidopsis thaliana, I* established controlled "hypoxia + flg22" (HF) treatments and identified RESPIRATORY BURST OXIDASE HOMOLOG D (RBOHD) as a central point of the hypoxia/flg22 crosstalk. This is evidenced by the distinct features of the canonical flg22-triggered ROS burst, which reduces its amplitude and becomes more sustained. Furthermore, the transcriptional profile of defence genes is differentially regulated under low O_2 in a RBOHD-dependent way. Immune response-associated transcriptional and post-transcriptional outcomes of RBOHD are also regulated by hypoxia in a developmental- and light-dependent mechanism. Specifically, two hypoxia-linked modules converge on RBOHD in HF: (i) hypoxia-stabilized ERF-VII transcription factors contribute to RBOHD expression, and (ii) the PTI negative regulator, calcium-dependent kinase CPK28, controls RBOHD protein levels under HF in a light-dependent way. These layers of regulation support a model in which plants switch from an energetically expensive immune responses to hypoxia-suitable immunity through a RBOHD-dependent signalling.

To investigate if similar principles occur in agricultural crop species, I screened ~100 *Brassica napus* varieties for waterlogging tolerance and for resistance to subsequent infection by *Sclerotinia sclerotiorum*. Through the study of photosynthetic parameters, waterlogging responses in *B. napus* were found to be highly genotype-dependent, enabling the ranking of tolerant and sensitive lines to waterlogging alone and to *S. sclerotiorum* infection after waterlogging. Genome-wide association and expression-marker analyses on waterlogged:control ratios highlighted a polygenic architecture but repeatedly pointed to processes that mirror the *Arabidopsis* work—Ca^{2+} signalling, energy/light pathways, and RNA/splicing regulators—providing candidate loci for breeding varieties that better withstand flooding-subsequent pathogen attacks. Together, the thesis shows that plants integrate oxygen status directly into immune output via RBOHD-centred modules, and that this molecular crosstalk between low O_2 and defence responses is mirrored in a major oilseed crop.

Abbreviation List

•OH	Hydroxyl Radical
AA	Antimycin A
ABI4	ABSCISIC ACID INSENSITIVE 4
ACA	CALCIUM-TRANSPORTING ATPASE
ACBP	Acyl-CoA-Binding Proteins
ACC	1-AMINOCYCLOPROPANE-1-CARBOXYLIC ACID
ACO	ACC Oxidase
ACS6	ACC SYNTHASE 6
ADH1	ALCOHOL DEHYDROGENASE 1
AGB1	ARABIDOPSIS GTP BINDING PROTEIN BETA 1
AGG1	ARABIDOPSIS G-PROTEIN GAMMA-SUBUNIT 1
AKT1	A-TYPE POTASSIUM TRANSPORTER
AlaAT	Alanine aminotransferase
AMT1;1	AMMONIUM TRANSPORTER 1
ANAC	ARABIDOPSIS NAC DOMAIN CONTAINING PROTEIN
AOAT2	ALANINE-2-OXOGLUTARATE AMINOTRANSFERASE 2
AOX1a	ALTERNATIVE OXIDASE 1a
APX	ASCORBATE PEROXIDASE
Ar	Argon
ARR	Age-Related Resistance
At	Arabidopsis thaliana
ATE1	ARGINYL-tRNA TRANSFERASE
ATG8e	AUTOPHAGY-RELATED 8e
ATL	ARABIDOPSIS TOXICOS EN LEVADURA
ATP	Adenosine Triphosphate
AXS1	UDP-D-AOPIOSE/UDP-D-XYLOSE SYNTHASE 1
B2	SECOND SUBUNIT
BAK1	BRI1-ASSOCIATED RECEPTOR KINASE
BBCH	Biologische Bundesanstalt, Bundessortenamt, and CHemische Industrie
BGAL13	BETA-GALACTOSIDASE 13

BIK1	BOTRYTIS–INDUCED KINASE 1
	Bayesian-information and Linkage-disequilibrium Iteratively Nested
Blink	Keyway
BRAVO	Brassica Rapeseed and Vegetable Optimisation
BRs	Brassinosteroids
BZR1	BRASSINAZOLE RESISTANT 1
CA1	CARBOXIC ANHYDRASE 1
Ca^{2+}	Calcium
CAT3	CATALASE 3
CAX2	CATION EXCHANGER 2
CBE1	CONSERVED BINDING OF eIF4E1
CBP60g	CALMODULIN-BINDING PROTEIN 60-LIKE G
CDPK/CPK	Ca^{2+}-dependent protein kinase
CHLM	MAGNESIUM-PROTOPRPHYRIN IX METHYLTRANSFERASE
Chr.	Chromosome
CI	Credible Intervals
CIP7	COP1-INTERACTING PROTEIN 7
CIPK	CBL-Interacting Protein Kinases
CML	Calmodulin-Like Proteins
CMLM	Compressed Mixed Linear Model
CNGC	CYCLIC NUCLEOTIDE-GATED CHANNELS
CO_2	Carbon Dioxide
CoQ	Coenzyme Q
CPR5	CONSTITUTIVE EXPRESSER OF PATHOGENESIS-RELATED GENES
CRK2	CYSTEINE-RICH RLK2
CRY1	CRYPTOCHROME 1
CTR1	CONSTITUTIVE TRIPLE RESPONSE 1
CYP71A12	CYTOCHROME P450 FAMILY 71 SUBFAMILY A POLYPEPTIDE 12
CYS6	CYSTATIN 6
Cyt c	Cytochrome c
DGK5	DIACYLGLYCEROL KINASE 5
DMTU	Dimethylthiourea
DORN1	DOES NOT RESPOND TO NUCLEOTIDES 1
DPB2	SECOND SUBUNIT of the DNA POLYMERASE EPSILON

DRP1A	DYNAMIN-RELATED PROTEIN1A
EBF1	EIN3 BINDING F-BOX1
EBS	EIN3-Binding Site
EIN3	ETHYLENE-INSENSITIVE 3
EIN4	ETHYLENE INSENSITIVE 4
ENAP1	EIN2 NUCLEAR ASSOCIATED PROTEIN 1
EP	Endopeptidases
ER	Endoplasmic Reticulum
ERF13	APETALA2/ETHYLENE-RESPONSIVE 13
ERF1A	ETHYLENE RESPONSE FACTOR 1A
ERFVIIs	Group VII Ethylene Response Factors
ERS1	ETHYLENE RESPOSE SENSOR 1
ET	Ethylene
ETR1	ETHYLENE RESPONSE 1
FAD	Flavin Adenine Dinucleotide
FAO	Food and Agriculture Organization
FarmCPU	Fixed and Random Model Circulating Probability Unification
FDR	False Discovery Rate
FLS2	FLAGELLIN-SENSING 2
FRK1	FLG22-INDUCED RECEPTOR-LIKE KINASE 1
GAPC1	GLYCERALDEHYDE-3-PHOSPHATE DEHYDROGENASE 1
GAPIT	Genome Association and Prediction Integrated Tool
GEM	Gene Expression Marker
GFP	Green Fluorescent Protein
GLIP1	GDSL LIPASE-LIKE 1
GLM	Generalized Linear Model
GLR	GLUTAMATE RECEPTOR-LIKE
GPA1	G PROTEIN ALPHA SUBUNIT 1
GR1	GLUTATHIONE REDUCTASE 1
GSH1	GLUTATHIONE SYNTHETASE1
GSNO	S-nitrosoglutathione
GSNOR	GSNO REDUCTASE
GSSG	Glutathione Disulfide
GWAS	Genome-Wide Association Study

H_2O_2	Hydrogen peroxide
HAD	Haloacid Dehalogenase
HF	Hypoxia flg22
HM	Hypoxia Mock
HPCA1	HYDROGEN-PEROXIDE-INDUCED CALCIUM INCREASES 1
HRE1	HYPOXIA RESPONSIVE 1
HRG	Hypoxia Responsive Gene
HRM1	HYPOXIA-RESPONSIVE MODULATOR 1
HRU1	HYPOXIA RESPONSIVE UNIVERSAL STRESS PROTEIN 1
HSF2A	HEAT STRESS TRANSCRIPTION FACTOR 2A
HSP18.2	HEAT SHOCK PROTEIN 18.2
HUP7	HYPOXIA RESPONSE UNKNOWN PROTEIN 7
HY5	ELONGATED HYPOCOTYL 5
ICS1	ISOCHORISMATE SYNTHASE 1
IM	Inner Mitochondrial Membrane
IP3	Inositol Phosphates
IRP9	INVOLVED IN RRNA PROCESSING 9
JA	Jasmonic Acid
JAZ1	JASMONATE ZIM-DOMAIN PROTEIN 1
KCN	Potassium Cyanide
LACS	LONG-CHAIN ACYL-CoA SYNTHETASE
LBD41	LOB DOMAIN-CONTAINING PROTEIN 41
MAF	Minor Allele Frequencies
MAPK	Mitogen-Activated Protein Kinase
MAPKK/MKK	MAP KINASE KINASE
MAPKKK/MEKK	MAP KINASE KINASE KINASE
MDM	Mitochondrial Dysfunction Motif
MDS	Mitochondrial Dysfunction Stimulon
MetAP	Methionine aminopeptidases
mETC	Mitochondrial Electron Transport Chain
MKS1	MAP KINASE SUBSTRATE 1
MLM	Mixed Linear Model
MLMM	Multi-Locus Mixed Model
MRL	Maximum Root Length

MYB2	MYB DOMAIN PROTEIN 2
N2	Nitrogen
NADPH	Nicotinamide Adenine Dinucleotide Phosphate
NASC	Nottingham Arabidopsis Stock Centre
NDA	NADH dehydrogenases
NF	Normoxia flg22
NH3	Ammonia
NHL10	NDR1/HIN1-LIKE 10
NM	Normoxia Mock
NO	Nitric Oxide
NOA1	NITRIC OXIDE ASSOCIATED 1
NPQt	Non-photochemical quenching
O_2	Oxygen
O_2^-	Superoxide Anion
OA	Oxalix Acid
ORA59	OCTADECANOID-RESPONSIVE ARABIDOPSIS 59
OXI1	OXIDATIVE SIGNAL-INDUCIBLE 1
PA	Phosphatidic Acid
PAD3	PHYTOALEXIN DEFINICENT 3
PAMP	Pathogen-Associated Molecular Patterns
PAR	Photosynthetically Active Radiation
PB1	PHAGOCYTOSIS OXIDASE/BEM1P
PB1CP	PHAGOCYTOSIS OXIDASE/BEM1P DOMAIN-CONTAINING PROTEIN
PBL13	PBS1-LIKE KINASE 13
PCA	Principal Component Analysis
PCD	Programmed Cell Death
PCO	PLANT CYSTEINE OXIDASE
PCRK1	PTI COMPROMISED RLCK 1
PCWDE	Plant Cell Wall Degrading Enzymes
PDC1	PYRUVATE DECARBOXYLASE 1
PDF1.2	PLANT DEFENSIN 1.2
PE	Phosphatidylethanolamine
PERE	Primary ET Response Element
PGB1	PHYTOGLOBIN 1

PHI1	PHOSPHITE-INSENSITIVE 1
PIF4	PHYTOCHROME INTERACTING FACTOR 4
PIP	PLASMA MEMBRANE INTRINSIC PROTEIN
PIRE	PBL13-INTERACTING RING TYPE E3 UBIQUITIN LIGASE
PLDa1	PHOSPHOLIPASE D ALPHA 1
POLε	DNA POLYMERASE EPSILON
PRR	Pattern Recognition Receptor
PRT6	PROTEOLYSIS 6
PRX34	PEROXIDASE 34
PSII	Photosystem II
Pst	Pseudomonas syringae pv tomato
PTI	Pattern-Triggered Immunity
PTM	Post-Translational Modifications
PUB25	PLANT U-BOX 25
PVE	Phenotypic Variance Explained
QTL	SIN DEFINICION
QTN	Quantitative Trait Nucleotides
RAP2.2	RELATED TO APELATA 2.2
RBCL	Large Subunit of RubisCO
RBL2	RHOMBOID-LIKE 2
RBOHD	RESPIRATORY BURST OXIDASE HOMOLOG D
RCD1	RADICAL-INDUCED CELL DEATH1
RG-II	Rhamnogalacturonan II
RLCK	Receptor-Like Cytoplasmic Kinases
RLK	Receptor-Like Kinases
RLP	Receptor-Like Proteins
RLU	Relative Light Unit
ROL	Radial Oxygen Loss
ROP2	HOMOLOGOUS-LIKE SMALL G PROTEIN OF PLANTS
RRTF1	REDOX RESPONSIVE TRANSCRIPTION FACTOR 1
SA	Salicylic Acid
SAA	Systemic Acquired Acclimation
SAR	Systemic Acquired Resistance
SD	Standard deviation

SDR	Seedling Death Rate
SEM	Standard Error of the Mean
SHAM	Salicylhydroxamic Acid
SHR	SHORT-ROOT
SID2	SALICYLIC ACID INDUCTION DEFICIENT 2
SIK1	SERINE/THREONINE KINASE 1
SMU1	SUPPRESSORS OF MEC-8 AND UNC-52 1
SNP	Single Nucleotide Polymorphisms
SOD	SUPEROXIDE DISMUTASES
SSR	Sclerotinia Stem Rot
Std. Error	Standard Errors
SUS1	SUCROSE SYNTHASE 1
SUS1	SUCROSE SYNTHASE 1
TCH3	TOUCH3
TCP1	TEOSINTE BRANCHED1, CYCLOIDEA, PROLIFERATING CELL FACTOR 1
TF	Transcription Factor
TOE1	TARGET OF EAT1
TPC1	TWO-PORE CHANNEL 1
UAV	Unnamed Aerial Vehicule
Ub	Ubiquitin
UPS	Ubiquitin Proteasome System
VQ12	SIN DEFINICION
VTC1	VITAMIN C DEFECTIVE1
WGR1	WRKY generating ROS 1
WRKY	WRKY DNA-binding protein
WRKY33	WRKY DNA-BINDING PROTEIN 33
XCP1	XYLEM CYSTEINE PEPTIDASE 1
XLG2	EXTRA-LARGE GTP-BINDING PROTEIN 2
ZAT10	ZINC FINGER ARABIDOPSIS THION 10
ΦII	PSII quantum yield

1. Chapter 1: Introduction

Some of the following sections contain passages and figures which I wrote or designed for a review I co-authored and that is published (García et al., 2024).

1.1. Overview of Research Questions

Plants are sessile organisms that live in a complex and ever-changing environment. Their growth, development and reproduction can be negatively affected by the environmental conditions in which they live, such as an excess or lack of water (flooding or drought, respectively), high or low temperatures, nutrient levels, high salinity or their interactions with other living organisms (e.g. insects, fungi, bacteria, etc.). When environmental conditions have the potential to disrupt plant homeostasis and negatively affect growth and/or reproduction, stress occurs.

As the global population grows and food demand increases, scientists, breeders and farmers have the challenge of maintaining crop yields and the food supply. However, in recent years, global climate change has increased the frequency and severity of extreme weather events and plants are exposed more often to (a)biotic stresses (Chaloner et al., 2020; Hanson et al., 2022; Liu et al., 2023; Mustroph, 2018). Heavy rainfall events, for example, have increased in recent years (Hirabayashi et al., 2013; Papalexiou and Montanari, 2019; Tie et al., 2025), causing up to USD 5.5 billion-valued crop production loss for the period between 1982 and 2016 (Kim et al., 2023). These rainfall events cause water to accumulate within the soil, filling natural occurring air pockets and leading to soil saturation surrounding plant roots with water instead of air (waterlogging; **Figure 1.1**). As oxygen (O_2) and carbon dioxide (CO_2) have slower diffusion in water, plant cells surrounded by water have reduced gas exchange, resulting in lower O_2 availability or hypoxia. In some extreme cases, flood water covers aerial parts of the plant, resulting in partial or complete submergence (**Figure 1.1**) (Sasidharan et al., 2017;Jiaet al., 2021; Striker, 2012).

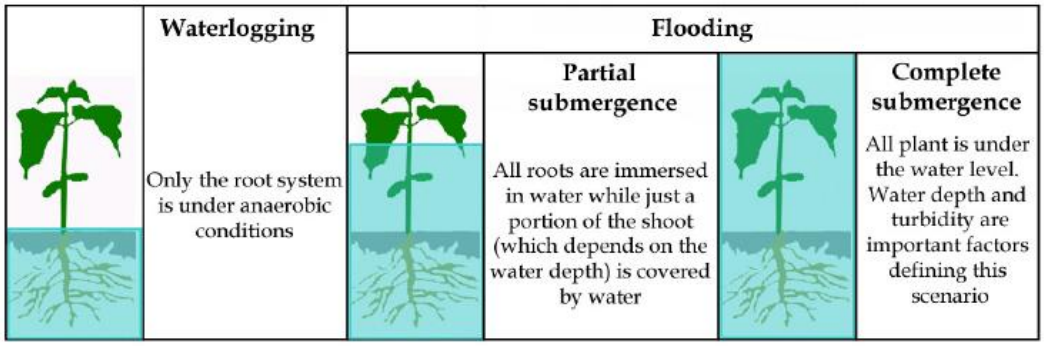

Figure 1.1. Definition of the different conditions resulting from an excess of water. Based on the parts covered by water after heavy rainfall events, plants can face (i) waterlogging, if only the root system is covered; (ii) partial submergence, if all roots and part of the aerial tissues are covered, and (iii) complete submergence, if all the plant is covered by water. Figure from Striker, 2012.

Waterlogging and submergence are in fact compound stresses, because they alter several additional environmental parameters other than O_2 availability – e.g. it can reduce light availability to the aerial parts of plants, given that flood water carries soil particles that limit the amount of light that reaches the plant (Pedersen et al., 2018; Vervuren et al., 2003). Consequently, photosynthesis can be limited, which decreases the production of carbohydrates, the release of O_2 and the generation of intermediate energy molecules such as ATP and NADPH from the light reactions of photosynthesis. Furthermore, reduced photosynthetic activity limits carbon assimilation, which subsequently impacts on mitochondrial respiration and ATP synthesis, resulting in carbon and energy starvation during prolonged hypoxic conditions (Geigenberger, 2003; Wagner et al., 2019). Flooding has also been linked to increased pathogen infection risks for plants, not only through increased host susceptibility caused by hypoxic stress (and associated limited photosynthesis or carbon starvation), but also by creating environmental conditions favourable to pathogen growth and disease development (Erayya et al., 2023; García et al., 2024; Garrett et al., 2016; Lahlali et al., 2024; Lamichhane et al., 2024; Maurya et al., 2022; Martínez-Arias et al., 2022; Tyagi et al., 2024). In aerial parts of the plant, prolonged leaf wetness and high humidity following intense precipitation events promote spore germination and bacterial proliferation, while in underground parts of the plant, excess moisture enhances the activity and mobility of root-infecting pathogens (Pokhrel, 2021; Velásquez et al., 2018). Hence, it is important to understand how flooding and associated hypoxia affect plants' ability to defend themselves against pathogens, not only from a fundamental point of view but also because of the important crop losses associated with plant disease alone. For example, it is estimated that

annually, between 20 to 40 percent of global crop production is lost to pests, and that plant diseases cost the global economy around $220 billion each year (FAO, 2021).

As rainfall events increase pathogen infection risk, plants likely face both hypoxia and pathogen infection at the same time. It has been suggested that plants perceive the combination of two (or more) stresses as a new state of stress rather than a sum of individual stresses (Mittler, 2006). This new state of stress can activate acclimation strategies that are different - and sometimes even antagonistic - to those triggered under each of the individual stresses (Kissoudis et al., 2014; Atkinson and Urwin, 2012; Pandey et al., 2015; Prasch and Sonnewald, 2013; Zandalinas et al., 2024; Zhang and Sonnewald, 2017). However, there are few studies focused on how plants respond to multiple simultaneous or sequential stresses, as the scientific community has mostly focused on plant responses to individual stresses. This has led to the discovery of several response pathways that have roles in response to distinct individual stresses, such as ROS production (Evans et al., 2016; Miller et al., 2009; Peláez-Vico et al., 2023; Wang et al., 2017). These common multi-stress (or cross-stress) responsive pathways will be termed 'convergence points' in this work (Baena-González and Sheen, 2008; Du et al., 2023). These convergent pathways are thought to play a role in mediating and integrating responses to combined stresses, however their role in this combined stress context remains poorly understood. One example of a convergence point is RESPIRATORY BURST OXIDASE HOMOLOG D (RBOHD), a plant enzyme that generates Reactive Oxygen Species (ROS), which act as second messengers that transduce external signals into their appropriate intracellular response pathways. Similarly, several transcriptional regulators that play roles in response to multiple stresses are also thought to play a predominant role as convergence points in response to combined stresses.

This PhD work focused on the dynamics of plant responses to the combination of hypoxic stress and the activation of plant immune responses. It aimed to answer the following key questions:

(i) How does hypoxia stress influence the onset of innate immune responses and the activation of defences against pathogens?

(ii) What is the role of *RBOHD* in the molecular response to the activation of innate immune responses under hypoxic conditions?

(iii) Is it possible to identify crop varieties that exhibit resilience to combined waterlogging and pathogen stress?

(iv) Can the genetic basis for this resilience trait be uncovered in crop plants?

Questions (i) and (ii) were approached using the plant *Arabidopsis thaliana* as a model system to dissect molecular mechanisms using a combination of genetic, molecular and biochemical approaches. Questions (iii) and (iv) were addressed using rapeseed (*Brassica napus*) - the world's second-largest oilseed crop (FAO, 2021). Rapeseed is grown not only for its oil, but also for human consumption, as animal fodder, or for its use as biodiesel or bioethanol (Kdidi et al., 2019). Rapeseed is grown in regions of the world that are regularly flooded (e.g. in Asia as a rotation crop on rice fields (Zou et al., 2015a), however, rapeseed is very sensitive to waterlogging (Voesenek et al., 1999a). Therefore, it is important to understand how hypoxia caused by flooding might affect rapeseed defences against pathogens. In that context, the necrotrophic fungal pathogen *Sclerotinia sclerotiorum* (the causal agent of Sclerotinia stem rot) was selected because of its impact on rapeseed crop yields (Neik et al., 2017).

In the sections below, the different mechanisms by which pathogens and O_2 are perceived or sensed, respectively, will be presented, followed by the signalling pathways that act downstream of the receptors and that are common to both hypoxia response and immunity. The latter are important because of their potential involvement in mediating plant responses to the combined stress conditions (i.e. as convergence points). Finally, transcriptional responses will be discussed, as one of the outputs of individual and combined hypoxia/pathogen stress.

1.2. Stress Perception

The detection of environmental cues associated with stress conditions constitutes the first step that enables plants to initiate molecular responses to acclimate and survive upon experiencing stress conditions. While the recognition of plant pathogens is well understood, sensors for abiotic stresses have remained more elusive, although several studies suggest that plants sense them at both the cell surface (cell wall and plasma membrane) and *via* intracellular compartments, such as the cytoplasm or the nucleus, triggering compartment-specific responses. In the case of hypoxia, for example, O_2 is sensed *via* intracellular mechanisms.

1.2.1. Pathogen perception by pattern recognition receptors

Transmembrane pattern recognition receptor (PRRs) recognise pathogen-associated molecular patterns (PAMPs; conserved molecular motifs from pathogens), initiating pattern-triggered immunity (PTI), the first branch of the plant innate immune response. PRRs are divided into receptor-like kinases (RLKs) and receptor-like proteins (RLPs) depending on the presence of a

protein kinase domain. FLS2 is a model plasma membrane-associated Leucine-Rich Repeat Receptor-Like Kinase (LRR–RLK) PRR, which is widely used to study PTI. FLS2 recognises the flg22 peptide, a 22-amino acid peptide present in the conserved N-terminal domain of eubacterial flagellin, the protein that makes up the bacterial flagellum (Chinchilla et al., 2006; Lourdes Gomez-Gomez and Boller, 2000; Sun et al., 2013).

Upon binding flg22, FLS2 undergoes conformational changes in its extracellular LRR domain, facilitating its interaction with the co-receptor BRI1-ASSOCIATED RECEPTOR KINASE (BAK1), a leucine-rich repeat receptor serine/threonine protein kinase that binds to different PRRs, leading to auto- and trans-phosphorylation reactions between them (Cao et al., 2013; Chinchilla et al., 2007; Schulze et al., 2010; Schwessinger et al., 2011; Sun et al., 2013). Afterwards, the phosphorylated FLS2-BAK1 complex activates a member of Receptor-Like Cytoplasmic Kinases (RLCKs) subfamily VII, BOTRYTIS–INDUCED KINASE 1 (BIK1) (Lin et al., 2014; Lu et al., 2010). In turn, BIK1 phosphorylates back FLS2 and BAK1 to further activate them and enhance the flg22 signalling events (**Figure 1.2**). At a later stage, BIK1 is released from the FLS2-BAK1 complex, triggering BIK1-dependent events essential for the onset of plant immunity, such as the activation of calcium (Ca^{2+}) channels or phosphorylation of RBOHD (Li et al., 2014; Lu et al., 2010; Tian et al., 2019).

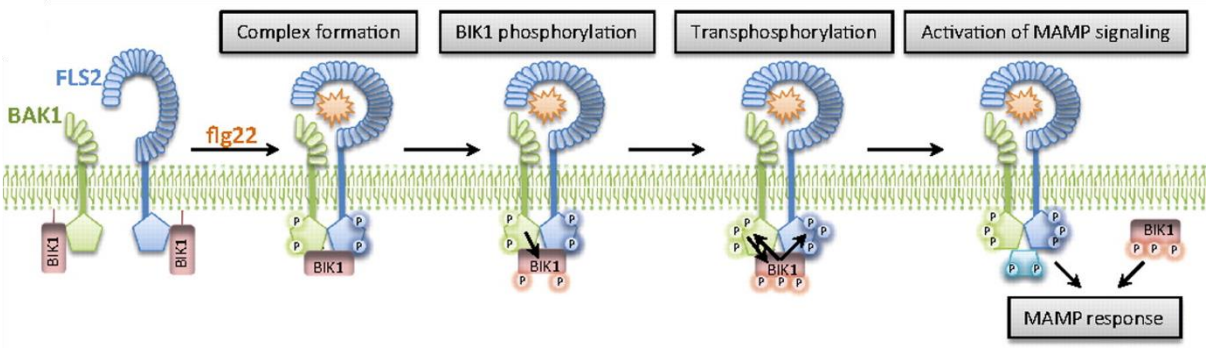

Figure 1.2. Early events after flg22 sensing by FLS2. After the binding of flg22 to FLS2, FLS2 dimerizes with BAK1, phosphorylating each other. Then BAK1 trans-phosphorylates BIK1, which will phosphorylate back FLS2 and BAK1, allowing the release of BIK1 from the complex and triggering PTI. Figure from Lu et al. 2010.

FLS2 is the target of multiple transcriptional and post-transcriptional regulatory mechanisms, even in the absence of its ligand flg22. For example, the microRNA miR172b controls the expression of *FLS2* throughout plant development *via* its regulation of the transcription factors TARGET OF EAT1 (TOE1) and TOE2, which bind directly to the *FLS2* promoter and inhibit its transcription in a development-controlled manner (Zou et al., 2018). This

mechanism controls the ontogeny of plant innate immunity, dampening PTI during early growth and boosting *FLS2* levels as the plant ages, thereby contributing to age-related resistance (ARR), a process in which plants become more pathogen-resistant as they age. In addition to developmental regulation, *FLS2* transcription is also sensitive to environmental stresses. For example, previous work has shown that hypoxia transcriptionally regulates *FLS2* levels, although the underlying mechanism remains unresolved (Mooney et al., 2024). This observation highlights the crosstalk between abiotic stress responses and immunity-related receptors, suggesting that plants could actively adjust *FLS2* (or more generally PRR) expression to balance immune responses when experiencing abiotic stresses, such as hypoxia.

Other members of the flg22 perception complex can also be regulated in the absence of flg22, as BAK1 can interact with several elements of the brassinosteroids (BRs) signalling pathway, preventing its interaction with FLS2 and regulating plant growth and development (Gao et al., 2009; Halter et al., 2014; Hee Nam and Li, 2002; Imkampe et al., 2017; Li et al., 2002; Ma et al., 2017). In addition, the non-activated BIK1 kinase is targeted for degradation by the plant U-box E3 ubiquitin ligases PUB25 and PUB26 to maintain BIK1 homeostasis and ensure robust yet appropriate immune activation upon pathogen attack (Wang et al., 2018). Altogether, these regulatory mechanisms ensure that PTI signalling components are tightly controlled in the absence of pathogen infection, allowing plants to balance immune readiness with growth and development. However, additional stress-responsive mechanisms (such as hypoxia-dependent transcriptional control of *FLS2*) could potentially regulate the energy-costly immune responses through these elements in response to hypoxic conditions, when energy availability is reduced.

Following flg22 binding, FLS2 in internalised in a ligand-triggered and clathrin-mediated unresolved process leading to FLS2 ubiquitination, which helps route FLS2 through late endosomes toward vacuolar degradation, attenuating sensitivity to flg22 (Lu et al., 2011; Smith et al., 2014; Spallek et al., 2013). This process is largely dependent on the phosphorylation status of FLS2 (Beck et al., 2012; Cui et al., 2023; Mbengue et al., 2016; Robatzek et al., 2006; Smith et al., 2014). This internalisation is essential to prevent prolonged or excessive immune responses which can be energetically costly. This unresolved process is synergically regulated by proteins such as the large dynamin GTPases DYNAMIN-RELATED PROTEIN1A (DRP1A) and DRP2B (Ekanayake et al., 2021). Other known regulators of FLS2 internalisation are two closely related U-box E3 ubiquitin ligases, PUB12 and PUB13, which are phosphorylated by BAK1 and subsequently polyubiquitinate FLS2, thereby promoting flg22-induced FLS2 degradation. As a result of their function, the *pub12* and *pub13* mutants displayed elevated immune responses to flagellin treatment (Lu et al., 2011).

Notably, in recent years, the FLS2 complex has been shown to play roles in the context of drought and salt stresses, together with RBOHD and PHYTOCHROME INTERACTING FACTOR 4 (PIF4) (Liu et al., 2022; Yu et al., 2023), but this has not been shown in the context of hypoxia stress. Altogether, protein abundance of key immune response proteins represents a crucial mechanism for regulating the amplitude and duration of immune responses, providing a potential target for hypoxia-regulatory mechanisms that allows plants to modulate immune responses in energy-limiting situations.

1.2.2. Oxygen sensing by PLANT CYSTEINE OXIDASE (PCO) enzymes

The first oxygen sensing pathway was reported in 2011 (Gibbs et al., 2011; Licausi et al., 2011), when it was demonstrated that the stability of five transcription factors (TFs) of the group VII Ethylene Response Factors (ERF-VIIs) was oxygen dependent. These five ERF-VIIs include *RELATED TO APELATA 2.2* (*RAP2.2*), *RAP2.3*, *RAP2.12* and *HYPOXIA RESPONSIVE 1* (*HRE1*) and *HRE2* (Gibbs et al., 2015; Loreti and Perata, 2023). ERF-VIIs are classified in two groups based on their mechanism of activation during hypoxia, *HRE1* and *HRE2* are characterised by their fast transcriptional up-regulation shortly after the onset of hypoxia, while *RAP2.2*, *RAP2.3* and *RAP2.12* are largely regulated *via* post-transcriptional mechanisms (Licausi et al., 2010). The degradation of these five ERF-VIIs was shown to be mediated by the ubiquitin dependent Arg/N-degron pathway, which recognises its substrates based on the identity of their amino-terminal residue (N-degrons) (reviewed in Holdsworth et al., 2020; Oldham and Mabbitt, 2024). In the case of the ERF-VIIs, their initial N-terminal methionine residue is first cleaved by methionine aminopeptidases (MetAPs) (**Figure 1.3**). This cleavage exposes the second residue of these TFs, which is a cysteine (Cys). This newly exposed N-terminal Cys is then converted to Cys-sulphinic acid ($CysO_2$) by PLANT CYSTEINE OXIDASE (PCO) enzymes that use oxygen as a substrate, establishing PCOs as the oxygen sensing component of the Arg/N-degron pathway and more broadly of hypoxia responses in plant cells (**Figure 1.3**) (Weits et al., 2014; White et al., 2018, 2017). Next, the ERF-VIIs are arginylated (i.e. newly exposed arginine residue is conjugated at their N-terminus) by ARGINYL-tRNA TRANSFERASE 1 (ATE1) and ATE2 (Yoshida et al., 2002), enabling the recognition of these ERF-VIIs by the E3 ubiquitin ligase PROTEOLYSIS 6 (PRT6), facilitating the ubiquitination and targeting for degradation by the 26S proteasome (**Figure 1.3**) (Garzón et al., 2007; Stary et al., 2003). In hypoxic conditions, the initial Cys residue can not be oxidised by the PCOs, this allows for the stabilization of the ERF-VIIs and allowing their translocation to the nucleus, where they act as the master regulators of Hypoxia-Responsive Genes (HRGs) (Hsu et al., 2011; Liu et al., 2005; Mustroph et al., 2009). The O_2-dependent mechanisms underlying the

degradation of ERF-VIIs rely on additional molecular players, such as nitric oxide (NO), which is also required for the degradation of the ERF-VIIs by the Arg/N-degron pathway (Gibbs et al., 2014). These regulatory mechanisms are redox-dependent, as recent work demonstrated that ERF-VIIs such as RAP2.3 and RAP2.12 can further be oxidised, forming sulfonate (Arg-Cys(SO_3^-)-ERF-VII) through a still unknown mechanism (Zubrycka et al., 2023). Moreover, hydrogen peroxide (H_2O_2) inactivates the PCOs, preventing the oxidation of ERF-VIIs and thereby enhancing their stability, contributing to the interplay between ROS signalling and hypoxia sensing mechanisms (Akter et al., 2024).

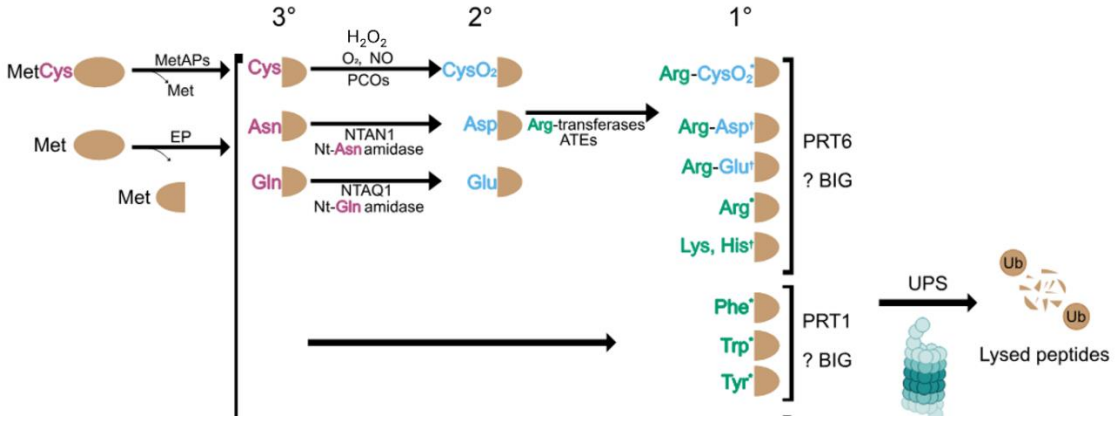

Fig. 1.3. Overview of the plant Arg/N-degron pathway. Methionine aminopeptidases (MetAPs) or endopeptidases (EP) cleave proteins, exposing new N-terminal amino acid residues. The tertiary (3°) destabilising residue Cys is oxidised by PCOs using O_2, resulting in the secondary destabilising residue $CysO_2$ (cysteine sulphinic acid). Cys can also be oxidised *via* nitric oxide (NO). The tertiary destabilising residues Asn and Gln are deamidated to Asp and Glu by specific amidases (NTAN1 and NTAQ1). Arg-tRNA transferases (ATEs) conjugate an Arg to the N-terminus of proteins starting with secondary (2°) destabilising residues ($CysO_2$, Asp and Glu). Proteins starting with primary destabilising residues are directly recognised by the E3 ubiquitin ligases PRT6 (for positively charged N-terminal residues such as Arg), or PRT1 (for hydrophobic residues). A third N-recognin, BIG, enhances the activity of both PRT1 and PRT6 (Zhang et al., 2024). Abbreviations: UPS, ubiquitin proteasome system; Ub: ubiquitin. Figure modified from Oldham and Mabbitt, 2024.

Once hypoxia is established, *HRE1* and *HRE2* are transcriptionally induced through distinct pathways, such as ethylene signalling (Hess et al., 2011; Yang, 2014) or apoplastic- and mitochondrial-located ROS signalling (De Clercq et al., 2013; Eysholdt-Derzsó et al., 2023; He et al., 2022; Liu et al., 2017; Yang, 2014; Yang and Hong, 2015). The *RAP2.2/3/12* ERF-VIIs that are not transcriptionally up-regulated during hypoxia rely on post-translational mechanisms to

ensure their presence in the nucleus upon hypoxic conditions. For example, RAP2.12 remains anchored at the plasma membrane in normoxic conditions through its interaction with the acyl-CoA-binding proteins ACBP1 and ACBP2. Whereas, upon hypoxia, polyunsaturation of long-chain acyl-CoA contributes to dissociation of the interaction between RAP2.12 and ACBP1/2, triggering RAP2.12 release and relocation to the nucleus (Licausi et al., 2011; Schmidt et al., 2018; Zhou et al., 2020). However, other lipids like phosphatidic acid (PA), a key intermediate in lipid metabolism, can also regulate nuclear localisation of RAP2.12 (Zhou et al., 2022).

In addition to their well-established roles in hypoxia response, both the Arg/N-degron pathway and the ERF-VII TFs have been shown to play roles in the regulation of plant defences against pathogens, becoming a convergence point of hypoxia and immune responses (**see also section 1.4.2.1 below**). For example, the Arg/N-degron pathway positively regulates the biosynthesis of plant defence secondary metabolites such as glucosinolates, as well as the biosynthesis and response to the phytohormone jasmonic acid (JA) (De Marchi et al., 2016). Arg/N-degron mutants were also shown to be affected for their response to pathogens such as the necrotrophic fungus *Sclerotinia sclerotiorum*, the hemi-biotrophic pathogen *Pseudomonas syringae pv tomato* (Pst) or the protist *Plasmodiophora brassicae* (De Marchi et al., 2016; Gravot et al., 2016; Vicente et al., 2019). These roles the Arg/N-degron pathway in defence responses are given by the potential immune-involved targets and their stabilization upon the establishment of hypoxia micro-environments during pathogen infection (Valeri et al., 2021).

Altogether, these findings illustrate the emerging regulatory role of the O_2-sensing Arg/N-degron pathway and the ERF-VIIs in the shaping of plant defence responses, thus suggesting connections between hypoxia response, plant defence and immunity. However, due to the complex molecular interplay between PAMP recognition and the manipulation of plant immunity by pathogen effectors, the use of pathogens in these studies makes it difficult to deconvolute the potential connection between hypoxia response and fundamental regulatory mechanisms of plant immunity. Instead of pathogens, the question could be deconvoluted by using purified PAMPs, such as the flg22 peptide, to elicit PTI and study the connection between hypoxia response and plant immunity. Considering the distinct perception and sensing mechanisms for flg22 and low oxygen levels, a key question is to identify the pathways and components (i.e. the convergence points) that might act in common to plant responses to hypoxia and to flg22. As with many other (a)biotic stresses, these common pathways are found downstream of the receptors and sensors, and include some of the main signal transduction pathways.

1.3. Hypoxia and immune responses share signal transduction pathways

The onset of plant responses to (a)biotic stresses requires signal transduction to relay the signal from the sensors or receptors to other subcellular compartments, such as the nucleus. This signal transduction is often accompanied by signal amplification and involves second messengers, including Ca^{2+}, ROS, inositol phosphates (IP_3), cGMP/cAMP, NO or even pH changes, as well as complex phosphorylation pathways such as mitogen-activated protein kinase (MAPK) signalling. These signal transduction pathways act as hubs downstream of signal perception/sensing and can also be a point of convergence in stress responses to multiple stresses, as (i) the same pathways can be activated in response to different stresses; (ii) they are directly regulated by the same signalling elements (second messengers), or (iii) they share the same downstream targets. The following section examines different signal transduction pathways and their possible role in combined stress responses. We focus on Ca^{2+} and ROS signalling in response to hypoxic stress and flg22 perception.

1.3.1. Calcium signalling

Ca^{2+} is essential for plant growth and development under both physiological and stress conditions. In the absence of stress, Ca^{2+} in the cytosol is kept at a low concentration (around 0.1 µM) through an active transport of Ca^{2+} from the cytosol into the apoplast or plant organelles, such as the vacuole, mitochondria or the endoplasmic reticulum, where Ca^{2+} concentrations are in the millimolar range (Lecourieux et al., 2002). This active Ca^{2+} transport is carried out by several Ca^{2+} channels (**Figure 1.4**) and results in electrochemical gradients across the plasma membrane, as well as membranes of the subcellular compartments.

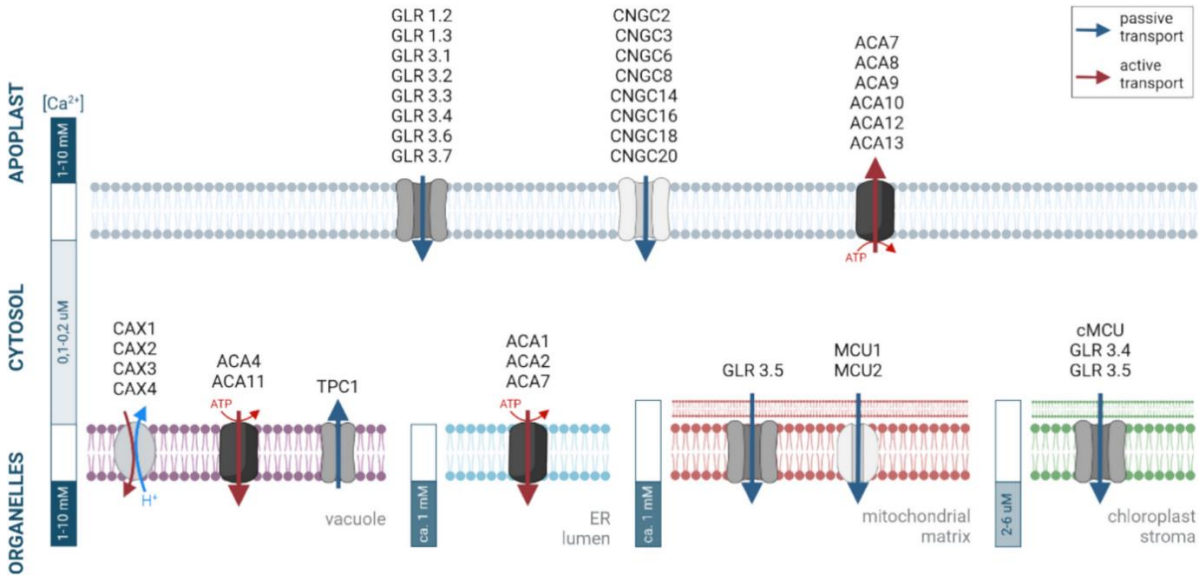

Figure 1.4. Set of Ca^{2+} channels present in different membranes of a plant cell. Distribution and mechanisms of active and passive Ca^{2+} transport across various cellular membranes, including the plasma membrane, tonoplast (vacuolar membrane), endoplasmic reticulum (ER), mitochondrial membrane, and chloroplast envelope. Figure from Wdowiak et al., 2024.

When stresses such as high salt concentrations (Choi et al., 2014), wounding (Kiep et al., 2015; Mousavi et al., 2013; Salvador-Recatalà, 2016; Salvador-Recatalà et al., 2014) or cold (Sulaiman et al., 2012; Zhu et al., 2013) are sensed, the Ca^{2+} stored in the organelles and the apoplast is released into the cytoplasm. This release of Ca^{2+} is mediated through the action of several Ca^{2+} channels such as TWO-PORE CHANNEL 1 (TPC1) (Evans et al., 2016; Ward and Schroeder, 1994) or several GLUTAMATE RECEPTOR-LIKE (GLR) channels (Mousavi et al., 2013; Salvador-Recatalà, 2016; Toyota et al., 2018). This fast increase in cytosolic Ca^{2+} concentrations (noted $[Ca^{2+}]_{cyt}$) has unique features depending on the stress that generated it, such as different period, amplitude, frequency and duration (McAinsh and Pittman, 2009).

In addition, stress-specific increase in $[Ca^{2+}]_{cyt}$ in one plant cell can propagate cell-to-cell through the plant vasculature at a slow but constant speed of approximately 1 µm/s (Nguyen et al., 2018; Zhang et al., 2025). The propagation of the increase in $[Ca^{2+}]_{cyt}$ can reach systemic (non-stressed) plant tissues, triggering pre-stress adaptation mechanisms called systemic acquired acclimation (SAA) if the stress that triggered the Ca^{2+} wave is abiotic, or systemic acquired resistance (SAR) if the Ca^{2+} wave is the result of an interaction with another organism (e.g., insect, bacteria, or fungi) (Choi et al., 2014).

Once the Ca^{2+} is in the cytosol, it can be detected by two types of sensors - sensor relays and sensor responders (Sanders et al., 2002). Sensor relays, which include calmodulins (CaMs) and calmodulin-like proteins (CMLs) (**Figure 1.5**), undergo a Ca^{2+}-induced conformational

change that is relayed to an interacting partner, which then responds with some change in its enzyme activity or conformation. On the other hand, sensor responders, which include Ca^{2+}-dependent protein kinase (CPK) and Calcineurin B-like proteins (CBLs) together with their CBL-interacting protein kinases (CIPKs) (**Figure 1.5**) undergo a Ca^{2+}-induced conformational change that alters the protein's activity.

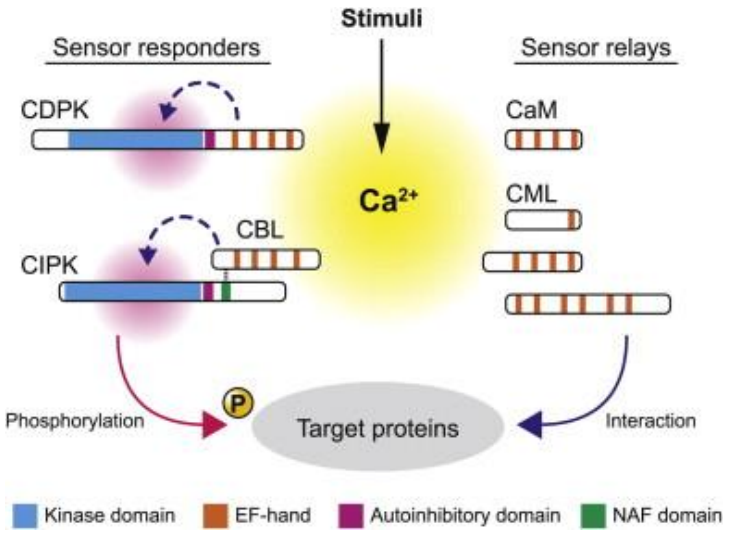

Figure 1.5. Classification of Ca^{2+} sensors in two groups. Sensor relays (CaM and CML) function through bimolecular interactions and sensor responders (CDPK/CPK and CBL together with CIPK) function through intramolecular interaction and rely on a kinase domain to trigger their function. Figure from Hashimoto and Kudla, 2011.

1.3.2. Calcium signalling in hypoxia

During hypoxic stress, an increase in $[Ca^{2+}]_{cyt}$ occurs as early as one minute after the onset of hypoxia (Bakshi et al., 2023; Subbaiah et al., 1994; Wagner et al., 2019; Yemelyanov et al., 2011) or waterlogging (Peláez-Vico et al., 2023). However, the Ca^{2+} channels responsible for triggering this $[Ca^{2+}]_{cyt}$ increase remain largely unidentified, although recent studies have begun to uncover a few candidates (Wang et al., 2017). During flooding, the use of GFP-based Ca^{2+} sensors such as YCNano-65, has shown that cytosolic Ca^{2+} levels increase, at least in the root meristematic and elongation zones (Bakshi et al., 2023). In the absence of stress, the CATION EXCHANGER 2 (CAX2) Ca^{2+} channel transports Ca^{2+} across the tonoplast into the vacuole (**Figures 1.4 and 1.6**) (Pittman et al., 2004). Consequently, in response to both waterlogging and hypoxic challenges, the *cax2* mutant showed a stronger and more sustained $[Ca^{2+}]_{cyt}$ increase in the root, leading to enhanced survival of *cax2* plants to waterlogging. These findings highlight the role for vacuolar Ca^{2+} transport and changes in $[Ca^{2+}]_{cyt}$ during flooding response (Bakshi et al., 2023).

During hypoxia, the increase in $[Ca^{2+}]_{cyt}$ post-translationally activates CPKs such as CPK12, which is rapidly activated through Ca^{2+}-dependent phosphorylation of its Ser186 residue. Phosphorylated CPK12 shuttles from the cytoplasm to the nucleus, where it interacts with and phosphorylates the ERF-VII TFs, thus contributing to increasing their stability (**Figure 1.6**) (Fan et al., 2023). Moreover, another CPK (CPK16), negatively regulates plant tolerance of hypoxia and submergence stress through the control of ROS production. Such control is mediated by the direct binding of CPK16 to RBOHD, and RBOHD phosphorylation at four different serine residues (Ser133, Ser148, Ser163, and Ser347), promoting RBOHD stability in response to hypoxia (Yu et al., 2024). Other Ca^{2+} sensors also have a role in hypoxia responses, such as CIPK25-dependent phosphorylation of the K^+ channel AKT1 or CIPK15-dependent phosphorylation of ammonium (NH^{4+}) channel Ammonium Transporter 1;1 (AMT1;1) (Chen and Ho, 2023; Tagliani et al., 2020).

In sum, Ca^{2+} signalling triggered by CAX2 and sensed by CPK12 and CPK16 along with other Ca^{2+} sensors such as CIPK15 (Chen and Ho, 2023) or CIPK25 (Tagliani et al., 2020) (**Figure 1.6**) establish the $[Ca^{2+}]_{cyt}$ elevations as one of the first signalling events of hypoxia responses and leading to acclimation of plants to hypoxic stress. Furthermore, hypoxia triggered Ca^{2+} signalling may influence a broad range of downstream targets of Ca^{2+} sensors, which can link hypoxia-triggered Ca^{2+} signalling to other events in PAMP and pathogen stress responses such as the ERF-VII activation of HRGs and RBOHD-triggered ROS production.

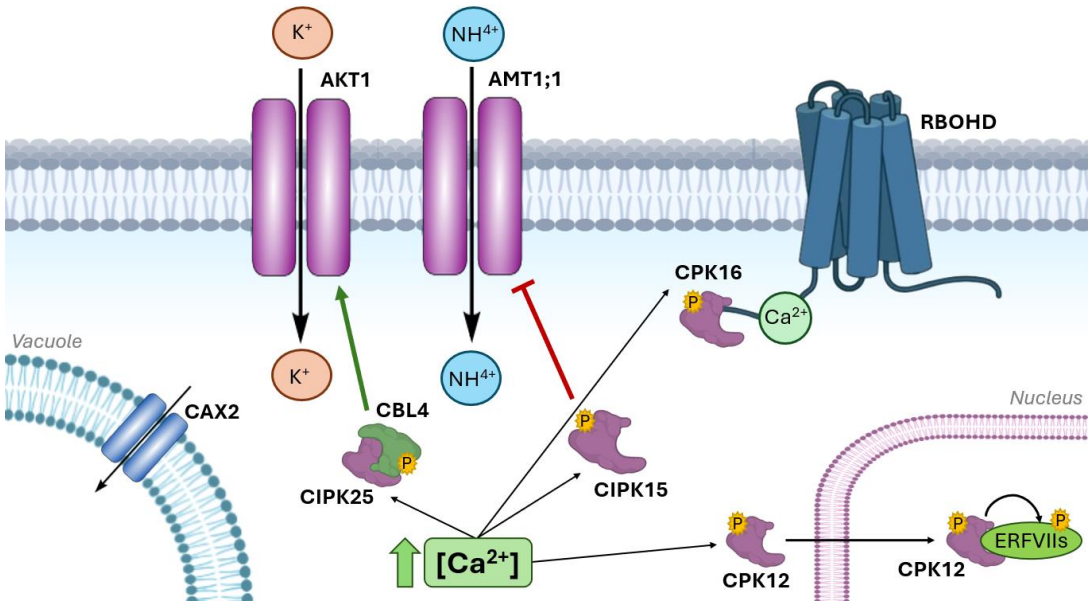

Figure 1.6. Ca^{2+}-dependent signalling in hypoxic conditions. Scheme showing the known signalling hubs dependent on Ca^{2+} triggered in hypoxic conditions. AKT1 - A-TYPE POTASSIUM TRANSPORTER; AMT1;1 – AMMONIUM TRANSPORTER 1.

1.3.3. Calcium signalling in response to flg22 perception

Increases in $[Ca^{2+}]_{cyt}$ after PAMP perception is known to be an oscillatory process (Keinath et al., 2015; Thor and Peiter, 2014), with desensitisation and re-sensitisation (Chi et al., 2021). However, although the characteristics of the increase of $[Ca^{2+}]_{cyt}$ after PAMP perception are well known, few proteins involved in this process have been characterized. After flg22 perception, BIK1 is phosphorylated and dissociates from the FLS2/BAK1 flg22-sensing complex, triggering BIK1-dependent signalling events (**Figure 1.2**). As an example, dissociated BIK1 interacts with a Ca^{2+} channel formed by CNGC2 and CNGC4, phosphorylates CNGC4, and thereby activates Ca^{2+} transport by these two proteins (**Figure 1.7**) (Tian et al., 2019). BIK1 also interacts and phosphorylates the vacuolar Ca^{2+} channels CAX1 and CAX3, independently of the phosphorylation of CAX1 and CAX3 by the Ca^{2+} sensors CIPK9, CIPK3 or CIPK26 (**Figure 1.7**). BAK1 also has a role in Ca^{2+} signalling, as it can phosphorylate and destabilise CNGC20 from the Ca^{2+} channel formed by CNGC19 and CNGC20 (Yu et al., 2019). FLS2, also has a role mediating Ca^{2+} signalling, as it interacts with the plasma membrane located Ca^{2+} pump CALCIUM-TRANSPORTING ATPASE 8 (ACA8), and together with ACA10 regulate the increase in $[Ca^{2+}]_{cyt}$ in response to flg22 (Frey et al., 2012). Independently of members of the flg22-sensing complex, the tonoplast-localised Ca^{2+} channels ACA4 and ACA11 transport Ca^{2+} into the vacuole in the absence of PAMP (**Figure 1.7**). However, in the presence of flg22, double mutant plants for both ACA4 and ACA11 genes displays larger increases of $[Ca^{2+}]_{cyt}$ during PTI, similar to the phenotype observed in the *cax2* mutant in hypoxia response (Bakshi et al., 2023; Hilleary et al., 2020).

Downstream of the increase in $[Ca^{2+}]_{cyt}$, Ca^{2+} can directly bind to two EF-Hands located in the N-terminal region of RBOHD (Torres et al., 1998). The downstream increase in $[Ca^{2+}]_{cyt}$ is sensed by several CPKs, of which CPK5 and CPK6 are the most studied in the context of PAMP perception. Specifically, CPK5 has been shown to regulate ROS production after flg22 perception by interacting and phosphorylating the N-terminus of RBOHD (**Figure 1.7 and Table 1.1**) (Dubiella et al., 2013). Furthermore, other Ca^{2+} sensors can also regulate RBOHD during the onset of plant immunity, as CPK1/2/4/11 can phosphorylate RBOHD's Ser148 residue, thus also regulating ROS production upon PAMP perception (**Figure 1.7 and Table 1.1**) (Gao et al., 2013). In addition to these mechanisms, Ca^{2+} channels can also be activated by the LRR receptor kinase HYDROGEN-PEROXIDE-INDUCED CALCIUM INCREASES 1 (HPCA1), which is activated by apoplastic ROS, increasing fast increases in $[Ca^{2+}]_{cyt}$ in response to pathogen infection (Wu et al., 2020). This process is a key step in the feedback loop established between Ca^{2+} and ROS signalling in stress responses (Fichman et al., 2022), demonstrating that Ca^{2+} signalling plays a critical role in plants response to biotic stress, functioning together with RBOHD to propagate stress perception

signals. Moreover, mutual phosphorylation can take place between different Ca^{2+} sensors, triggering a synergistic activation. This mechanism synergistically enhances NADPH oxidase activation by CPK5 and CBL1/CIPK26 after flg22 treatment (Köster et al., 2025) (**Table 1.1**).

Table 1.1. List of Ca^{2+}-dependent regulators of RBOHD activity in response to stress. List of post-translational regulators of RBOHD activity related to Ca^{2+}, specifying the residues affected by this regulation, the functional involvement of the regulatory process and the studies where these mechanisms were discovered.

Regulator	Phosphorylated Residue-Regulation		Functional Involvement	Reference
CPK2/4/11	Ser-148		Enhance plant immunity	(Gao et al., 2013)
CPK5	Ser-8	Ser-163	Enhance plant immunity	(Dubiella et al., 2013; Köster et al., 2025)
	Ser-39	Ser-343		
	Ser-148	Ser-347		
	Ser-162	Ser-692		
CPK16	Ser-133	Ser-163	Enhance plant hypoxia response and increase RBOHD stability	(Yu et al., 2024)
	Ser-148	Ser-347		
HPCA1	Upstream of RBOHD		Acclimation to high light stress	(Fichman et al., 2022)
CBL1/CIPK26	Ser-8	Ser-343	Enhance ROS production	(Köster et al., 2025)
	Ser-162	Ser-347		
	Ser-163	Ser-692		
CPK4/5/6/11	Ser-133	Ser-163	Enhance plant defence responses	(Kadota et al., 2014)
	Ser-148	Ser-347		
	Ser-152			
	Upstream of RBOHD		Enhance plant immunity	(Boudsocq et al., 2010)
CPK28	Interaction		Inhibit plant immunity	(Monaghan et al., 2014)

In addition to RBOHD, in response to the increase in $[Ca^{2+}]_{cyt}$, both CPK5 and CPK6 can phosphorylate downstream targets such as the WRKY33 TF (**Figure 1.7**), a key transcriptional regulator of plant defence responses against pathogens (Yang et al., 2020; Zhou et al., 2020) (**see**

also section 1.4.2.2 below), as well as WRKY8/28/48 (**Figure 1.7**) (Gao et al., 2013). In addition, the calmodulin-like protein TOUCH3 (TCH3) can bind to Ca^{2+} and relieve autoinhibition of CPK5 to phosphorylate and activate, CALMODULIN-BINDING PROTEIN 60-LIKE G (CBP60g), a transcriptional activator involved in the positive regulation of immune responses (Sun et al., 2022).

These are all positive roles of CPKs in the activation of plant immunity, however, CPKs can also act as negative regulators of PTI. For example, one key negative regulator is CPK28, which is located at the cytosolic side of the plasma membrane, where it interacts with several other proteins such as RBOHD (Monaghan et al., 2014), BIK1 (Monaghan et al., 2014), PLASMA MEMBRANE INTRINSIC PROTEIN 2;7 (PIP2;7) (Zhu et al., 2025) and several E3 ubiquitin ligases like PUB25/26 (Wang et al., 2018) or ARABIDOPSIS TOXICOS EN LEVADURA 6 (ATL6) and ATL31 (Liu et al., 2022). In the absence of PAMP, CPK28 phosphorylates PIP2;7, an aquaporin that acts as H_2O_2 transporter (**Figure 1.7**), inhibiting its function and preventing the transport of H_2O_2 from the apoplast into the cytoplasm (Zhu et al., 2025). However, the most studied CPK28 target is BIK1. BIK1 is phosphorylated by CPK28 in the absence of PAMP, promoting its turnover *via* the two E3 ubiquitin ligases PUB25 and PUB26 to prevent over-accumulation of BIK1 and hyper-activation of immunity (**Figure 1.7**) (Monaghan et al., 2014; Wang et al., 2018). In contrast, after PAMP perception, CPK28 directly phosphorylates PUB25/26 enhancing their activity and promoting BIK1 degradation to enhance BIK1 turnover and dampen immunity (Wang et al., 2018). To ensure adequate immune responses, after flg22 perception, CPK28 undergoes both intermolecular autophosphorylation and BIK1-mediated phosphorylation, which positively regulates its interaction with ATL6/31, promoting CPK28 degradation and favouring the stabilization of BIK1 and the activation of PTI (**Figure 1.7**) (Liu et al., 2023, 2022).

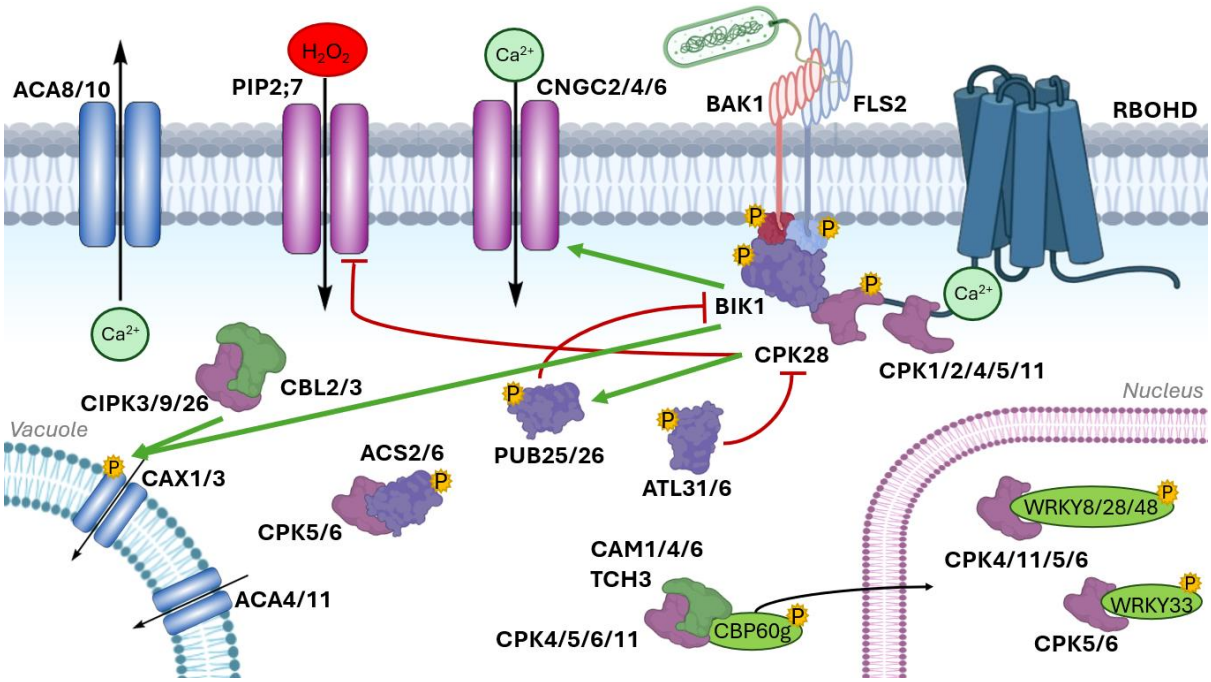

Figure 1.7. Ca^{2+}-dependent signalling after PAMP perception. Scheme showing the known signalling hubs dependent on Ca^{2+} triggered after flg22 perception by FLS2.

Taken together, CPKs play dual roles in regulating plant immunity, acting as both positive and negative regulators of defence responses to allow the fine-tuning of plant immunity and preventing excessive immune responses. However, critical knowledge gaps remain: (i) it is unclear whether specific CPKs discriminate between downstream targets in different signalling contexts (e.g. hypoxia or flg22); (ii) if CPKs interplay with other signalling modules (e.g., MAP kinases or hormone signalling pathways) when shaping immune outcomes; and (iii) what is the role of CPKs and other Ca^{2+} sensors in the convergence between hypoxia and immune responses. Also, while Ca^{2+} acts as a central secondary messenger in response to both hypoxia and PAMP perception through increases in $[Ca^{2+}]_{cyt}$, it remains unclear how stress-specific Ca^{2+} signatures are decoded without signal conflict when different stresses occur simultaneously or sequentially. Additionally, stress sensing mechanisms and Ca^{2+} signalling pathways converge on the NADPH oxidase RBOHD in stress responses. The interaction between Ca^{2+} and RBOHD establishes a feedback loop between Ca^{2+} and ROS once stress is perceived and enables rapid and robust responses to stress by amplifying and propagating stress signals from local to distal tissues. This mechanism may function as a convergent pathway that allows integration of the different stress-specific signals at the level of one enzyme (RBOHD), thus highlighting a potential crucial role of RBOHD in mediating responses to multiple stresses, including hypoxia and immunity.

1.4. ROS signalling

ROS are a group of molecules derived from O_2 (**Figure 1.8**), characterised by their reactivity towards biomolecules such as lipids, proteins, RNA or DNA, by donating an electron or transfer of an excited energy state to these biomolecules (Mittler, 2017; Mittler et al., 2022). As they are extremely reactive, their production, scavenging and transport are tightly regulated to avoid cellular damage. This extensive regulation allows the plant to use ROS as second messengers to contribute to signal transduction and the triggering of biotic and abiotic stress responses by producing stress-specific signatures that travel from local to distal (non-stressed) tissues together with Ca^{2+} and other second messengers (Fichman et al., 2019).

ROS are formed after O_2 accepts electrons in a stepwise manner, producing superoxide anion (O_2^-) in different subcellular compartments. This reaction can take place passively as in chloroplasts as a by-product of photosynthesis (Exposito-Rodriguez et al., 2017), or mitochondria as the result of mitochondrial electron transport chain (mETC) malfunction (Schwarzländer et al., 2009). However, superoxide anion can also be produced actively, by dedicated oxidases that generate ROS for the purpose of signalling after stress sensing, and by NADPH oxidases (**Figure 1.8**) (Mittler et al., 2022). The production of superoxide anion by RBOHD takes place by using electrons from its nicotinamide adenine dinucleotide phosphate (NADPH) oxidase domain at the cytosolic side of the plasma membrane to produce superoxide in the apoplast (De Torres Zabela et al., 2002; Keller et al., 1998). Once produced, superoxide is extremely reactive, unstable, and unable to diffuse through membranes, making it unsuitable to act as a second messenger in stress responses. Two molecules of superoxide are transformed into one molecule of H_2O_2 by superoxide dismutases (SODs) involving the action of a metal ion at the enzyme's active site. In contrast to superoxide, H_2O_2 is more stable and can diffuse through membranes, making it the ideal molecule to act as a second messenger in stress signalling.

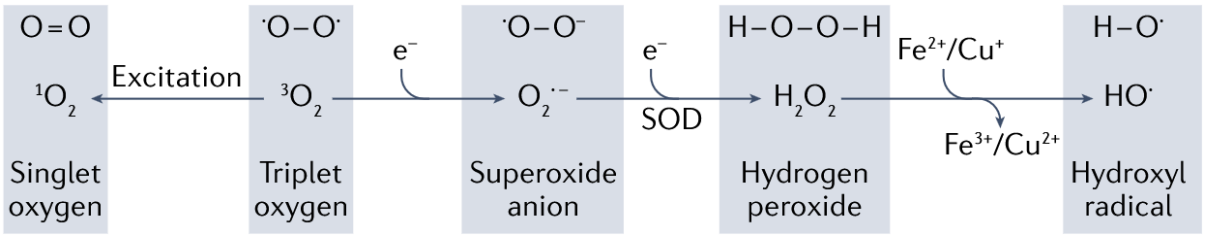

Figure 1.8. Different forms of ROS are produced by excitation or reduction of O_2. O_2 can accept electrons in a sequential manner, producing (i) superoxide anion (O_2^-); (ii) hydrogen peroxide (H_2O_2) after dismutation of two superoxide anions; (iii) a hydroxyl radical (•OH) *via* the Fenton reaction. Figure from Mittler et al., 2022.

As described in the following sections, (i) ROS production occurs shortly after stress perception in multiple compartments by multiple mechanisms, (ii) they carry general- and stress-specific signatures across plant tissues, and (iii) they interact with other second messengers and signalling networks, triggering downstream mechanisms that result in stress-responsive transcriptional and post-translational changes to increase plant survival upon stress conditions. Therefore, ROS serve as a convergent point in stress responses that integrates signals from stress sensing mechanisms into transcriptional and post-translational outputs. Due to their relevance in the context of hypoxia and flg22 responses, the following sections will focus on mitochondrial and RBOHD-dependent ROS production, as well as the downstream signalling events.

1.4.1. Mitochondrial ROS production

The mETC is a series of protein complexes in the inner mitochondrial membrane that transfers electrons from metabolic fuels (like NADH, $FADH_2$) to oxygen, creating a proton gradient that drives ATP synthesis via oxidative phosphorylation, essentially generating cellular energy (ATP) (**Figure 1.9**). The mETC comprises four inner-membrane complexes (I–IV) and two mobile electron carriers, ubiquinone (CoQ) and cytochrome c (Cyt C) (**Figure 1.9**). During stress conditions such as low levels of O_2, the electron carriers in the mETC become over-reduced, leading to electron leakage from complexes I and III and the formation of ROS (Chang et al., 2012; Møller, 2001; Schwarzländer et al., 2009; Vishwakarma et al., 2018; Wagner et al., 2019). This superoxide is then released to the mitochondrial matrix or the intramembrane space, where it is dismuted to H_2O_2 by SOD enzymes. Afterwards, H_2O_2 can travel to different parts of the plant cell, triggering retrograde signalling, the process by which plant organelles send signals to the nucleus, modulating nuclear gene expression in response to changes in organelle function.

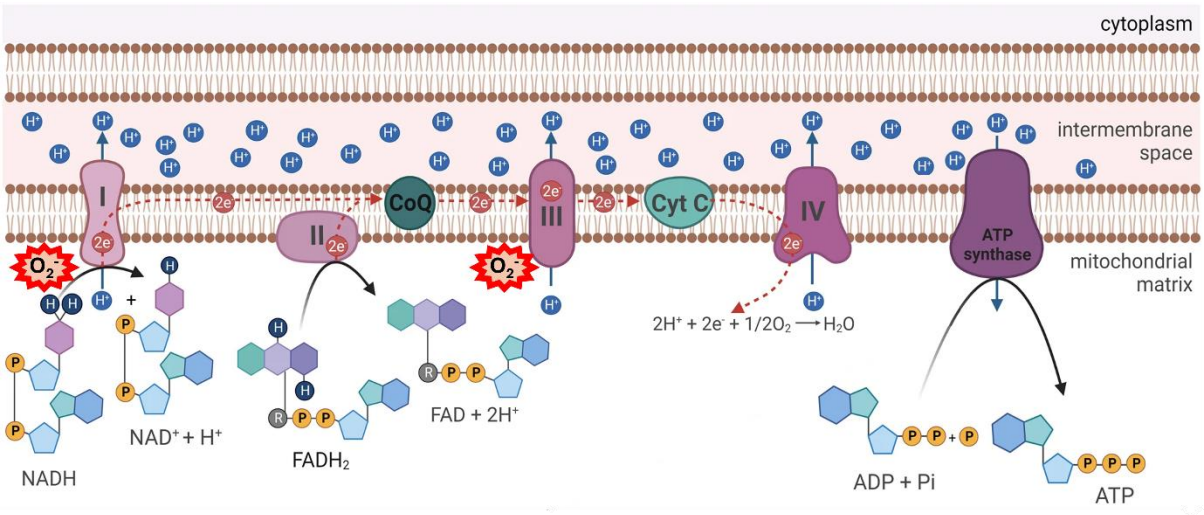

Figure 1.9. Illustration of the mitochondrial electron transport chain (mETC). Electrons move through the inner-membrane complexes (I–IV) and the two mobile electron carriers, ubiquinone (CoQ) and cytochrome c (Cyt C), generating a proton gradient across the membrane, which powers ATP synthase to produce ATP. This figure also shows the main ROS producing sites during mETC disfunction. Figure adapted from Palma et al., 2024.

Mitochondrial ROS production under hypoxia is regulated by HYPOXIA-RESPONSIVE MODULATOR 1 (HRM1), through association with complex I (Tsai et al., 2023). Mitochondrial alternative NADH dehydrogenases NDA1 and NDA2 can also regulate mitochondrial ROS production upon hypoxia (Jethva et al., 2023). These proteins are part of an overflow mechanism that provides metabolic plasticity under environmental stress conditions. Once mitochondrial ROS exit the mitochondria in the initial phases of hypoxia stress, they can travel to the endoplasmic reticulum (ER), where they trigger RHOMBOID-LIKE 2 (RBL2)-dependent cleavage of ER-anchored transcription factors ARABIDOPSIS NAC DOMAIN CONTAINING PROTEIN 13 (ANAC013), ANAC016 and ANAC017 (Eysholdt-Derzsó et al., 2023). This cleavage facilitates their translocation to the nucleus, where they transcriptionally induce genes belonging to the "mitochondrial dysfunction stimulon" (MDS) such as *NDA1* (Jethva et al., 2023). These target genes are characterised by the presence of a mitochondrial dysfunction motif (MDM) in their promoter, which is bound by the ANAC013/16/17 TFs (De Clercq et al., 2013). Among them, several Hypoxia Responsive Genes (HRGs) are included, such as *PHYTOGLOBIN 1* (*PGB1*), *ALCOHOL DEHYDROGENASE 1* (*ADH1*) or *PYRUVATE DECARBOXYLASE 1* (*PDC1*) (De Clercq et al., 2013; Eysholdt-Derzsó et al., 2023; Ng et al., 2013).

Intriguingly, mitochondrial ROS production in hypoxic conditions can be a potential convergence point between hypoxia and flg22 responses, as the inhibition of the terminal step of the mETC by mETC inhibitors antimycin A (AA) and potassium cyanide (KCN), which stimulates

mitochondria-associated ROS production, transiently activates MITOGEN-ACTIVATED PROTEIN KINASE 3 (MPK3), MPK4 and MPK6 (Chang et al., 2012) (**see also Section 1.3.3 below**), which play a central role in transducing flg22-dependent immune signals downstream of PRRs (Asai et al., 2002). However, how this activation takes place is still unclear and highlights the need for further investigation into how ROS modulates MAPK cascades.

As indicated above, ROS production is tightly regulated in the plant cell and mitochondria have enzymes to prevent excessive ROS formation. One of these enzymes, ALTERNATIVE OXIDASE 1a (AOX1a), can use excess reductants that surpass the cytochrome pathway capacity, thereby preventing ROS formation from an over-reduced ubiquinone pool (Umbach et al., 2005). This enzyme is another convergence point in response to both hypoxia and flg22, as AOX1a has been shown to play a role in regulating ROS and NO accumulation in both hypoxia and flg22 stress responses (Vishwakarma et al., 2018a). Consistent with its role in regulating mitochondrial ROS production, *AOX1a* is one of the MDS genes, whose expression is transcriptionally activated by several TFs related to hypoxia and mitochondrial malfunction, including ANAC013 and ANAC017 (He et al., 2022; Ng et al., 2013). Other hypoxia responsive TFs that control *AOX1a* expression are the ERF-VIIs, as observed by the binding of RAP2.12 to the *AOX1a* promoter and evidenced by the transcriptional downregulation of *AOX1a* in *rap2.12* mutants in response to flooding (Yao et al., 2017a). *HRE2* is another ERF-VII included in the MDS gene list and consequently, it is transcriptionally upregulated by ANAC013 (Eysholdt-Derzsó et al., 2023). Hence, *HRE2* is not only a target of mitochondrial malfunction response, but also a mediator of it, as it binds *AOX1a* promoter, establishing a feedback regulatory loop to regulate mitochondrial malfunction (He et al., 2022; Ng et al., 2013).

Altogether, mitochondrial ROS might be a key hub in the crosstalk between hypoxia and pathogen/PAMP response and could potentially play a role when these stresses are combined as a hypoxia-dependent regulator of plant immunity. In addition, these studies suggest a role of ERF-VIIs in the regulation of mitochondrial ROS production and scavenging, consistent with previous studies suggesting a role of ERF-VIIs regulating genes involved in redox regulation (Giuntoli et al., 2017). A recent report showed that ROS inhibit PCOs (Akter et al., 2024), raising the possibility that mitochondrial ROS could contribute to regulating ERF-VII stability in hypoxic conditions and perhaps in response to PAMPs too, establishing a feedback loop in which ERF-VIIs and mitochondria interact with and regulate each other in combined stress conditions.

1.4.2. ROS production by RBOHD

As mentioned previously, RBOHD is a plasma membrane–localised NADPH oxidase that plays a central role in ROS production during stress responses. It is activated in response to several environmental cues such as PAMPs and pathogens (Dubiella et al., 2013; Kadota et al., 2014; Li et al., 2014; Torres et al., 2002), hypoxia (Wang et al., 2017; Yu et al., 2024), high light stress (Miller et al., 2009; Zandalinas et al., 2020) or phytohormones (Kwak et al., 2003). Given the central role of RBOHD in plant stress responses, its regulation has been extensively studied, but much more is known about the regulation of RBOHD upon flg22 perception than in response to hypoxia.

RBOHD comprises six plasma membrane-spanning domains (**Figure 1.10**) responsible for RBOHD location in dynamic spots in the plasma membrane (Hao et al., 2014). In this previous studies, it was also shown how RBOHD activity, in response to stress perception (flg22, abscisic acid (ABA) or salt), increased the diffusion and oligomerization of RBOHD itself. This dynamic behaviour is cooperatively regulated by clathrin- and microdomain-dependent endocytic pathways, indicating the importance of RBOHD stability in stress conditions.

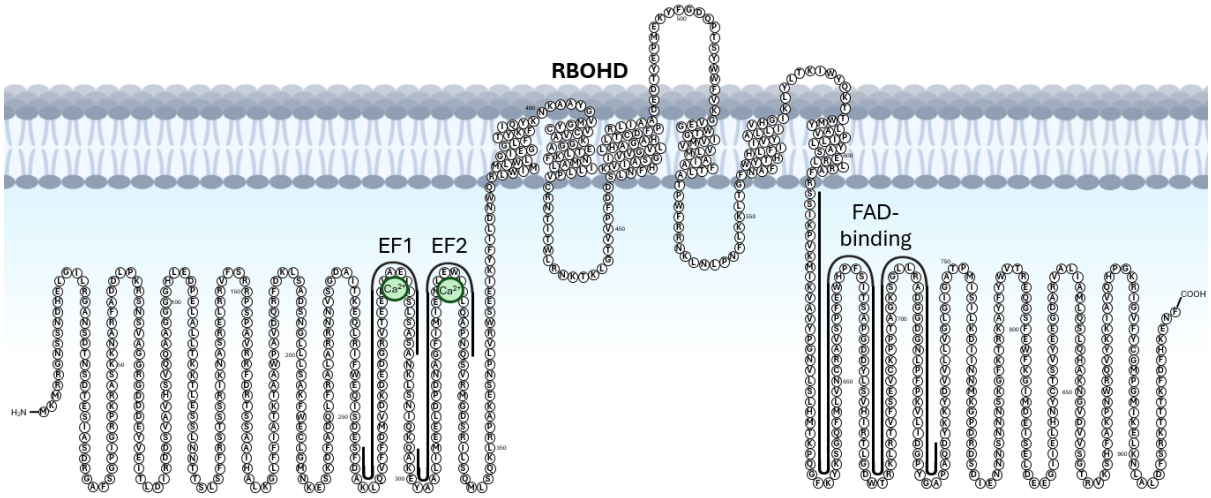

Figure 1.10. Structure of RBOHD. The RBOHD amino acid sequence is shown, with its different domains: EF-Hands 1 (EF1; amino acids (aa) 253-288) and EF2 (aa 297-332), FAD-binding domain (aa 611-732) and the six transmembrane domains (aa 377-397; 462-482; 517-537; 560-580; 589-606; 735-755). Adapted from Köster et al., 2025.

The cytoplasmic C-terminal domain of RBOHD harbours NADPH- and FAD-binding sites (Keller et al., 1998) (**Figure 1.10**). This domain is in charge of transferring electrons from cytosolic NADPH to apoplastic O_2, leading to the production of superoxide anion in the apoplast (**Figure 1.8).** This domain also plays an important role in the regulation of RBOHD activity and stability *via*

different mechanisms: (i) S-nitrosylation of Cys-890 by NO abolishes RBOHD ability to synthesise ROS in the context of pathogen-induced cell death (**Table 1.2**) (Yun et al., 2011); (ii) phosphorylation of Ser-611, Ser-703 and Ser-862 by CYSTEINE-RICH RLK2 (CRK2) is required to fine-tune flg22-triggered ROS production by RBOHD and regulate resistance to virulent bacterial pathogens (**Table 1.2**) (Kimura et al., 2020); and (iii) phosphorylation of Ser-862 and Thr-912 by PBS1-LIKE KINASE 13 (PBL13) negatively regulates RBOHD activity by enhancing the subsequent ubiquitination by PBL13-INTERACTING RING TYPE E3 UBIQUITIN LIGASE (PIRE), which triggers the subsequent vacuolar degradation of RBOHD (Lee et al., 2020). While both mechanisms are active in the absence of flg22, in the presence of this PAMP, PIRE is phosphorylated by an unknown kinase, which inhibits its function and thus stabilises RBOHD in the plasma membrane (**Table 1.2**) (Lee et al., 2020). These regulatory mechanisms of RBOHD highlight the role of the C-terminal domain as the catalytic domain responsible for ROS production, but also as a critical regulatory hub that integrates information from diverse post-translational modifications.

The cytoplasmic N-terminal domain of RBOHD comprises two Ca^{2+}-binding motifs called EF-Hands (Torres et al., 1998) (**Figure 1.10**). This domain plays an important role in regulating RBOHD activity and stability in response to stress perception (Kimura et al., 2012; Ogasawara et al., 2008). For example, phosphorylation of four serine residues in this domain (Ser-39, Ser-339, Ser-343 and Ser-347) by BIK1 activates RBOHD activity after flg22 treatment (Kadota et al., 2014; Li et al., 2014). At the same time, PHAGOCYTOSIS OXIDASE/BEM1P (PB1) DOMAIN-CONTAINING PROTEIN (PB1CP) can also interact with RBOHD after flg22 treatment, competing with BIK1 and leading to the dissociation of phosphorylated BIK1 from RBOHD (Goto et al., 2024b). In addition, phosphorylation of other 4 serine residues (Ser-8, Ser-9, Ser-339, and Ser-347) by the MAP4 kinase SERINE/THREONINE KINASE 1 (SIK1) enhances ROS production by RBOHD after flg22 treatment. SIK1 also stabilises BIK1 in the absence of flg22 through direct phosphorylation or indirectly through heterotrimeric G protein subunit EXTRA-LARGE GTP-BINDING PROTEIN 2 (XLG2) (Liang et al., 2018; Liang et al., 2016; Zhang et al., 2018).

In addition to this role in regulating BIK1 stability, different heterotrimeric G proteins are also involved in the regulation of RBOHD function through different ways. For example, the Gβ subunit ARABIDOPSIS GTP BINDING PROTEIN BETA 1 (AGB1), similar to XLG2, associates with the FLS2–BIK1 receptor complex and is required for flg22-triggered ROS burst in a BIK1-dependent mechanism (Ishikawa, 2009; Liang et al., 2018; Wang et al., 2023; Liang et al., 2016). Furthermore, the canonical Gα subunit G PROTEIN ALPHA SUBUNIT 1 (GPA1) constitutively associates with RBOHD to enhance flg22-induced ROS independently of BIK1 (Ishikawa, 2009; Lahong Xu et al., 2019). Beyond immunity, the heterotrimeric G proteins regulate RBOHD

function, for example, GPA1 mediates high-concentration CO_2-induced stomatal closure through interacting with CARBOXIC ANHYDRASE 1 (CA1) and CA4 to promote H_2O_2 accumulation in *A. thaliana* guard cells (Zhang et al., 2025). Furthermore, in response to ABA GPA1 couples with PHOSPHOLIPASE D ALPHA 1 (PLDα1) to produce Phosphatidic Acid (PA), which binds to Arg-149, Arg-150, Arg-156 and Arg-157 residues of RBOHD positively regulating its activity (Zhang et al., 2009). Briefly, PA is a phospholipid that acts as a second messenger in stress responses. It accumulates in plant cells in response to PAMPs (Cao et al., 2022; Kalachova et al., 2022; Kong et al., 2024), pathogen infection (*Pst DC3000*) (De Torres Zabela et al., 2002) and hypoxic conditions (Fan et al., 2023; Premkumar et al., 2019; Xie et al., 2015; Zhou et al., 2022) among other stresses. Intriguingly, PA-activated RBOHD is more stable and remains in the plasma membrane after ROS production (Qi et al., 2024).

Hence, several mechanisms are at play for the regulation of RBOHD (i) phosphorylation of residues at both C- and N-terminal domains, leading to RBOHD endocytosis and subsequent degradation; (ii) PA binding to Arg residues, leading to RBOHD retention at the plasma membrane and stabilisation; and (iii) Ca^{2+}-dependent regulation mediated by Ca^{2+} itself, and different kinases such as CPK2/4/5/11 as positive immunity regulators or CPK28 as negative immune regulator, as outlined in **Section 1.3.1.2 above** (**Table 1.1 and Figure 1.11**).

These mechanisms allow us to generate an up-to-date model for ROS production by RBOHD upon flg22 perception by FLS2. In this model, activated-BIK1 phosphorylates RBOHD at different residues, resulting in RBOHD initial activation and local extracellular ROS production (**Figure 1.11**). In addition, other regulators of RBOHD are thought to phosphorylate RBOHD in early stages of PTI, such as SIK1 or CRK2 (**Figure 1.11**). Once RBOHD is activated, BIK1 dissociates from RBOHD through the action of PB1CP and together with the activation of HPCA1 by the initial ROS production, Ca^{2+} channels become active and allow for $[Ca^{2+}]_{cyt}$ increases to take place (**Figure 1.11**). Cytosolic Ca^{2+} binds the EF-hand domains of RBOHD triggering conformational changes. In addition, cytosolic Ca^{2+} also activates different Ca^{2+} sensors involved in RBOHD regulation, such as the CBL1/CIPK26 and CPK2/4/5/11/28 (**Figure 1.11**). The conformational changes triggered by Ca^{2+} binding, together with the post-translational modifications triggered by CPKs, further activate RBOHD. Afterwards, CBL1/CIPK26 and CPK5, and potentially other CPKs, can further phosphorylate each other to maintain ROS production by RBOHD (**Figure 1.11**). However, there are still aspects of this model that are poorly understood, such as how PA-dependent activation is integrated in this model, which regulators interact with each other similar to CBL1/CIPK26 and CPK5 or the mechanisms that regulate the stability of RBOHD via internalisation or degradation after RBOHD becomes active.

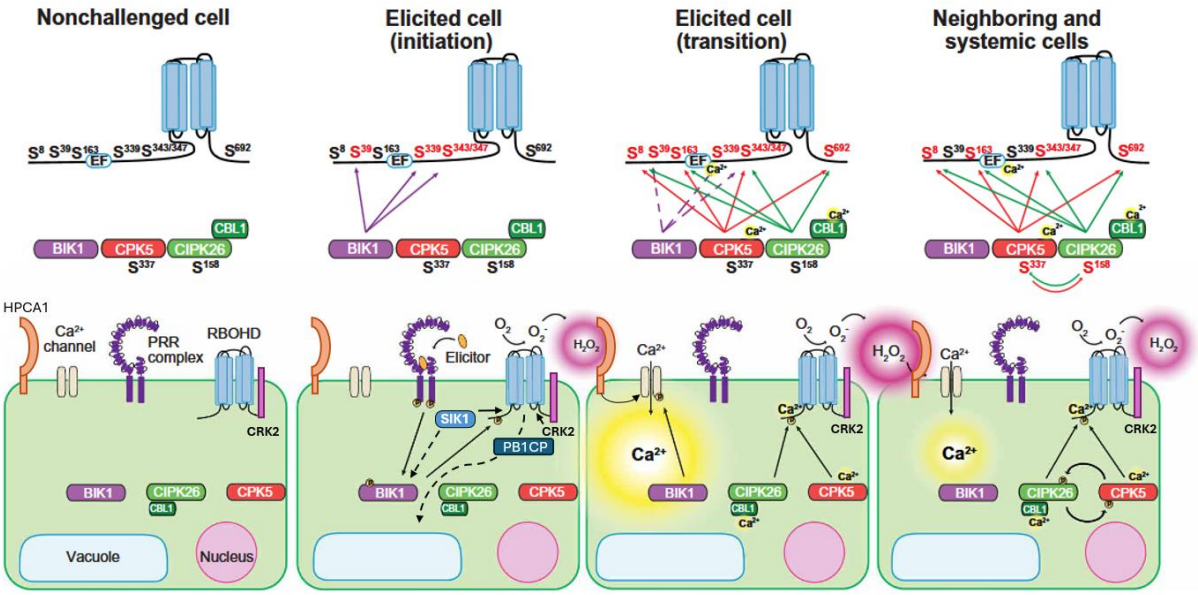

Figure 1.11. Current models for RBOHD regulation in response to pathogens and to PAMPs. First, after PAMP perception, BIK1 phosphorylates RBOHD triggering an initial ROS burst, which triggers Ca^{2+} increases, triggering complete activation of RBOHD and allowing ROS burst to propagate to neighbouring cells. Figure adapted from Köster et al., 2025.

RBOHD is also important for the onset of plant responses to hypoxia, but much less is known about its regulation in low O_2 conditions. In addition to previously mentioned CPK16 (**see also section 1.3.1.1 above**), in response hypoxic conditions, the ERF-VIIs induce HYPOXIA RESPONSIVE UNIVERSAL STRESS PROTEIN 1 (HRU1) re-location to the plasma membrane, favouring its interaction with RBOHD (**Figure 1.12**) (Gonzali et al., 2015a). When interacting with RBOHD, HRU1 can also interact with Ras HOMOLOGOUS-LIKE SMALL G PROTEIN OF PLANTS (ROP2), which was previously reported to activate ROS production in hypoxic conditions (**Figure 1.12**) (Baxter-Burrell et al., 2002). This data allowed us to generate a similar model for RBOHD function and regulation in response to hypoxia than the one in response to flg22.

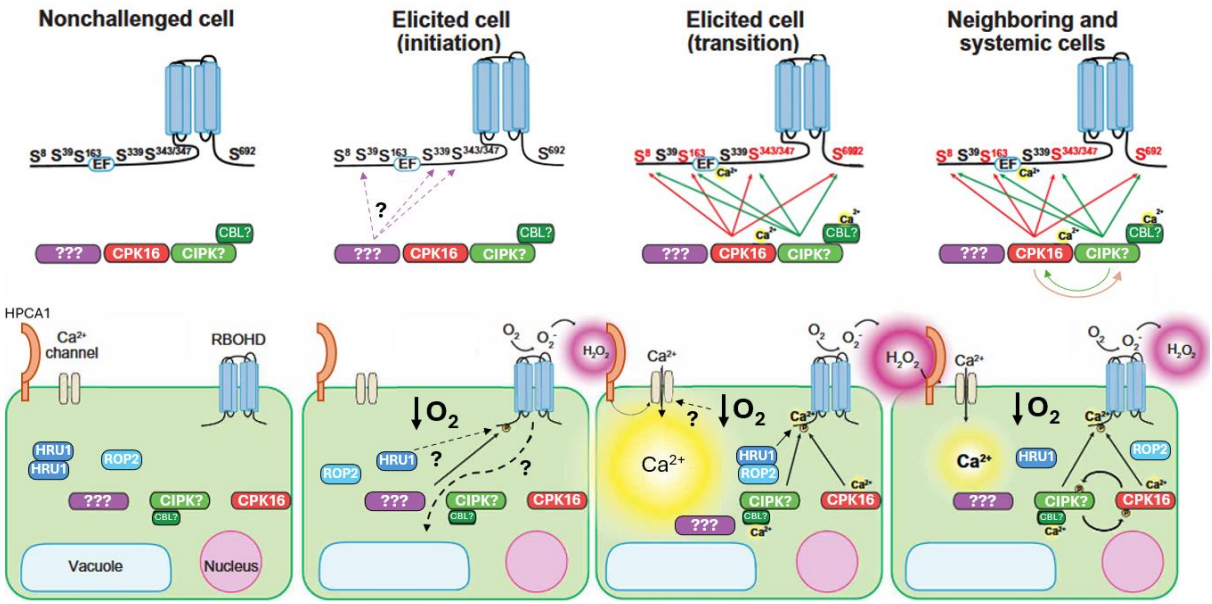

Figure 1.12. Current model for RBOHD regulation in systemic signal initiation and propagation adapted for hypoxic conditions. First, hypoxia sensing, an unknown element will activate RBOHD, then the ROS produced triggers Ca^{2+} increases, triggering complete activation of RBOHD and allowing ROS burst to propagate to neighbouring cells. Figure adapted from Köster et al., 2025.

However, when comparing the proposed model of RBOHD activation in hypoxic conditions and flg22, several mechanisms remain unclear. For example, (i) what initiates RBOHD activation under hypoxia, HRU1 is one plausible candidate as it monomerizes upon hypoxia when ATP levels decrease; (ii) are there additional Ca^{2+} sensors involved in RBOHD activation upon hypoxia, and could any of them phosphorylate CPK16, analogous to the CBL1/CIPK26 and CPK5 phosphorylation mechanisms. Moreover, different regulators of RBOHD upon flg22 have known roles in hypoxia response, but their role in RBOHD regulation upon hypoxia remains undiscovered. Lastly, although several regulatory mechanisms of RBOHD function have been discovered, its function has not been clearly integrated in the most recent module of RBOHD regulation (**Table 1.2**). Integrating these modules into the most recent RBOHD regulatory models will clarify how individual components fit together and highlight shared convergence points that coordinate ROS output across contexts and therefore underline potential convergent points with a role in combined stress responses.

Table 1.2. List of regulators of RBOHD function. List of regulators of RBOHD activity whose function has not been studied in terms of residue-specific regulation or timely integration into the current model, including the functional involvement of the regulation and the studies where these mechanisms were discovered.

Regulators	Known Regulation	Functional Involvement	Reference
FLS2	Interaction	Enhance immune responses	(Li et al., 2014)
AGB1	Interaction and phosphorylation	Enhance immune responses	(Liang et al., 2016)
XLG2/3	Interaction and phosphorylation	Enhance immune responses	
CPK28	Interaction	Unknown	(Monaghan et al., 2014)
RIPK	Phosphorylation of Ser-347 Ser-343	Enhance immune responses	(Goto et al., 2024)
OXI1	Interaction and phosphorylation	Enhance immune responses	(Ma et al., 2024)
PUB2/4	Interaction	Enhance immune responses	(Wang et al., 2022)
QSK1	Interaction	Enhance immune responses	(Goto et al., 2024)
PLC2	Interaction	Enhance immune responses	(D'Ambrosio et al., 2017)
S-nitrosothiols	S-nitrosylation of Cys-890	Suppress immunity responses	(Yun et al., 2011)
XCP1 - CYS6	Interaction	Enhance immune responses	(Liu et al., 2024)
ALR1	Phosphorylation of Ser-39	Heavy metal stress response	(Z. J. Ding et al., 2024)
OST1	Phosphorylation of Ser-347	Acclimate to high light stress	(Fichman et al., 2022; Wang et al., 2019)
LSK4	Phosphorylation of Ser-39	K+ Uptake	(Wang et al., 2021)
H_2S	S-sulfhydration of Cys-825 Cys-890	Stomatal closure	(Shen et al., 2020)
DORN1	Phosphorylation of Ser-22 Thr-24	Stomatal closure	(Chen et al., 2017)

Taking both models for RBOHD regulation, other unanswered questions arise in terms of RBOHD regulation:

(i) What are the negative regulators (e.g. protein phosphatases) of RBOHD that prevent excessive ROS production in stress responses.

(ii) Are there different regulatory pathways depending on the tissue or the cell type where RBOHD is located.

(iii) Phosphorylation of RBOHD is well established, however other post-translational modifications (PTMs) such as ubiquitination, sumoylation, S-nitrosylation, or oxidation together with RBOHD stability in the plasma membrane are much less understood.

(iv) How do plants integrate the different activation mechanisms when plants face combined stress conditions.

Considering the central role of RBOHD in the response to a wide range of (a)biotic stresses integrating complex regulatory mechanisms which can be stress-specific or common to different stresses, RBOHD is one of the main and most studied convergence points that could potentially regulate plant responses to combined stresses, including combined PAMP/hypoxia or pathogen/hypoxia.

1.4.3. Signalling pathways downstream of ROS production

Once ROS are produced in different compartments of the plant cell, they can follow different pathways to activate stress responses, including protein oxidation or movement of ROS to neighbouring cells.

1.4.3.1. A ROS wave contributes to systemic signalling

ROS can propagate stress signals to neighbouring cells *via* RBOHD-dependent apoplastic ROS production in a process called “ROS wave”, which enables rapid signal transduction from local tissues to systemic (not-stressed) tissues. This ROS wave relies on three main mechanisms to propagate the ROS signal to neighbouring cells, (i) apoplastic H_2O_2 enters cells through aquaporin membrane proteins and covalently modifies cytoplasmic proteins (Dynowski et al., 2008), (ii) apoplastic H_2O_2 triggers an influx of Ca^{2+} ions to the cytoplasm through the activation of HPCA1 and subsequent phosphorylation of Ca^{2+} channels (**Figures 1.11-13**) (Fichman et al., 2022; Wu et al., 2020), or (iii) H_2O_2 enters neighbouring cells through plasmodesmata, which are channels that provide direct cytoplasmic connections between plant cells (Fichman et al., 2021). This cell-to-cell mode of signal propagation is evidenced by the inhibition of ROS production in systemic tissues when inhibitors of Ca^{2+} and ROS signalling were applied between systemic and local tissues (Miller et al., 2009).

Moreover, other waves (Ca^{2+}, electric and redox waves) have been identified to coordinate each other through different regulators to propagate the stress signal to distal tissues in response

to stress conditions such as waterlogging (Peláez-Vico et al., 2024, 2023), pathogens (Dubiella et al., 2013; Fichman et al., 2019; Morales et al., 2016), salinity (Evans et al., 2016; Miller et al., 2009), wounding (Fichman et al., 2019; Lew et al., 2020; Miller et al., 2009; Yosef Fichman and Ron Mittler, 2021), or high light (Fichman et al., 2022, 2021; Yosef Fichman and Ron Mittler, 2021) (**Figure 1.13**).

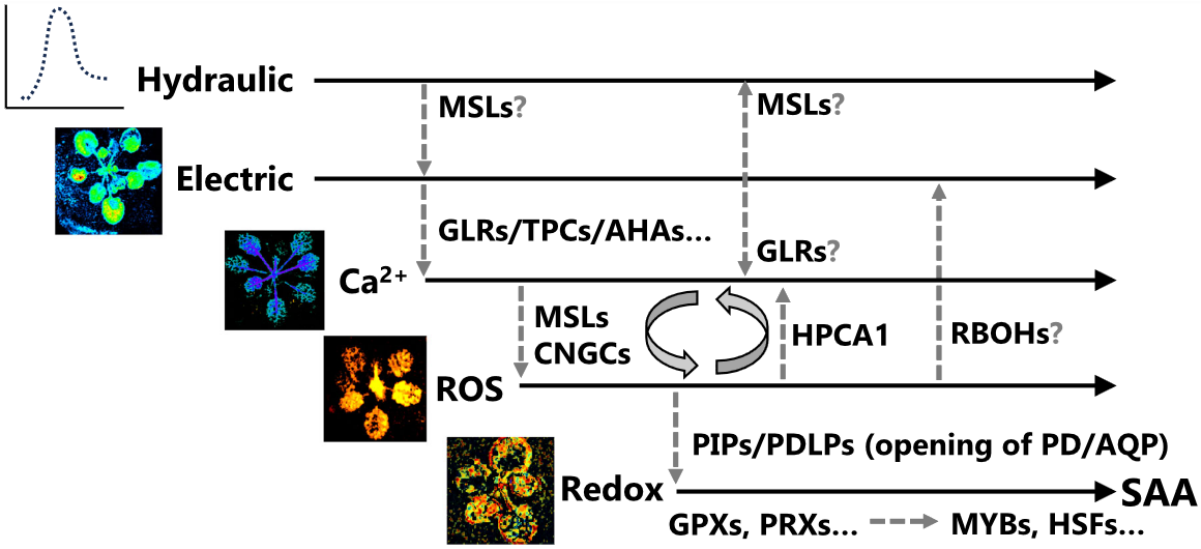

Figure 1.13. Scheme of the hierarchy and known or proposed interactions between the fast-propagated signals (waves) after stress sensing. The diagram illustrates the interconnected and hierarchical roles of the hydraulic, electric, Ca^{2+}, ROS, and redox waves in mediating systemic acquired acclimation (SAA) and systemic acquired resistance (SAR). Dotted lines represent studied and hypothetical connections between waves and the known or proposed regulators of the connections. Figure from Peláez-Vico et al., 2024.

Several gaps of knowledge remain in the context of systemic signalling, especially for combined stresses. It has nevertheless been shown that plants can integrate two different systemic signals simultaneously generated during stress combination (high light and heat stress). However, the way plants sense the different stresses that trigger these signals makes a significant difference to how fast and how efficiently they induce systemic ROS signals, and therefore plant acclimation to these combined conditions (Zandalinas et al., 2020). Little is known about RBOHD regulation and role in these combined ROS waves at the molecular level.

1.4.3.2. ROS contribution to transcriptional changes

Once ROS are produced upon stress conditions, they can react with a wide range of redox-sensitive proteins to regulate the function, localisation, or DNA-binding capacity of downstream

transcription factors. Through this redox-dependent regulation, ROS links cellular redox status to gene expression changes in stress responses. Furthermore, this ROS-dependent transcriptional activation has the ability to integrate stress signals from different cell compartments such as the apoplast, the cytosol, chloroplast or mitochondria. One example of ROS-dependent regulation of transcriptional changes is the indirect transcriptional upregulation of several HRGs upon hypoxia by *RBOHD* and *RBOHF*, such as *ADH1, PDC1, MYB2, SUS1/4, HEAT STRESS TRANSCRIPTION FACTOR (HSFA2)* or *HEAT SHOCK PROTEIN 18.2 (HSP18.2)* (Liu et al., 2017). This is evidenced by the transcriptional downregulation of *HSF2A* in the *rbohd* mutant in comparison with wild type plants in response to anoxia (Liu et al., 2017). In another study in which hypoxia and ROS responsive transcriptomic datasets were compared, *HSFA2* and *HSP22* were identified as genes transcriptionally induced in response to ROS and hypoxia (Pucciariello et al., 2012). Several genes from HSF and HSP families were also shown to be induced in response to mitochondrial malfunction (Kuzmin et al., 2004; Miller and Mittler, 2006), suggesting that not only RBOHD-dependent ROS production, but also mitochondrial ROS regulate transcriptional changes during hypoxia, underpinning ROS role as integrators of stress signalling pathways.

In addition, RBOHD acts as a central regulator linking early ROS production to transcriptional immune reprogramming, yet its regulatory role has not been extensively studied. In response to flg22, RBOHD-dependent ROS production modulates the expression of oxidative stress and secondary metabolism genes such as *PRX34, CYP71A12, CYP79B2, CYP81B2,* and *MYB51* (Daudi et al., 2012), and is required for induction of *NHL10* in distal tissues after flg22 treatment (Dubiella et al., 2013). Furthermore, chemical inhibition of RBOHD activity by spermine reduces expression of early PTI marker genes such as *WRKY22*, *WRKY29*, *FRK1* and *NHL10* (Zhang et al., 2023). However, another study showed lack of involvement of RBOHD in the transcriptional regulation of the same PTI marker genes (Macho et al., 2012; Yuan et al., 2021). These contrasting findings highlight how different experimental approaches to study RBOHD function can change the transcriptional outputs of the experiments, where one approach could allow for compensatory mechanisms (ROS produced in other sources of the plant cell such as RBOHF or mitochondria). Similarly, *PR1* expression is enhanced in *rbohD* plants upon *Pst DC3000 hrcC* infection (Kadota et al., 2015), although other studies reported no effect of RBOHD on *PR1* induction following flg22 perception (Smith et al., 2014). These studies suggest that RBOHD regulation of immunity-related genes is highly dependent on the context of the immune response.

Altogether, these studies highlight the role of ROS in the regulation of transcriptional changes in response to hypoxia and PAMPs, but further study is needed on this topic to

understand how different ROS signals are integrated into transcriptional changes during combined hypoxia and flg22 combined stress responses.

1.4.3.3. Protein oxidation by ROS

Once ROS accumulates in plant cells, they affect the redox state of many proteins through oxidative post-translational modifications, activating, modifying or integrating multiple stress-response signal transduction pathways, redox regulation or metabolic pathways. One of the main mechanisms involves the reaction of ROS with the thiol group of cysteine (Cys) and methionine (Met) residues. However, the presence of positively charged residues or hydrogen bonds, also influences protein reactivity to ROS (Zaffagnini et al., 2016). Oxidation of proteins involved in signal perception and transduction include the oxidation of two cysteine residues (Cys421 and Cys424) located in the extracellular domain of the LRR receptor kinase HPCA1. These cysteine residues are oxidised in response to pathogen infection to activate plasma membrane-localised Ca^{2+} channels and propagate the ROS and Ca^{2+} waves to from local to distal tissues (Fichman et al., 2022; Wu et al., 2020).

Proteins involved in redox regulation are themselves susceptible to oxidative modifications, including ASCORBATE PEROXIDASEs (APXs), which act as ROS-scavenging enzymes (Kubo et al., 1992). Among them, cytosolic APX1 is a central component of ROS signalling, as its activity is regulated by ROS during developmental transitions such as bolting (Zimmermann et al., 2006) or in response to both individual (Davletova et al., 2005) and combined stress conditions (Koussevitzky et al., 2008; Zandalinas et al., 2021, 2016). Oxidation of proteins regulates metabolic pathways such as glycolysis and photosynthetic carbon assimilation with the oxidation of NAD-dependent GLYCERALDEHYDE-3-PHOSPHATE DEHYDROGENASE 1 (GAPC1) in response to H_2O_2 (Vescovi et al., 2013) and flg22 treatment (Henry et al., 2015). Indeed, ROS oxidation of the catalytic cysteine residue (Cys149) of GAPC1 results in the loss of GAPC1 enzymatic activity, resulting in its translocation to the nucleus and subsequent interaction with different transcription factors, where it can regulate defence-related gene expression. However, no role of GAPC1 has been studied in hypoxia responses, which could be relevant, as primary metabolism is severely affected by the decrease in O_2 levels.

Altogether, the role of ROS as second messengers is a crucial component of stress responses. Their ability to regulate redox and metabolic signalling in response to different stresses establishes them as key convergent points during plant stress responses and therefore, potential regulators of combined stress conditions.

1.5. Importance of MAPK cascades in response to hypoxia and immune signalling

The mitogen-activated protein kinase (MAPK) cascade is a key signal transduction pathway that contributes to plant responses to a wide range of signals, including developmental cues and environmental stresses (Arthur and Ley, 2013; Kumar et al., 2020; Zhang and Zhang, 2022). The ubiquitous role of MAPK cascades have made them interesting candidates as components that could integrate different extracellular signals into cue-specific targets (Ma et al., 2024). MAPK cascades involve serine/threonine protein kinases that interact and activate each other in a sequential and hierarchical manner, starting with MAP KINASE KINASE KINASEs (MAPKKKs or MEKKs; 60 members in *A. thaliana*) that are activated by phosphorylation, and then interact and phosphorylate different MAP KINASE KINASEs (MAPKKs or MKKs), of which there are 10 members in *A. thaliana*. Activated MAPKKs then phosphorylate subsets of MAP KINASEs (MAPKs or MPKs), with 20 MPKs identified in *A. thaliana* (Ma et al., 2022). This last kinase component phosphorylates a wide range of targets with different biochemical functions, including TFs (**Figure 1.14).**

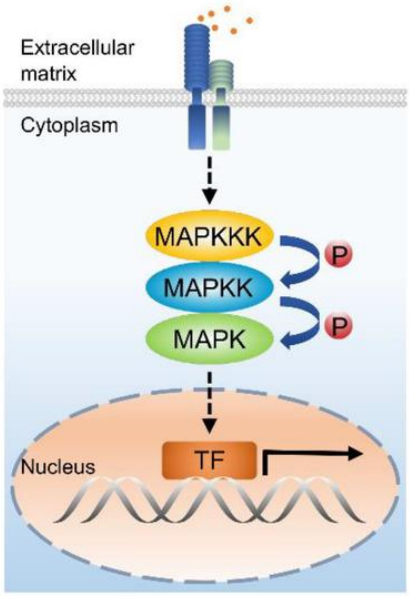

Figure 1.14. Mode of action of MAPKs in response to developmental or stress cues. MAPK cascades consist in the phosphorylation of MAPKKKs downstream of stress perception. MAPKKK phosphorylate MAPKKs, which subsequently phosphorylate MAPKs. MAPKs will phosphorylate several target proteins, including TFs, that regulate plant acclimation to abiotic stresses and defence responses. Figure from Wang and Gou, 2020.

One of the main challenges in MAPK signalling is to elucidate how the specificity of the signal received by the MAPKKKs is transduced to the substrates of the MPKs to activate a cue-specific response. In the stress response context, although the specific molecular mechanisms are unknown, it is known that this specificity is given by (i) the spatiotemporal-specific expression of the stress sensing machinery, which determines when and in which cells the MAPK cascade is activated; (ii) the interaction between MAPK cascade elements and second messengers; (iii) the interactions between different components of MAPK cascades; and (iv) the availability and function of the MAPK substrates, however, only some of them have been identified and studied (Dhatterwal et al., 2024).

1.5.1. Activation of MAPK cascades in response to flg22 or hypoxia

In *A. thaliana*, the first evidence of MAPK signalling demonstrated the activation of MPK3/MPK6 in a receptor-ligand-dependent manner during PTI, in response to flg22 sensing by FLS2 (Asai et al., 2002). In the context of both flg22 and plant pathogen infection, arguably one of the best understood MAPK cascades is the MKKK3/5–MKK4/5–MPK3/6 pathway, which was first discovered when MKK4 and MKK5 were identified as the upstream kinases of MPK3 and MPK6 in *A. thaliana* (Asai et al., 2002; Ren et al., 2002). MKKK3/5 were subsequently identified as the upstream kinases of MKK4 and MKK5 in response to flg22 (Bi et al., 2018; Sun et al., 2018). However, additional unidentified MKKKs are likely involved in the activation of MPKs, as MPK3/6 phosphorylation was not completely abolished in *mapkkk3 mapkkk5* double mutants upon PAMP perception (Bi et al., 2018). Additionally, MPK6 can phosphorylate MKKK5, enhancing MPK3/6 activation and disease resistance, suggesting that MAPK cascades are not strictly linear, but instead can include regulatory feedback loops that amplify signalling outputs (**Figure 1.15**) (Bi et al., 2018). The connection between PRRs and the activation of MAPKKKs after PAMP perception were partially discovered more recently, as analysis of various high-order mutants for six members of RLCK VII-4 subgroup (*PBL19*, *PBL20*, *PBL37*, *PBL38*, *PCRK1*, and *PCRK2*) showed that these RLCKs play crucial roles in the activation of MAPK signalling during PTI. However, MPK phosphorylation still occurs in the *rlck vii-4* sextuple mutant backgrounds tested, suggesting that additional RLCKs likely contribute to the activation of MAPK signalling during PTI (Bi et al., 2018; Rao et al., 2018; Tian et al., 2021).

Another important MAPK cascade in the context of plant immunity is the MEKK1–MKK1/2–MPK4/11 pathway, which was first discovered when a study demonstrated that MPK4 plays a negative role in plant immunity suppressing salicylic acid (SA)-dependent defence signalling (Berriri et al., 2012; Brodersen et al., 2006; Morten Petersen et al., 2000; Qiu et al., 2008). In

addition, MPK11, a close homolog of MPK4, was also found to be activated after PAMP treatment (Bethke et al., 2012). Subsequently, MEKK1 was identified as the upstream MAPKKK of MPK4 (Ichimura et al., 2006; Nakagami et al., 2006; Suarez-Rodriguez et al., 2007), followed by the discovery that MKK1 and MKK2 acted downstream of MEKK1 and upstream of MPK4 (**Figure 1.15**) (Gao et al., 2008; Qiu et al., 2008). Interestingly, the MEKK1–MKK1/2–MPK4/11 pathway was also shown to be activated by H_2O_2 treatment (Nakagami et al., 2006), in contrast to the MKKK3/5–MKK4/5–MPK3/6 cascade which is not regulated by H_2O_2 after flg22 treatment (Xu et al., 2014).

Both hypoxia and reoxygenation activate the two MAPK cascades outlined above. In addition, upon submergence stress, PA binds to MPK3 and MPK6, activating them (**Figure 1.15**) (Zhou et al., 2022). However, only the MKKK3/5–MKK4/5–MPK3/6 pathway is activated by mitochondrial ROS produced under hypoxic conditions, which is evidenced by activation of MPK3/6 after treatment with the mETC inhibitors antimycin A (AA) and potassium cyanide (KCN) (**Figure 1.15**) (Chang et al., 2012). These studies demonstrate that MAPK cascade elements not only depend on upstream phosphorylation events in the cascade, but also on second messengers generated during stress.

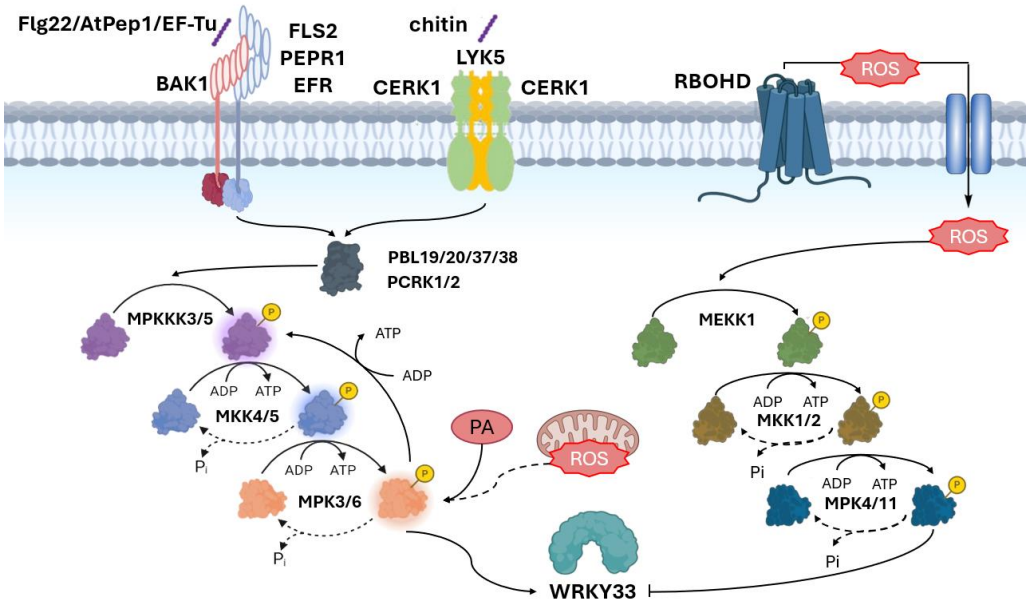

Figure 1.15. Different modes of MAPK cascade activation during either hypoxia or immune responses. The two main MAPK cascades downstream of PAMP and hypoxia sensing are depicted, including regulatory mechanisms.

Altogether, these findings highlight the complexity of MAPK cascades activation in plant stress responses. The involvement of multiple signals downstream of the stress sensing machinery that activate MAPK cascades such as different RLCKs, mitochondrial ROS or PA

suggests a potential role of MAPKs as convergent points of hypoxia and flg22 responses, potentially coordinating the integration of stress signals upon combined stress.

1.5.2. MAPK signalling activates regulators of hypoxia and immune responses

Once MPKs are activated in response to stress, they phosphorylate a wide number of targets with different biological function that regulate stress response pathways. The known substrates of MPK3/4/6 are summarized in **Table 1.3**.

Table 1.3. List of known substrates of MPK3/4/6 that are relevant in the context of hypoxia and PAMP or pathogen infection.

MPK	Target	Functional Involvement	Reference
MPK3/4/6	CAMTA3	Suppress plant immune responses	(Jiang et al., 2020)
MPK3/6	PLDα1	Plant Hypoxia Response	(Zhou et al., 2022)
	RAP2.12 (ERF74)	Plant Hypoxia Response	(Zhou et al., 2022)
	ASC2/6	Enhance plant immune responses	(Han et al., 2010; Liu and Zhang, 2004)
	EIN3	Enhance ethylene signalling	(Yoo et al., 2008)
	ERF1a	Suppress plant immune responses	(Wang et al., 2022)
	ERF5	Enhance plant immune responses	(Son et al., 2012)
	ERF6	Enhance plant immune and oxidative responses	(Meng et al., 2013; Wang et al., 2013; Xu et al., 2016)
	MAPKKK5	Enhance plant immune responses	(Bi et al., 2018; Wang et al., 2024)
	MVQ1	Enhance plant immune responses	(Pecher et al., 2014)
	MYB44	Enhance plant immune responses	(Wang et al., 2023)
	PTI1-4	Only interaction known	(Forzani et al., 2011)
	PHOS32	Enhance plant immune responses	(Merkouropoulos et al., 2008)
	RAP2.3 (ERF72)	Enhance plant immune responses	(Li et al., 2022)
	VLN3	Enhance plant immune responses	(Zou et al., 2021)

	WRKY7	Enhance plant immune responses	(Adachi et al., 2015)
	WRKY8		
	WRKY11		
	WRKY9		
	WRKY18	Enhance plant immune responses	(Wang et al., 2023)
	WRKY33	Enhance plant immune responses	(Mao et al., 2011; Qiu et al., 2008; Ren et al., 2008; Zhou et al., 2020)
	WRKY46	Enhance plant immune responses	(Sheikh et al., 2016)
	WRKY62	Only interaction known	(Popescu et al., 2009)
	ZAT10	Only interaction known	(Nguyen et al., 2012)
MPK3	MYB4	Enhance plant immune responses	(Lin et al., 2022)
	VIP1	Enhance plant immune responses	(Djamei et al., 2007)
MPK4	C3H14	Enhance plant immune responses	(Wang et al., 2022)
	ERF8	Enhance plant immune responses and ABA signalling	(Cao et al., 2018)
	MEKK1	Enhance plant immune responses	(Bi et al., 2018)
MPK6	ERF104	Enhance plant immune responses	(Bethke et al., 2009)

Among MPK substrates, there are several transcription factors of the WRKY family, which are key regulators of stress responses, as outlined previously in **section 1.4.2.2 above**. WRKY33 is arguably one of the best studied substrates of MAPK signalling, and is well-established as a key regulator of plant immunity and defences against pathogens (Chen et al., 2025; Chen and Zhang, 2024; Zheng et al., 2006). In response to pathogens, WRKY33 is rapidly activated and translocates to the nucleus, where it binds to specific W-box elements in the promoter of target genes, transcriptionally inducing genes involved in the synthesis of secondary metabolites, such as camalexin, and in the modulation of hormone signalling pathways, including jasmonic acid (JA) and ethylene (ET), which are two key hormones involved in pathogen responses (Birkenbihl et al., 2012; Zheng et al., 2006) as well as hypoxia responses (Hartman et al., 2021; Shukla et al., 2020). WRKY33 has been shown to be directly phosphorylated by MPK3/6 at Ser-54, Ser-59, Ser-65, Ser-72, and Ser-85 in response to *B. cinerea* infection, and then regulates the expression of camalexin biosynthesis genes and SAR-related genes (Mao et al., 2011; Wang et al., 2018). This phosphorylation of WRKY33 by MPK3/6 was later shown to enhance WRKY33's transactivation

activity and further induce camalexin biosynthesis (Zhou et al., 2020). MPK4 also regulates WRKY33 by forming a trimeric complex together with MAP KINASE SUBSTRATE 1 (MKS1) in the nucleus, inhibiting WRKY33 activity. However, when MPK4 is phosphorylated upon PAMP perception, it phosphorylates MKS1 on multiple sites triggering the release of WRKY33 from the complex, and activating the expression of its target genes (**Figure 1.16**) (Andreasson et al., 2005; Caspersen et al., 2007; Qiu et al., 2008).

In hypoxic conditions, few MPK substrates have been identified. Submergence activates PLDα1 and PLDδ, which hydrolyse phosphatidylethanolamine (PE) to generate PA and activates MPK3/6 (Xie et al., 2015). Once activated, MPK3/6 phosphorylate the ERF-VII RAP2.12 to activate its transcriptional activity of downstream HRGs and PLDα1 and PLDδ enzymes to reduce their protein levels, thus inhibiting submergence-induced PA accumulation as a part of a feedback regulatory loop (**Figure 1.16**) (Li et al., 2022). Other ERF-VII identified as a MPK3/6 substrate is RAP2.3, and is involved in both hypoxia and pathogen responses. Specifically, MPK3/6 phosphorylates RAP2.3 at Ser-151, which allows this ERF-VII to up-regulate *PAD3*, *CYP71A13* and *WRKY33*, resulting in increased camalexin biosynthesis in response to *B. cinerea* (Li et al., 2022). In addition MPK3/6 substrates also play roles in hormonal regulation of stress responses, as the EIN3 TF is phosphorylated by MPK3/6 at Thr-174, promoting EIN3 stability and boosting ethylene-responsive transcription (**Figure 1.16**) (Yoo et al., 2008). MPK3/6 also directly phosphorylate ACS6, reducing its turnover and contributing to the regulation of ethylene synthesis (**Figure 1.16**) (Han et al., 2010; Joo et al., 2008; Li et al., 2012; Liu and Zhang, 2004). Considering the important roles of ethylene in both hypoxia and pathogen responses (Hartman et al., 2021; Shekhawat et al., 2023), these regulatory mechanisms could be of importance when plants experience the two stresses simultaneously.

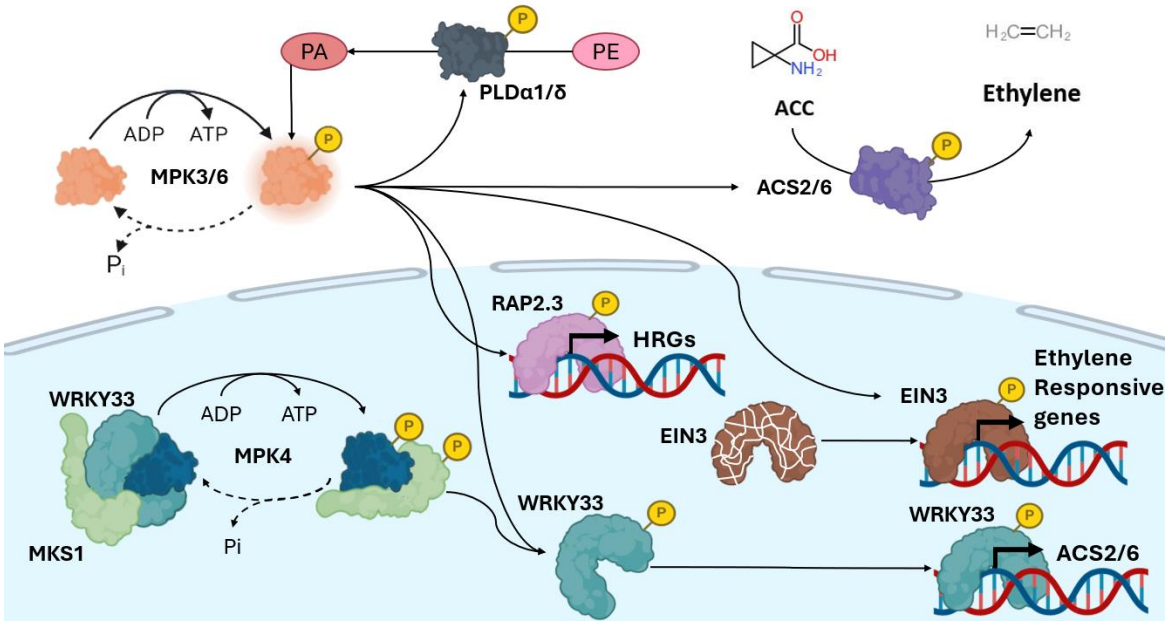

Figure 1.16. Summary of MPK targets relevant to either hypoxia or pathogen responses. Following their activation, MPKs phosphorylate a wide range of substrates (**Table 1.3**) involved in either pathogen or hypoxia responses and hypoxic conditions, such targets are mainly involved in ethylene biosynthesis, secondary metabolite production and signal transduction. In addition, most of the identified MPK targets are transcription factors, establishing transcriptional activation, the main signalling event downstream of MPKs.

As with the other signalling pathways discussed above, the roles of MAPK signalling have been mostly studied under individual stress conditions. However, a recent study from our laboratory highlighted differential phosphorylation of MPK3/6 under combined hypoxia/flg22 treatment compared to flg22 treatment alone. Specifically, applying at the same time hypoxia and flg22 resulted in significantly lower levels of MPK3/6 phosphorylation compared to treatment with flg22 alone (Mooney et al., 2024). This finding strongly suggests that MAPK signalling via MPK3/6 could play an important role in mediating plant responses to combined hypoxia/flg22.

1.6. Hypoxia and immune responses share transcriptional regulators and changes

Plants exposed to hypoxia, pathogens or PAMPs undergo extensive transcriptional reprogramming, with the hypoxia transcriptional response being centred on anaerobic metabolism and energy conservation, while PTI or pathogen-associated gene expression changes activate immune and defence-related pathways that lead to physical changes, such as

stomatal closure or callose deposition, as well as chemical changes (e.g. the synthesis of secondary metabolites and anti-microbial molecules). While hypoxia and immune transcriptional responses are different, some of the TFs that contribute to the reprogramming of gene expression are common to both, and there is overlap in the transcriptional response programs to hypoxia and to flg22 (Mooney et al., 2024). In the following sections, I will discuss the roles and regulatory mechanisms of specific transcription factor families involved in both hypoxia and flg22-induced signalling pathways, because of their potential relevance in the context of combined hypoxia/flg22 stress.

1.6.1. Transcriptional response programmes to hypoxia, flg22 and combined treatment

At the single-cell level, Liu et al., 2023 showed an overlap between hypoxia and immunity transcriptional responses. Gene ontology analysis revealed that genes involved in hypoxia signalling were upregulated in almost all cell types in response to the activation of innate immunity. Subsequent analysis indicated that hypoxia signalling interacts with immune response signalling and plays a role in the development of immune response-induced cells (IMC). Transcription factor network analysis and subsequent loss-of-function analysis revealed that the TF APETALA2/ETHYLENE-RESPONSIVE 13 (ERF13) plays an important role in regulating IMC differentiation both in innate immunity and hypoxia. Nobori et al., 2025, also showed the overlap between hypoxia and immunity transcriptional programs at single-cell level. Marker genes of clusters identified for mesophyll (clusters 3, 7 and 11) and epidermis (cluster 12) cell populations were enriched with defence-related and decreased oxygen levels genes. Furthermore, this study previously uncharacterized transcription factor, GT-3A, which contributes to plant immunity. Consistently, genes downregulated in a bystander cluster of gt3a-KO mutants (vs. WT) were enriched for “response to hypoxia” and “response to decreased oxygen levels”. These studies highlight that hypoxia-associated programs are co-activated with PTI, with TFs ERF13 and GT-3A emerging as regulators that potentially integrate hypoxia-stress and defence responses.

Additionally, meta-Analysis of RNA-seq datasets from *A. thaliana* and Rice (*Oryza sativa*) under hypoxia, revealed that in *Arabidopsis*, gene set enrichment analysis showed that hypoxia-inducible upregulated genes were enriched for immunity-related terms, including defence responses to fungi and bacteria. This analysis also allowed for the identification of hypoxia-induced genes that had previous known roles in plant immunity, such as WRKY33/46/53 or CYP73A5 (Tamura and Bono, 2022). Whole plants transcriptomics and meta-analysis carried out by Mooney et al., 2024 showed that transcriptional responses to individual stresses hypoxia and

flg22 substantially overlap, as GO terms for "response to oxygen levels/hypoxia" are enriched within flg22 transcriptomic datasets, and hundreds of genes are co-regulated by both stresses. Furthermore, combined hypoxia/flg22 treatments displayed substantial increase in transcriptional changes compared to hypoxia and flg22 individual stresses, indicating that the combined stress elicits a distinct transcriptional response. Analysis of individual genes upon combined hypoxia/flg22 treatments demonstrated transcriptional downregulation of *EFR*, *FLS2* and *MYB51*. Additionally, Hsu et al., 2013 observed the transcriptional upregulation of several innate immunity marker genes (e.g. *WRKY29, FRK1* and *PHI1*) by submergence.

Taken together, these studies position oxygen availability as a core regulator of plant immunity, as hypoxia-associated transcriptional programs are co-activated with PTI across cell types and shape immune and defence transcriptional outputs. At the network level, this crosstalk results in a specific combined-stress transcriptome, that can potentially be caused by the function of different regulators; the following section highlights candidate regulators and mechanisms underlying this crosstalk.

1.6.2. Some transcription factors have dual roles in response to hypoxia or flg22/pathogens

1.6.2.1. ERF-VII transcription factors are involved in both hypoxia and defence responses

In recent years, several members of the ERF-VII family have been shown to play roles in the regulation of plant defences against pathogens, in addition to their well-known functions in plant responses to hypoxia. For example, through the study of Arg/N-degron pathway mutants, it was found that the constitutive accumulation of the ERF-VIIs in these mutant plants contributed to their increased susceptibility to the pathogen *Plasmodiophora brassicae* (Gravot et al., 2016). Interestingly, the ERF-VIIs were also proposed to play roles in the formation of galls during infection by the bacterial pathogen *Agrobacterium tumefaciens*, as *erf-VII* quintuple mutant plants showed reduced gall development (Kerpen et al., 2019). The roles of the TFs ERF-VIIs in this context may be linked to their function as regulators of hypoxia response, as gall formation triggers a hypoxic environment. The fungal pathogen *Botrytis cinerea* has also been shown to trigger the formation of local hypoxic niches during infection. This appears to be the result of increased respiration at the site of infection, leading to a drop in O_2 levels, which is evidenced by the transcriptional upregulation of HRGs such as *HRE2* or *PCO1* and the stabilization of RAP2.12 in the nucleus upon *B. cinerea* infection (Valeri et al., 2021). In agreement with this, the ERF-VIIs have been implicated in defence responses against *B. cinerea*. For example, *RAP2.2* is

transcriptionally induced by *B. cinerea* infection and overexpression of *RAP2.2* in *Arabidopsis* resulted in increased resistance to *B. cinerea* (Zhao et al., 2012). More recently, during *B. cinerea* infection, the OCTADECANOID-RESPONSIVE ARABIDOPSIS 59 (ORA59) TF was found to interact with ERF-VIIs and repress their activity (except for HRE2), resulting in reduced induction of HRGs such as *ADH1,* a hypoxia response marker gene whose role is to maintain cellular energy production converting acetaldehyde to ethanol during anaerobic fermentation (Brunello et al., 2024; Pré et al., 2008). Specifically, the interaction between ORA59 and RAP2.3 in the nucleus is important for ORA59 positive role in ethylene-regulated responses, which could be involved in hypoxia responses (Kim et al., 2018; Pré et al., 2008). The ERF-VII RAP2.12 also appears to have roles in the regulation of salicylic acid (SA) as RAP2.12 binds directly to the *SALICYLIC ACID INDUCTION DEFICIENT 2* (*SID2*) promoter, which codes for one of the main enzymes in the SA biosynthesis pathway, and activates its transcription (Koo et al., 2024).

The HRE1 and HRE2 ERF-VIIs could also play dual roles in the regulation of hypoxia and defence responses, as they regulate the expression of target genes that have roles in both hypoxia response and pathogen defence. A good example is the link between HRE1 and RBOHD. Specifically, *HRE1* is transcriptionally regulated by ROS produced by RBOHD in hypoxic conditions (Liu et al., 2017; Yang, 2014; Yang and Hong, 2015). In addition, as a negative feedback loop in hypoxic conditions, *hre1* mutant plants have increased expression of *RBOHD* in response to hypoxia, therefore, HRE1 may act as a negative regulator of ROS production in hypoxia (Yang et al., 2017a). This role of HRE1 could, especially in the context of pathogens that trigger local hypoxic niches, affect plants' ability to defend themselves against those pathogens. However, these mechanisms have not been studied upon pathogen infection. In addition, *HRE2* is up-regulated by both hypoxia and *B. cinerea*, but not by flg22 treatment (possibly because PAMPs do not appear to induce the formation of hypoxic microenvironments) (Valeri et al., 2021). Intriguingly, HRE2 is the only ERF-VII that does not interact with ORA59, and consequently, its potential role in pathogen responses may not be negatively affected by this TF (Brunello et al., 2024). When the ERFVIIs are stabilised and locate to the nucleus, they will trigger the expression of several hypoxia- and pathogen-related genes shown in **Figure 1. 17** (Li et al., 2022; Tang et al., 2021; Yang et al., 2017; Zhao et al., 2012).

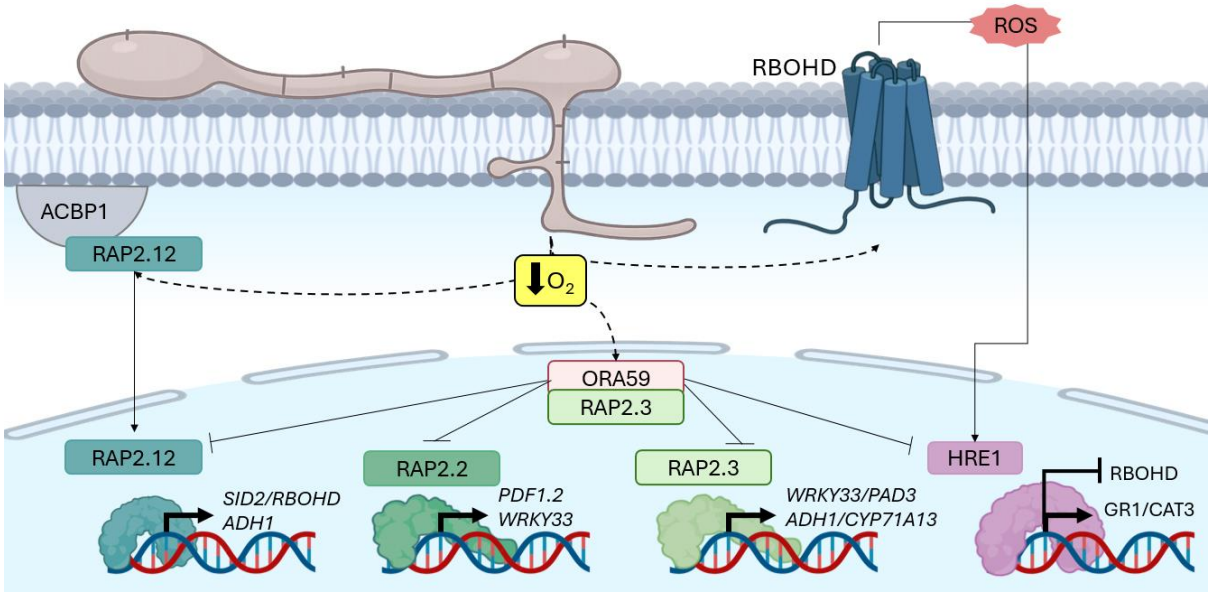

Figure 1.17. Summary of potential roles of ERF-VIIs in plant immunity and defences against pathogens. RAP2.12 induces *SID2* and *RBOHD* to trigger SA biosynthesis and ROS production, respectively. RAP2.2 induces *PDF1.2* to trigger ethylene signalling, and induces *ChiB* and *WRKY33* to trigger plant immunity. RAP2.3 induces *WRKY33*, *PAD3* and *CYP71A13* to trigger plant immunity and camalexin production. HRE1 induces *GR1* and *CAT3* to trigger redox regulation and inhibit *RBOHD* expression to regulate ROS production.

In sum, the master regulators of hypoxia response, the ERF-VIIs play dual roles in mediating both hypoxia response and defences against pathogens. Roles in the latter may be linked to the formation of local hypoxic niches at the site of infection by some pathogens such as *B. cinerea*, or in galls. Overall, many open questions remain regarding the molecular mechanisms that could underpin a role of ERF-VIIs in the regulation of plant defences against pathogens, as well as in mediating aspects of immune responses, including PTI and ETI (**Figure 1.17**).

1.6.2.2. WRKY transcription factors have dual roles in hypoxia and immunity

WRKY transcription factors are one of the largest families of transcriptional regulators in plants (Rushton et al., 2010). Their defining feature is the presence of an N-terminal DNA-binding WRKY domain that recognises the W-box (TTGACC/T) (Rushton et al., 1996). Some members of the WRKY family, such as WRKY33, also bind to non-W-box motifs, such as the TC Box (TCTCTC) (Zhang et al., 2021). As mentioned in **section 1.3.3.2 above**, WRKY33 is regulated by MPK3/6 and is involved in response to *B. cinerea via* its ability to regulate camalexin biosynthesis and phytohormone signalling (Birkenbihl et al., 2012; Zheng et al., 2006). Interestingly, the ERF-VII RAP2.3 contributes to camalexin biosynthesis during pathogen infection, in part through the

promoter binding and transcriptional activation of *WRKY33* (**Figure 1.17**) (Li et al., 2022). In addition to its known roles during pathogen infection, *WRKY33* is also considered to be a HRG that contributes to hypoxia response together with WRKY12 at least in part by binding to the promoter of *RAP2.2*, activating its transcription and promoting the activation of the hypoxia response program (**Figure 1.17**) (Tang et al., 2021). The roles of *WRKY33* and its links with ERF-VIIs during either infection or submergence/hypoxia, suggest that *WRKY33* may play a role in regulating plant responses to pathogens under hypoxic or flooding conditions. However, WRKY33 target genes have been identified mostly in response to pathogens, and little is known about its target genes during hypoxia treatment or submergence (**Figure 1.18 and Table 1.4**).

Table 1.4. Identified WRKY33 targets in response to pathogens or hypoxic stresses that might be potentially involved in the molecular crosstalk between both stresses.

Target	Functional Involvement	Reference
ACS2/6	Redox Potential	(Datta et al., 2015; Li et al., 2012)
RAP2.2	Submergence responses	(Tang et al., 2021)
PEPR1	Plant immune responses	(Birkenbihl et al., 2017)
PROPEP2/3		
CYP71A13	Plant immune responses	(Birkenbihl et al., 2012)
ORA59		
GLIP1		
JAZ8/10		
RBOHD	Plant immune responses	(Zhao et al., 2020)
PAD3	Plant immune responses	(Birkenbihl et al., 2012; Mao et al., 2011)
YDD4/5/6/7/11/13/15/17/26	Plant immune responses	(Cai et al., 2021)

To date, the only WRKY transcription factor with a demonstrated role in mediating the crosstalk between submergence and pathogen response is *WRKY22*. This WRKY TF is transcriptionally upregulated in response to both pathogen infection (Jiang et al., 2024; Macho et al., 2012; Yuan et al., 2021) and submergence (Hsu et al., 2013). In response to flg22, WRKY22 directly regulates the expression of *FRK1* (Asai et al., 2002) and it has a similar role during infection by the pathogen *Verticillium dahliae* (Gkizi et al., 2016). Hsu *et al*. showed that pre-

treating plants with submergence prior to inoculation with the bacterial pathogen *Pseudomonas syringae*, resulted in increased resistance to this pathogen compared to plants that had not experienced submergence pre-treatment. Notably, the use of *wrky22* mutants showed that this transcription factor was essential in mediating this waterlogging-induced increase in defence against *P. syringae* (Hsu et al., 2013). In addition, these authors showed that submergence could induce, in a WRKY22-dependent manner, the expression of PTI-associated genes, such as for example *FRK1* (**Figure 1.18**) (Hsu et al., 2013).

Perhaps another WRKY TF to consider for the potential crosstalk between hypoxia and defence responses is WRKY70, which is a well-known regulator of SA-dependent immunity and suppressor of JA-responsive genes, thereby modulating resistance to different pathogens (Hu et al., 2012; Li et al., 2017, 2006; Ülker et al., 2007). Beyond this role in plant immunity, Lou et al., 2022 demonstrated that WRKY70 binds to the WT-box and W-box motifs present in the promoter of *RAP2.12*, thus potentially linking this TF to hypoxia response (**Figure 1.18**).

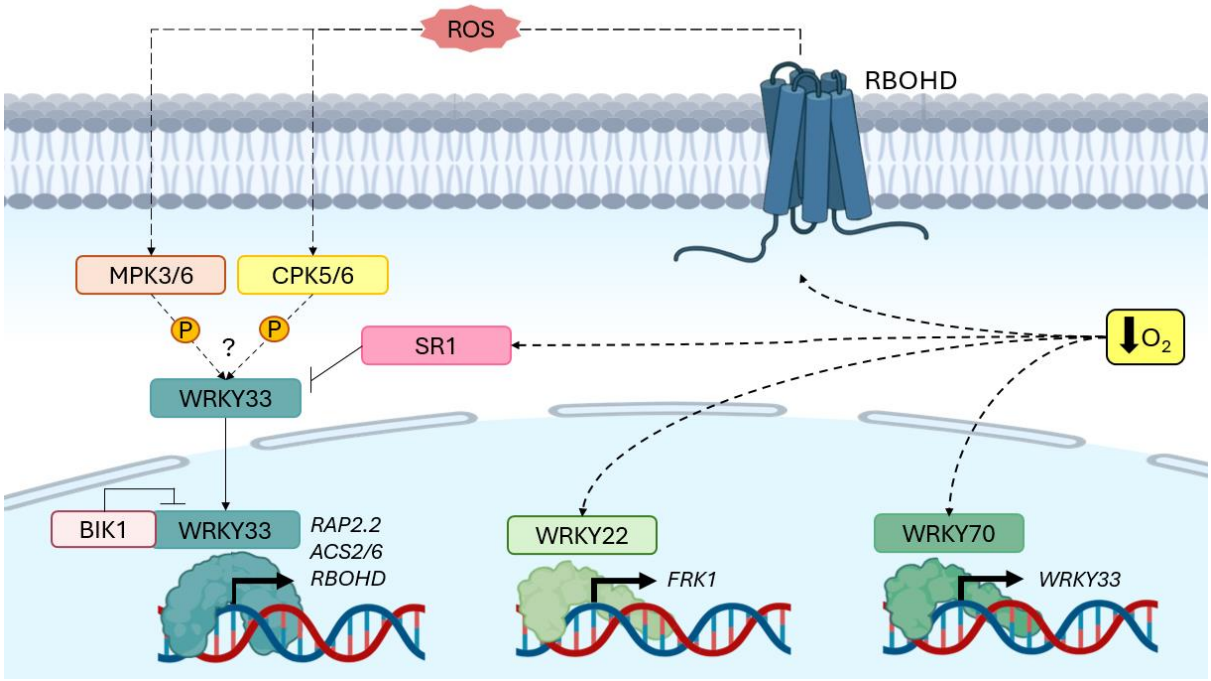

Figure 1.18. Dual roles of regulators of plant defences against pathogens in hypoxia response. WRKY33 induces *RAP2.2* to trigger HRGs expression, including *ACS2/6* and *RBOHD*. WRKY22 up-regulates *FRK1*, *WRKY53,* and *WRKY49* thus playing a role in plant immunity. WRKY70 induces WRKY33 to trigger plant immunity.

In sum, some TF families, such as the ERF-VIIs and WRKYs have dual roles downstream of hypoxia sensing or pathogen/PAMP perception. This dual function is the outcome of (i) their activation by signal transduction pathways that are involved in relaying information downstream

O2 sensing or pathogen perception and (ii) their mutual regulation. How their target genes overlap is another important question to establish links between the genome-wide transcriptional reprogramming that takes place in response to the individual stresses, and more importantly when plants might activate immune and defence responses while also experiencing hypoxia.

1.7. Hormone signalling also integrates multiple stress signals and contributes to transcriptional reprogramming

In response to stresses, phytohormone signalling pathways are also activated and contribute to the gene expression changes that enable a cue-specific response. Phytohormones work as regulatory molecules, functioning at very low concentrations in a local or systemic way. The molecular pathways triggered by phytohormones rarely act in isolation, and instead, form a complex web of synergistic and antagonistic interactions that integrate environmental and developmental cues. In response to hypoxia or pathogens/PAMPs, the most studied (and probably relevant) interactions among phytohormone signalling pathways involve ET, JA and SA signalling, with ET playing a particularly important role. During submergence, ET entrapment due to low gas diffusion is one of the earliest signals perceived by the plant (Hartman et al., 2019a), and it regulates adaptative traits such as aerenchyma formation, adventitious root initiation or shoot elongation. In the context of plant defences against necrotrophic pathogens (which trigger cell death in the early stages of infection and feed on the dead tissue), ET acts synergistically with JA signalling and ET can act antagonistically to SA signalling, regulating defences against biotrophic pathogens (which feed on living tissue) (Li et al., 2019; Mur et al., 2013; Yang et al., 2015). Intriguingly, the necrotrophic pathogen *B.* cinerea was shown to trigger hypoxic niches at the site of infection (Valeri et al., 2021). Hence, when plants face hypoxic conditions together with a pathogen infection, ethylene could mediate the molecular crosstalk between plant responses to both stresses, through the control of its biosynthesis and of ET-dependent transcriptional regulators, which could act as points of convergence between hypoxia and pathogen response.

1.7.1. ET biosynthesis is an important regulatory step

The regulation of ET biosynthesis is a key step in controlling downstream ET signalling and gene expression changes, because ET is a gas and it cannot be conjugated. Several elements of ET biosynthesis act as convergence points between hypoxia and pathogen stresses. In the first reaction of ET biosynthesis, S-adenosyl-L-methionine (SAM) is transformed into the ET precursor 1-aminocyclopropane-1-carboxylic acid (ACC) by ACC Synthase (ACS) enzymes (reviewed in

Pattyn et al., 2021). In *A. thaliana*, ACS enzymes belong to a multigene family of 12 members, divided in three major groups based on their C terminal domains: type 1 (ACS1/2/6) has MAPK and CPK target sites, type 2 (ACS4/5/8/9) has CPK and E3 ligases binding sites and type 3 (ACS7/11) has no target sites (reviewed in Yoon, 2015). In the second step of ET synthesis, ACC is transformed into ET by the 5 ACC oxidase (ACO) enzymes in *Arabidopsis* (**Figure 1.19**) (reviewed in Pattyn et al., 2021).

During the activation of pathogen defence responses, WRKY33 has been shown to bind to the promoter of *ACS2/6* to activate their expression (**Table 1.4**), together with that of *ACO1* (Datta et al., 2015), while WRKY29 binds to the W-boxes present in the promoters of *ACS5/6/8/11* and *ACO5* to regulate ET biosynthesis (Wang et al., 2023). In addition, *ACS2/6* are indirectly negatively regulated by ETHYLENE RESPONSE FACTOR 1A (ERF1A) in response to *B. cinerea*. ERF1A acts downstream of *B. cinerea*-induced ET signalling, establishing a negative feedback loop in which ET regulates its own biosynthesis during the onset of plant responses to pathogens. In addition, one potential convergence point of hypoxia and flg22 signalling, MPK3/6, directly phosphorylate ERF1A at Thr-116 and Ser-134 residues to enhance its transcriptional activity, suggesting different roles of MPKs in ET biosynthesis regulation, having enhancing roles through the phosphorylation of WRY33 and ACS2/6, and having negative roles through the phosphorylation of ERF1A (**Figure 1.19**) (Wang et al., 2022).

During hypoxia, ET synthesis is regulated through different pathways. First, 4 of the 12 ACS genes, *ACS2/6/7/9*, are induced following three different patterns: for *ACS9* hypoxic induction, ET is needed, but not sufficient; for *ACS2* hypoxia-dependent induction in roots, ET production has an inhibitory effect, and lastly, ET has no effect on the hypoxic induction of *ACS6* and *ACS7* (Peng et al., 2005). One mechanism for *ACS7* induction was discovered by Yang and Hong, 2015, in which *ACS7/8* are induced during hypoxic stress in a RBOHD-dependent manner. Another example of hypoxia-dependent transcriptional upregulation of ET biosynthesis is *via* the MYB30 TF, which contributes to plant response to submergence by repressing *ACS7* expression and consequently negatively regulating ET biosynthesis (**Figure 1.19**) (Zhang et al., 2023). A crosstalk between mitochondrial ROS and ET signalling comes from ANAC017, which in response to mitochondrial stress treatments, binds to the promoter of *ACS2*. In addition, this study also demonstrates that mitochondrial malfunction induces the expression of several ET-related genes involved not only in biosynthesis (*ACS2/6/11*), but also in ET signalling (*ERF019/042/100*) (He et al., 2022).

Few studies have been published regarding crosstalk between hypoxia and pathogen responses, however, WRKY22, previously shown to confer immunity when plants faced submergence stress (**see also section 1.4.2.2 above** and Hsu et al., 2013), binds to promoter

regions of *ACS5/11* and *ACO5*, thus promoting ET production (**Figure 1.19**) (Wang et al., 2024). However, these ET biosynthesis-related genes are not the only ones regulates by WRKY22, as *wrky22* mutants have lower *ACS7* transcript levels upon submergence, suggesting that the already established role of WRKY22 as one of the regulators of hypoxia and pathogen responses could involve the regulation of ET biosynthesis genes (Hsu et al., 2013).

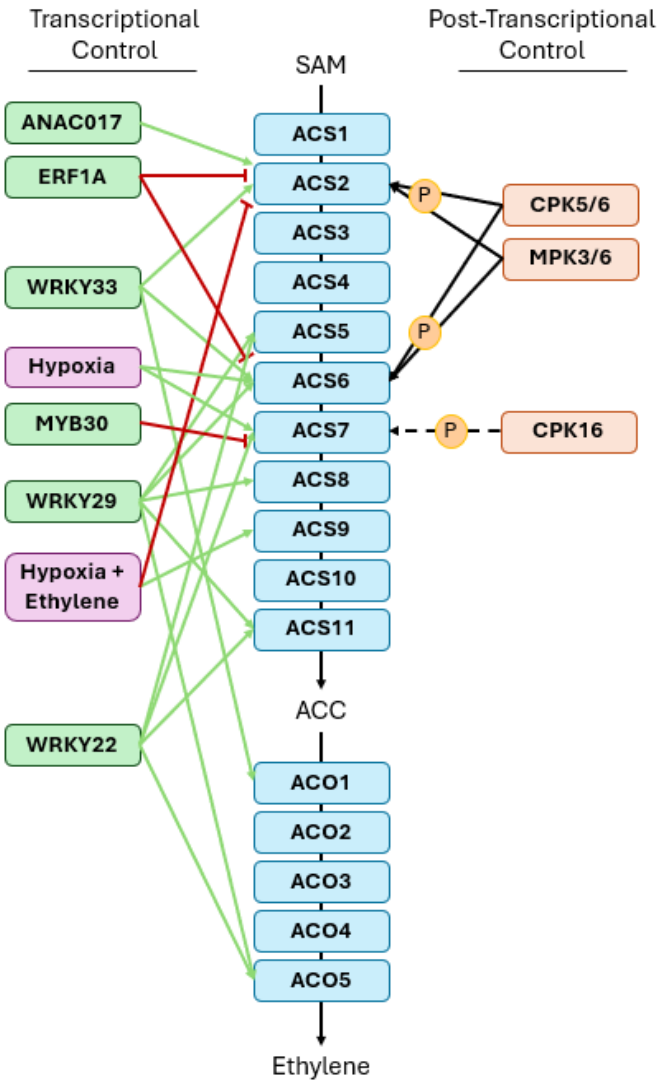

Figure 1.19. Hypoxia and defence-dependent regulatory pathways of ET **biosynthesis.** *ACS2* is regulated by hypoxia through ANAC017 and ET, and by pathogens through MPK3/6, CPK5/6, ERF1A and WRKY33; *ACS5* is regulated by hypoxia through WRKY22 and by pathogens through WRKY29; *ACS6* is regulated by hypoxia through an unknown mechanism and by pathogens through ERF1A, WRKY29 and WRKY33; *ACS7* is regulated by hypoxia through WRKY22 and MYB30; *ACS8* is regulated by pathogens through WRKY29; *ACS9* is regulated by hypoxia through an ET -dependent unknown mechanism; *ACS11* is regulated by hypoxia through WRKY22 and by pathogens through WRKY22. *ACO1* is regulated by pathogens through WRKY33; and *ACO5* is

regulated by hypoxia through WRKY22 and by pathogens through WRKY29. Dashed arrows involve regulatory mechanisms in other stress responses other than hypoxia and pathogens.

Although the core enzymatic steps of ET biosynthesis are well studied, significant gaps remain in our understanding of how these pathways are differentially regulated during hypoxia, and also when plants have to activate their immunity or defence responses while experiencing hypoxia. Importantly, the interplay between ET and other immunity-related phytohormones such as JA and SA also requires more studies. Because these are not the focus of this PhD, they will not be detailed here, but the following reviews are informative (Hartman et al., 2021; Li et al., 2019; Miricescu et al., 2018; Shekhawat et al., 2023; Yang et al., 2015).

1.7.2. ET signalling & crosstalk with other hormone signalling pathways during hypoxia or defence responses

Once it is synthesised, ET diffuses from its site of production to neighbouring cells, where it is perceived by ET receptors, including ETHYLENE RESPONSE 1 (ETR1), ETR2, ETHYLENE RESPOSE SENSOR 1 (ERS1), ERS2, and ETHYLENE INSENSITIVE 4 (EIN4), which are located in the ER (Bleecker et al., 1988; Chang et al., 1993; Hua et al., 1998, 1995; Sakai et al., 1998). In the absence of ET binding, these 5 receptors phosphorylate the CONSTITUTIVE TRIPLE RESPONSE 1 (CTR1) kinase, keeping it active and resulting in the phosphorylation and subsequent ubiquitination and degradation by the 26S proteasome of the ET-dependent TF ETHYLENE INSENSITIVE 2 (EIN2) (Qiao et al., 2009). Other ET-dependent TFs, EIN3, ETHYLENE INSENSITIVE3-like 1 (EIL1) and EIL2 are also targeted for degradation in absence of ET *via* the E3 ubiquitin ligase components EIN3 BINDING F-BOX1 (EBF1) and EBF2 (**Figure 1.20 A**) (reviewed in Binder, 2020). After ET perception, ET receptor's function is inhibited, resulting in the accumulation of EIN2 and its proteolytic cleavage. The latter released C-terminal portion of EIN2, can either (i) bind to the *EBF1/2* mRNAs, triggering their degradation and stabilising EIN3 and EIL1/2, or (ii) translocate to the nucleus, where it associates with EIN2 NUCLEAR ASSOCIATED PROTEIN 1 (ENAP1) to regulate EIN3- and EIL1/2-dependent transcription (**Figure 1.20 B**) (Binder, 2020). EIN3 stability has also been shown to be regulated by other pathways, including MAPK signalling, so that MPK3/6 phosphorylate EIN3 at residue Thr-174, resulting in EIN3 stabilisation (Yoo et al., 2008). Once EIN3 is stabilised, it binds to EIN3-binding site (EBS) or primary ET response element (PERE), triggering the expression of ET-responsive genes (Solano et al., 1998).

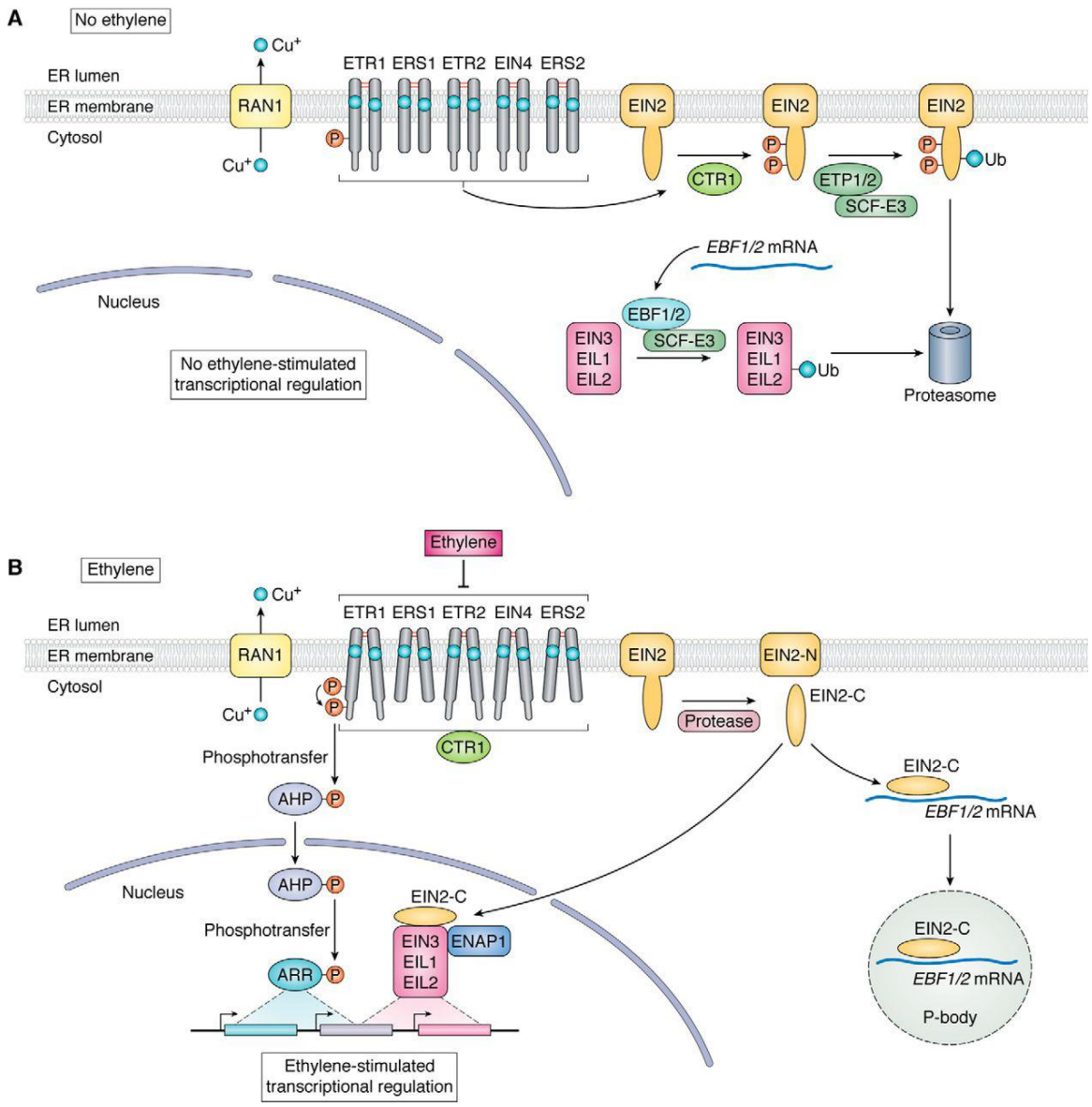

Figure 1.20. Proposed model for ET **signalling**. A, in the absence of ET, the receptors signal to CTR1, phosphorylating EIN2, resulting in its degradation by the proteasome. Because EIN2 levels are low, EIN3 and EIL1/2 are degraded by the mechanism regulated by the F-box proteins EBF1 and EBF2 which recognize these EIN3/EIL proteins and recruit them to an SCF E3 ubiquitin ligase complex, which polyubiquitinates the substrates and targets them for degradation by the 26S proteasome, preventing them from affecting transcription in the nucleus. B, in the presence of ET, CTR1-dependent phosphorylation of EIN2 is reduced, allowing EIN2 cleavage of its C-terminal domain triggering EIN3, EIL1/2-dependent transcription. Ethylene can also trigger a non-canonical pathway by phosphorylating AHP proteins, which then shuttle to the nucleus and phosphorylate ARR response regulators which modulate transcription of downstream genes (Hass et al., 2004; Scharein et al., 2008). Figure from Binder, 2020.

EIN3 and EIL1 targets relevant to defence against pathogens includes *SID2* (Chen et al., 2009), which encodes ISOCHORISMATE SYNTHASE 1 (ICS1; Wildermuth et al., 2001) - a key gene in the SA biosynthesis pathway together with ICS2 (Garcion et al., 2008; Wildermuth et al., 2001). This mechanism is an example of the crosstalk between SA and ET in pathogen response, although it is not known whether such a mechanism is relevant in the context of plants experiencing pathogen infection at the same time as hypoxia. More recently, Koo et al., 2024 showed that RAP2.12 could bind directly to the *SID2* gene promoter and activate SA biosynthesis, which could serve to link hypoxia response and immunity or defences against pathogens.

ET and JA frequently act together to regulate stress responses, largely through the coordinated activities of the transcription factors EIN3 and MYC2, MYC3, and MYC4, which together control the expression of JA-responsive genes (Song et al., 2014). For instance, EIN3 and MYC2 physically interact, enabling reciprocal regulation between the ET and JA signalling pathways (Song et al., 2014). Consistent with these regulatory pathways, ET and JA can act synergistically to activate defence-related genes such as *PLANT DEFENSIN 1.2* (*PDF1.2*), *ERF1*, and *OCTADECANOID-RESPONSIVE ARABIDOPSIS AP2/ERF 59* (*ORA59)* (Berrocal-Lobo et al., 2002; He et al., 2017; Lorenzo et al., 2003; Penninckx et al., 1998; Zhu et al., 2011). Beyond pathogen defence, JA also has a role in hypoxia response, where MYC2 participates in submergence and reoxygenation responses by regulating antioxidant-related genes through direct binding to the promoters of *VITAMIN C DEFECTIVE1* (*VTC1*) and *GLUTATHIONE SYNTHETASE 1* (*GSH1*) (Yuan et al., 2017). In addition, ERF-VIIs have been shown to partially regulate JA marker genes upon hypoxia, including *AT2G4790* and *JASMONATE ZIM-DOMAIN PROTEIN 1* (*JAZ1*), a negative regulator of JA signalling (Shukla et al., 2020).

Altogether, ET and its interaction with other phytohormone signalling pathways could serve as a point of convergence in hypoxia and pathogen responses. However, how plants coordinate these signalling hubs when plants face combined hypoxia/pathogen stress remains unknown.

1.8. Project objectives

As previously stated, plants can encounter hypoxic conditions at the same time as pathogen infection, so that hypoxia response and immunity or defence responses against pathogens could interact with each other in the context of this combined stress. Despite growing evidence for this crosstalk, our understanding of how these pathways are coordinated at the molecular level remains limited. Addressing these gaps requires a specific framework to study

immune activation within the physiological context of low-oxygen stress. Therefore, the objectives of this PhD project were:

I. Explore the effect of hypoxia on plant immunity, and the potential role of RBOHD under combined hypoxia/flg22
II. Identify novel genes that mediate plant resilience to combined waterlogging/pathogen using rapeseed as a model crop

1.8.1. Exploring the effect of hypoxia on plant immunity, and the potential role of RBOHD under combined hypoxia/flg22

The early regulatory pathways triggered after hypoxia or PAMP sensing are common, consisting in Ca^{2+} movements, ROS production by the NADPH oxidase RBOHD, activation of MAPK cascades, transcriptional activation of genes and the induction of phytohormone signalling. The similarities between hypoxia and flg22 responses underscores shared regulatory elements that may act as convergence points, integrating both signals to regulate plant stress responses when these stresses occur simultaneously or in sequence. RBOHD is one of these convergence points. Therefore, studying RBOHD expression, abundance and function during combined hypoxia and flg22 exposure can provide mechanistic insights into how plants coordinate stress responses when plants encounter oxygen limitation and immune challenges simultaneously. Understanding this crosstalk could reveal how hypoxia modulates defence amplitude, duration, or specificity, as previously demonstrated, and identify RBOHD as a key integrator of abiotic and biotic stress signalling networks.

1.8.2. Identifying novel genes that mediate plant resilience to combined waterlogging/pathogen using rapeseed as a model crop

1.8.2.1. Use of A. thaliana as a model plant versus crops

Many of the molecular mechanisms involved in stress responses to hypoxia and pathogens were discovered using *A. thaliana* as a model system, because this species has the most resources available, as well as a faster pace of research (Provart et al., 2016; Roeder et al., 2025). While *A. thaliana* offers many advantages as a model species, plant research should broaden to include a wider range of species. Unlike crop species, *A. thaliana* does not have many critical traits, such as large seeds, large starch reserves or complex root systems have

biochemical pathways absent or different from several crop species. From the genetic point of view, gene function and regulatory pathways can be dramatically different between species due to genetic divergence. For example, the previously discovered degradation of RBOHD by PIRE and PBL13 in *A. thaliana* could not provide resistance to diseases caused by root pathogens in tomato after the editing of its *PIRE* gene (Castro et al., 2025; Lee et al., 2020). Additionally, crop genomes are frequently polyploid and contain large repetitive segments. From the food security point of view, research directly done on crops can speed up breeding for yield or stress tolerance, while translating findings from *A. thaliana* to crops can take longer and not always be successful (Simmons et al., 2021).

For many decades, crop species were more difficult to work with to dissect molecular mechanisms due to practical issues (e.g. space needed and long generation times), as well as their more frequent polyploid genomes or difficulties to transform them using *Agrobacterium tumefaciens*. However, the development of new and affordable techniques have greatly contributed to making research work with crops more accessible. This includes (i) low-cost next-generation sequencing, that allows a more rapid and affordable genome sequencing, assembly and annotation of crop species (Della Coletta et al., 2021); (ii) CRISPR/Cas9 approaches for precise, effective and low-cost genome editing in crop species (Saini et al., 2025); and (iii) bioinformatics methods, that allowed the development of crop-specific databases (Chen et al., 2024).

1.8.2.2. Using rapeseed as a model crop to study plant responses to combined waterlogging and pathogen infection

Rapeseed (*Brassica napus* L.) is the world's second-largest oilseed crop and is of significant economic importance in the production of edible oil, cattle feed, and as a source of biodiesel, or bioethanol (FAO, 2021; Kdidi et al., 2019a). *B. napus* is an allotetraploid species (genome AACC, n=19), which is the result of hybridisation event between ancestors of *B. rapa* (Asian cabbage or turnip, genome AA, n=10) and *B. oleracea* (Mediterranean cabbage, genome CC, n=9) about 7,500 years ago (Chalhoub et al., 2014; Rousseau-Gueutin et al., 2021). This genome complexity allows for multiple copies of genes (homoeologs), which make it complicated to carry out genetic studies and to identify genes relevant to stress tolerance.

Climate change is expected to increase the frequency of extreme precipitation and flooding events, increasing rapeseed exposure to waterlogging stress (Madsen et al., 2014). For example, Ireland has experienced more frequent and intense heavy rainfall events, especially in the east and southeast, and climate models project that this trend will continue, with winter and

autumn seeing roughly 20% more extreme rainfall events by mid-century (Nolan et al., 2017; Ryan et al., 2022). In other regions of the globe, such as in China (one of the largest rapeseed growing countries in the world), 80% of this crop is planted along the Yangtze river as a rotation crop after rice. While this rotation system has many agricultural advantages (e.g. improvement of soil fertility, decrease in pests and weeds (Cao et al., 2025), it also causes waterlogging of rapeseed fields at the seedling and flowering stages, when they are especially vulnerable (Guo et al., 2020; Hong et al., 2024; Wollmer et al., 2018; Xu et al., 2015; Zhou and Lin, 1995; Zou et al., 2014). One particularly problematic effect of flooding is that it causes an increased risk of pathogen infection. This is thought to result from increased dampness, changes to the soil and plants' microbiome (Gschwend et al., 2020; Hartman and Tringe, 2019), and a generally elevated stress exposure that affects overall plant responses to biotic stresses (Velásquez et al., 2018). Therefore, in this PhD thesis I will use rapeseed as a model crop to dissect the physiological and molecular mechanisms underpinning rapeseed responses to combined waterlogging and pathogen infection, and to identify key pathways/genes that contribute to tolerance under these concurrent stresses.

1.8.2.3. Identifying rapeseed varieties with tolerance to waterlogging and resilience to combined waterlogging/pathogen

Here, a subset of the Brassica Rapeseed and Vegetable Optimisation (BRAVO) collection of 96 commercial rapeseed varieties (kindly provided by collaborators at the John Innes Centre: Dr. Rachel Wells, Prof. Chris Ridout and Prof. Lars Østergaard) was screened for waterlogging tolerance, as well as for resilience to combined waterlogging and infection with the necrotrophic fungal pathogen *Sclerotinia sclerotiorum*. This pathogen causes important crop losses for rapeseed (Mei et al., 2011), justifying the need to identify varieties with resilience to both waterlogging and *Sclerotinia*. The analysis of this screening carried out in collaboration with Prof. Rafael de Andrade Moral (MU, Department of Mathematics and Statistics), led to a varietal ranking that could be relevant to future breeding efforts, and through the subsequent and still on-going genome-wide association study (GWAS) in collaboration with Dr. Rachel Wells and Dr. Emmanuel Solomon, this project also seeks to identify the genetic basis for waterlogging tolerance in rapeseed, as well as for resilience to combined waterlogging/pathogen.

2. Chapter 2: Materials and Methods

2.1. Materials

2.1.1. *Arabidopsis thaliana* lines used

The *Arabidopsis thaliana* accession Columbia-0 (Col-0) was used as the wild type for this study. Mutant *Arabidopsis* lines were ordered from the Nottingham Arabidopsis Stock Centre (NASC) and are listed in Table 2.1.

Table 2.1. List of *A. thaliana* lines used in this study.

Name of Mutant	AGI	T-DNA	Accession	Reference
rbohd-3	AT5G47910	CS9555	Col-0	(Torres et al., 2002)
cpk28-1	AT5G66210	GK-523B08	Col-0	Matschi et al., 2012. Seeds were donated by Prof. Cyril Zipfel (The Sainsbury Laboratory, UK).
erfVII	AT1G72360 AT2G47520 AT3G14230 AT3G16770 AT1G53910	-	Col-0	(Abbas et al., 2015)
hre1hre2	AT1G72360 AT2G47520	SALK_039484 x SALK_052858	Col-0	(Gibbs et al., 2014)
rap2.2rap2.3rap2.12	AT3G14230 AT3G16770 AT1G53910	SAIL_184_G12 x SAIL _1031_D10 x GK_503A1_11	Col-0	(Gibbs et al., 2014)
gsnor1-3	AT5G43940	GK-315D11.03	Col-0	(Feechan et al., 2005; Lee et al., 2008)
hb1 (pgb1-1)	AT2G16060	SALK_058388	Col-0	(Hartman et al., 2019)
noa1	AT3G47450	SALK_047882	Col-0	(Guo et al., 2003)

2.1.2. Brassica napus lines used

Germplasm used in this study consisted of approximately 100 varieties from the BRAVO collection of commercial rapeseed varieties. These accessions come from the BnASSYST diversity panel which originated from different countries and includes winter, semi-winter and spring oilseed rape (OSR, grown primarily for seed oil and meal), fodder (grown mainly for vegetative biomass as animal feed), kales (human consumption), and rutabaga/swede morphotypes (cultivated for its enlarged storage root used for feed and, in some cases, human consumption). These accessions were kindly donated by collaborators at the John Innes Centre: Dr. Rachel Wells, Prof. Chris Ridout and Prof. Lars Østergaard. Rapeseed varieties used in this study and are listed in **Table 2.2**.

Table 2.2. List of *B. napus* accessions used in this study.

BRAVO #	Line	Assyst #	Crop type
	Victor	BnASSYST-	Winter_OSR
1	Capitol	BnASSYST-028	Winter OSR/Modern winter OSR
2	Apex	BnASSYST-040	Winter OSR/Modern winter OSR
3	Verona	BnASSYST-053	Winter OSR/Modern winter OSR
4	Expert	BnASSYST-055	Winter OSR/Modern winter OSR
	Viking	BnASSYST-060	Winter_OSR/Modern winter OSR
5	APEX-93_5 X GINYOU_3 DH LINE	BnASSYST-090	Winter OSR
6	BIENVENU DH4	BnASSYST-091	Winter OSR
7	CANBERRA x COURAGE DH LINE	BnASSYST-093	Winter OSR
8	HANSEN X GASPARD DH LINE	BnASSYST-096	Winter OSR
9	MADRIGAL x RECITAL DH LINE	BnASSYST-097	Winter OSR
10	RAFAL DH1	BnASSYST-098	Winter OSR
11	TAPIDOR DH	BnASSYST-099	Winter OSR
12	EUROL	BnASSYST-101	Winter OSR
13	Lesira	BnASSYST-102	Winter OSR
14	LICROWN X EXPRESS DH LINE	BnASSYST-105	Winter OSR
15	SHANNON x WINNER DH LINE	BnASSYST-106	Winter OSR
16	Janetzkis Schlesischer	BnASSYST-107	Winter OSR
17	LEMBKES MALCHOWER (LENORA)	BnASSYST-108	Winter OSR
18	NORIN	BnASSYST-109	Winter OSR
19	Samourai	BnASSYST-113	Winter OSR
	Askari	BnASSYST-118	Winter_OSR
	Jetneuf	BnASSYST-121	Winter_OSR
20	Baltia	BnASSYST-133	Winter OSR
21	Coriander	BnASSYST-137	Winter OSR
22	Dippes	BnASSYST-139	Winter OSR

23	Kromerska	BnASSYST-150	Winter OSR
24	Matador	BnASSYST-160	Winter OSR/Semi-Winter
25	Ramses	BnASSYST-168	Winter OSR
26	Slovenska Krajova	BnASSYST-172	Winter OSR
27	CANARD	BnASSYST-185	Winter fodder
28	MOANA, MOANA RAPE	BnASSYST-186	Winter fodder
29	Aphid resistant rape	BnASSYST-190	Winter fodder
30	Dwarf Essex	BnASSYST-193	Winter fodder
31	English Giant	BnASSYST-194	Winter fodder
32	Taisetsu	BnASSYST-203	"Exotics": Winter vegetable
33	Q100	BnASSYST-204	"Exotics": synthetic
34	BRAUNER SCHNITTKOHL	BnASSYST-206	"Exotics": Siberian kale
35	CHEMBERE DZAGUMHANA	BnASSYST-207	"Exotics": unspecified
36	COUVE NABICA	BnASSYST-208	"Exotics": cauve nabica
37	RAGGED JACK	BnASSYST-209	"Exotics": rape kale
38	SIBERISCHE BOERENKOOL	BnASSYST-211	"Exotics": Siberian kale
39	SLAPSKA, SLAPY	BnASSYST-212	"Exotics": unspecified/Winter
40	ABUKUMA NATANE	BnASSYST-213	"Exotics": Winter OSR
41	GROENE GRONINGER SNIJMOES	BnASSYST-218	"Exotics": unspecified
42	RAPID CYCLING RAPE (CrGC5)	BnASSYST-221	"Exotics": rape kale
43	SWU Chinese 1	BnASSYST-229	Semiwinter OSR/Exotics Semiwinter OSR
44	SWU Chinese 2	BnASSYST-230	Semiwinter OSR/Exotics Semiwinter OSR
45	Zhouyou	BnASSYST-237	Semiwinter OSR/Exotics Semiwinter OSR
46	Drakkar	BnASSYST-238	Spring OSR
47	STELLAR DH	BnASSYST-239	Spring OSR
48	WESTAR DH	BnASSYST-240	Spring OSR
	Brutor	BnASSYST-242	Spring OSR
49	CRESOR	BnASSYST-245	Spring OSR
50	KARAT	BnASSYST-251	Spring OSR
51	KAROO-057DH	BnASSYST-256	Spring OSR
52	MONTY-028DH	BnASSYST-257	Spring OSR
53	N01D-1330	BnASSYST-258	Spring OSR
54	N02D-1952	BnASSYST-259	Spring OSR
55	SURPASS400-024DH	BnASSYST-260	Spring OSR
56	CUBS ROOT	BnASSYST-261	Spring OSR/Semi Winter
57	ERGLU	BnASSYST-263	Spring OSR/Spring_fodder
58	HELIOS	BnASSYST-264	Spring OSR
59	MAZOWIECKI	BnASSYST-268	Spring OSR
60	TANTAL	BnASSYST-269	Spring OSR
61	WEIHENSTEPHANER	BnASSYST-270	Spring OSR
62	Liho	BnASSYST-271	Spring fodder
63	Bronowski	BnASSYST-273	Spring OSR
64	Ceska Krajova	BnASSYST-274	Spring OSR
65	Duplo	BnASSYST-275	Spring OSR
66	Topas	BnASSYST-283	Spring OSR
67	Tribune	BnASSYST-307	Spring OSR
68	Willi	BnASSYST-394	Spring OSR

69	VIGE DH1	BnASSYST-401	Swede
70	HUGUENOT	BnASSYST-410	swede
71	JAUNE A COLLET VERT	BnASSYST-411	swede
72	SENSATION NZ	BnASSYST-414	swede
73	Altasweet	BnASSYST-418	swede
74	Tina	BnASSYST-436	swede
75	YORK	BnASSYST-438	swede
76	Wilhelmsburger	BnASSYST-448	swede
77	Cabernet	BnASSYST-509	Winter OSR
78	Cabriolet	BnASSYST-510	Winter OSR
79	Castille	BnASSYST-511	Winter OSR
80	Catana	BnASSYST-512	Winter OSR
81	Chuanyou 2	BnASSYST-513	Semiwinter OSR/Exotics Semiwinter OSR
82	Dimension	BnASSYST-514	Winter OSR
83	Excalibur	BnASSYST-515	Winter OSR
84	Flash	BnASSYST-516	Winter OSR
85	Huron x Navajo	BnASSYST-517	Winter OSR
86	Inca x Contact	BnASSYST-518	Winter OSR
87	Ningyou 7	BnASSYST-520	Semiwinter OSR/Exotics Semiwinter OSR
88	Palmedor	BnASSYST-521	Winter OSR
89	POH 285, Bolko	BnASSYST-522	Winter OSR
90	Quinta	BnASSYST-523	Winter OSR
91	Rocket	BnASSYST-524	Winter OSR
92	Shengliyoucai	BnASSYST-526	Semiwinter OSR/Exotics Semiwinter OSR
93	Temple	BnASSYST-527	Winter OSR
94	Vision	BnASSYST-528	Winter OSR
95	Xiangyou 15	BnASSYST-529	Semiwinter OSR/Exotics Semiwinter OSR
96	Zhongshuang II	BnASSYST-530	Semiwinter OSR/Exotics Semiwinter OSR

2.2. Methods

2.2.1. Growth conditions

2.2.1.1. *Arabidopsis thaliana*

For experiments requiring growth in sterile conditions, *Arabidopsis* seeds were sterilised using the vapor-phase sterilisation method (Lindsey et al., 2017). Briefly, an aliquot of seeds in an Eppendorf tube was placed in a closed desiccator with a beaker containing 100 mL of bleach and 3 mL of 37% HCl. Sterilisation took place for 3 hours. Then, seeds were sown on Petri dishes containing 0.5x Murashige and Skoog (MS) medium (pH 5.7) and 6 g/L agar with 0.5% sucrose (w/v). For stratification, plates were kept at 4°C for 3 days before transferring to growth rooms.

Unless otherwise stated, growth was in a controlled environment room at 20 °C ± 2 °C under continuous light for 9 days, after which, seedlings were placed in liquid 0.5x MS medium (pH 5.7) with 0.5% sucrose (w/v) and kept in continuous light on a shaker at 120 rpm for 24 hours. Then, treatments were applied as stated in **section 2.2.2 below**.

Adult plants were grown for 9 days in continuous light as indicated above and were placed in pots with autoclaved soil (5:3:2 compost : vermiculite : perlite, v/v/v) and then grown in a controlled-environment room at 20 °C ± 2 °C under a short-day photoperiod (8 hours light / 16 hours dark) with a photosynthetic photon flux density of ~80 µmol m^{-2} s^{-1} and ~65% relative humidity.

2.2.1.2. *Brassica napus*

For *B. napus* plants, seeds were placed in pots with autoclaved soil (5:3:2, compost : vermiculite : perlite, v/v/v) and then grown in a temperature-controlled (~22 °C ± 2 °C) greenhouse for 3 weeks (reaching the state in which the 2^{nd}-3^{rd} leaf is fully unfolded) maintaining spacing between pots to minimize shading and adjusting the watering frequency (approximately every 3-4 days) to keep substrate moisture.

Environmental conditions were maintained under a neutral-day regime with a minimum photoperiod of 12 h light and 12 h dark. Natural daylight was supplemented with LED lighting (Valoya RX600 Solray 385) when required to ensure that plants received at least 12 h of light (neutral days). During summer, supplementary lighting was switched off when natural day length exceeded this threshold. To minimise abrupt transitions in irradiance during switching on and off of the lights, light intensity was gradually increased when switching on at the end of the summer and gradually decreased at the end of the spring, with the timing of these adjustments varying according to the season.

2.2.1.3. *Sclerotinia sclerotorium*

Sclerotinia sclerotiorum was maintained on potato dextrose agar (PDA) at 20 °C ± 2 °C under short-day photoperiod (8 hours light / 16 hours dark) with a photon flux density of ~80 µmol m^{-2} s^{-1}. Humidity was maintained by keeping the plate sealed with parafilm. These conditions support active mycelial growth and subsequent sclerotial development.

2.2.2. Hypoxia treatments

2.2.2.1. Hypoxia chambers

For hypoxia treatments, the experimental material was prepared according to plant developmental stage before transfer to the hypoxia chambers (transparent PhO2X boxes (Baker-Ruskinn)). 10-day old seedlings were placed in plates containing liquid medium (0.5x MS + 0.5% Sucrose) and then kept in continuous light for 24 h in a shaker and later transferred into the hypoxia chambers. 4-week old plants leaf discs were cut and floated in water before being placed in the hypoxia chambers.

For all hypoxic treatments, nitrogen gas was pumped in the chamber until the desired O_2 concentrations were reached (as indicated for each specific experiments). CO_2 levels were also kept constant at atmospheric levels. Normoxic control plates were maintained on adjacent shelves outside the hypoxia chambers, where they were exposed to the same light conditions as the hypoxia-treated plates, but at ambient oxygen concentrations.

2.2.2.2. Anaerojars

An Anaerogen sachet (Oxoid) was placed into an anaerojar (Oxoid), which was sealed after introduction of the plants, and placed back into the plant culture rooms to keep temperature and light conditions as constant as possible. Normoxic control plates were maintained on adjacent shelves outside the anaerojars, where they were exposed to the same light conditions as the hypoxia-treated plates, but at ambient oxygen concentrations.

2.2.2.3. Waterlogging

For waterlogging treatments, pots with 3-week old *B. napus* plants were placed in plastic boxes and water was added to ~1 cm above the soil surface. This water level was maintained for the duration specified for each experiment. When applying waterlogging treatment, plants were moved between benches to reduce positional effects in the greenhouse. Control plants were watered as normal (every 3-4 days).

2.2.3. Pathogen and flg22 treatments

2.2.3.1. Treatments with flg22 to elicit PTI

The synthetic flg22 peptide (Alpha Diagnostic International; FLG22-P-5) was resuspended in sterile deionised water to a stock concentration of 1 mM and aliquoted in 25 µL aliquots to avoid repeated freeze-thaw cycles. Aliquots were stored at −80 °C and thawed on ice immediately before use. Plants were treated by applying freshly prepared working solutions (concentrations specified on each experiment) from the 1 mM stock in sterile dH_2O, directly to the liquid medium surrounding the tissue material (seedling or leaf disc). Mock controls received carrier only (sterile dH_2O).

2.2.3.2. *Sclerotinia sclerotiorum* inoculations

S. sclerotiorum detached leaf assays with *B. napus* were performed by Dr. Shreenivas Singh as in Mullins et al., 1999. Briefly, *S. sclerotiorum* sclerotias were placed on PDA plates at 20 °C ± 2 °C in short-day conditions (8 hours light / 16 hours dark). After 48 hours of growth, *S. sclerotiorum* mycelia agar plugs (5 mm of diameter) were placed on PDA for 48 hours after which agar plugs were excised from the edges of actively growing colonies and placed onto detached *B. napus* leaves (i.e. the 3rd leaf of 5-week old plants grown in control/waterlogging conditions for 15 days prior to the detached leaf assays – **section 2.2.2.3 above**). Leaves were placed on water agar (1%) plates and left in short-day conditions. At 24 and 48 hours post inoculation (hpi) pictures of the leaves were taken. The lesion size area was then calculated using Image J.

2.2.4. Molecular biology methods

2.2.4.1. Genomic DNA extraction

Genomic DNA was extracted from plant tissue using a protocol adapted from Edwards et al., 1991 for tissue grinding with a TissueLyser (Qiagen). Briefly, a small piece of leaf material was immersed in 400 µL of Edward's buffer (200 mM Tris–HCl, pH 7.5–8.0; 250 mM NaCl; 25 mM EDTA) with a metal bead and broken up with a TissueLyser (2 cycles of 120 seconds at 30 rpm) at room temperature. Metal beads were removed and 20 µL of 0.5% (w/v) SDS was added to each sample. The tube was centrifuged for 1 minute at 14,000 rpm (~16,000×g) at room temperature to pellet cell debris. 300 µL of the supernatant was transferred to a new tube and mixed 1:1 (v/v) with 100% isopropanol, gently inverted 10–15 times to precipitate nucleic acids, and then centrifuged for 5 minutes at 14,000 rpm at room temperature. The resulting pellet was rinsed with 70% (v/v)

ethanol, recentrifuged for 3 minutes at 14,000 rpm, air-dried for approximately 1 hour in a fume hood, and resuspended in 100 µL of nuclease-free water. DNA was then stored at 4 °C until use.

2.2.4.2. Genotyping by PCR

T-DNA insertion mutants were genotyped by PCR using T-DNA and gene-specific primers. The OligoAnalyzer online tool (Integrated DNA Technologies) was used to assess primer melting temperatures, hairpin formation, self-dimerisation and hetero-dimerisation properties. DNA primers were diluted to 100 µM in nuclease-free H_2O and stored at -20°C. All the oligos used in this study for genotyping are listed in Table 2.4.

Table 2.4. Primers used in this study for genotyping.

Line	Primer name	Sequence
rbohd-3	BM rbohd LP	GTTATTGCGTTTGTGTCGCCAAAG
	BM rbohd RP	GGTCAGGACCTTTCATGTTGTTGATG

For the genotyping PCR reactions, 3 µL of extracted genomic DNA (**see also section 2.2.4.1 above**) was mixed with 0.2 µM of each primer , 0.2 mM dNTP mixture and Taq polymerase following manufacturer's instructions. The PCR program used was as follows: 94°C, 30 sec; 55°C for 30 sec and 72°C for 1 minute per 1 kb of DNA . The products of the PCR reactions were separated using agarose gel electrophoresis and visualised using SYBR safe DNA stain (ThermoFisher).

2.2.4.3. Total RNA extraction

Total RNA was isolated from leaf tissue that had been frozen in liquid nitrogen and stored at -80°C by using column-based plant RNA kits according to the manufacturers' instructions (GeneJET Plant RNA Purification Kit (Thermo Scientific - K0802), Spectrum Plant total RNA kit (Merck - STRN250-1KT) and *EasyPure*® RNA Purification Kit (TransGen - ER701-01)). Kits changed depending on commercial availability, as there were disruptions in supply for the brand normally used in the lab. The tissue was lysed in a TissueLyser (Qiagen) using blocks previously cooled to -80°C to prevent tissue thawing during the lysing process. After RNA extraction, RNA quantity and purity were assessed by spectrophotometry (NanoDrop, DeNovix), with typical values of A_{260}/A_{280} ≈ 2.0 and A_{260}/A_{230} ≈ 2.0–2.2. Purified RNA was stored at −80 °C until use.

2.2.4.4. Reverse Transcription (RT)

1 µg of extracted total RNA was reverse transcribed to complementary DNA (cDNA) by incubating with 1X Reaction Buffer (Thermo Fisher), RevertAid Reverse Transcriptase (Thermo Fisher), RiboLock RNase inhibitor (Thermo Fisher), oligo(dT)18 (IDT) and 1 mM dNTP mixture (volumes shown in **Table 2.4**) in a thermocycler at 42°C for 60 minutes. The cDNA was used directly for qPCR analysis and was stored at -20°C.

Table 2.5. Volumes used for Reverse Transcription (RT) reaction.

Reagents	Volume
Diluted total RNA	12 µL
5X Reaction Buffer (Thermo Fisher)	4 µL
100 µM Oligo(dT)18 (IDT)	0.5 µL
RiboLock RNase inhibitor (Thermo Fisher)	0.5 µL
10 mM dNTP	2 µL
RevertAid Reverse Transcriptase (Thermo Fisher)	1 µL
Total Reaction Volume	**20 µL**

2.2.4.5. Quantitative PCR (qPCR)

For the Quantitative PCR (qPCR), cDNA was mixed with a primer pair mixture (1 µM final concentration each primer), water and 2X SYBR green master mix (Roche) (volumes shown in **Table 2.6**) in each well of a LightCycler 480 96-well plate (Roche) that was placed in a LightCycler 480. The qPCR amplification was performed for 40 cycles consisting of denaturation at 95 °C for 30 s, annealing at 60 °C for 20 s, and extension at 72 °C for a duration adjusted to amplicon length (approximately 1.5 kb min^{-1}, kept as short as possible).

Table 2.6. Volumes used for Quantitative PCR (qPCR) reaction.

Reagents	Volume
2X SYBR green master mix (Roche)	5 µL
cDNA	1 µL
Primer pair mixture	1 µL
dH_2O	3 µL
Total Reaction Volume	**10 µL**

The LightCycler 480 software provided crossing point (CP) values based on the Absolute Quantification/Second Derivative Maximum method, which were used to calculate the gene expression (CP reference gene – CP gene of interest = ΔCP), and assuming a PCR efficiency value of 2 (PCR products double each cycle), relative expression was calculated as 2^ΔCP . *MON1* (AT2G28390) was used as a reference gene for *Arabidopsis* samples because previous expression-stability studies identified AT2G28390 as a comparatively stable transcript across a range of tissues and conditions, supporting its suitability for normalization of gene expression data (Czechowski et al. 2005). Primers used in this study for qPCR analysis are listed in **Table 2.7**.

Table 2.7. Primers used in this study for qPCR.

Target Gene	Sequence (5' à 3')
RBOHD (AT5G47910)	TGGATGTTGTGTCGGGTACACG
	TGGCATTCCACAGTAGAAGACTCCTA
WRKY33 (AT2G38470)	GGAGTGAACCTGAAGCAAAGAGATGGAA
	CGTTGTCTGCACTACGATTCTCGGC
BIK1 (AT2G39660)	CATGTCATCAGGTCACTTGAATGCAAG
	CGGTCTGTTATGATCCAACGCTCG
FRK1 (AT2G19190)	TGAGAACTTAGGAGACTATTTGGCAGGTAA
	ACCATTGTGAAGATACTCTAGTCCTTGCG
CPK28 (AT5G66210)	AGTCTTGAAGAGATGAGACAGGCACT
	CCCATCAGTGTTGCTATCAATCGCTTC
PHI1 (AT1G35140)	CGACGTTGGTTTAGACGGGATGG
	AGACTCCAGTACAAGCCGATCCA
CYP71A13 (AT2G30770)	ATCTTGGATATGTTTATCGGAGGAACGTC
	AGCACCTCTTTAATCACGGCTTTTAAGT
NHL10 (AT2G35980)	GCCTTCTACGGTCCATCA
	TGACGAATAAGCTGAGGAGG
WRKY22 (AT4G01250)	GAATTACGGTGTGTCGGAGCTGG
	CGATGTCTGGGCATGGCGA

2.2.5. Biochemical methods

2.2.5.1. Protein extraction

Frozen tissue was ground in a TissueLyser (Qiagen) by keeping samples in blocks stored at -80ºC to prevent tissue thawing during the lysing process. After grinding, the tissue powder was mixed with Laemmli protein extraction buffer (2xSDS loading dye) in a 1:1 ratio (v/v) of 2xSDS (µL):volume of powder (µL) ratio. After mixing, samples were kept at 95ºC for 5 minutes to denature proteins, centrifuged at 14,000 rpm for 10 minutes at room temperature to pellet and remove cell debris, supernatant was transferred to fresh Eppendorf tubes.

2.2.5.2. Immunoblot analysis

Protein extracts (25 µL) were loaded directly on acrylamide SDS-PAGE gels (10%) alongside 10 µL of PageRuler of pre-stained protein ladder (ThermoFisher) and run through the gel using 1x running buffer (25 mM Tris base, 192 mM glycine, 0.1% SDS, pH 8.3) at 90 volts. Separated proteins were transferred to a PVDF membrane through a wet/semi-dry transfer system at 60 mA (transfer buffer: 10 mM Tris base, 100 mM glycine, 10% ethanol (v/v)). To assess equal protein loading, membranes were incubated with Ponceau S staining (0.4% (w/v) Ponceau S, 10% (v/v) acetic acid in water) for 5 minutes after equilibrating the membrane in a 7.5% acetic acid solution for 3 minutes. Then, the membranes were rinsed with 1xPBS-T and blocked with 5% milk in PBS-T (PBS (OXOID #BR0014G)) containing 0.05% (v/v) Tween-20) for 30 minutes (3x 10 minutes) at room temperature. Membranes were placed in 50 mL Falcon tubes containing 5 mL of PBS-T with 5% (w/v) non-fat dry milk and the relevant primary antibody and incubated overnight at 4°C with constant rotation on a tube roller (Stuart). RBOHD protein was detected using a rabbit polyclonal anti-RBOHD antibody (Agrisera, AS15 2962), raised against *Arabidopsis thaliana* RBOHD (AT5G47910). The primary antibody was used at a dilution of 1:2,000 for immunoblot analysis.

After incubation with the primary antibody solution, the PVDF membranes were washed with PBS-T for 3x 5 minutes and incubated with the secondary antibody for 2 hours at room temperature with constant shaking. An HRP-conjugated anti-mouse secondary antibody (Sigma, A9044) was used at a dilution of 1:50,000 for immunoblot detection. Membranes were washed with PBS-T for 3x 5 minutes and immunoblots were imaged using WesternBright ECL substrate (Advansta) in a G:BOX gel documentation system with the GeneSys software.

2.2.6. ROS measurement

ROS burst triggered by flg22 was quantified using *Arabidopsis thaliana* leaf discs using a luminol–horseradish peroxidase (HRP) chemiluminescence assay with minor adaptations for plate-based kinetics and optional hypoxia pre-treatment (Bisceglia et al., 2015; Smith and Heese, 2014; Wagner et al., 2019). Briefly, plants were grown to 4–5 weeks as outlined in **section 2.2.1.1 above**, and fully expanded, non-senescent rosette leaves of similar, intermediate age (Sew et al., 2015) were sampled to minimise developmental variation; 3 leaf discs per plant were excised with a (7 mm diameter) cork borer. Each leaf disc was placed abaxial side up at the bottom of each well of a black 96-well plate (Thermo Scientific) prefilled with 372 µL sterile deionized water and 4 µL of fresh 100x stocks of luminol (17.7 mg mL^{-1} in 200 mM KOH; Sigma) and HRP (10 mg mL^{-1} in dH_2O; Fisher Scientific) to reach a final concentration of 1x. Intercellular spaces were then infiltrated with the water surrounding the leaf discs by applying three rounds of vacuum and release for 10 minutes each.

The plates were then dark-adapted for 60 minutes at room temperature. This period also allowed for wounding recovery. The plates were then introduced in a hypoxia chamber (**see also section 2.2.3.1 above**) set to 21% (normoxia control) or 1% O_2 (hypoxia) for 4 hours in the dark. At the end of the hypoxia treatment, the plates were sealed with a transparent gas-tight qPCR film (Roche) to maintain the hypoxic environment during handling. Plates were loaded into a POLARstar Omega microplate reader (BMG LABTECH) configured for luminescence for 6 min in in the dark to establish a baseline. A flg22 working solution was prepared at 20 µM so that addition of 20 µL to each well (initially 380 µL) yielded a final flg22 concentration of 1 µM in 400 µL total volume. Controls received the same volume of the mock solution (sterile water). flg22 or mock solution was dispensed rapidly (manual pipetting under dim light), and luminescence was recorded immediately for 60 min with a 120-s integration time per read, using top-read optics at room temperature. Raw relative light units (RLU) were exported and the values for each disc within a biological replicate and treatment were averaged. The area under the curve for the averages was then determined using GraphPad Prism v10. This software was also used for statistical analyses of the data - exact sample sizes, tests and *P* values are reported with the relevant figures. Wells exhibiting bubbles, splashing, unstable baselines, or other handling artefacts were excluded *a priori*.

2.2.7. MultispeQ measurements

Measurements of fluorescence-derived parameters were performed with the MultispeQ device (PhotosynQ Inc.), which is a portable leaf fluorometer/spectrophotometer that enables rapid, non-destructive measurement of photosynthesis-related and environmental parameters. Using the RIDES 2.0 protocol, light-adapted leaves can be assessed for chlorophyll fluorescence traits associated with PSII performance and non-photochemical quenching together with environmental conditions.

To perform the measurements, the 3rd leaf of *B. napus* plants after control or waterlogging treatment (**see also section 2.2.2.3 above**) for 15 days were measured between 09:00 am and 12:00 pm (noon) to minimize diurnal variability. Leaf photosynthetic parameters were measured using a MultispeQ fluorometer controlled *via* the PhotosynQ Desktop app v1.10.59 following the PhotosynQ protocol "Photosynthesis RIDES 2.0" with default pulse amplitudes and timing. Leaves were gently cleaned of surface moisture prior to clamping. For each plant, 2 technical replicates were taken on independent leaf positions avoiding the midrib and major veins; 3-4 biological replicates were measured per treatment/cultivar, as outlined in the relevant sections.

2.3. Statistical Analyses

2.3.1. Statistical analysis of *A. thaliana* experiments

The number of biological replicates is indicated in the corresponding figure legends, as well as the statistical tests applied. These were performed using GraphPad Prism v10 (GraphPad, San Diego, California, USA).

2.3.2. Statistical analysis of *B. napus* screening

Effect size analysis was used to quantify the magnitude of differences between control and waterlogging conditions independently of statistical significance. Effect sizes for group comparisons of screening conditions optimization experiments were expressed as Hedges' g, which is a small-sample–corrected version of Cohen's d (Hedges, 1981; Ialongo, 2016). Hedges' g was chosen because several of the comparisons in this study involved relatively small group sizes, conditions under which uncorrected d tends to be positively biased. For each comparison, Hedges' g was reported along with its direction and magnitude. Values of about 0.2, 0.5, and 0.8

were interpreted as small, medium, and large effects, respectively, but interpretation was ultimately made in the substantive context of the study.

$$g = \frac{|\bar{x}_1 - \bar{x}_2|}{\sqrt{\frac{(n_1 - 1)s_1^2 + (n_2 - 1)s_2^2}{n_1 + n_2 - 2}}}$$

Figure 2.1. Formula used to calculate Hedge's g. Hedge's g was calculated following the formula explained in (Ialongo, 2016).

Statistical analysis was then carried out with n = 3 using R. All source codes are available upon request.

To analyse the phenotypic data generated in the *Brassica napus* screening, all measurements made during the screening of the rapeseed collection were entered in an Excel file where all measurements made with individual plants were averaged to consider a single value which was then used by Prof. Rafael de Andrade Moral for statistical analysis.

Bayesian mixed-effects models were fitted separately for each measured trait using the brms package in R. For the "absolute" approach, raw trait values were modelled assuming a Gaussian error distribution. Fixed effects included biological replicate, environmental covariates such as table location, age of lamps, ambient humidity, ambient temperature, time of day, photosynthetically active radiation (PAR), and treatment, together with the interaction between treatment and the two internal control varieties present across all batches (C1 (#240) and C2 (#229)). Random effects were included to account for variation among batches and varieties, with treatment-specific random slopes fitted for each variety. The model structure was:

$y \sim \text{bio\_rep} + \text{Location} + \text{Age\_of\_Lamps} + \text{Ambient\_Humidity} + \text{Ambient\_Temperature} + \text{Time\_of\_Day} + \text{PAR} + \text{treatment} \times (C1 + C2) + (1 \mid batch) + (0 + \text{treatment\_Control} \mid\mid variety) + (0 + \text{treatment\_WL} \mid\mid variety)$.

In addition, a "relative" approach was used in which the ratio between waterlogged and control values was calculated and then modelled for each trait. These ratio data were analysed using a

simpler Bayesian mixed-effects model with biological replicate, and environmental covariates such as location, age of lamps, and the two internal control varieties (C1 and C2) as fixed effects, and batch and variety as random intercepts:

$$y \sim \text{bio\_rep} + \text{Location} + \text{Age\_of\_Lamps} + C1 + C2 + (1 \mid batch) + (1 \mid variety).$$

For all models, four Markov chains were run for 2,000 iterations each, with 1,000 warm-up iterations, resulting in 4,000 post-warm-up posterior draws. Model outputs were summarised using posterior estimates and 95% credible intervals, which were used to identify varietal responses differing from the population mean.

2.3.3. Genome-wide association studies (GWAS) and associated transcriptomics

Genome-wide association studies (GWAS) were conducted to identify loci associated with variation in rapeseed responses to waterlogging, S. sclerotiorum infection, and combined waterlogging + S. sclerotiorum stress. Analyses were performed by our collaborators Dr. Rachel Wells and Dr. Emmanuel Solomon (John Innes Centre; UK) in R using the GAPIT software package. The phenotypic input for GWAS consisted of the fitted mixed-effects models fitted by Prof. Rafael de Andrade Moral. Using model-derived phenotypes allowed the association analyses to be based on values already adjusted for environmental covariates and experimental structure. Parameters chosen to perform the GWAS were SPAD, Fv'/Fm', ΦII, ΦNO, NPQt, plant weight and lesion size at 24 hpi.

Markers were filtered according to standard quality criteria, including thresholds for minor allele frequency and missing data, and only accessions with complete genotype–phenotype information were retained. GWAS was performed using several models implemented in GAPIT, including GLM, MLM, CMLM, MLMM, FarmCPU and Blink, to compare their performance and identify the best-fit model for each trait. Population structure and relatedness were accounted for by incorporating principal components and kinship matrices.

Model performance was assessed using GAPIT diagnostic outputs, particularly Manhattan and QQ plots, and the best-fit models were selected for downstream interpretation. Significant marker–trait associations were identified using FDR = 0.05, and for each associated SNP, the estimated effect size and proportion of phenotypic variance explained were extracted from the GAPIT results.

3. Chapter 3: Regulation of RBOHD during combined hypoxia and flg22 responses: effects of light availability, developmental stage, and *CPK28*.

3.1. Introduction

3.1.1. Background Information

Plants are sessile organisms that often experience simultaneous abiotic and biotic stresses, for example, flooding conditions provide adequate conditions for pathogen infections (increased leaf wetness, high humidity, anaerobic and humid soils…), but also pathogens can cause the establishment of hypoxic microenvironments at the site of infection (Chung et al., 2019; Gravot et al., 2016; Valeri et al., 2021). Combined stress responses often involve trade-offs between individual stress response pathways. Previous studies have highlighted negative trade-offs between hypoxia and flg22 responses for example (Brunello et al., 2024; Mooney et al., 2024). However, hypoxia and pathogen responses have common molecular components that are activated in both individual stress responses and may act as convergence points to regulate the response to this combined stress.

One of these common components is RBOHD, which, as detailed in **section 1.3.2.2**, is a plasma membrane–localised NADPH oxidase that plays a central role in ROS production during stress responses. During early stress responses, RBOHD is the target of multiple multilayered regulatory pathways involving transcriptional to post-translational levels, leading to the rapid yet balanced production of ROS. For example, at the transcriptional level, hypoxia induces *RBOHD* transcript levels through the action of different ERFVII TFs and EIN2 (Yang et al., 2017; Yang and Hong, 2015; Yao et al., 2017), whereas immune responses induce *RBOHD* transcriptional expression through the WRKY DNA-BINDING PROTEIN 33 (WRKY33) TF and other second messengers such as PA (Birkenbihl et al., 2012; Qi et al., 2024; Zhao et al., 2020). At the post-translational level, both hypoxia and flg22 treatment trigger sequential phosphorylation and Ca^{2+}-dependent feedback loops to dynamically activate RBOHD ROS production, however these stresses differ in the direct activators of RBOHD. While flg22 responses activate RBOHD through kinases like BIK1, SIK1 or GPA1, hypoxia activates RBOHD through HRU1 or ROP2 (**Table 1.1-2 and Figures 1.11-12**). Most studies on flg22 have mainly focused on these activation pathways, while transcriptional control and protein abundance of RBOHD have been a more recent focus. In the context of hypoxia, transcriptional control of *RBOHD* has been studied to some extent, whereas RBOHD activation

at the protein level remains poorly understood compared to flg22, with few identified activators (**Table 1.1-2**). The integrated control of RBOHD under combined hypoxia and flg22 is poorly understood.

3.1.2. Aims of this chapter

The two aims of this chapter were (i) to determine how hypoxia influences the onset of innate immune responses and (ii) to dissect the role of *RBOHD* during the onset of innate immune responses under hypoxic conditions**.** Transcriptional and post-transcriptional analyses were conducted in this chapter in order to better understand a potential role of RBOHD in regulating plant responses to combined hypoxia/flg22. For these experiments, the role of the ERF-VIIs was considered as hypoxia sensing mechanisms converge on the transcriptional control of gene expression through the induction and/or stabilisation of the master regulators of hypoxia, the ERFVIIs (Gibbs et al., 2011; Licausi et al., 2011). Recent studies on this group of TFs underscore the roles of the N-degron pathway, more specifically the ERFVIIs, in both hypoxia and immune responses (Brunello et al., 2024; De Marchi et al., 2016; Gravot et al., 2016; Mooney et al., 2024; Valeri et al., 2021; Vicente et al., 2019). Given the existing evidence that the ERFVIIs stabilise and interact with regulators of immune responses, such as RBOHD (Yao et al., 2017), one question is: do the ERFVIIs also participate in modulating defence pathways, such as ROS production, triggered by flg22, especially when hypoxia and flg22 are applied at the same time? Recent studies have demonstrated that hypoxia inhibits immune responses (Brunello et al., 2024; Mooney et al., 2024). Therefore, potential hypoxia-dependent activation of negative regulators of immunity may contribute to the trade-off between hypoxia and immune responses. Here, we explored this possibility by focusing on negative regulators of immunity, such as CPK28, which is a common response element to hypoxia and flg22 treatments (Bakshi et al., 2023; Chi et al., 2021; Keinath et al., 2015; Peláez-Vico et al., 2023; Subbaiah et al., 1994; Thor and Peiter, 2014; Wagner et al., 2019; Yemelyanov et al., 2011).

3.2. Optimisation of experimental conditions

3.2.1. Exploring chemical induction of mitochondrial malfunction as a readout for hypoxia response

As stated in the introduction, mitochondria play a key role in mediating responses to hypoxia. Wagner et al. (2019) demonstrated that treatment with antimycin A (AA), which inhibits the mETC, partially mimics the cytosolic responses to hypoxic conditions, including a decrease

in cytosolic $MgATP^{2+}$ levels, an increase in $[Ca^{2+}]_{cyt}$, a transient reduction of the NAD pool, acidification of the cytosol, and oxidation of the glutathione pool. These findings indicate that inhibition of the mETC is sufficient to account for some of the hypoxia-associated cellular changes.

As previously mentioned in Section 1.3.2.1, *AOX1a* transcriptional expression can be used to assess mitochondrial malfunction (Clifton et al., 2005; Vanlerberghe and Mclntosh, 1996). AOX1a bypasses two proton translocation sites in the cytochrome pathway (complexes III and IV), thereby uncoupling respiration from ATP synthesis, and can be pharmacologically inhibited through salicylhydroxamic acid (SHAM) treatment. Wagner et al. (2019) demonstrated that further mitochondrial inhibition through treatment with a combination of AA+SHAM resulted in cellular responses that mimicked more closely those obtained under O_2 depletion. These authors concluded that the impairment of mitochondrial function by AA+SHAM was sufficient to trigger hypoxia-induced cytosolic changes. This gene

Transcriptional changes are one of the main outputs downstream of the cytosolic changes triggered by hypoxia. Notably, the main known transcriptional regulators of mitochondrial malfunction also have a role in hypoxia response. These include the transcription factors ANAC013, ANAC016 and ANAC017 (De Clercq et al., 2013; Eysholdt-Derzsó et al., 2023; Jethva et al., 2023; Ng et al., 2013). These transcription factors trigger the expression of target genes by binding to the MDM *cis*-regulatory element present in their promoter regions. A classic example of this is the binding of ANAC017 to the *AOX1a* promoter (Ng et al 2013). Among the MDM-containing genes are several HRGs and ANAC013/16/17 have been shown to bind to the *cis*-regulatory elements in the promoters of these genes, such as *HRE2*, *ADH1*, *PGB1* and *PDC1* (Eysholdt-Derzsó et al 2023; Ng et al 2013). The presence of MDM elements in several HRGs further links mitochondrial malfunction to hypoxia responses, suggesting that chemically induced mitochondrial malfunction could regulate HRG expression and could be used as a method to study hypoxia responses at cellular level.

This link was further supported by Schmidt et al (2018), who showed that decreasing the cellular ATP level constitutes limiting conditions for LONG-CHAIN ACYL-CoA SYNTHETASE (LACS) activity. When ATP is limiting, LACS activity drops, which is associated with induction of low-oxygen (hypoxia)–responsive genes. This reduction in ATP levels was achieved by chemically inhibiting the mETC through AA treatment. Notably, AA treatment not only triggered the induction of ANAC017 target genes, but also other HRGs such as *HYPOXIA RESPONSE UNKNOWN PROTEIN* 7 (*HUP7)*, which lacks the MDM motif (Eysholdt-Derzsó et al., 2023). Additionally,

another treatment that induced the expression of several HRGs was the combination of AA and dimethylthiourea (DMTU), an H_2O_2 scavenger (Schmidt et al., 2018). Since DMTU was hypothesised to inhibit the mitochondrial ROS produced by AA treatment, these results suggest that cellular energy status is involved in the regulation of hypoxic gene expression and therefore that factors other than ANAC013/16/17 contribute to controlling the expression of HRGs in a mitochondrial-dependent manner.

Altogether, these findings support the view that mitochondrial malfunction is a central trigger of hypoxia-associated signalling, integrating energy status, ROS, and ANAC-mediated transcriptional regulation. To study the extent of mitochondrial malfunction in hypoxia responses and to identify a potential chemical treatment for co-application with flg22, we compared the responses of plants subjected to the combined AA+SHAM treatment or to hypoxic conditions by monitoring the expression of selected genes (**Figure 3.1**).

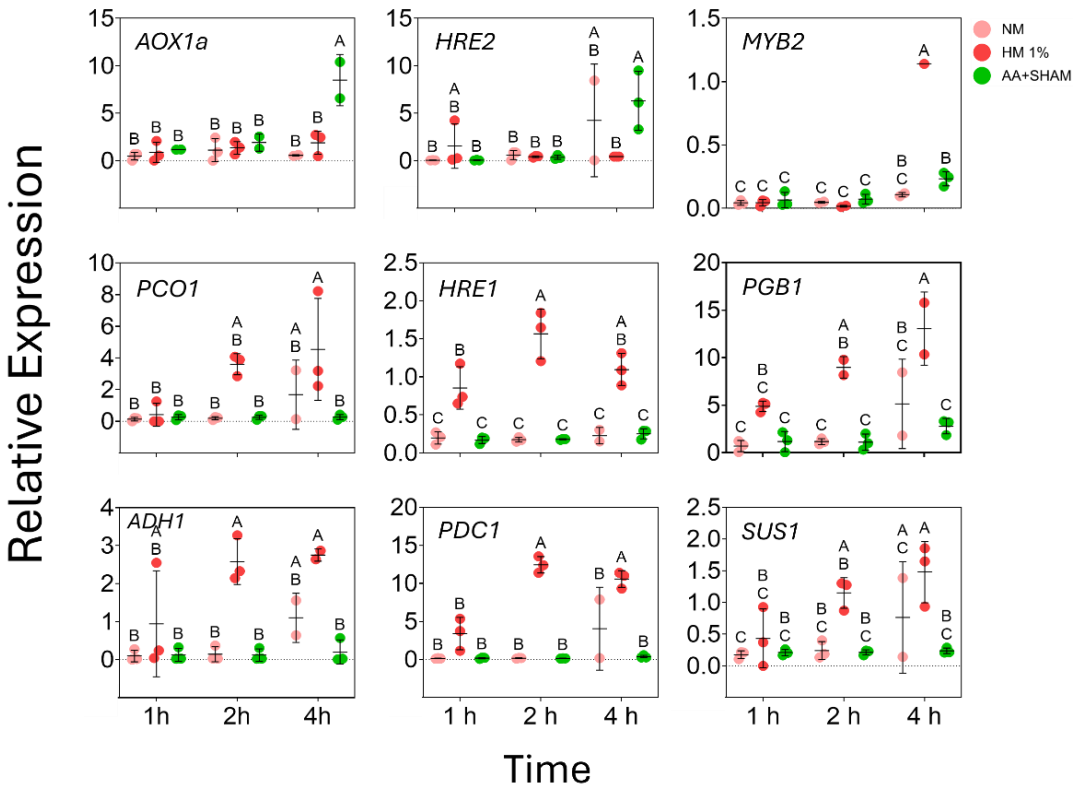

Figure 3.1. Mitochondrial malfunction triggered by AA+SHAM does not induce HRG expression. Expression analysis of mitochondrial malfunction responsive genes in 10-day old wild-type (Col-0) seedlings treated in the dark with ethanol (control, 21% O_2, light pink symbols), AA+SHAM (green symbols) or hypoxia (1% O_2; red symbols) for 1, 2 or 4 hours. The mean relative expression to the *MON1* reference gene is shown. Results are means ± standard deviation (SD) of 3 biological replicates (n = 3). Statistical analysis: two-way ANOVA with Tukey's test ($p < 0.05$);

different letters indicate statistically different groups. AA concentration was 100 µM and SHAM concentration was 10 mM.

As expected, the transcription of the two previously known mitochondrial malfunction marker genes, *AOX1a* and *HRE2*, were induced upon AA+SHAM treatment (**Figure 3.1**), showing that the treatment applied efficiently disrupts mitochondrial function. Next, the expression of seven additional HRGs (*MYB2*, *PCO1*, *HRE1*, *PGB1*, *ADH1*, *PDC1* and *SUCROSE SYNTHASE 1* (*SUS1)*) was tested, and revealed that apart from *MYB2*, the expression of the remaining HRGs was not affected by AA+SHAM treatment (**Figure 3.1**). The extent of *MYB2* induction was smaller compared to that observed in hypoxic conditions caused by hypoxia chambers. MYB2 is known to bind to the GT-motif (5'-TGGTTT-3') present in the promoter of *ADH1* (Hoeren et al. 1998). However, despite MYB2 binding sites in the *ADH1* promoter, together with the presence of an MDM motif, the *ADH1* gene was not transcriptionally induced by AA+SHAM treatment. Similarly, the transcription of other HRGs with an MDM motif present in their promoters, such as *PDC1*, were not induced by AA+SHAM compared to the mock treatment (21% O_2 + ethanol) (**Figure 3.1**). This contrasts with the induction of *PDC1* by AA alone observed in previous studies (Schmidt et al., 2018). Together, these results indicate that the simultaneous inhibition of both the cytochrome and alternative respiratory pathways through AA+SHAM treatment can trigger the expression of canonical mitochondrial malfunction marker genes (*AOX1a* and *HRE2*), but these chemical treatments were not sufficient to induce the expression of HRGs despite the presence of the MDM *cis*-regulatory motif. Therefore, AA+SHAM application was not considered further for co-treatment with flg22.

3.2.2. Comparing the use of anaerojars and hypoxia chambers

We next compared the use of anaerojars and hypoxia chambers, as each of these experimental approaches has a unique set of characteristics that can potentially impact on plant hypoxia responses. In hypoxia chambers, O_2 is displaced by flushing the chamber with another gas (nitrogen (N_2) or argon (Ar)) under a positive pressure (**Figure 3.2 A**). In anaerojars, plant samples are introduced in a sealed chamber where an O_2-consuming chemical reaction removes O_2 (**Figure 3.2 B**). Importantly, this system also increases local levels of CO_2, potentially leading to sample acidification or an increase in the rate of photosynthesis in the light (Donahue et al., 1997; Wurts and Durborow, 1992), and O_2 levels cannot be as tightly controlled as in a hypoxia chamber. In addition, anaerojars (Oxoid) commonly reach <1% O_2 within ~30 minutes in a sealed

jar, whereas in hypoxia chambers (Baker-Ruskinn) take shorter periods of time to reach <1% O_2 (15 mins approx.).

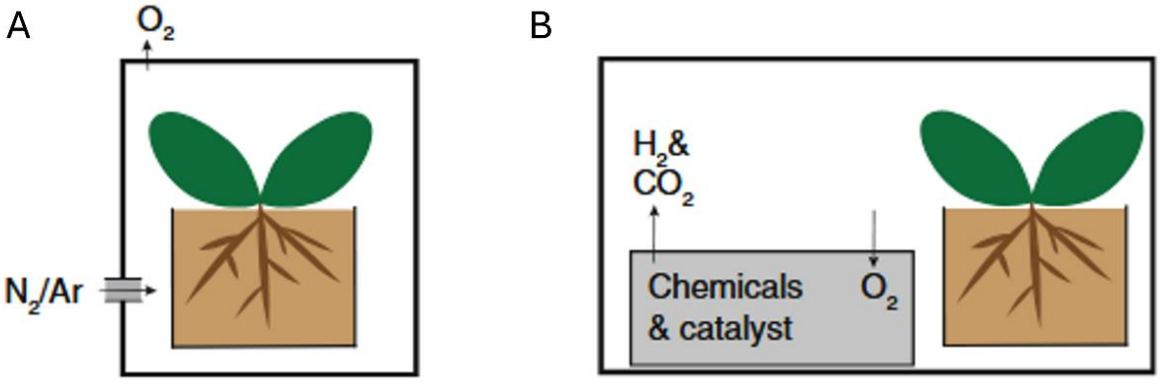

Figure 3.2. Different experimental approaches to induce hypoxia in plant tissues. (A) Hypoxia chambers can reduce O_2 levels through O_2 displacement by blowing gas mixtures over a sample under a positive pressure. **(B)** Anaerojars can reduce O_2 levels through gas replacement by the use of an O_2-reacting catalyst. Figure from (Brazel and Graciet, 2023).

For these experiments, we combined the hypoxia treatments with flg22 and monitored the expression of two HRGs (*HRE2* and *AOX1a*) and two genes associated with pathogen response (*AGB1* and *ARABIDOPSIS G-PROTEIN GAMMA-SUBUNIT 1 (AGG1)*) (**Figure 3.3**). When comparing the results from the anaerojars and hypoxia chambers, *HRE2* showed the most important differences, with a robust induction in hypoxia chambers (with or without flg22; hypoxia/mock (HM) or hypoxia/flg22 (HF)) compared to normoxia/mock (NM), but not in anaerojars (**Figure 3.3**). In hypoxia chambers, the induction of *HRE2* was consistent with previous reports (Brunello et al., 2024; Licausi et al., 2010; Park et al., 2011). The other HRG tested, *AOX1a*, did not show such a strong discrepancy between anaerojars and hypoxia chambers and was not induced by the hypoxia treatment applied, perhaps because longer treatments or lower O_2 levels are needed (Vishwakarma et al., 2018; Yao et al., 2017). The two defence-related genes, *AGG1* and *AGB1*, also behaved similarly in anaerojars and hypoxia chambers, and their expression was not regulated by hypoxia treatment (**Figure 3.3**). When comparing the effects of flg22 under normoxia (NF) or hypoxia (HF), the expression of *HRE2* was not affected by flg22 consistent with previous reports (Valeri et al., 2021), suggesting that *HRE2* expression is largely regulated by hypoxia (**Figure 3.3**). In contrast, *AOX1a* was transcriptionally induced in HF compared to NF in hypoxia chambers but not in anaerojars, (**Figure 3.3**), although for the latter variation between replicates

and reproducibility may be the problem. The defence-related genes *AGB1* and *AGG1* were induced under HF compared to NF in anaerojars but not in hypoxia chambers (**Figure 3.3**). These data suggest that different experimental approaches to trigger hypoxic conditions influence transcriptional dynamics of hypoxia responses alone, but also influence responses to combined hypoxia/flg22.

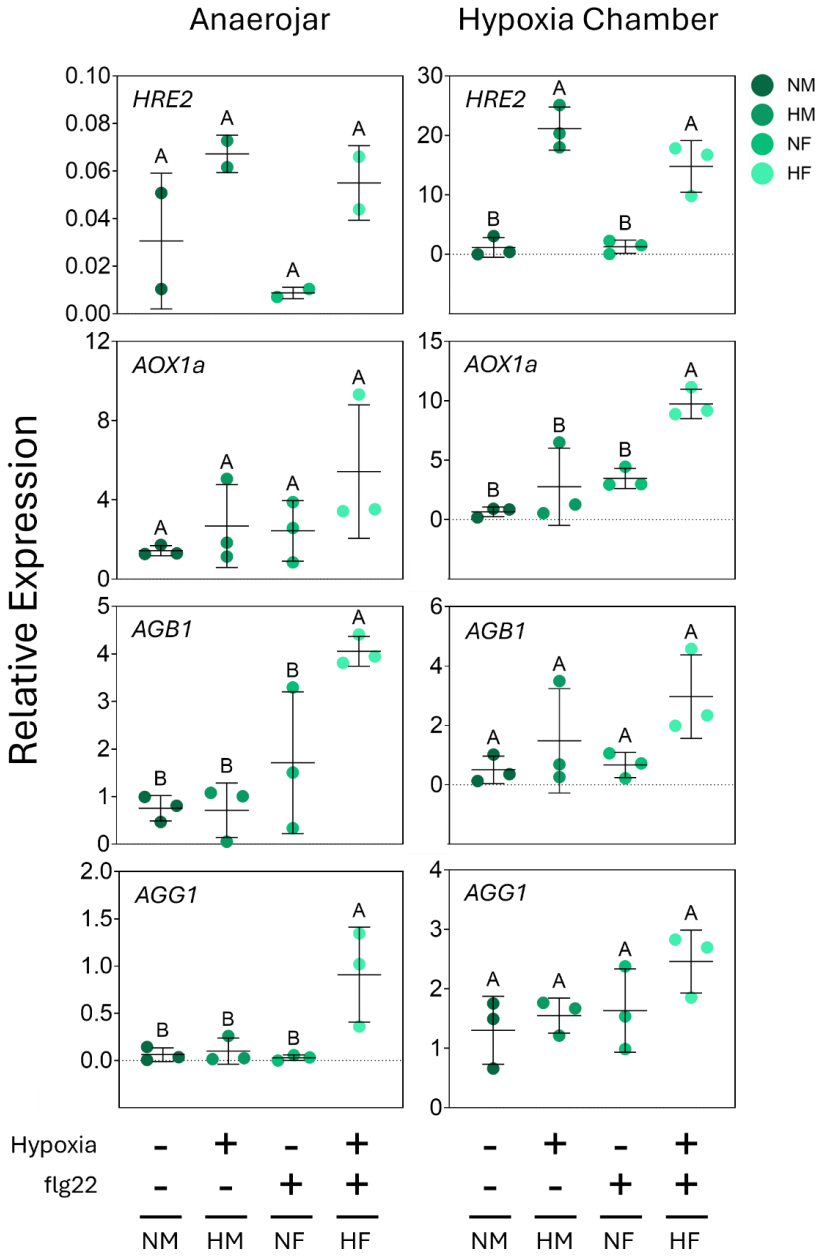

Figure 3.3. Differential expression of selected genes in response to hypoxia and flg22 individually and in combination. Expression analysis of hypoxia and flg22-response genes in 10-day old seedlings treated for 2 hours with a mock solution under normoxia (21% O_2; NM) or hypoxia (1% O_2; HM) and treated with 100 nM flg22 under normoxia (NF) or in combination with

hypoxia (1% O_2; HF) . Results are means ± standard deviation (SD) of 2-3 biological replicates (n = 2 or 3). Statistical analysis: one-way ANOVA with Tukey's test ($p < 0.05$); different letters indicate statistically different groups.

Based on these results, as well as the technical specifications of the hypoxia chambers, it was decided that the latter would be more suitable for our experiments due to (i) reduced time to achieve hypoxic conditions, (ii) possibility of maintaining atmospheric CO_2 levels (allowing a normal photosynthesis rate when treatments were done in the light) in contrast to the elevated CO_2 levels in anaerojars, and (iii) the possibility of controlling more accurately O_2 levels, over a wider range. However, these experiments also highlighted the need to identify the best possible O_2 levels to be used for the experiment (i.e. if hypoxia stress is too strong, this could mask the effects of flg22 when comparing HF to NF, for example), as well as the best duration of the hypoxia treatment.

3.2.3. Optimizing hypoxia treatments in hypoxia chambers

Here, we sought to identify the O_2 levels and duration of hypoxia treatments, as both can affect the outcome of hypoxia responses and therefore, the subsequent hypoxia/flg22 combined stress responses. For example, Licausi et al., (2011) showed that mild hypoxic conditions (8% O_2) induced upregulation of a small number of TF genes after 30 min and 2 h after the onset of hypoxia (7 and 11 genes, respectively), while lower oxygen levels (4% and 1% O_2) increased the number of upregulated TF after 30 min of hypoxia to 29 and 24, respectively. This finding suggests that different sets of transcriptional regulators are differentially activated depending on O_2 levels. Furthermore, Kosmacz et al., (2015) showed that the subcellular localisation of RAP2.12 in the nucleus was lower upon mild hypoxia (10% O_2) compared to lower O_2 levels ranging between 0 and 5%. However, the peak induction of some hypoxia-responsive genes at 1 h does not match the timing of RAP2.12 nuclear accumulation, which is only observed after ~3–4 h of hypoxia. This suggests that early hypoxia transcription is controlled by mechanisms other than RAP2.12 (or other ERF-VIIs) nuclear localisation. Similarly, different durations of hypoxia treatment affect hypoxia response differently. For example, at 1 hour of hypoxia, different regulators of hypoxia response have been shown to be transcriptionally induced, such as *HRE1* and *HRE2* (Licausi et al., 2010). Genes involved in anaerobic metabolism such as *ADH1*, *PDC1*, *LOB DOMAIN-CONTAINING PROTEIN 41 (LBD41)* or *SUS1* are also induced at early timepoints of hypoxia (1 hour) (Gasch et al., 2016; Kosmacz et al., 2015; Licausi et al., 2010; Liu et al., 2017; Wagner et al., 2019; Yang and Hong, 2015; Zhou et al., 2020). In addition, these studies show that these same

genes are further induced at later stages of hypoxia response. This likely represents additional events in the hypoxia response activated at later timepoints (Gasch et al., 2016; Kosmacz et al., 2015; Schippers et al., 2024).

To optimise the experimental conditions, O_2 levels of 0.1%, 1% , 4% and 10% were tested in addition to 21% O_2 (normoxia), for different durations (1, 2, 4 and 6 h), and the expression of several HRGs was monitored taking into account the previously observed transcriptional expression dynamics in hypoxia responses: *HRE2* (Licausi et al., 2010; Park et al., 2011), *AOX1a* (Vishwakarma et al., 2018; Wany et al., 2018; Yao et al., 2017), *PCO1* (Gasch et al., 2016; Valeri et al., 2021; Weits et al., 2014) and *ADH1* (Bakshi et al., 2023; Gasch et al., 2016; Giuntoli et al., 2014; Hsu et al., 2011; Kosmacz et al., 2015; Licausi et al., 2010; Liu et al., 2017; Loreti et al., 2005; Yang and Hong, 2015; Zubrycka et al., 2023). The latter codes for alcohol dehydrogenase, whose activity is important to maintain cellular energy production by regenerating NAD+ under hypoxic conditions.

The four genes tested showed different dynamics of gene expression depending on O_2 levels and duration of the hypoxia treatment. Induction of *PCO1* was largely dependent on O_2 levels, in that its expression was higher at 0.1% and 1% O_2 compared to 4%, 10% and 21% (normoxia) O_2 and its level of induction did not increase further beyond one hour of treatment (**Figure 3.4**). *ADH1, HRE2* and *AOX1a* induction was clearer at 0.1% O_2, although also detected at 1% O_2. In contrast to *PCO1*, the expression of these three HRGS continued to increase with longer hypoxia treatments.

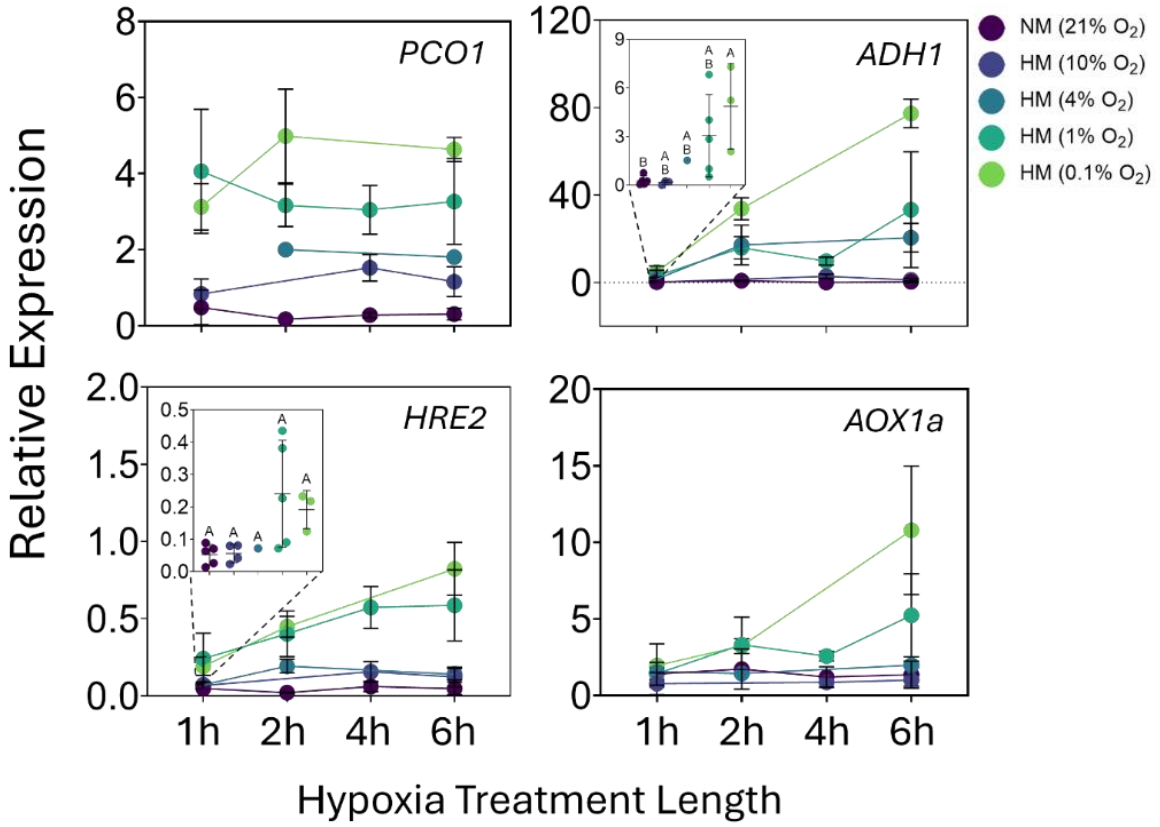

Figure 3.4. Transcriptional changes of hypoxia marker genes depend on O_2 levels and duration of the hypoxia stress. Expression analysis of different hypoxia marker genes (*PCO1*, *ADH1*, *HRE2* and *AOX1a*) with different O_2 levels (21% O_2-purple; 10% O_2-dark blue; 4% O_2-blue; 1% O_2-light blue; 0.1% O_2-green) for 1, 2, 4 and 6 hours. Results are means ± standard deviation (SD) of 2-6 biological replicates (n = 2 to 6). Statistical analysis: two-way ANOVA with Tukey's test ($p < 0.05$); different letters indicate statistically different groups.

These results suggests that in terms of O_2 levels, 0.1% or 1% could be suitable for combined hypoxia/flg22 experiments, and that the duration of the treatment is important to optimise. For the next optimisation steps, 1% O_2 was chosen because (i) 1% O_2 represents a level of oxygen that is low enough to trigger hypoxia responses and sufficient to avoid effects where the plant is energy-deprived; (ii) it is more widely used in the community, so this will allow comparison with a broader range of published studies that also used 1% O_2 (Bui et al., 2015; Eysholdt-Derzsó et al., 2023; Kosmacz et al., 2015; Licausi et al., 2010; Liu et al., 2017; Schmidt et al., 2018; Triozzi et al., 2024; Zhou et al., 2020),and (iii) 1% O_2 represents a level of oxygen that is high enough so plants can still produce ROS (Pucciariello et al., 2012), which is important for the questions addressed.

Finally, careful comparison of the data obtained to previously published results indicated that the expression pattern of *HRE2* and *PCO1* differed from previous reports (Kosmacz et al., 2015; Licausi et al., 2010). While here, *HRE2* was not significantly induced within 1 hour of hypoxia treatment (1% O_2), Licausi et al., (2010) reported differences in *HRE2* expression levels at this timepoint. Similarly, while Kosmacz et al., (2015) reported increased *PCO1* expression levels upon 1% O_2, where *PCO1* expression increased with time, in contrast to our results, where the transcriptional levels remained stable across time (**Figure 3.4**). In addition, Kosmacz et al., (2015) studied *PCO1* expression at different O_2 levels, which in contrast to our results, peaked at 1% O_2 instead of 0.1% O_2. One main difference between our experimental conditions and those of Licausi et al., 2010 and Kosmacz et al., 2015 is that we applied hypoxia in light conditions as opposed to dark. Hence, in subsequent experiments, light availability was also considered as a factor that could affect how hypoxia interacts with the onset of PTI.

3.2.4. Effect of combined hypoxia/flg22 on *RBOHD* expression

One of the main questions addressed in this PhD is "*What is the role of RBOHD in the molecular response to the activation of innate immune responses under hypoxic conditions?*". *RBOHD* expression levels are induced rapidly upon either hypoxia or flg22 stress (**Section 1.4.2**), and RBOHD-dependent ROS production regulates downstream hypoxia and flg22 signalling (Dubiella et al., 2013; Peláez-Vico et al., 2023). We therefore hypothesised that RBOHD could act to regulate plant responses in the context of a hypoxia/flg22 co-treatment, and presumed that hypoxia-dependent changes in *RBOHD* expression could modulate flg22 responses differently under hypoxia compared to normoxic conditions. In this scenario, *RBOHD* expression levels could be differently regulated under the combined HF treatment compared to NF.

To assess the dynamics of *RBOHD* expression under HF conditions, we investigated the effect of different durations of hypoxia pre-treatment prior to the addition of flg22. For HF conditions, plants were maintained under hypoxia for one hour after the addition of flg22, or for NF treatment, plants were kept under normoxic during the entire duration of the experiment. The duration of the hypoxia pre-treatments were chosen as follows:

- 1 hour of hypoxia pre-treatment accounted for early hypoxia transcriptional responses and genes with roles in both hypoxia and immunity, such as *ADH1* (Barreto et al., 2022; Brunello et al., 2024; Castellana et al., 2024; Hsu et al., 2013; Licausi et al., 2010; Loreti et al., 2005; Yang et al., 2011), *CPK28* (Bakshi et al., 2023; Monaghan et al., 2014), *APX1*(Hong et al., 2023; Yang et al., 2017), *WRKY22* (Asai et al., 2002; Hsu et al., 2013) and *RBOHD* (Zabela et al., 2002; Dubiella et

al., 2013; Kadota et al., 2014; Li et al., 2014; Yang et al., 2017; Yang and Hong, 2015). We hypothesised that this early hypoxic-dependent induction of plant immunity regulators could potentially regulate subsequent flg22 responses in combination with hypoxia.

- 2 hours of hypoxia pre-treatment should result in hypoxia-dependent ROS production, which could affect flg22 response. As shown in Pucciariello et al. (2012), low O_2 levels trigger ROS production between 1 and 2 hours after the establishment of anoxic conditions. In addition, these authors suggested that this ROS production is probably mediated by a member of the RBOH family, characterised by presenting NADPH oxidase activity, which was later demonstrated by Gonzali et al., 2015 and Yu et al., 2024. In addition, hypoxic ROS production could modulate flg22 responses through the induction of ROS-responsive genes such as *RBOHD* (Nakagami et al., 2006), *OXIDATIVE SIGNAL-INDUCIBLE 1 (OXI1)* (Nakagami et al., 2006), *REDOX RESPONSIVE TRANSCRIPTION FACTOR 1* (*RRTF1*) (Hong et al., 2023), *ERF6* (Meng et al., 2013; Wang et al., 2013), or *ZINC FINGER ARABIDOPSIS THION 10 (ZAT10)* and *ZAT12* (Davletova et al., 2005; Rossel et al., 2007).

- 4 hours of hypoxia pre-treatment was used because it gives sufficient time to stabilise RAP2.2 and RAP2.12 in the nucleus (Kosmacz et al., 2015). This is a major event in hypoxia response and it is also relevant to combined hypoxia and flg22 responses, as it has been demonstrated that RAP2.12 can induce the expression of several immunity regulators such as *SID2* (Koo et al., 2024a) or *RBOHD* (Yao et al., 2017). In addition, Kosmacz et al., 2015 showed that together with RAP2.12 nuclear location, several HRGs reached their maximal expression levels within 3-4 hours of hypoxic conditions, suggesting that hypoxia signalling could crosstalk with the onset flg22 responses at this timepoint.

Consistent with previous reports, under NF conditions, *RBOHD* expression levels were reproducibly induced within 1 hour after the addition of flg22 (Bai et al., 2023; Trujillo et al., 2008). Under HF conditions (with either a 1-hour or 2-hour hypoxia pre-treatment), *RBOHD* induction was similar as that observed under NF conditions (**Figure 3.5**). However, 4 hours of hypoxic conditions prior to flg22 treatment triggered a stronger transcriptional induction of *RBOHD* in HF compared to NF conditions (**Figure 3.5**).

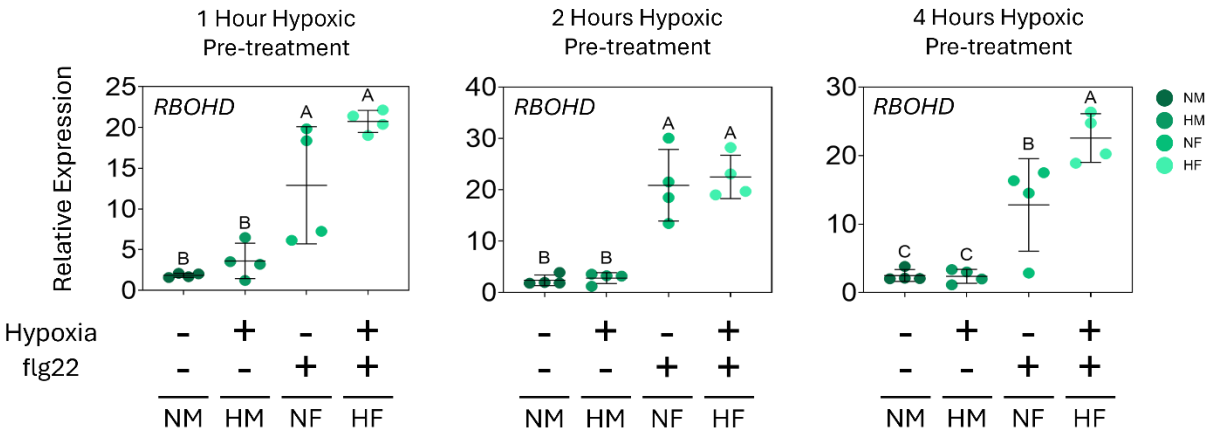

Figure 3.5. *RBOHD* transcriptional levels in seedlings upon combination of hypoxia and flg22 with different duration of hypoxia pre-treatment. Expression analysis of *RBOHD* upon normoxia (21%O_2+mock solution (NM)); hypoxia (1%O_2+mock solution (HM)); flg22 (21%O_2+100 nM flg22 (NF)) or hypoxia+flg22 (1%O_2+100 nM flg22 (HF)), with different lengths of hypoxia or normoxia pre-treatments (1, 2 and 4 hours). Ten-day old wild-type Col-0 seedlings were used. Results are means ± standard deviation (SD) of 4 biological replicates (n = 4). Statistical analysis: one-way ANOVA with Tukey's test ($p < 0.05$); different letters indicate statistically different groups.

3.2.5. Conclusions

Altogether, these findings indicate that depending on the duration of the hypoxia pre-treatment, *RBOHD* could respond differently to flg22 treatment. At 1% O_2, a 4-hour hypoxia pre-treatment is needed to observe an effect of hypoxia on flg22-dependent transcriptional regulation of *RBOHD*. Therefore, for this study, a 4-hour of hypoxia pre-treatment followed by flg22 treatment for 1 hour were therefore chosen for studying the role of *RBOHD* in mediating plant responses to the combination of hypoxia and flg22 treatments because (i) it gives hypoxia response programmes sufficient time to be activated, and (ii) longer treatment lengths could trigger secondary effects such as cell death or large-scale metabolic shifts that would make it more difficult to study the role of ROS. These conditions were used in all assays below.

3.3. Contributions and role of RBOHD in HF stress responses

3.3.1. Apoplastic ROS dynamics under combined hypoxia and flg22 treatment

As stated in **section 1.4.2**, RBOHD functions in both hypoxia and flg22 responses, triggering apoplastic ROS production in response to environmental cues in a tightly regulated process. In hypoxia response, several activators of RBOHD regulate its activity, such as CPK16, ROP2 or HRU1 (**Figure1.12**) (Baxter-Burrell et al., 2002; Gonzali et al., 2015; Yu et al., 2024). In the context of plant immunity, activators of RBOHD include BIK1, XLG2, CRK2, SIK1, DIACYLGLYCEROL KINASE 5 (DGK5) or CPK5 (**Figure 1.11**) (Dubiella et al., 2013; Kadota et al., 2015; Kimura et al., 2020; Kong et al., 2024; Li et al., 2014; Köster et al., 2025; Qi et al., 2024; Liang et al., 2016; Zhang et al., 2018). This differential mechanism of activation highlights that the context-specific signal integration of RBOHD into distinct signalling networks may not be only at the transcript and protein level, but also at the ROS production level, enabling plants to fine-tune the magnitude, duration and spatial distribution of ROS production in response to combined stress conditions.

Experiments performed by Dr. Catherine Doorly indicated that in NF samples, the characteristic transient ROS production previously attributed to RBOHD activation was detected, with maximum luminescence reached within 15-20 minutes after flg22 treatment. By contrast, RBOHD function was differently regulated in HF, where plants were pre-treated with 2 hours of hypoxia treatment in anaerojars prior to flg22 treatment. This assay showed that the oxidative burst triggered by flg22 was markedly altered under hypoxic conditions, in terms of both the kinetics and the amplitude of the ROS production. Specifically, under hypoxia the flg22-triggered ROS production failed to reach the peak observed under normoxia, and the subsequent desensitisation was altered, leading to a more sustained ROS production over time (**Figure 3.6**). These features indicate that RBOHD activity was not simply reduced by lack of oxygen but rather was regulated through alternative signalling events.

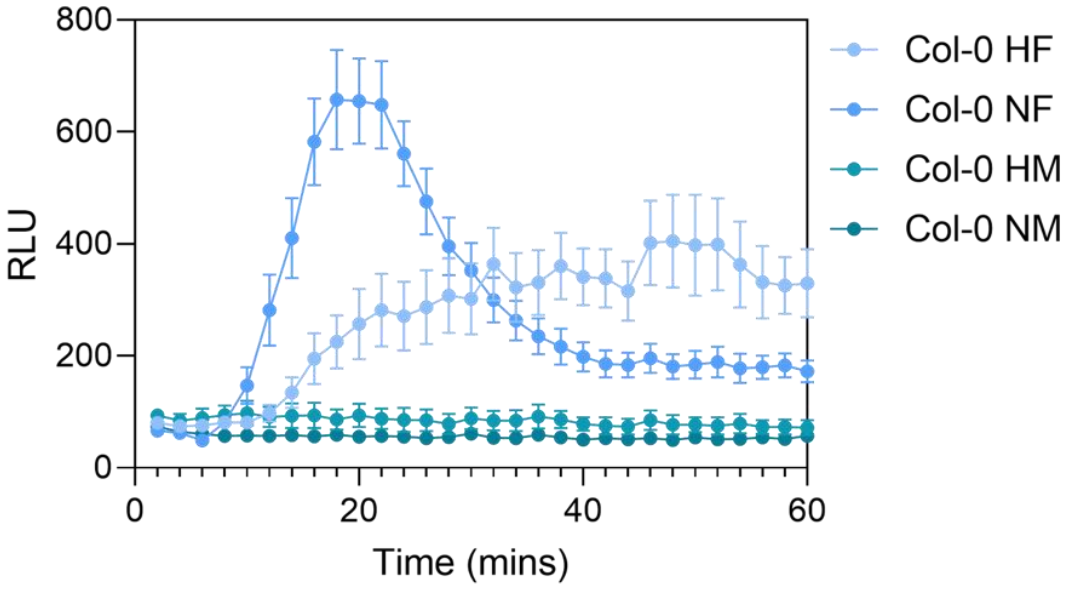

Figure 3.6. Apoplastic ROS production in HF conditions. The luminol-based approach was used to measure apoplastic ROS production upon Normoxia Mock (NM), hypoxia mock (HM), normoxia flg22 (NF), and hypoxia flg22 (HF). Leaf discs of 4-week old plants grown in short-day conditions were used. Results are means ± Standard Error of the Mean (SEM) of the average of 12 biological replicates (n = 12).

This experiment was performed by Dr. Catherine Doorly rather than by the author because it was undertaken under significant time constraints and required a highly time-sensitive assay workflow. Although suitable for longer hypoxia treatments, hypoxia chambers were not technically compatible with the CLARIOstar-based ROS measurement workflow, as it was difficult to maintain hypoxic conditions consistently during sample transfer, flg22 application, and plate-reader measurements. Nevertheless, future optimisation of this assay could employ reader-integrated atmospheric control systems, such as the Atmospheric Control Unit (ACU) for the Clariostar, which enables independent regulation of O_2 and CO_2 within the plate reader chamber during kinetic measurements.

3.3.2. Transcriptional reprogramming under HF conditions reveals RBOHD as a component of hypoxia–flg22 crosstalk

To further confirm a role of *RBOHD* in combined hypoxia/flg22 responses, we analysed the expression of different PTI marker genes in 4-week old plants, together with that of genes previously identified to participate in the crosstalk between hypoxia and immunity and in the

regulation of RBOHD function. As expected, PTI marker genes such as *FRK1* or *NHL10* were induced in samples treated with flg22 (**Figure 3.7**), and the hypoxia marker gene *ADH1* was only induced in samples treated with hypoxia (**Figure 3.7**). Expression analysis demonstrated slight transcriptional upregulation, although not statistically significant, of *BIK1* in HF conditions compared to NF (**Figure 3.7**). Although none of these genes were transcriptionally differentially regulated upon HF compared to NF in the wild type, in the *rbohd* mutant, *BIK1* was hyper-induced in HF compared to NF (**Figure 3.7**). Similarly, although *WRKY22* expression did not differ between NF and HF in the wild type, it was hyper-induced in HF compared to both NF in the *rbohd* mutant and also compared to HF in the wild type. This suggests a specific role of WRKY22 in combined hypoxia/flg22 experiments, in line with previous findings in *Arabidopsis* using waterlogging and the bacterial pathogen *Pseudomonas syringae* (Hsu et al., 2013). Furthermore, although *WRKY33* was not differentially regulated in HF, one of its target genes, *CYP71A13*, was transcriptionally upregulated in *rbohd* mutant in NF compared to the wild type, this upregulation was reduced in HF conditions compared to NF in the *rbohd* mutant (**Figure 3.7**). Collectively, these data indicate that, while early PTI transcriptional markers respond largely as expected to flg22 and hypoxia when applied individually, combined hypoxia/flg22 uncovers RBOHD-dependent layers of regulation that are not present when stresses are applied individually. However, due to the central role of RBOHD in stress responses the mechanisms behind this expression patterns upon HF remain undiscovered, as they can be loss of RBOHD-dependent negative feedback, compensatory activation of other pathways, altered redox signalling, changes in calcium and kinase signalling, developmental or physiological differences in the mutant, etc.

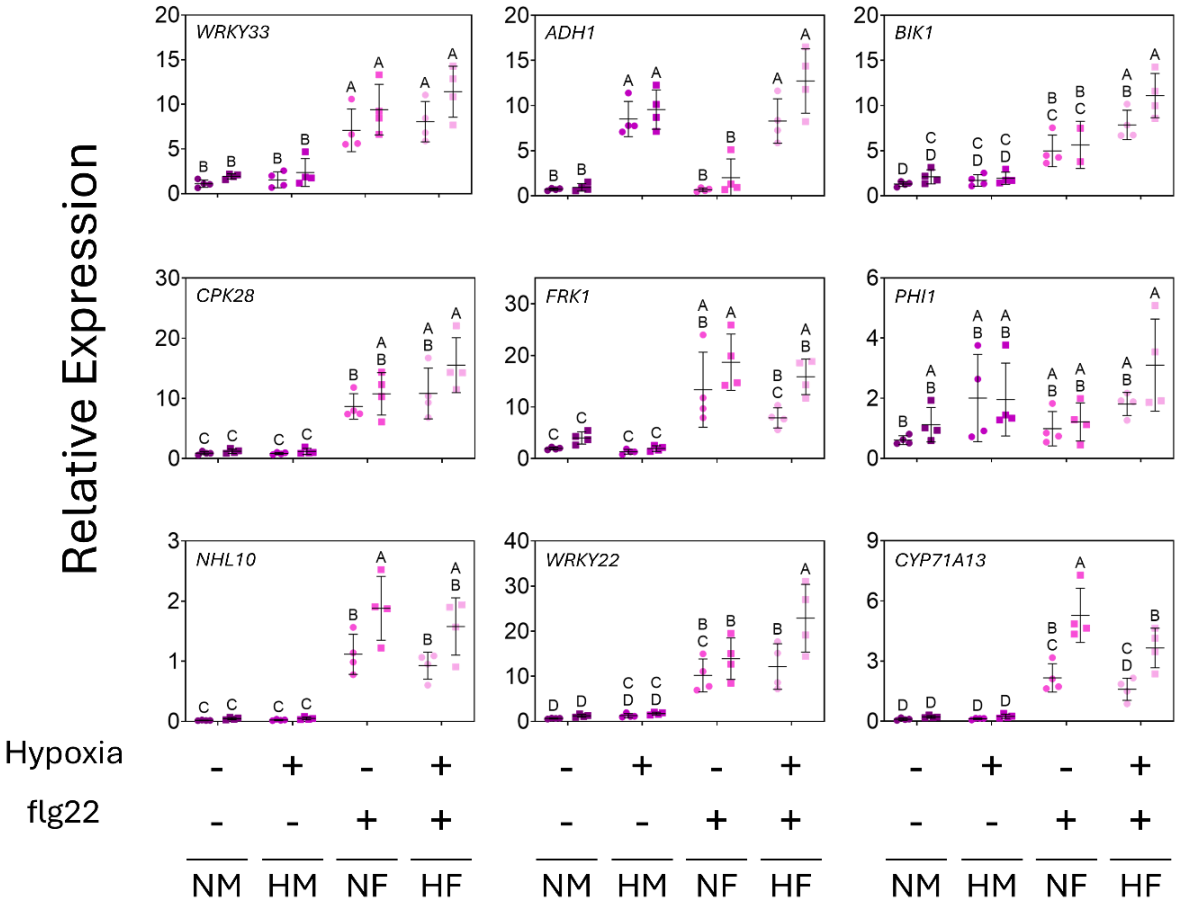

Figure 3.7. Transcriptional changes of hypoxia and PTI associated genes in HF conditions. 4-week old wild type (circles) and *rbohd* (squares) plants undergoing NM, HM, NF or HF treatment in the light (pink). Here, a 4-hour hypoxia pre-treatment, followed be 1 hour combined treatment was used (hypoxia: 1% O_2). Results are means ± standard deviation (SD) of 4 biological replicates (n = 4). Statistical analysis: two-way ANOVA with Tukey's test ($p < 0.05$); different letters indicate statistically different groups.

3.3.3. Conclusions

Altogether, the combination of both luminol assays performed by Dr. Catherine Doorly and the expression patterns of hypoxia and PTI-associated genes in wild-type and *rbohd* mutant plants show that the combination of hypoxia and flg22 treatments triggers unique stress responses and RBOHD plays a role in the differential regulation of PTI-associated genes in these unique stress responses.

3.4. Regulation of *RBOHD* expression in combined hypoxia and flg22 experiments

3.4.1. Effect of light availability on *RBOHD* expression in combined hypoxia/flg22

As outlined in section 3.2.3, some of the transcriptional responses to hypoxia that we observed were different from previous reports, and we hypothesised that light availability in our hypoxia pre-treatments could explain some of the differences. Given that plants generate their energy primarily through photosynthesis, which is a light-dependent process, dark conditions during hypoxic conditions inhibit (i) the plant local production of O_2 and (ii) glucose production for downstream use in anaerobic fermentation. Therefore, in the dark, the plant experiences an energy deficit, leading to stronger activation of hypoxic stress responses (Kunkowska et al., 2023). In addition, light has emerged as a critical environmental cue influencing plant-pathogen interactions. Specifically, light can influence plant immunity through light receptors, such as blue-light photoreceptor CRYPTOCHROME 1 (CRY1) (Hao et al., 2025; Wu and Yang, 2010) and CRY2 (Jeong et al., 2010) or through regulators of light signalling such as ELONGATED HYPOCOTYL 5 (HY5) (Liu et al., 2025). In addition to light signalling, the circadian rhythm also influences plant responses to hypoxia and pathogens. Intriguingly, hypoxia response genes and plant immunity genes show opposite transcriptional trends, whereby hypoxia responses are transcriptionally induced upon dark conditions (Triozzi et al., 2024) while immunity genes are transcriptionally induced upon light conditions (Bhardwaj et al., 2011; Goodspeed et al., 2012; Korneli et al., 2014; Lai et al., 2012; Wang et al., 2011). These findings suggest that depending on light availability during HF treatment, the effect of hypoxia on the onset of flg22 responses could be different, perhaps as the result of plants prioritizing response to one stress over the other. To test this, we subjected seedlings to NM, HM, NF, HF conditions with 4 hours of hypoxia pre-treatment followed by treatment with flg22 for 1 hour in the dark and determined the transcriptional changes of *RBOHD*, which was compared to our results obtained when plants were treated with these conditions in the light (**Figure 3.8**).

In contrast to light conditions, *RBOHD* expression levels in HF did not differ from NF, indicating that the HF-dependent hyper-induction of *RBOHD* observed in the light was absent in darkness (**Figure 3.8**). Interestingly, though, comparing *RBOHD* expression in NF conditions in the dark and in the light, indicated that *RBOHD* is already more strongly induced in the dark under NF and HF conditions compared to those conditions in the light. This comparison suggests that dark flg22-treated samples induce more strongly *RBOHD*, potentially masking any hypoxia-

dependent hyper-induction in HF conditions. These results suggest that light availability during HF conditions is a factor that needs to be taken into account as it contributes to modulating the synergistic interaction by which hypoxia further induces flg22-induced *RBOHD*.

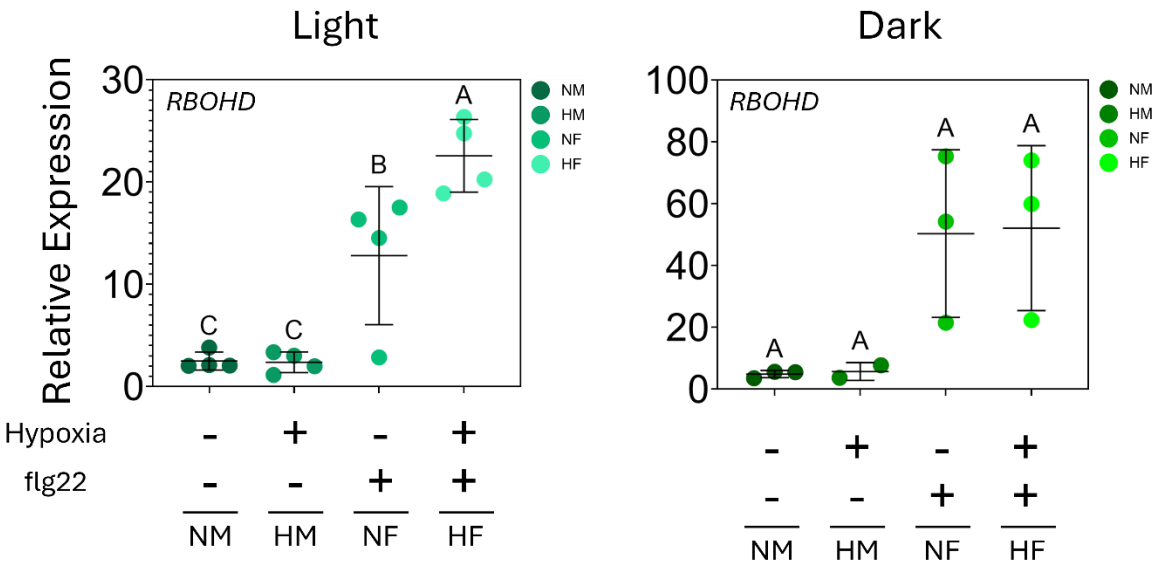

Figure 3.8. Light availability contributes to regulating *RBOHD* transcriptional changes in HF conditions in seedlings. Expression analysis of *RBOHD* in the light and in the dark under NM, HM, NF and HF (same conditions as in **Figure 3.5**). The data for samples obtained in the presence of light are the same as in **Figure 3.5** but added here to facilitate comparison. Ten-day old wild-type Col-0 seedlings were used. Results are means ± standard deviation (SD) of 3 or 4 biological replicates (n = 3 or 4). Statistical analysis: one-way ANOVA with Tukey's test ($p < 0.05$); different letters indicate statistically different groups.

3.4.2. Effect of development on *RBOHD* expression in combined hypoxia/flg22

Responses to single stresses (including hypoxia and flg22) differ depending on the developmental stage at which plants encounter them. In hypoxic conditions, age-dependent regulation of plant responses rely on ANAC017 differential regulation of target genes, as they are in genomic regions that move towards a heterochromatic state as development proceeds, hindering ANAC017-dependent transcriptional activation (Bui et al., 2020). In addition, an age-dependent mechanism also restrains ERF-VII activity on core HRGs, independently of the N-degron pathway (Giuntoli et al., 2017). Altogether, these mechanisms suggest that juvenile plants

possess better tolerance to low O_2 levels than adult plants, although the age-dependent mechanism governing hypoxia responses are not fully understood.

Plant immunity is also regulated by plant development as proceeds through a process called Age-Related Resistance (ARR), which allows plants to gain or reinforce defences against pathogens during the process of host maturation (reviewed in Hu and Yang, 2019). An example of this is the age-dependent regulation of *FLS2* (the receptor for flg22), whose expression is repressed at early developmental stages but not at later stages (Winter et al., 2011; Zou et al., 2018). It is intriguing as well to note that that hypoxia and immunity have opposite outcomes when it comes to age-dependent responses, in that juvenile plants are more tolerant to hypoxic conditions, but more susceptible to pathogens, while adult plants are more sensitive to hypoxic conditions and more resistant to pathogen infection.

To determine which developmental stage might be best to use to study the role of *RBOHD* in mediating the effect of hypoxia on the onset of PTI, *RBOHD* expression levels were analysed across NM, HM, NF and HF treatments in both light and dark conditions in 4-week old plants as opposed to 10-day old seedlings used pre viously. This also allowed us to determine whether the developmental stage could affect how *RBOHD* expression is regulated under HF treatment. As shown in **Figure 3.8-9**, in the light, *RBOHD* expression in 4-week old plants had the same pattern as in seedlings, as it was hyper-induced in HF compared to the already induced NF-treated plants. In 4-week-old plants, *RBOHD* transcript levels were higher in dark HF compared to dark NF, indicating that, in contrast to 10-day old seedlings, mature plants further induce RBOHD when exposed to combined hypoxia and flg22 in the dark. Moreover, when HF samples were compared across light/dark conditions during stress treatments, *RBOHD* expression was significantly higher in the dark than in the light. This mirrors the pattern observed in seedlings, where *RBOHD* transcripts were generally higher in the dark than in light, but in 4-week-old plants the dark treatment under HF led to an additional hypoxia-driven increase over NF, revealing a dark-dependent induction at this developmental stage. This comparison indicates that *RBOHD* expression dynamics upon HF treatment are different depending on the developmental stage of the plants and light status during the treatment. These differences suggest additional layers of transcriptional control for *RBOHD* dependent on both light availability during the treatment and the developmental stage of the plant.

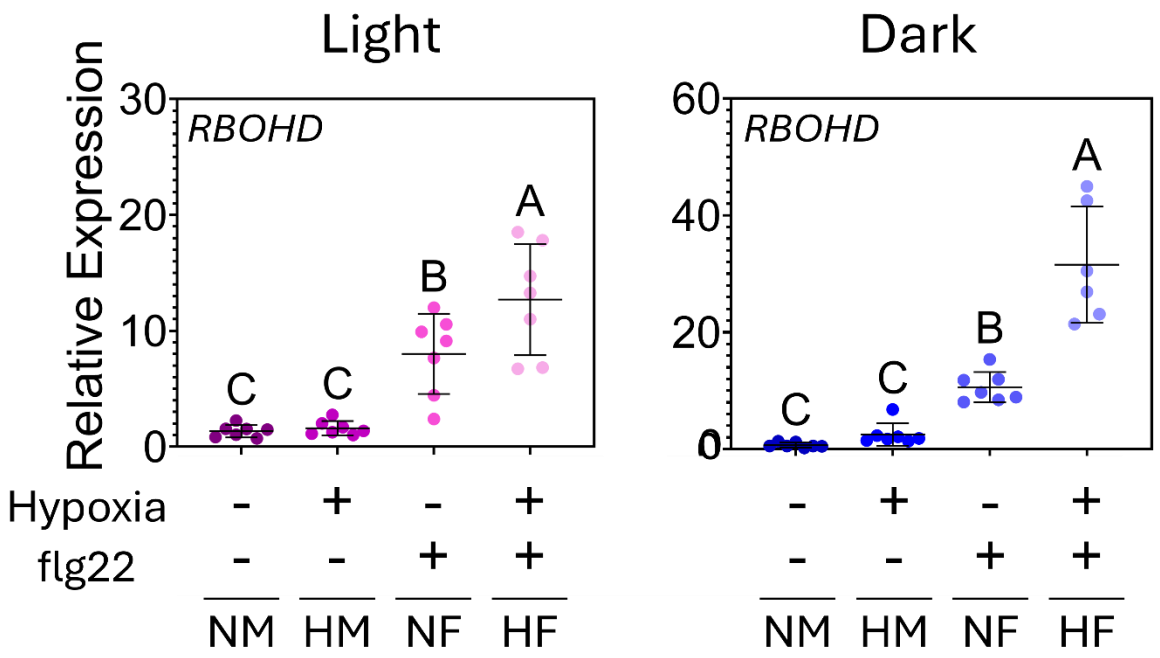

Figure 3.9. Differential expression of *RBOHD* upon HF treatment in 4-week old wild-type Col-0 plants. Expression analysis of *RBOHD* in the light (pink) and in the dark (blue) in NM, HM, NF and HF (conditions as in **Figure 3.5**). Results are means ± standard deviation (SD) of 3 biological replicates (n = 3). Statistical analysis: two-way ANOVA with Tukey's test ($p < 0.05$); different letters indicate statistically different groups.

Because *RBOHD* transcripts were differentially regulated by light availability during the combined hypoxia/flg22 treatment, we next asked whether the absence of RBOHD in the dark (i.e. in a *rbohd* mutant) would alter the expression of candidate genes under HF. To address this, the same experiment as in **Figure 3.7** was performed, but in the dark and the results were compared (**Figure 3.10**). *ADH1*, a hypoxia response marker gene, was more strongly induced in dark HM compared to light HM conditions. The wild type and the *rbohd* mutant behaved similarly, suggesting that *RBOHD* is not implicated in this stronger expression of *ADH1* in the dark. *NHL10* expression was induced to the same extent in NF or HF, in the wild type as well as the *rbohd* mutant. Light/dark also did not affect this up-regulation, so that RBOHD or light/dark or hypoxia do not impact on *NHL10* induction. *WRKY22* up-regulation in NF was not influenced by RBOHD or light/dark conditions. In contrast, in HF conditions, the hyper-induction of WRKY22 in dark HF compared to light HF was lost in the *rbohd* mutant, suggesting that in HF conditions, RBOHD could contribute to a stronger expression of *WRKY22* in the dark compared to the light. Similar observations were made for the hyper-induction of *CPK28* and *BIK1* in dark HF compared to light

HF, with a dependency on *RBOHD*. These data indicate that the *CPK28* and *BIK1* transcriptional hyper-induction observed in the dark under combined hypoxia and flg22 requires functional RBOHD. Lastly, for *FRK1*, dark conditions with NF significantly reduced the expression of this gene in both wild type and *rbohd* mutant compared to light NF conditions. This dark-dependent repression of *FRK1* was lost in the wild type in HF, while it was retained in the *rbohd* mutant in HF, suggesting that RBOHD could contribute to the regulation of *FRK1* in HF conditions, in a light/dark dependent manner.

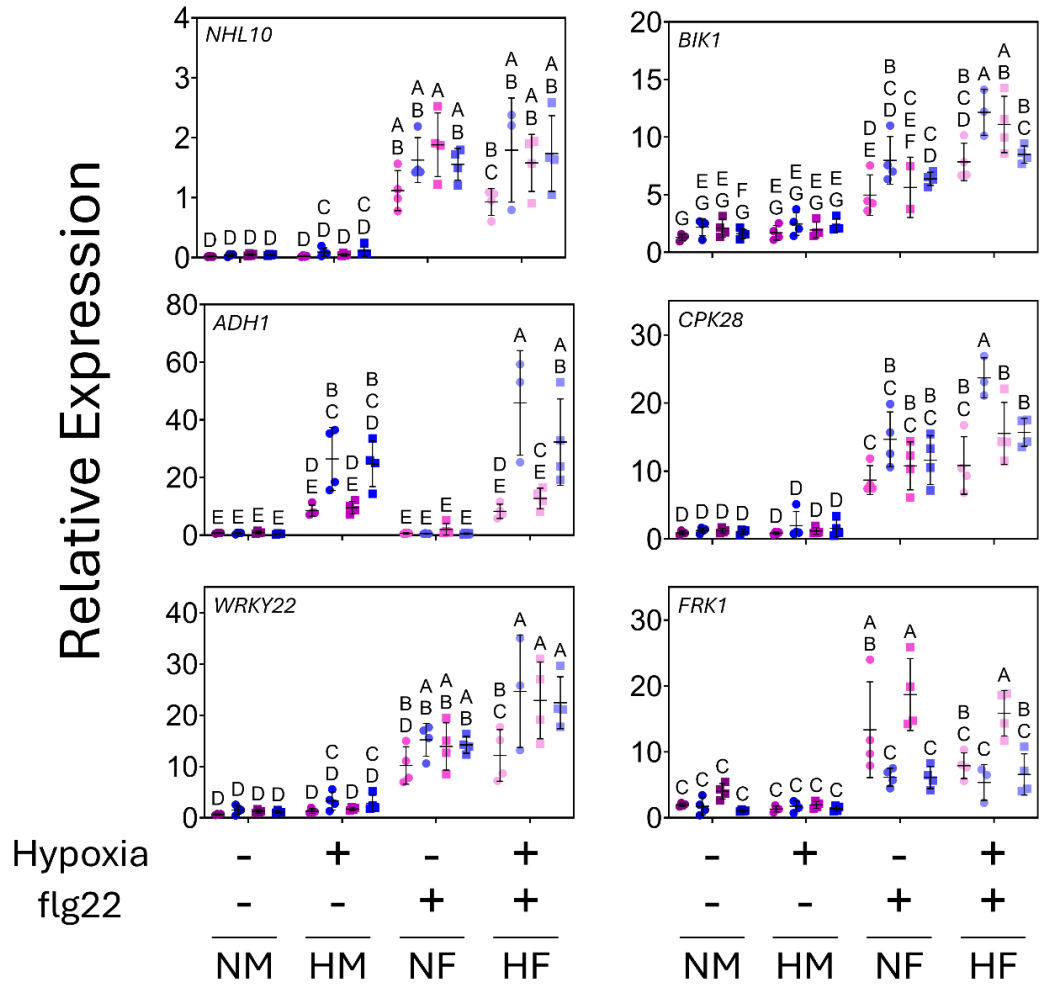

Figure 3.10. Transcriptional changes of candidate genes involved in the crosstalk of hypoxia/flg22 comparing light and dark conditions. Expression analysis of candidate genes involved in HF crosstalk (*NHL10, ADH1, WRKY22, BIK1, CPK28* and *FRK1*) in 4-week old wild type (circles) and *rbohd* (squares) plants undergoing NM, HM, NF or HF treatment in the light (pink) from **Figure 3.7** or in the dark (purple). Results are means ± standard deviation (SD) of 3-4 biological replicates (n = 3-4). Statistical analysis: two-way ANOVA with Tukey's test ($p < 0.05$); different letters indicate statistically different groups.

In summary, the data indicate that (i) *RBOHD* expression is differentially regulated upon HF treatment, with differences between light/dark or developmental stage; and (ii) in a *rbohd* mutant, PTI associated genes do not have the same expression pattern in HF compared to NF, again also depending on light/dark conditions. Together, this points to a role of *RBOHD* in the regulation of plant responses to HF, and to the need to identify which TFs might contribute to the differential regulation of *RBOHD* expression in HF conditions compared to NF.

3.4.3. Identifying potential regulators of *RBOHD* expression in HF

Identifying the transcription factors that could mediate the differential expression of *RBOHD* in HF compared to NF conditions would be important to understand how *RBOHD* is integrated in the molecular crosstalk between hypoxia and flg22 responses. Several TFs have been shown to be involved in the transcriptional regulation of *RBOHD* during development and single stresses (**Table 3.1**).

Table 3.1. List of identified *RBOHD* transcriptional regulators that directly bind to the *RBOHD* promotor.

Gene	Functional Involvement	Reference
WRKY33	Response to fungi	(Zhao et al., 2020)
WRKY55	Leaf Senescence	(Wang et al., 2020)
Brassica napus WRKY generating ROS 1 (WGR1)		(Yang et al., 2018)
BRASSINAZOLE RESISTANT 1 (BZR1) and SHORT-ROOT (SHR)	Periclinal division	(Tian et al., 2022)
ABSCISIC ACID INSENSITIVE 4 (ABI4)	Salinity stress responses	(Luo et al., 2021)
RAP2.12	Hypoxia stress responses	(Yao et al., 2017)
WRKY46 and MYC2	Herbivore responses	Hao et al., 2024)

Among these *RBOHD* transcriptional regulators, WRKY33 has a well-established role in immune responses but has also been shown to contribute to hypoxia responses, and RAP2.12 is

a central regulator of hypoxia responses, but has emerging roles in plant immunity (sections 1.4.2.2 and 1.4.2.3). However, whether these TFs modulate *RBOHD* transcription under combined hypoxia and flg22 treatment is unknown and was tested as outlined below.

3.4.3.1. WRKY33 expression under HF conditions

In a first step to determine if WRKY33 is involved in regulating *RBOHD* expression during combined hypoxia/flg22 treatments at both developmental stages used in this work (10-day old seedlings and 4-week old plants) and light/dark conditions, we monitored the expression of this TF across NM, HM, NF and HF treatments. In seedlings, conclusions were difficult to draw due to experimental variability and the lack of statistically significant differences, even though the data showed a trend towards increased expression of *WRKY33* in NF and HF samples (compared to NM and HM), both in the dark and in the light (**Figure 3.11**). Although not significant, *WRKY33* expression in light HF in seedlings seemed to be in average higher than in NF, thus mimicking (with more variability) the expression pattern of *RBOHD* in the same conditions (**Figure 3.11**). However, the opposite trend is seen in seedlings treated with dark HF conditions, where on average, *WRKY33* expression levels seem to be lower compared to dark NF (**Figure 3.11**). Similarly to seedlings, in 4-week old plants undergoing treatment under different light regimes, average *WRK33* expression did not change significantly when comparing NF and HF conditions (**Figure 3.11**), which is different from the expression of *RBOHD* in the same experimental conditions, in that *RBOHD* was more strongly upregulated in HF than NF (**Figure 3.7**). Taken together, these results suggest that the hyper-induction of *RBOHD* expression in HF conditions may be independent of *WRKY33*. However, considering the level of variation, specifically in dark HF, additional replicates are needed to confirm this result.

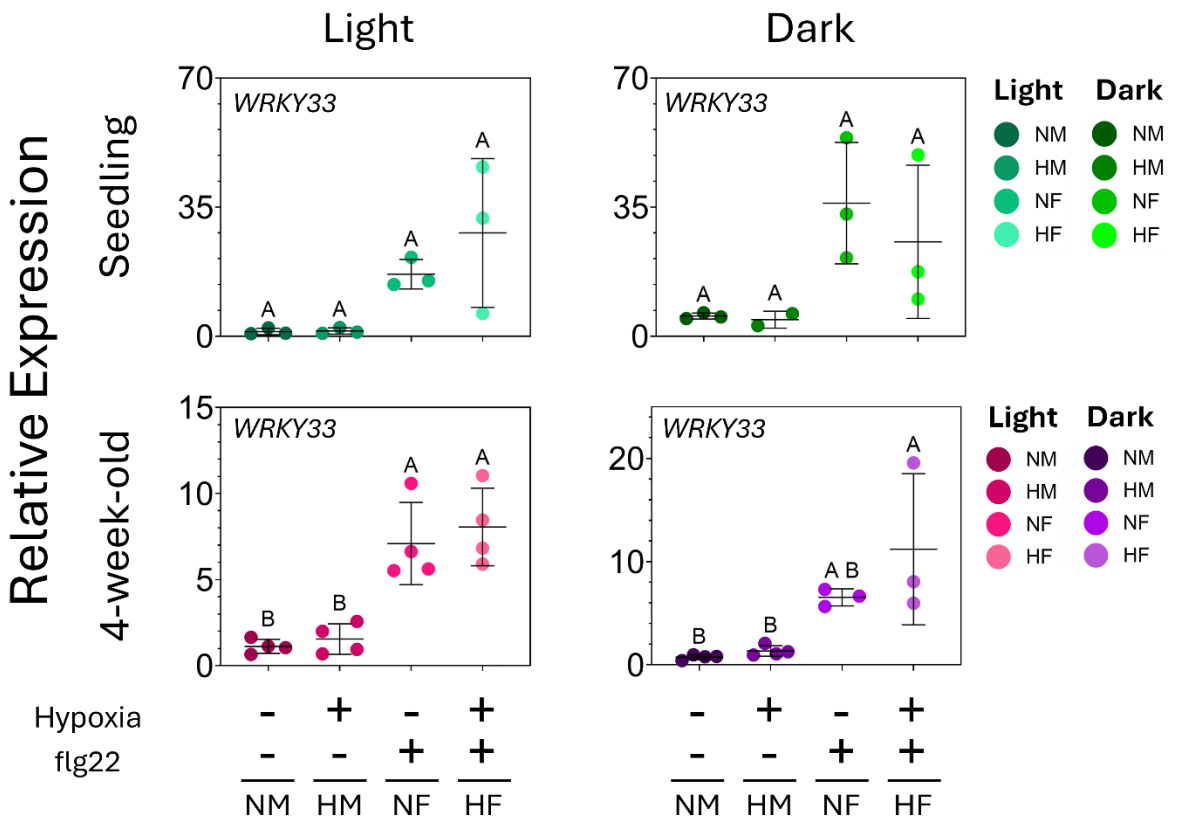

Figure 3.11. *WRKY33* transcriptional levels upon combination of hypoxia and flg22 depending on light availability and developmental stage. Expression of *WRKY33* in 10-day old seedlings (green datapoints) or in 4-week old plants (purple datapoints) undergoing NM, HM, NF or HF treatment in the light or in the dark. Results are means ± standard deviation (SD) of 3 biological replicates (n = 3). Statistical analysis: one-way ANOVA with Tukey's test ($p < 0.05$); different letters indicate statistically different groups.

3.4.3.2. Exploring a link between RBOHD expression in HF and ERFVII TFs

As stated in the introduction, three ERFVII TFs, RAP2.2, RAP2.12 and HRE1 are known to regulate *RBOHD* expression upon hypoxia treatment through both direct and indirect mechanisms (Yang et al., 2017; Yao et al., 2017), we hence sought to test a potential regulatory role of ERFVIIs in the hyper-induction of *RBOHD* expression during HF treatment in the light. To do so, we assessed *RBOHD* expression levels in seedlings in different *ERFVII* mutant backgrounds. 10-day old seedlings was chosen as the developmental stage for these experiments as the activities of the ERFVIIs are at their highest and decrease as development proceeds (Giuntoli et al., 2017). The mutants used were the *erfvii* quintuple mutant, which carries T-DNAs in all 5 *ERFVII*-coding genes (RAP2.2/3/12 and HRE1/2), as well as the *rap2.2/3/12* triple and *hre1/2 double* mutants so that the potential role of either the 3 *RAP*s or the 2 *HRE*s could be determined (Abbas et al., 2015).

Triple mutant *rap2.2/3/12* was used instead of single *rap2.12* mutant, as these transcription factors have partially redundant functions, and the phenotype of *rap2.12* alone may therefore be masked by compensation from RAP2.2 and RAP2.3. The latter could be relevant because Licausi et al., 2010 showed that *HRE1* and *HRE2* are transcriptionally induced during hypoxia, while *RAP2.2*, *RAP2.3* and *RAP2.12* are not transcriptionally induced also independently of hypoxic conditions.

Despite having 4 biological replicates for each set of conditions, the RT-qPCR data obtained remained variable, making it difficult to draw conclusions with confidence. In the quintuple *erfvii* mutant, *RBOHD* hyper-induction upon HF in the light appeared to be suppressed (**Figure 3.12**). The *rap2.2/3/12* and *hre1/2* mutants displayed the same transcriptional dynamics for *RBOHD* as the quintuple *erfvii* mutant, but with slightly higher expression levels (**Figure 3.9 and 3.12**), presumably because of the remaining ERFVII activity in the double and triple mutants. These results suggest that the ERFVIIs could play a role in the hyper-induction of RBOHD during HF treatment in the light in seedlings, and that these were functionally redundant, which is consistent with previous reports (Bui et al., 2015; Gasch et al., 2016; Papdi et al., 2015; Yao et al., 2017).

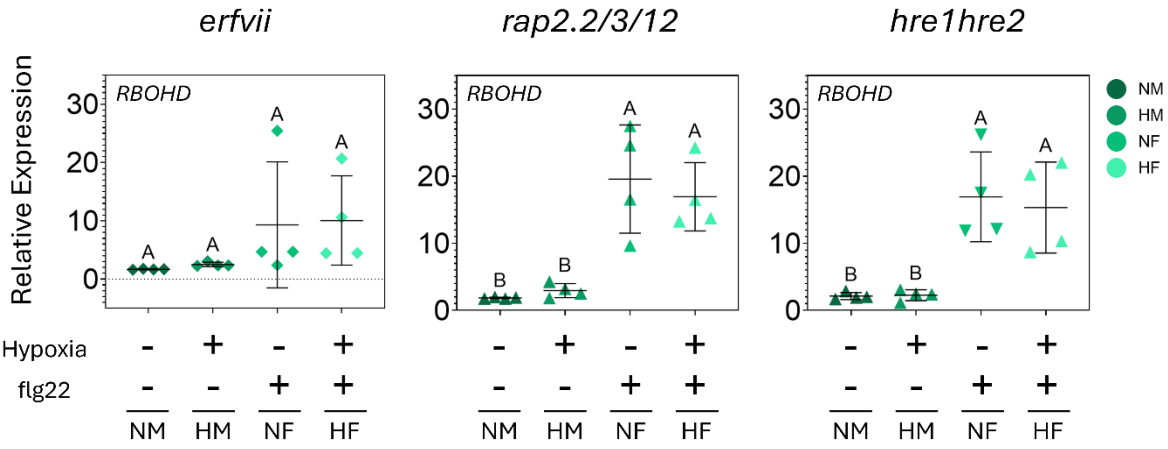

Figure 3.12. ERFVIIs contribute to the transcriptional regulation of *RBOHD* in HF conditions. Expression analysis of *RBOHD* in 10-day old seedlings in NM, HM, NF and HF conditions in the light. Results are means ± standard deviation (SD) of 4 biological replicates (n = 4). Statistical analysis: one-way ANOVA with Tukey's test ($p < 0.05$); different letters indicate statistically different groups.

3.4.3. Conclusions

Altogether, *RBOHD* transcript levels were shown to be hyper-induced in a combination of hypoxia and flg22 treatments. Light availability plays a role in the hyper-induction of *RBOHD* expression under HF compared with NF conditions in seedlings, but darkness likely masks the hypoxia-dependent transcriptional regulation of *RBOHD* in dark HF. However, in 4-week old plants, hyper-induction of RBOHD in HF compared to NF is present irrespective of dark/light conditions. Noteworhty, *RBOHD* transcript levels were further induced in dark HF compared to light HF, indicating distinct mechanisms in charge of controlling transcriptional regulation of *RBOHD* in HF conditions. We examined the roles of previously identified *RBOHD* transcriptional regulators, including *WRKY33* and the *ERFVIIs*. Although too variable, the data obtained suggest a potential role of the ERFVIIs in this hyper-induction of *RBOHD* in HF compared to NF.

3.5. Combined hypoxia and flg22 signalling differentially regulates RBOHD protein abundance and reveals CPK28 as a candidate regulator

Although transcriptional profiling revealed differential *RBOHD* dynamics in HF conditions, transcript abundance does not necessarily correlate with protein levels. We therefore complemented the transcriptional expression analysis of *RBOHD* with the monitoring of endogenous RBOHD at the protein level under NM, HM, NF and HF conditions, thereby providing a more comprehensive understanding of RBOHD regulation in combined hypoxia/flg22 conditions. The regulation of RBOHD protein levels has not been studied under hypoxic conditions. In contrast, regulation of RBOHD stability is understood to some extent in the context of plant immunity, such as (i) the PBL13 and PIRE1- dependent ubiquitination of RBOHD (Lee et al., 2020), or (ii) PA-dependent enhanced stability of RBOHD (Kong et al., 2024; Qi et al., 2024). The latter might also be relevant under hypoxic conditions, considering the dual role of PA in regulating plant responses to hypoxia and pathogens. The different genes known to be involved in regulasting RBOHD protein levels are summarised in **Table 3.3**.

Table 3.3. List of regulators of RBOHD protein stability.

Gene	Functional Involvement	Role in RBOHD Stability	Reference
CONSTITUTIVE EXPRESSER OF PATHOGENESIS-RELATED GENES (CPR5)	Resting conditions	Negative	(Qi et al., 2023)
CONSERVED BINDING OF eIF4E1 (CBE1)	Resting conditions	Negative	(George et al., 2023)
PBL13 & PIRE1	Resting conditions and PAMP-enhanced RBOHD stability	Negative	(Lee et al., 2020)
	PAMP- and PA-enhanced RBOHD stability	Negative	(Kong et al., 2024; Qi et al., 2024)
PB1CP	PAMP-triggered RBOHD stability	Negative	(Goto et al., 2024)
XYLEM CYSTEINE PEPTIDASE 1 (XCP1)	PAMP-triggered RBOHD stability	Negative	(Liu et al., 2024)
CYSTATIN 6 (CYS6)		Positive	
DGK5	PAMP- and PA-enhanced RBOHD stability	Positive	(Kong et al., 2024; Qi et al., 2024)
CPK16	In vitro experiments	Positive	(Yu et al., 2024)

3.5.1. RBOHD protein dynamics in combined hypoxia/flg22

Here, we explored whether (i) RBOHD protein levels were differentially regulated in HF compared to NF in wild-type Col-0 seedlings and 4-week old plants, and (ii) there was a correlation between the loss of hyper-induction in the *erfvii* quintuple mutant and RBOHD protein levels in HF. To do so, we analysed endogenous RBOHD protein abundance in both seedlings and 4-week old plants in light and dark conditions, with NM, HM, NF and HF treatments.

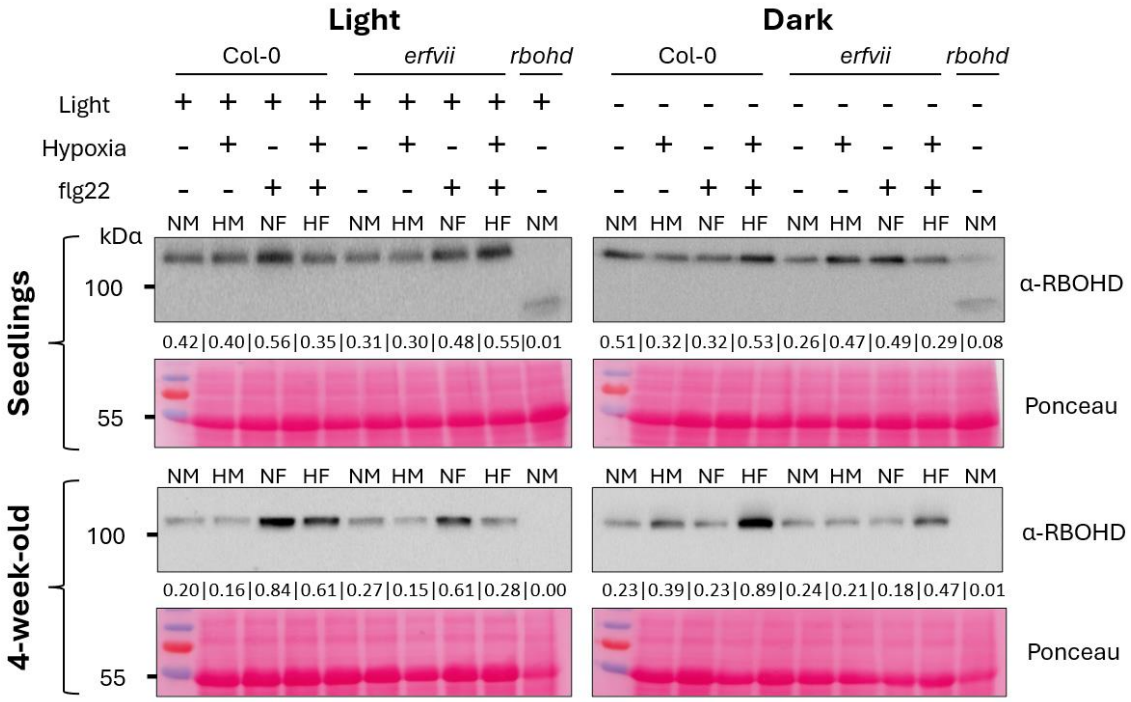

Figure 3.13. RBOHD protein abundance in NM, HM, NF and HF conditions in the wild type and the *erfvii* mutant. Total proteins were extracted after 4 hours of normoxia/hypoxia pre-treatment followed by one hour of combined hypoxia/flg22 treatment or equivalent control (i.e. same experimental conditions as in section 3.4). The endogenous RBOHD protein was detected using the anti-RBOHD antibody (Agrisera #AS15 2962) by immunobloting. Ponceau S staining serves as a control for protein loading. The band corresponding to the large subunit of RubisCO (RBCL) is shown here. Numbers between the immunoblot and the Ponceau S staining indicate the relative levels of RBOHD protein normalised with RBCL levels. Blots are representative of n = 2 for seedlings, n=3 for 4-week old plants.

In the wild type, we obtained the same RBOHD abundance dynamics in both seedlings and 4-week old plants, indicating that the behaviour of RBOHD protein levels across treatments is not dependent on developmental stage (**Figure 3.13**). In the light, as previously observed, both seedlings and 4-week old plants presented increased RBOHD protein levels in NF compared to the control conditions (NM) (Kong et al., 2024) (**Figure 3.13**). Furthermore, hypoxia treatment alone (HM) did not affect RBOHD levels, but when combined with flg22 in HF, RBOHD protein abundance decreased in both wild-type seedlings and 4-week old plants compared to NF in the light (**Figure 3.13**). In contrast, in the dark, for both wild-type seedlings and 4-week old plants, we did not detect an increase in RBOHD protein abundance in NF relative to NM, suggesting that dark conditions prevent the accumulation of RBOHD in NF (**Figure 3.13**). Similarly to light conditions,

HM did not affect RBOHD levels, but when combined with flg22 in HF, RBOHD protein abundance increased compared to NM, HM and NF in wild-type 4-week-old plants in the dark, and to a lesser extent in seedlings (**Figure 3.13**).

Taken together, these results indicate that HF conditions in the light reduce RBOHD protein abundance in comparison to NF, but under HF conditions in the dark, RBOHD protein abundance increases compared to NF. However, when comparing protein an mRNA levels, they do not align. Although *RBOHD* transcripts were strongly induced under HF in the light, RBOHD protein abundance decreased. However, in the dark, mRNA and protein levels mirrored each other. These contrasting dynamics suggest that post-transcriptional or post-translational mechanisms (e.g. translation efficiency or protein turnover,) play a role in determining RBOHD protein abundance in HF compared to NF, especially in light conditions.

As our transcriptional data suggested that the ERFVIIs could contribute to the regulation of *RBOHD* expression in HF treatment in seedlings treated in the light (**Figure 3.9**), we also tested how RBOHD protein abundance was affected in the *erfvii* quintuple mutant (**Figure 3.13**). In the light, RBOHD protein levels increased in NF treated plants in the *erfvii* mutant background (both seedlings and 4-week old plants), similarly to that seen in wild type plants. In light HF treated seedlings RBOHD protein levels increased rather than decline in contrast with the trend observed in the wild type, indicating that the ERFVIIs might play a role in decreasing RBOHD abundance in light HF in seedlings (**Figure 3.13**). In contrast, in 4-week old plants, the lack of ERFVIIs resulted in RBOHD protein levels between NF and HF that are similar to the ones observed in the wild type (**Figure 3.13**), albeit with generally lower RBOHD levels. In the dark, *erfvii* seedlings displayed reduced RBOHD levels in HF compared to NF, indicating that the ERFVIIs are required for the increased RBOHD levels in dark HF (**Figure 3.13**). Conversely, in 4-week old plants, the lack of ERFVIIs resulted in the reduction of RBOHD levels in HF in comparison with wild type, however, it remained higher than those observed in dark NF (**Figure 3.13**), and hence the dynamics of RBOHD level showed similar behaviour in wild type and *erfvii*.

In sum, ERFVIIs contribute to regulating RBOHD protein levels in HF conditions in seedlings, as evidenced by the inverted trend of RBOHD abundance present in *erfvii* mutants compared to the wild type. However, in 4-week old, the trends do not change in comparison to wild type plants, but the overall protein levels are reduced. This suggests that the ERFVIIs still contribute to the regulation of RBOHD abundance, but their role is limited to maintaining basal levels.

3.5.2. Exploring a role of NO in RBOHD regulation under HF treatment

Nitric Oxide (NO) in plants is a small redox-active molecule that functions primarily as a gaseous second messenger in stress responses (Borrowman et al., 2023; Gupta et al., 2020; Yu et al., 2014). In hypoxic conditions, mitochondria play a major role in NO production through different pathways, such as for example AOX1a-dependent production of NO upon hypoxia (Vishwakarma et al., 2018). During the onset of plant immunity and defences against pathogens, NO also plays a major role and has been shown to S-nitrosylate different components involved in PTI (Cui et al., 2024; Yang et al., 2015; Yun et al., 2011). Notably, NO directly S-nitrosylates RBOHD, thus decreasing its activity (via interference with FAD binding) upon pathogen infection (Yun et al., 2011). BIK1 is another key regulator of PTI that is directly S-nitrosylated, this modification promotes BIK1 phosphorylation, which activates and stabilises BIK1, together with an increase in its physical interaction with RBOHD, promoting ROS production (Cui et al., 2024). Altogether, these results indicate an important, as well as dynamic role of NO in hypoxia and pathogen responses, with direct and indirect effects on RBOHD activity. Here, we studied RBOHD protein levels in HF in different mutant backgrounds that are affected for NO levels and capacity of S-nitrosylation.

3.5.2.1. RBOHD protein levels in a pgb1 mutant

PGB1 is involved in NO scavenging during hypoxia (Hebelstrup et al., 2008) and pathogen infection (Mur et al., 2012; Qu et al., 2006; Terrón-Camero et al., 2023). When plants experience hypoxia, *PGB1* expression is rapidly induced by ethylene, thereby preventing the accumulation of NO and maintaining redox balance (Hartman et al., 2019). One effect of this induced expression of *PGB1* is the stabilisation of the ERFVIIs, which enables the activation of the transcriptional hypoxia response program (Gibbs et al., 2014; Hartman et al., 2019; Vicente et al., 2017). Here, we used the *pgb1-1* mutant that has increased levels of NO upon stress treatment (Hartman et al., 2019) to determine if NO-dependent mechanisms play a role in the regulation of RBOHD protein levels in HF compared to NF, HM and NM, in the dark or in the light. This work focused on 4-week old plants to ensure consistency across experiments, as the tissue used in ROS measurements (**Figure 3.6**) was also collected from 4-week-old plants. The immunoblot analysis with the anti-RBOHD antibody suggests that RBOHD protein levels change in a similar way in HF compared to NF in both the wild type and the *pgb1-1* mutant, suggesting that hypoxia-triggered NO scavenging by PGB1 in hypoxic conditions does not influence the dynamics of RBOHD protein abundance in HF (**Figure 3.14**).

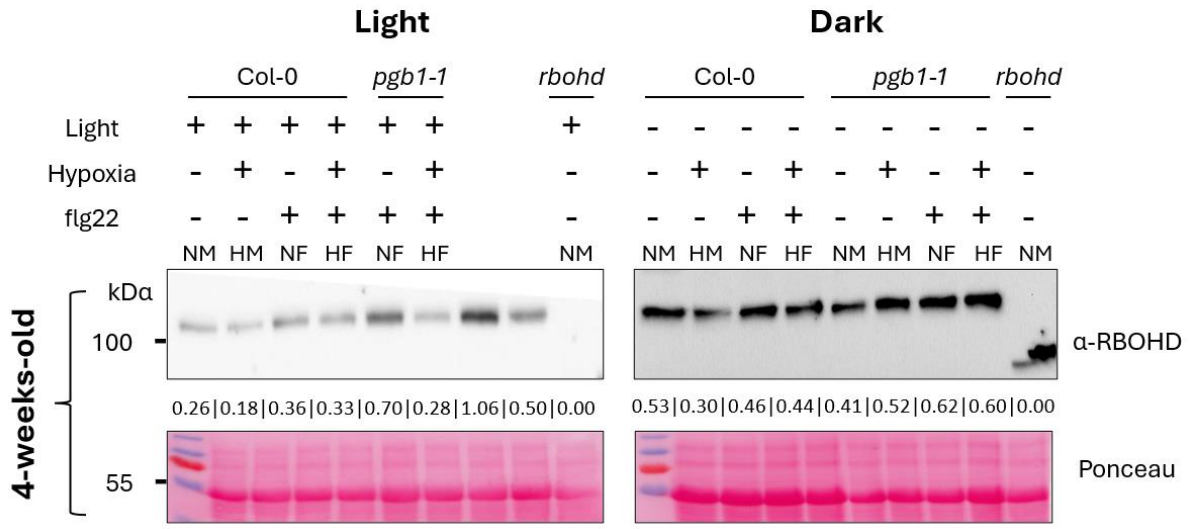

Figure 3.14. RBOHD protein abundance in NM, HM, NF and HF conditions in the wild type and the *pgb1-1* mutant. Total proteins were extracted from leaves of 4-week old plants after 4 hours of normoxia/hypoxia pre-treatment followed by one hour of combined hypoxia/flg22 treatment or equivalent control (i.e. same experimental conditions as in section 3.4). The endogenous RBOHD protein was detected using the anti-RBOHD antibody (Agrisera #AS15 2962) by immunobloting. Ponceau S staining serves as a control for protein loading. The band corresponding to the large subunit of RubisCO (RBCL) is shown here. Numbers between the immunoblot and the Ponceau S staining indicate the relative levels of RBOHD protein normalised with RBCL levels. Blots are representative of n = 2.

3.5.2.2. RBOHD protein levels in a noa1 mutant with decreased NO levels

The regulation of RBOHD protein levels was also monitoredusing mutants with decreased levels of NO, and focused on a mutant for *NITRIC OXIDE ASSOCIATED 1* (*NOA1*), which is a conserved mitochondrial GTP-binding protein essential for ribosome assembly and mitochondrial translation in plants (Sudhamsu et al., 2008) with an indirect role in NO synthesis (Guo et al., 2003; Feechan et al., 2005; Lee et al., 2008; Moureau et al., 2008). Additionally, in response to PAMPs, an *noa1* mutant can regulate transcriptional levels of immunity-regulated genes such as the RBOHD regulator WRKY33 or the immunity regulator MPK3, inhibiting the immunity induced by the PAMPs and caused increased bacterial growth in plants pre-inoculated with PAMPs (Ma et al., 2013). Because of these roles in NO biosynthesis, we would expect *noa1* mutants to accumulate lower NO levels than WT. As these pathways can potentially regulate RBOHD protein abundance in HF conditions, we subjected 4-week old *noa1* mutant plants to HF

treatment in light or dark conditions and assessed RBOHD protein levels by immunoblotting with an anti-RBOHD antibody.

Data shown in **Figure 3.15** show that in 4-week old plants, RBOHD protein levels in the *noa1* mutant treated with HF in the light behave different than in the wild type. Specifically, while RBOHD protein levels are lower in HF compared to NF in the wild type, in the *noa1* mutant, RBOHD protein levels are increased in HF and NF to a similar level. This suggests that in the wild-type, NO might play a role in mediating downregulation of the abundance of RBOHD in HF compared to NF. In the dark, RBOHD protein levels are the same in the wild type and *noa1* mutant.

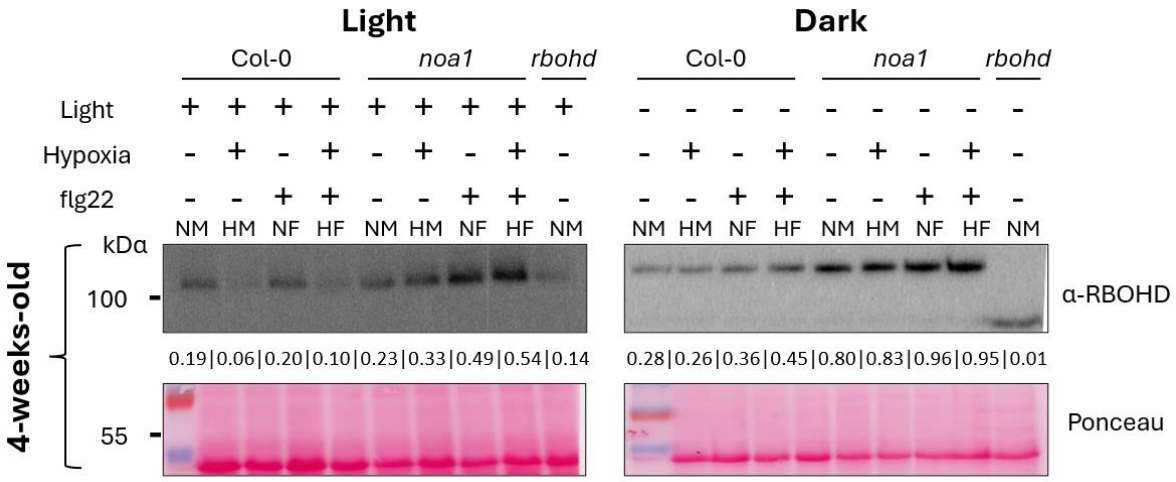

Figure 3.15. RBOHD protein abundance in NM, HM, NF and HF conditions in the wild type and the *noa1* mutant. Total proteins were extracted after 4 hours of normoxia/hypoxia pre-treatment followed by one hour of combined hypoxia/flg22 treatment or equivalent control (i.e. same experimental conditions as in section 3.4). The endogenous RBOHD protein was detected using the anti-RBOHD antibody (Agrisera #AS15 2962) by immunobloting. Ponceau S staining serves as a control for protein loading. The band corresponding to the large subunit of RubisCO (RBCL) is shown here. Numbers between the immunoblot and the Ponceau S staining indicate the relative levels of RBOHD protein normalised with RBCL levels. Blots are representative of n = 2

3.5.2.3. Exploring a potential role of GSNOR in the regulation of RBOHD in HF

S-nitrosoglutathione (GSNO) is the product derived from the reaction of NO with glutathione (GSH) and is a major source of bioavailable NO species to mediate protein S-nitrosylation (Hess et al., 2005). However, GSNO can be converted to glutathione disulfide (GSSG) and ammonia (NH_3) by GSNO REDUCTASE (GSNOR), thus decreasing GSNO levels and

protein S-nitrosylation (Jahnová et al., 2019; Sakamoto et al., 2002). The GSNOR-mediated GSNO/NO reduction is thus an important pathway to scavenge excess NO in plants (Gupta et al., 2011), in addition to the PGB1-dependent scavenging of NO.

GSNOR is widely involved in responses to various biotic and abiotic stresses, such as hypoxia response and plant immunity, and has a strong link with second messengers such as Ca^{2+}, NO itself and ROS. GSNOR is itself S-nitrosylated in hypoxic conditions, which triggers conformational changes that promote the interaction of GSNOR with AUTOPHAGY-RELATED 8e (ATG8e), leading to the degradation of GSNOR via autophagy (Frungillo et al., 2014; Zhan et al., 2018). In addition, this pathway has been shown to have a role in disease resistance in fruit (Yu et al., 2020). In the context of plant defences against pathogens, *gsnor* mutant plants have been shown to have increased RBOHD activity due to decreased S-nitrosylation and subsequent increased cell death in response to pathogen (*Pst* DC3000) infection, controlling the hypersensitive response (Yun et al., 2011). Because of these roles in NO biosynthesis, we would expect *gsnor1-3* mutants to accumulate lower NO levels than WT. In addition, this dual role in regulating individual stress responses to both hypoxia and pathogens suggests that GSNOR could also potentially play a role in the differential regulation of RBOHD protein levels in HF conditions. This was tested using 4-week old *gsnor1-3* mutant plants treated with HF in dark and light conditions.

The data obtained in the light was not of sufficient quality to draw conclusions (**Figure 3.16),** but in the dark, the *gsnor1-3* mutant behaved similarly to the wild type, suggesting that GSNOR does not play a major role in the regulation of RBOHD abundance in HF in the dark. In conclusion, NO does not appear to be a key regulator of RBOHD protein levels when 4-week old plants are treated with combined HF.

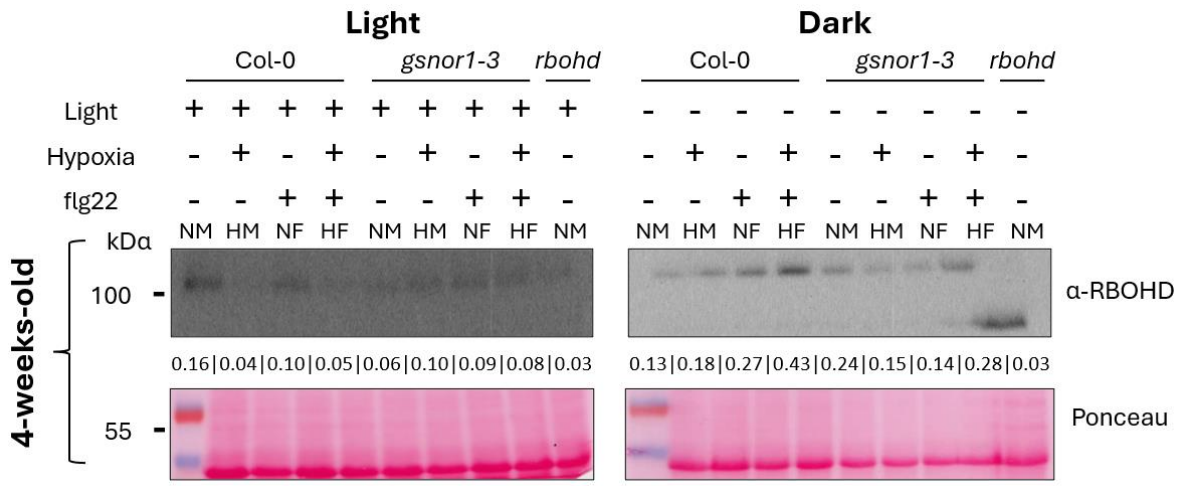

Figure 3.16. RBOHD protein abundance in NM, HM, NF and HF conditions in the wild type and the *gsnor1-3* mutant. Total proteins were extracted after 4 hours of normoxia/hypoxia pre-treatment followed by one hour of combined hypoxia/flg22 treatment or equivalent control (i.e. same experimental conditions as in section 3.4). The endogenous RBOHD protein was detected using the anti-RBOHD antibody (Agrisera #AS15 2962) by immunobloting. Ponceau S staining serves as a control for protein loading. The band corresponding to the large subunit of RubisCO (RBCL) is shown here. Numbers between the immunoblot and the Ponceau S staining indicate the relative levels of RBOHD protein normalised with RBCL levels. Blots are representative of n = 2 for seedlings, n=3 for 4-week old plants.

3.5.3. Exploring a potential role of CPK28 in the regulation of RBOHD levels in HF

CPK28 is a Ca^{2+}-regulated protein kinase that plays a negative role in plant immunity via the indirect repression of RBOHD function and also has roles in hypoxia response. For example, *CPK28* has been shown to be transcriptionally induced within 30 minutes of low O_2 levels (Bakshi et al., 2023), as well as phosphorylated together with other CPKs (Fan et al., 2023; Yu et al., 2024). In the context of PTI, the main identified target of CPK28 is BIK1, a key regulator of RBOHD upon flg22 perception by FLS2. Specifically, CPK28 phosphorylates BIK1 in the absence of PAMP, promoting its turnover and inhibiting immune responses (Monaghan et al., 2014). CPK28 can also promote BIK1 turnover indirectly by phosphorylating the E3 ligases PUB25 and PUB26, which target non-activated BIK1 for degradation (Wang et al., 2018). Interestingly, CPK28 also interacts with RBOHD at the plasma membrane, although no phosphorylation of RBOHD by CPK28 has been reported (Monaghan et al., 2014).

Therefore, we hypothesised that the potential activation of CPK28 in hypoxic conditions might alter RBOHD levels in HF conditions. To address this hypothesis, expression analysis in the *cpk28-1* mutant was performed. Unexpectedly, *RBOHD* transcript levels were already elevated in *cpk28-1* under NF, suggesting an additional negative role for CPK28 in restraining *RBOHD* expression upon flg22 treatment (**Figure 3.17**). Furthermore, the genes tested (*RBOHD, ADH1* and *BIK1*) were genes with light-dependent expression patterns in HF in the wild type, however, when expression levels were analysed in the *cpk28-1* mutant, the significant transcriptional induction of these genes upon dark HF in comparison with light HF observed in the wild type was lost (**Figure 3.17**). These results suggest that *CPK28* is required to control the light-dependent component of the HF response.

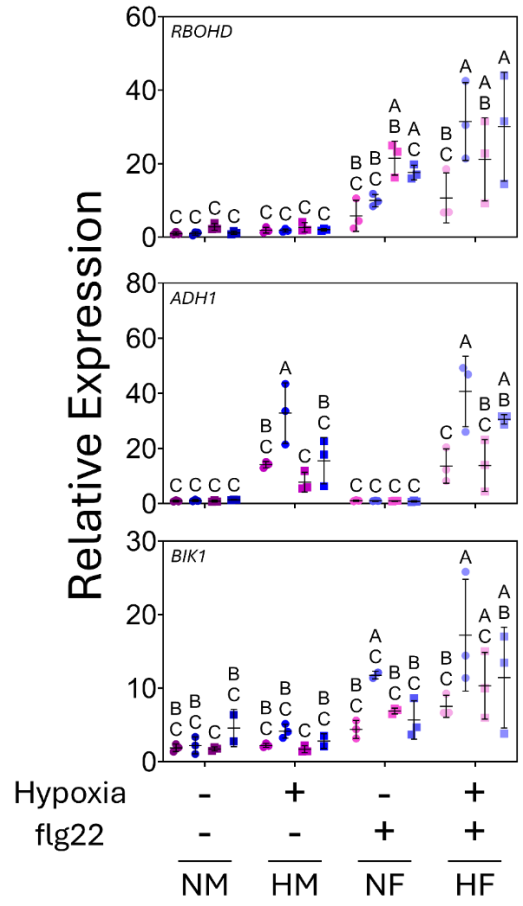

Figure 3.17. Transcriptional changes of candidate genes involved in the crosstalk of hypoxia/flg22 comparing light and dark conditions in 4-week old plants. Expression analysis of candidate genes involved in HF crosstalk (*RBOHD, ADH1* and *BIK1*) in 4-week old wild type (circles) and *cpk28-1* (hexagons) plants undergoing NM, HM, NF or HF treatment in the light (pink) or in the dark (purple). Results are means ± standard deviation (SD) of 3 biological replicates (n = 3). Statistical analysis: two-way ANOVA with Tukey's test ($p < 0.05$); different letters indicate statistically different groups.

As *CPK28* can regulate RBOHD expression levels and the CPK28 protein interacts with RBOHD, we hypothesised that CPK28 could also play a role in the regulation of RBOHD protein abundance in HF. To address this, we subjected 4-week old *cpk28-1* mutant plants (Monaghan et al., 2014) to HF treatment under light and dark conditions to monitor endogenous RBOHD protein levels.

In contrast with *RBOHD* expression levels, where the role of CPK28 was only observed in samples treated with flg22, RBOHD protein levels were higher in the *cpk28-1* mutant compared to the wild type in absence of flg22 and independently of light availability during the treatments. When plants underwent treatment in light conditions, the levels of RBOHD increased in NF in both wild type and *cpk28-1* plants. Although the decrease in RBOHD levels was not obvious in HF *versus* NF in the wild type in this experiment, in the *cpk28-1* mutant, the results showed that RBOHD abundance decreased in HF compared to NF, therefore suggesting that CPK28 does not play a role in regulating RBOHD stability in HF conditions in the light (**Figure 3.18**). In the dark, in the *cpk28-1* mutant (but not in the wild type), HM treatment decreased RBOHD protein levels compared to those found in NM conditions. In addition, a comparable decrease in RBOHD protein levels was visible under HF compared to NF (or NM). These results suggests that CPK28 has a role in the regulation of RBOHD stability in the absence of any stress, and CPK28 has a light- and hypoxia-dependent role on the ability of plants to increase the levels of RBOHD under combined HF (**Figure 3.18**).

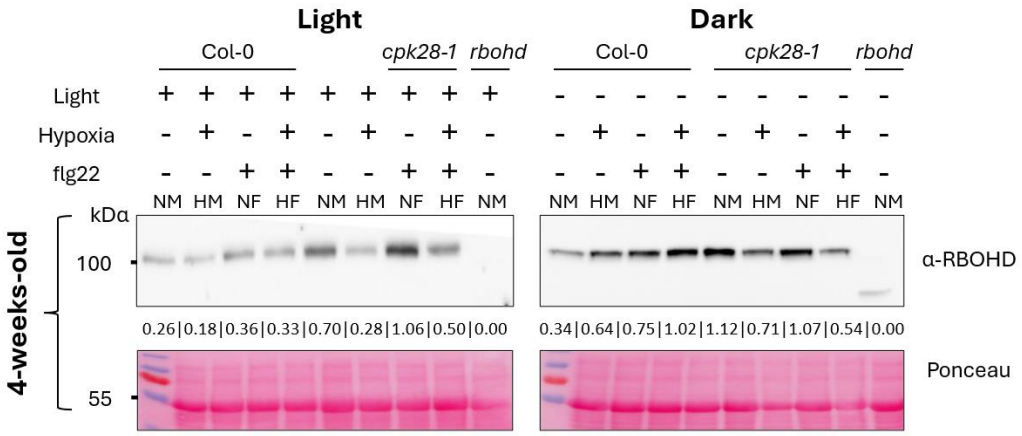

Figure 3.18. RBOHD protein abundance in HF conditions and role of CPK28 controlling of RBOHD protein abundance. 4-week old plants in the light and dark normoxia (21%O_2+mock solution (NM)); hypoxia (1%O_2+mock solution (HM)); flg22 (21%O_2+100nM flg22 (NF)) or hypoxia+flg22 (1%O_2+100nM flg22 (HF)). Total proteins were extracted after 4 hours of normoxia/hypoxia pre-treatment prior to mock solution/flg22 and RBOHD abundance was

detected by immunoblot analysis (Agrisera #AS15 2962) using the Ponceau S staining of the large subunit of Rubisco (RBCL) as a loading control. Numbers between the blot and the Ponceau S staining indicate the relative levels of RBOHD proteins normalized with RBCL levels. n=2

3.5.4. Conclusions

The results presented in section 3.5 indicate that in HF conditions, RBOHD transcript levels do not correlate with protein abundance, as RBOHD protein levels are reduced in light HF comparison to light NF, and RBOHD protein levels increase in dark HF comparison with dark NF. In seedlings, subjected to HF conditions, the data suggest that ERFVII-dependent transcriptional regulation of *RBOHD* might explain both mRNA and protein levels. However, in 4-week old, CPK28 appears to be more important to control the dynamics of RBOHD protein levels between NF and HF in the dark.

3.6. Discussion

This chapter provides evidence that RBOHD is a key point of integration between hypoxia and flg22 signalling, and that its regulation during combined hypoxia/flg22 treatment occurs at multiple levels (transcriptional and post-transcriptional). Rather than simply suppressing PTI output as it has been previously observed (Mooney et al., 2024), prior hypoxia reconfigured the flg22 response by altering the kinetics of the apoplastic ROS burst, *RBOHD* transcript accumulation, and RBOHD protein abundance in a manner that dependeds strongly on other environmental factors such as light availability and developmental stage. Together, these findings suggest that the contribution of RBOHD to immune responses is not fixed but instead is shaped by the physiological and environmental context in which immune signalling is initiated.

The experimental framework used in this chapter was designed to identify conditions under which hypoxia pre-treatment would modify RBOHD regulation during the early phase of flg22 signalling. This optimisation identified 4 hours of hypoxia (1% O_2) pre-treatment as suitable, and hence this 4 hour pre-treatment was used in conjunction with a subsequent one-hour flg22 treatment under maintained hypoxia. Interestingly, the 4 hour time point of hypoxia pre-treatment coincides with RAP2.12 nuclear localisation (Kosmacz et al., 2015), consistent with previous evidence that this transcription factor regulates *RBOHD* expression upon hypoxia (Yang et al., 2017). We also tested the effects of light and developmental stage on experimental outcomes because both are known to influence the balance between hypoxia and immune signalling.

Hypoxia response genes are transcriptionally induced upon dark conditions, when plants are not able to produce local O_2 via photosynthesis (Triozzi et al., 2024) while immunity genes are transcriptionally induced upon light conditions (Bhardwaj et al., 2011; Goodspeed et al., 2012; Korneli et al., 2014; Lai et al., 2012; Wang et al., 2011). In addition, ERFVII activity and immune responsiveness differ between different developmental stages (seedlings and adult plants), making developmental context an important variable for interpreting combined stress responses.

The first outcome of this chapter is that hypoxia pre-treatment altered the shape of the flg22-triggered apoplastic ROS burst. In HF conditions the ROS burst failed to reach the peak amplitude seen in NF and instead showed a flatter, more sustained ROS production over time (**Figure 3.6**). This flatter and more sustained ROS burst suggests that hypoxic conditions changes the balance between burst activation and burst attenuation producing lower-intensity defence signalling over acute oxidative responses.

We hypothesise that the mechanisms causing this can range from (i) different expression dynamics of RBOHD in combined HF conditions, (ii) energy constrains on energy produced by hypoxia, limiting NADPH availability, a substrate needed for RBOHD activity (Torres et al., 1998; Triozzi et al., 2024), (iii) disturbance of Ca^{2+} signalling by hypoxia responses (Bakshi et al., 2023; Subbaiah et al., 1994; Wagner et al., 2019; Yemelyanov et al., 2011), (iii) inhibition of flg22 canonical desensitization machinery to (iv) disturbance of apoplastic environment by hypoxia, such as apoplastic pH or peroxidase activity (Felle, 2006; Hofmann et al., 2020). Among these potential mechanisms, the data presented here most strongly support the idea that RBOHD abundance and/or regulation are distinctively influenced under HF, although the contribution of altered metabolism and signalling attenuation is also likely to be important. In addition, downstream of this ROS production, transcriptional analyses showed that the absence of RBOHD disrupted the transcriptional dynamics normally observed under HF conditions (**Figure 3.7**).

To address the first potential mechanism, we studied the transcriptional dynamics of *RBOHD*, which showed that RBOHD was hyper-induced in HF relative to NF at both developmental stages. These dynamics of *RBOHD* indicate that prior hypoxia modifies how it responds to flg22 perception (**Figures 3.8-9**). This finding agrees with previous studies that demonstrated that the short, combined stress treatment of hypoxia and flg22 increases the amplitude of gene expression change for DEGs common to HF and NF (Mooney et al., 2024). Importantly, this effect was more pronounced in the dark, suggesting that light availability strongly influences the extent to which hypoxia preconditions the immune response. A possible

explanation for this enhancement of hyper-induction is the plant's energy metabolism becomes limited due to reduced photosynthesis, therefore further activating hypoxia responses (Triozzi et al., 2024), and increasing *RBOHD* transcript abundance. Consistently, RBOHD is required for full induction of HF unique response (**Figure 3.10**), further supporting RBOHD role in HF responses.

An important question given the hyper-induction of RBOHD in HF which regulators might account for this transcriptional behaviour. Lack of regulation of *WRKY33* across developmental stages and light availabilities suggests that *RBOHD* regulation upon HF conditions is independent of WRKY33 (**Figure 3.11**). However, due to variability between replicates, additional experiments need to be performed. On the other hand, ERFVIIs contributed to *RBOHD* hyper-induction, as in seedlings it was reduced in the light (**Figure 3.12**). This was only tested in seedlings, as ERFVII activity decreases with development, and hence might be most relevant at the seedling stage rather than in 4-week old plants. Mechanistically, it is plausible, as stabilised ERFVIIs could act directly through hypoxia-responsive motifs in the RBOHD promoter or indirectly via downstream transcriptional regulators (Yao et al., 2017). We therefore propose a model where stabilised ERFVIIs induce *RBOHD* transcription additively to flg22-triggered RBOHD induction (**Figure 3.19**). Whether the ERFVIIs act in the dark to hyper-induce RBOHD expression in HF conditions remains to be determined in the future.

One of the main findings from this chapter is that RBOHD transcript abundance did not always predict RBOHD protein abundance, as previously observed in hypoxic stress (Branco-Price et al., 2008; Lee and Bailey-Serres, 2019; Mustroph et al., 2009; Sorenson and Bailey-Serres, 2014). Therefore, combined hypoxia/flg22 stress-triggered transcriptional changes may not reflect changes in protein levels. Consistent with previous reports that demonstrated increased RBOHD protein levels upon PAMP treatment, flg22 induced RBOHD accumulation NF in the light (Kong et al., 2024b; Qi et al., 2024) (**Figure 3.13**). One of the most important conceptual advances from this chapter is that RBOHD transcript abundance did not always predict RBOHD protein abundance (**Figure 3.13**). This data indicates that hypoxia influences RBOHD stability triggered by flg22. Possible mechanisms causing this could be selective translational repression or sequestration of RBOHD mRNA, altered ribosome association or degradation of RBOHD protein.

Light availability further shaped this post-transcriptional behaviour. In dark NF conditions, we observed reduced RBOHD protein levels in comparison to light NF conditions, indicating that darkness alone inhibit flg22-triggered RBOHD stability (**Figure 3.13**). By contrast, upon dark HF conditions, RBOHD protein abundance increased relative to dark NF, mirroring transcriptional hyper-induction of *RBOHD* (**Figure 3.10**). This data indicates that hypoxia

inhibition or deactivation of mechanisms ensuring RBOHD internalisation and/or degradation in the dark by flg22. One possible interpretation is that under strong energy limitation, such as dark hypoxia endocytosis, vesicle trafficking, and proteolytic routes are altered, reducing RBOHD turnover. Other possibility is that under these strong energy limitations, plants actively stabilise RBOHD at the plasma membrane prioritizing signalling capacity, enabling defence responses and stress-triggered ROS production. Altogether, these data indicate that the relationship between RBOHD transcript and protein is context-dependent, and that the HF response cannot be understood from transcriptional data alone.

The effect of ERFVIIs on RBOHD protein accumulation further emphasised the developmental specificity of this regulation. In seedlings, as activity of ERFVIIs is not reduced (Giuntoli et al., 2017), the *erfvii* quintuple mutant increased levels of RBOHD protein upon light HF conditions and decreased under dark HF conditions (**Figure 3.13**). In contrast, 4-week old *erfvii* mutants exhibited reduced RBOHD protein levels but do not display altered RBOHD dynamics in comparison with wild type plants (**Figure 3.13**). This is consistent with previous reports that ERFVII activity declines with development (Bui et al., 2020; Giuntoli et al., 2017), and suggests that while ERFVIIs are important contributors to RBOHD regulation in seedlings, their influence becomes more limited in adult plants. Taken together, the data support a developmental layer in the control of RBOHD, in which ERFVII-dependent regulation is stronger in seedlings, whereas other regulatory mechanisms become dominant in adult plants.

To identify these regulators of RBOHD protein levels in adult plants, we examined the roles of NO and CPK28. Despite NO directly modifying RBOHD protein, none of the mutants affecting hypoxia-associated NO scavenging or basal NO production altered the trends of RBOHD protein abundance observed in wild type (**Figure 3.14-16**). This suggests that NO is unlikely to be the principal determinant of the HF-dependent RBOHD protein phenotype, and other mechanisms account for RBOHD stability upon HF conditions.

Among the candidate regulators tested, CPK28 emerged as the strongest regulator of RBOHD behaviour under HF conditions. This was plausible given the role of CPK28 as a negative regulator of immunity controlling E3 ubiquitin ligases that control the stability of BIK1, and therefore controlling RBOHD function (Monaghan et al., 2014), and its transcriptionally induction and phosphorylation upon hypoxic conditions (Bakshi et al., 2023; Fan et al., 2023; Yu et al., 2024). Moreover, both CPK28 and BIK1 displayed transcriptional behaviour in HF that mimics *RBOHD* transcriptional dynamics (**Figure 3.10**). Indeed, transcriptional expression analysis in the *cpk28-1* mutant revealed that CPK28 controls the light-dependent hyper induction of *RBOHD, ADH1* and

BIK1, therefore establishing CPK28 not only as an immune regulator, but also as a regulator of hypoxia responses prior to flg22 treatment. Subsequent immunoblotting showed that loss of CPK28 displayed reduced RBOHD abundance in dark HF conditions instead of the expected hyper-accumulation of RBOHD protein, reaching levels even lower than those under dark NF conditions (**Figure 3.13**). These findings suggest two different possibilities: either CPK28 hypoxic activation only takes place in severe hypoxic conditions observed in dark hypoxia, or the CPK28-dependent regulation of RBOHD stability is highly dependent on light signalling pathways. Several potential CPK28-dependent mechanisms may regulate RBOHD stability upon HF conditions: (i) through direct phosphorylation of RBOHD by CPK28, altering RBOHD ubiquitination and degradation, which would be in line with the direct interaction of RBOHD and CPK28 (Monaghan et al., 2014) or (ii) through an indirect pathway that consists on the phosphorylation of RBOHD stability regulators like BIK1 or other E3 ligases in a similar mechanism as CPK28-dependent control of BIK1 turnover (Monaghan et al., 2014; Wang, 2018).

However, several limitations should be considered when interpreting these findings and should be taken care in the future. First, ERFVIIs contribution to the dark HF response remains unresolved because the relevant experiments were not completed. Second, the current experiments studying RBOHD protein levels do not distinguish whether this occurs primarily at the level of translation, membrane trafficking, internalisation, or degradation. Third, the role of CPK28 is strongly supported genetically, but its direct biochemical mode of action on RBOHD remains to be established. Future work combining polysome profiling, protein turnover assays, phosphosite analyses, and trafficking-based approaches will be required to distinguish between these potential mechanisms.

We therefore propose a model in which prior hypoxia reprogrammes flg22-triggered RBOHD regulation at both transcriptional and post-transcriptional levels. Seedlings that face hypoxia prior to flg22 treatment present active ERFVIIs which regulate transcriptional and post-transcriptional dynamics of RBOHD in seedlings. However, in adult plants, the ERFVIIs only control basal levels of RBOHD protein abundance, and other elements of the hypoxia stress response, most notably CPK28 control RBOHD transcription and protein levels. This regulatory mechanism is determined by light availability, possibly due to a stronger activation of hypoxia responses in the dark and the energetic state of the tissue (**Figure 3.19**).

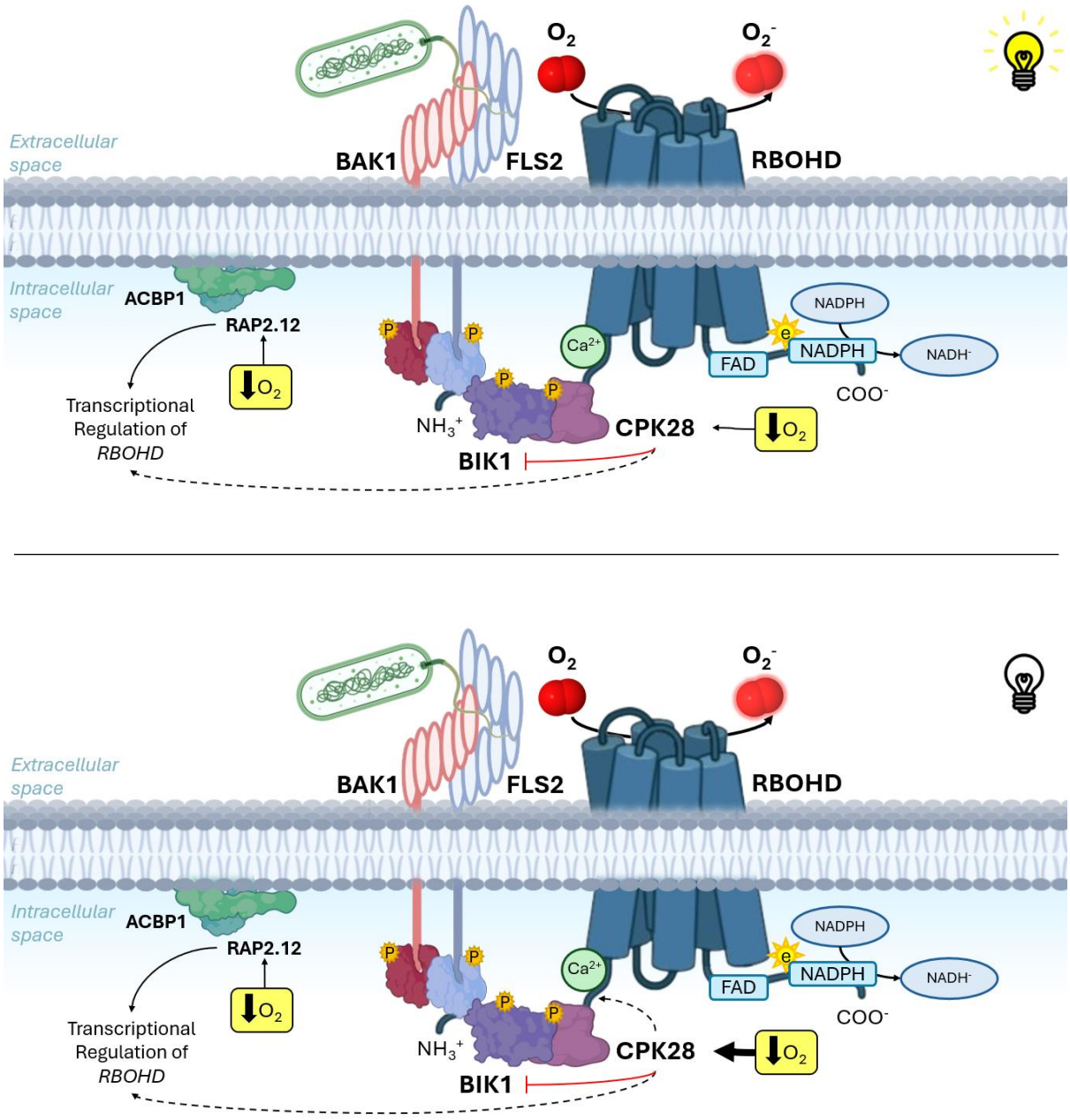

Figure 3.19. Regulatory mechanisms controlling RBOHD transcript and protein abundance upon HF. In this diagram, the identified hypoxia-activated mechanisms regulating dynamics of *RBOHD* transcript and protein abundance are shown in response to HF conditions. In addition, identified regulators highlighted with the hypoxia icon (yellow square) with arrows pointing at them. Dashed lines indicate indirect and still unknown mechanisms that influence the regulation of *RBOHD* transcriptional levels.

Altogether, these mechanisms suggests that RBOHD represents a convergence point at the intersection of abiotic and biotic stress pathways, integrating oxygen sensing and immune

signalling through context-specific (light availability and development stages) regulatory modules that ensure adequate RBOHD transcript and protein abundance in combined HF conditions. Furthermore, the convergence of ERFVIIs and CPK28 on RBOHD likely reflects a broader principle: plants integrate O_2 sensing and immune signalling at the RBOHD level to ensure that immune competence is preserved under low O_2 levels without compromising survival under energy-limiting conditions such as submergence. Future work should determine how these layers of transcriptional and post-translational control RBOHD transcript and protein levels and how they interact with additional signalling networks, including circadian regulation, hormone pathways, and metabolic status.

4. Chapter 4: Screening for combined waterlogging and pathogen stress tolerance in rapeseed

4.1. Introduction

4.1.1. Background Information

The *Brassicaceae* family, which *Arabidopsis* is a member of, is composed of ~3700 species (Al-Shehbaz, 2012), which have great importance in agricultural, scientific and economic sectors. Among them, rapeseed (*Brassica napus* L.) is the world's second largest oilseed crop after soybeans (FAO, 2021). Rapeseed plays a central role in breaking crop rotation systems that are often dominated by cereals, and is used to produce edible oil, cattle feed, and as a source of biodiesel or bioethanol (Kdidi et al., 2019). However, this role in crop rotation systems means that rapeseed plants experience waterlogging as part of their life cycle, one example of which is in China along the Yangtze River, where rapeseed is cultivated in rotation with rice, and therefore exposed to frequent waterlogging during the vulnerable seedling and flowering stages. This severely reduces its yield (Guo et al., 2020; Hong et al., 2024; Wollmer et al., 2018; Xu et al., 2015; Yang et al., 2024; Zhou and Lin, 1995; Zou et al., 2014). Globally, rapeseed plants can face waterlogging in emerging cultivation regions (Canada, Europe, India, and Australia (FAO, 2021)), where climate change driven increases in heavy rainfall and flooding further threaten productivity (Madsen et al., 2014). Although rapeseed plants are frequently subjected to waterlogging conditions, rapeseed exhibits high susceptibility to waterlogging conditions mainly due to (i) lack of aerenchyma, a tissue with enlarged gas spaces that increase the porosity of the root and thus reduces the resistance for gas movement from the shoot to the root tips; and (ii) lack of Radial Oxygen Loss (ROL) barrier formation, which prevents oxygen from leaking from the roots to the soil (Voesenek et al., 1999). Although physiological traits such as fresh and dry weight, seed oil content or plant yield are mainly used in studies assessing rapeseed tolerance to waterlogging, photosynthetic-related parameters are emerging as reliable traits to measure waterlogging tolerance (Lee et al., 2014; Li et al., 2023; Nabloussi et al., 2019; Song et al., 2025; Zhou and Lin, 1995).

In field conditions, waterlogging can increase the risk of pathogen infection. One pathogen that favours the increased humidity during waterlogging is *Sclerotinia sclerotiorum* (Zamani-Noor and Jedryczka, 2025). *S. sclerotiorum* is a fungal pathogen that causes sclerotinia stem rot (white mould) on the stems of the host plant and results in substantial yield and oil-

quality losses across major producing regions (Derbyshire and Denton-Giles, 2016; Ding et al., 2021; Shahoveisi et al., 2020). Humidity is important for the germination of the sclerotias (resting bodies) through two different processes: (i) myceliogenic germination, which produces hyphae to infect plant roots, and (ii) carpogenic germination, leading to the production of apothecia from which ascospores are released into the air to inoculate aerial parts of the plant (Chen et al., 2023). Although *S. sclerotiorum* is considered a necrotrophic pathogen, it has been proposed to have a transient biotrophic phase after initially colonizing plant tissues before transitioning into a necrotrophic pathogen (Kabbage et al., 2015). During this initial biotrophic phase, the pathogen releases plant cell wall degrading enzymes (PCWDEs) to weaken cell walls, helping penetration so that the nutrients can be taken up by the appressorium, then the pathogen also releases oxalic acid (OA) to suppress host oxidative defences by affecting the normal metabolism of the host cells (Ding et al., 2021). Then, the pathogen transitions into a necrotrophic lifestyle in which ROS accumulation and programmed cell death (PCD) in host cells promote tissue maceration and nutrient release, enabling full colonisation (Liang et al., 2009).

4.1.2. Aims of this chapter

The study of combined stress is emerging in model plant species like *A. thaliana*, where it has been recently demonstrated that hypoxia can repress flg22-triggered immunity and regulate early defence programs (Mooney et al., 2024). However, in crop species the literature regarding this field of study is divided across species, abiotic stresses and pathosystems. Some examples include (i) soybean, in which the combination of flooding with *Phytophthora sojae* infection was applied to evaluate the response of soybean seedlings, and demonstrated that traits such as maximum root length (MRL) and shoot and root dry weight were affected by interaction between inoculation and flooding (Tada et al., 2021); (ii) wheat and barley, for which yield components, grain composition and quality were significantly affected by combined *Fusarium poae* infection and waterlogging treatment (Martínez et al., 2019). These studies pinpoint specific outcomes of stress combination between waterlogging and pathogen infection. It has been suggested that plants perceive the combination of two (or more) stresses as a new state of stress rather than a sum of individual stresses (Mittler, 2006). Despite the connection between *S. sclerotiorum*, rapeseed and waterlogging, little is known about how waterlogging influences rapeseed plants' ability to defend against *S. sclerotiorum* infection. The main aims of this work were to determine a work frame that allowed us to elucidate if:

i. Waterlogging treatment affected rapeseed ability to fight off *S. sclerotiorum*.

ii. Rapeseed varieties that are tolerant (or sensitive) to waterlogging tend to be either more susceptible or resistant to *S. sclerotiorum*.

iii. And that allows us to identify genes associated with waterlogging tolerance, *S. sclerotiorum* resistance or resilience to combined waterlogging + *S. sclerotiorum* (see next chapter).

Indeed**,** early studies demonstrated that waterlogging at different developmental stages decreased leaf chlorophyll content and leaf photosynthetic rate of rapeseed (Zhou and Lin, 1995). Later, Lee et al., 2014 reported that waterlogging caused a significant decrease in leaf chlorophyll content and premature senescence of the leaves, together with a decrease in a parameter noted Fv/Fm which corresponds to the maximal quantum efficiency of photosystem II (PSII) in rapeseed. More recently, photosynthetic-related parameters have been used by Nabloussi et al., 2019 to demonstrate that waterlogging-tolerant varieties display relative high chlorophyll content to sustain photosynthesis and tolerate waterlogging stress, and additional studies have used similar parameters to distinguish waterlogging tolerant and sensitive rapeseed varieties (Li et al., 2023; Song et al., 2025). Altogether, these studies show that the measurement of different photosynthesis-related parameters is a suitable approach to distinguish between waterlogging sensitive or tolerant rapeseed varieties. To this aim, a screen was completed to monitor the response of ~100 rapeseed varieties, as it is a set of genetically diverse rapeseed lines supported by established genotyping resources makes it practical and powerful for a screening-first, GWAS-second strategy to identify loci controlling your waterlogging and waterlogging + *S. sclerotiorum*. Therefore, in this work, we treated these varieties with 4 different treatment conditions: control, waterlogging, *S. sclerotiorum* inoculation and combined waterlogging + *S. sclerotiorum* treatment. Response to *S. sclerotiorum* was assessed by measuring lesion size, and waterlogging resilience was assessed by measuring photosynthesis related traits.

4.2. Optimization of experimental conditions

4.2.1. Exploring different methods to apply hypoxia

In order to optimise the experimental conditions that could be used to screen the rapeseed collection for resilience to combined waterlogging and *S. sclerotiorum* treatment (as well as the individual stresses as controls), we first considered different experimental approaches to apply hypoxia. Common approaches to study hypoxia responses in rapeseed include waterlogging, submergence, de-oxygenated hydroponic media, or anoxic/stagnant agar (Ambros et al., 2022; Li

et al., 2023; Voesenek et al., 1999). Submergence, which would be ideal to restrict O_2 supply to aerial as well as underground tissues (Wittig et al., 2021) could not be used here because of the need to also inoculate leaves or stems with *S. sclerotiorum* either after or during submergence treatment. Hence, to reproduce this whole-plant hypoxic experience, we first carried out some preliminary experiments with hypoxia chambers.

4.2.1.1. Using hypoxia chambers with rapeseed seedlings

Hypoxia chambers enable (i) controlled O_2 levels during the hypoxic treatment, (ii) control of additional environmental factors that could potentially affect hypoxia responses, such as CO_2 or light availability, and (iii) could improve reproducibility of the results. One week old seedlings (Westar variety due to its wide use in published *B. napus* molecular studies) grown in short day conditions (8 h light / 16 h dark) conditions were kept in a hypoxia chamber (1% O_2) for 24 hours with the same light regime at the start of the dark period to test their response to hypoxic conditions. After a one-week recovery period in normal O_2 conditions, root length, shoot length, and overall seedling size were measured and compared with seedlings that were not subjected to hypoxic conditions. The data suggest that exposure to hypoxia did not significantly affect rapeseed growth, as observed in plant, root and shoot lengths one week after hypoxia treatment (**Figure 4.1**). These results indicate that longer hypoxia treatments may be needed, which would not be convenient using hypoxia chambers in the context of a large screen.

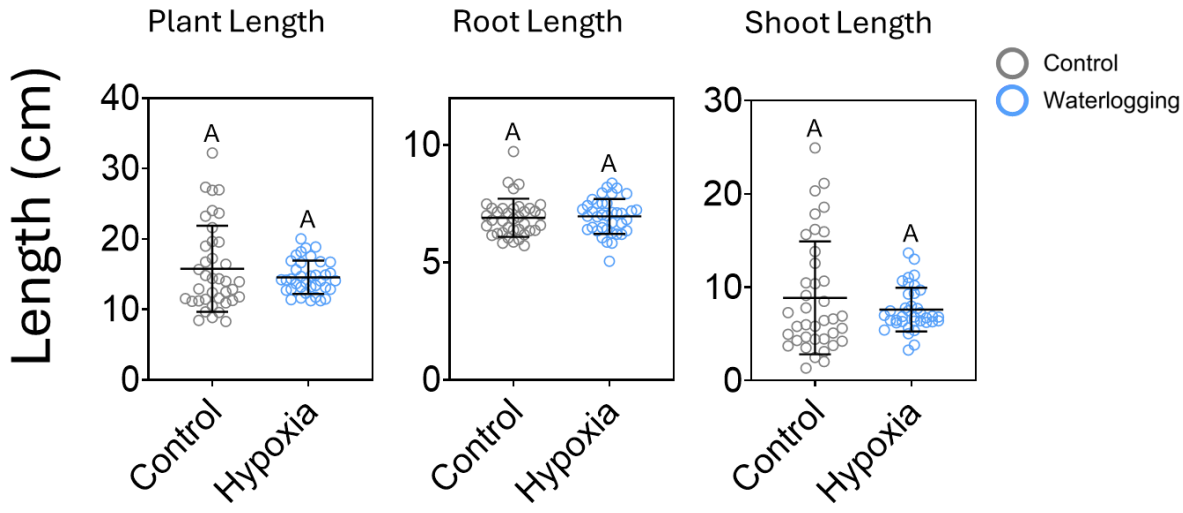

Figure 4.1. Effect of hypoxia treatment on one week old rapeseed seedlings growth. Means and standard deviations are shown for rapeseed seedlings treated with hypoxia for 24 hours (1% O_2; grey circles) or for control seedlings (21% O_2; blue circles). Statistical analysis: unpaired t-test ($p < 0.05$); different letters indicate statistically different groups.

4.2.1.2. Effect of waterlogging on 4-week old rapeseed plants

To apply hypoxic conditions for longer, we tested waterlogging treatments by immersing plant pots in a plastic container and raising the water level to 1-2 cm above soil surface, which is a method commonly used to test for waterlogging tolerance using rapeseed as well as other crops (Hong et al., 2023; Hong et al., 2024; Kuai et al., 2020; Li et al., 2024; Xu et al., 2016). Several parameters can be measured to score plants for waterlogging tolerance, many of which rely on determining the photosynthetic capacity of plants and transpiration rate (Li et al., 2023; Liu et al., 2020; Liu and Zwiazek, 2022; Ploschuk et al., 2018; Zhou and Lin, 1995), reduced chlorophyll content (Ashraf and Mehmood, 1990; Lee et al., 2014; Men et al., 2020; Nabloussi et al., 2019; Le Xu et al., 2019; Zhou and Lin, 1995) or reduced chlorophyll fluorescence (Lee et al., 2014; Li et al., 2023; Ploschuk et al., 2018; Xu et al., 2019). To measure these parameters, we used a portable MultispeQ (PhotosynQ) to allow rapid, non-invasive, and multiparametric assessment of light-adapted photosynthesis parameters *in vivo* (Kuhlgert et al., 2016), including PSII quantum yield (ΦII), non-photochemical exciton quenching (NPQt), light-driven proton translocation and thylakoid proton motive force, regulation of the chloroplast ATP synthase and leaf chlorophyll content (**Table 4.1**). These parameters are sensitive indicators of photosynthetic processes and of the onset of photoinhibition and photodamage, which in turn are useful indicators of plant health status (Baker, 2008; Baker and Rosenqvist, 2004; Murchie and Lawson, 2013). The MultispeQ is also equipped with a series of actinic and measuring lights, allowing the measurements of environmental conditions (light intensity and quality, temperature, humidity, CO_2 levels, time and location), which can be useful in the context of a large screen.

Table 4.1. Photosynthesis-related parameters used in this study.

Parameter	Definition	Physiological relevance	References
Fm'	Maximal chlorophyll fluorescence measured in a light-adapted state	Level of fluorescence when primary quinone electron acceptor of PSII (Q_A) is maximally reduced (PSII centers are closed). Estimates capacity of PSII to perform photochemistry in the light-adapted state.	(Baker, 2008; Baker and Rosenqvist, 2004; Genty et al., 1989)
Fo'	Minimal fluorescence measured in a light-adapted state	Level of fluorescence when primary quinone electron acceptors of PSII (Q_A) are maximally oxidized (PSII centres are open).	(Baker, 2008; Baker and Rosenqvist, 2004; Genty et al., 1989)

Fs	Steady-state chlorophyll fluorescence measured in a light-adapted state	Provides little information on photosynthetic performance, as it depends on plant status or environmental factors. Measures the fluorescence emitted when the photosynthetic apparatus is actively engaged in photosynthesis.	(Baker, 2008; Baker and Rosenqvist, 2004; Genty et al., 1989)
Fv'/Fm'	Maximum efficiency of PSII	PSII efficiency if all PSII centers were open (with Q_A oxidized), and all harvested light was converted to chemical energy	(Baker, 2008; Baker and Rosenqvist, 2004; Genty et al., 1989)
NPQt	Non-photochemical quenching	Estimates the share of excess energy dissipated as heat in photosystem II (PSII) associated antenna complexes.	(Tietz et al., 2017)
ΦII	Quantum yield of PSII	Estimate the operating efficiency of PSII with the available PSII open centers. Estimates the proportion of light absorbed by PSII that is used in photochemistry.	(Genty et al., 1989)
ΦNO	Quantum yield of non-regulatory energy dissipation	Estimates the proportion of light energy absorbed by PSII that is lost through processes other than photochemistry or regulated non-photochemical quenching (NPQ).	(Tietz et al., 2017)
SPAD	Chlorophyll content in leaves	Estimates photosynthetic pigment status and nitrogen allocation to the photosynthetic apparatus.	(John Markwell et al., 1995)

In a first preliminary experiment, four-week old rapeseed plants of the Westar variety were subjected to waterlogging treatment and photosynthesis-related parameters were measured over this time during waterlogging to determine the optimal duration of the treatment that elicits different responses in waterlogged *versus* control plants kept under normal watering conditions. Measurements were performed on the third leaf of all plants, as this is a developmentally mature leaf and consistently present among rapeseed plants at this developmental stage. It also provides a sufficient surface area to carry out the measurements. Growth of the aerial part of the plant was also determined at the end of the treatment by measuring fresh and dry weight together with its length.

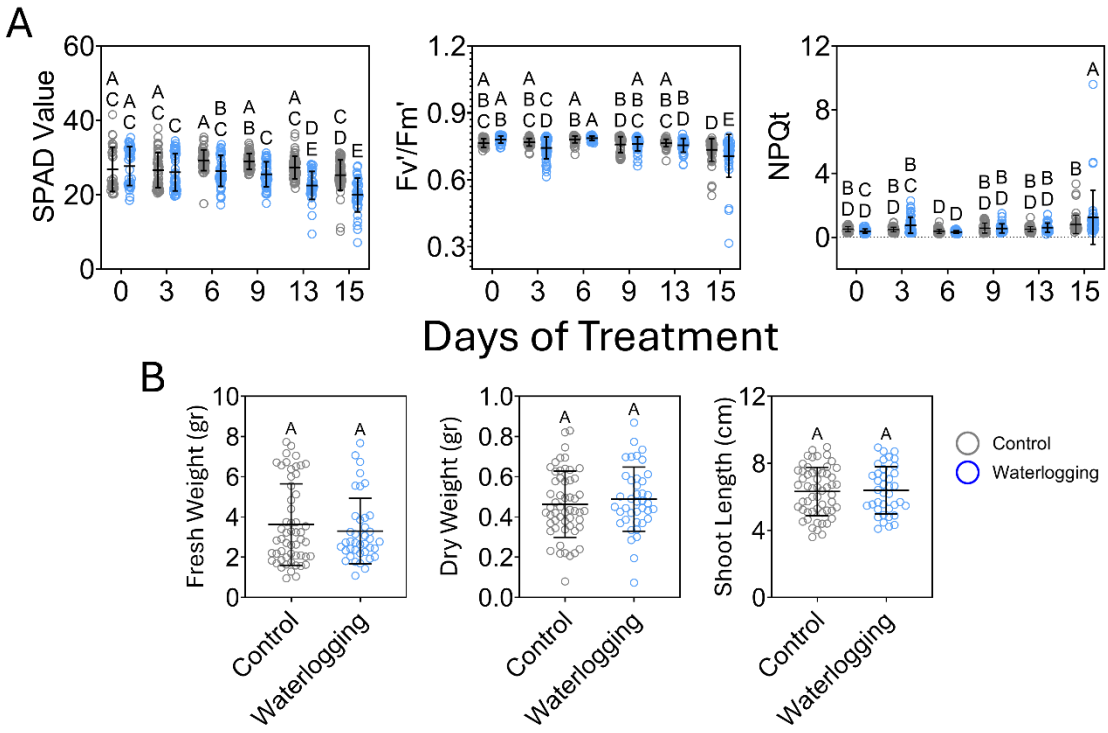

Figure 4.2. Waterlogging treatment did not impact growth of 4-week old Westar plants, but affected photosynthetic parameters. (A) Time course measurement of photosynthetic parameters on rapeseed plants using MultispeQ (SPAD, Fv'/Fm', NPQt (**Table 4.1**)) during 15 days of waterlogging (blue circles) or for control plants kept with normal watering (grey circles). **(B)** Physiological parameters of the aerial part of the plant were taken at day 15 of waterlogging (blue circles) and control (grey circles) treatment. Results are means ± standard deviation (SD) of 3 biological replicates (n = 3). Statistical analysis: unpaired t-test ($p < 0.05$) for physiological parameters and two-way ANOVA with Tukey's test ($p < 0.05$) for photosynthetic parameters; different letters indicate statistically different groups.

Decreased SPAD values were observed within 6 days of waterlogging treatment (**Figure 4.2 A**), indicating that waterlogging had an impact on rapeseed, and suggesting that nitrogen status might be affected early in the treatment. This reduction in nitrogen, combined with the maintenance of waterlogging (and low O_2 conditions for the roots) could subsequently affect the photosynthetic apparatus, reducing the quantity of harvested light that is converted to chemical energy, which is observed here at day 15 by the reduction of Fv'/Fm' values (**Figure 4.2 A**). This was accompanied by an increase in NPQt values (**Figure 4.2 A**), which would suggest an increase in the excess energy that is dissipated as heat in PSII. Despite these changes in photosynthetic-related parameters, growth of rapeseed plants did not show significant differences between treated and control plants at the end of the waterlogging treatment (**Figure 4.2 B**). These

preliminary experiments suggest that these conditions are sufficient to alter the photosynthetic apparatus, but not to affect biomass production. However, it is possible that an impact on growth would become visible at later stages of development, after plants have been returned to normal watering conditions after waterlogging (e.g. Miricescu et al., 2021; Ploschuk et al., 2018).

4.2.2. Identifying a suitable developmental stage to study waterlogging tolerance

The developmental stage at which plants experience waterlogging or hypoxia can affect their responses and ability to survive. In rapeseed, earlier stages appear to be more sensitive to waterlogging. For example, Nabloussi et al., (2019) demonstrated that germination and post-emergence seedling stages were the most sensitive to waterlogging stress in field experiments in the Gharb region (Morocco). Similarly, waterlogging treatment of rapeseed seedlings impacted plants more strongly than if applied at later stages (Liu et al., 2020), as plant dry weight, gas exchange, leaf water potentials and root hydraulic conductivity decreased more at early stages of development. Wollmer et al., (2019) also showed that the occurrence of micronutrient deficiencies or toxicities depended on the developmental stage at which the plant was flooded.

In order to optimise the developmental at which the screen could be conducted, we subjected 2, 3, and 4-week old Westar plants to 15 days of waterlogging treatment and assessed their photosynthetic capacity by performing MultispeQ measurements on the third leaf as it was the only fully unfolded leaf on the 2, 3, and 4-week old Westar plants at the end of the waterlogging treatment. However, this third leaf did not always have a sufficient area to carry out the measurements. This was the case at days 4 and 8 of waterlogging when the treatment was applied to 2-week old, and at day 4 for 3-week old plants at the start of treatment.

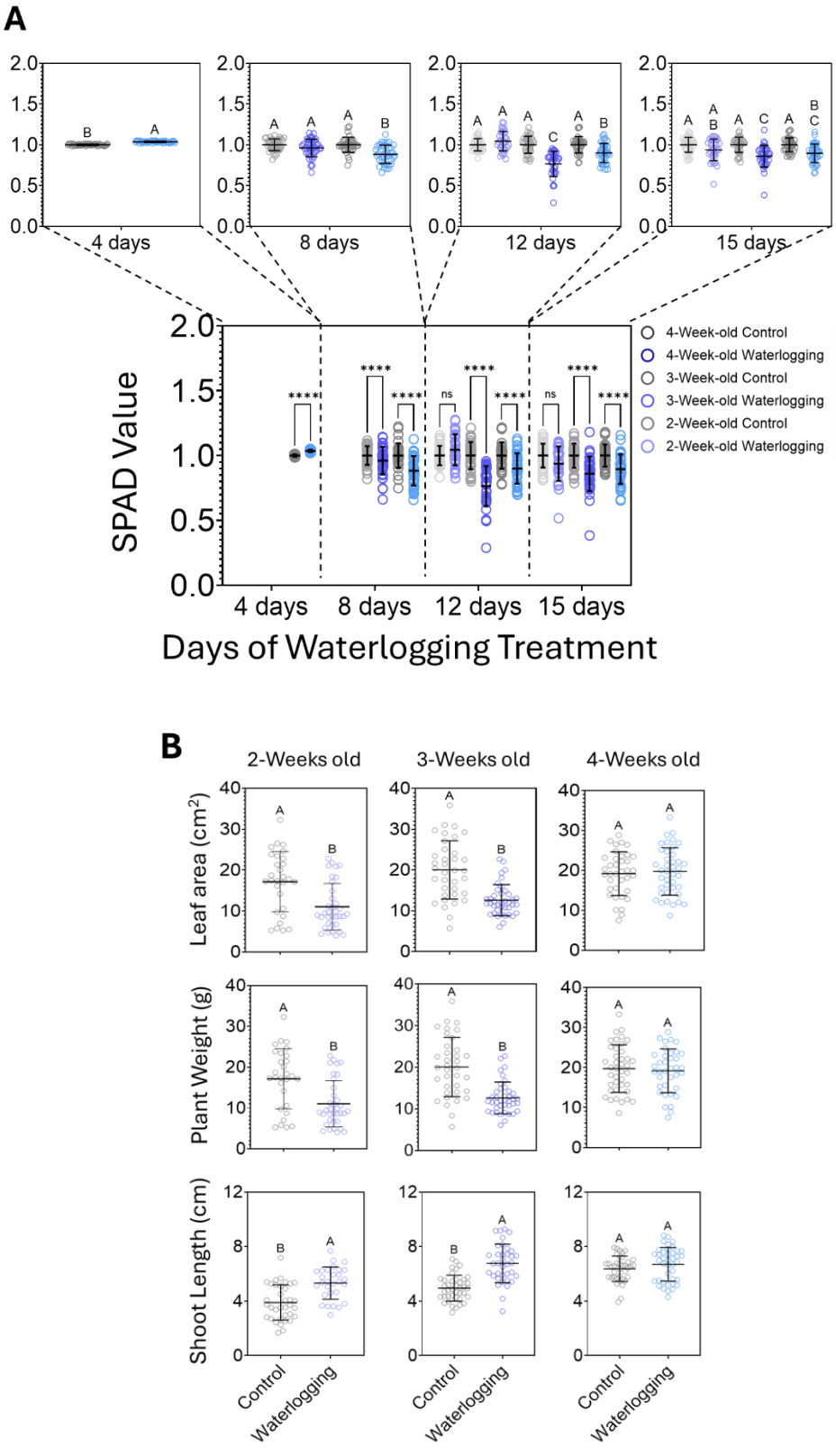

Figure 4.3. Waterlogging treatment affects rapeseed growth and photosynthetic parameters depending on developmental stage. (A) Time course of SPAD measurements with a multispeQ device during 15 days of waterlogging (blue circles) or control (grey circles) treatments. Values were normalised relative to the control measurements. **(B)** Physiological parameters (leaf area,

plant weight and shoot length) taken at day 15 of waterlogging (blue circles) and control (grey circles) treatment. Results are means ± standard deviation (SD) of 3 biological replicates (n = 3). Statistical analysis: unpaired t-test ($p < 0.05$) for physiological parameters, unpaired multiparametric t-test corrected for multiple comparisons using the two-stage step-up method of Benjamini, Krieger, and Yekutieli (FDR < 0.05) for the time course of the SPAD values and two-way ANOVA with Tukey's test ($p < 0.05$) for photosynthetic parameters on each day of the waterlogging treatment; different letters indicate statistically different groups.

For 4-week old plants at the start of treatment, SPAD values changed within the first 4 days of waterlogging. While these values were higher in waterlogged plants at 4 days of treatment, at later time points, these SPAD values were lower under waterlogged conditions compared to normal watering (**Figure 4.3 A**). SPAD values of plants that were 3 weeks old at the start of waterlogging were not affected until day 12 of treatment, when they became lower in waterlogged plants compared to the control. For 2-week old plants at the start of treatment, no differences were detected for SPAD values during the 15 days of waterlogging. When physiological parameters were measured, we observed reduced leaf area and plant weight, and increased shoot length in 2- and 3- week old plants that experienced waterlogging (**Figure 4.3 B**), while for plants that were 4 weeks old, 15 days of waterlogging did not cause changes in physiological parameters, as also found in **Figure 4.2 B**. Hence, plants that were 3 weeks old when starting the waterlogging treatment seemed to be the most consistently affected by waterlogging, both for photosynthetic and physiological measurements.

4.2.3. Conclusions

Taken together, these results indicate that, for a large screening to assess the differences in waterlogging tolerance among approximately 100 rapeseed varieties, the most adequate approach would be to use (i) waterlogging to induce hypoxic conditions, and (ii) plants that are 3 weeks old at the start of treatment. These preliminary experiments also allowed us to identify some measurements (photosynthetic and physiological) that could be taken to assess the response of rapeseed plants to waterlogging.

4.3. Screening for rapeseed waterlogging tolerance and resilience to combined waterlogging and *S. sclerotiorum*

4.3.1. Selection of internal controls

Before screening approximately 100 varieties for waterlogging tolerance +/- *S. sclerotinia*, we verified whether the experimental conditions chosen would allow us to indeed detect tolerance/sensitivity to waterlogging amongst rapeseed varieties, while also identifying some varieties that could be used as internal controls for the screen. To this end we performed a pilot experiment with 15 different varieties to (i) check throughput and reproducibility of measurements, (ii) provide estimates of trait variability within and between varieties and (iii) identify tolerant and sensitive varieties that could serve as controls to account for batch effects and other environmental factors. We selected the 15 test varieties based on geographical origin, considering local annual precipitations and time of sowing, with the idea that varieties from areas with high precipitation, may have been selected by breeders for waterlogging tolerance, while varieties bred in regions with lower precipitation may be more sensitive to waterlogging.

Among all the parameters analysed, SPAD was the only photosynthesis-related parameter that consistently showed decreased values in all the varieties treated with waterlogging compared to control-treated plants from the same variety (**Figure 4.3 A**). To quantify by how much waterlogged-treated groups differed from control-treated plants from the same variety, an effect size analysis was performed using Hedge's g formula (**see section 2.3.2 above**; Hedges, 1981; Ialongo, 2016) (see g values obtained on top of bars in each of the graphs in **Figure 4.3 A**). In this analysis, g values close to 0.5 are considered as medium effects, while g values of at least 0.8 are considered as a strong effect. Based on this, we only considered |g values| > 0.5 in our analysis. In addition, negative values indicate that waterlogging negatively affects plants compared to control-treated plants from the same variety, while positive values would indicate that waterlogged plants perform better. Effect size analysis for SPAD values yielded negative g values for all varieties, indicating that waterlogging treatment impacted in a negative manner to all the 15 tested varieties. This analysis also revealed that variety #240 had the smallest g value (-3.00), suggesting that, based on SPAD measurements, among the 15 varieties tested, #240 could be the most affected by waterlogging. In contrast, varieties #275 and #242 had the highest g values (-0.63 and -0.61, respectively), suggesting that they may perform better under waterlogging (**Figure 4.4**).

A similar analysis was performed for the other photosynthesis-related measurements, namely Fv'/Fm', ΦII and NPQt. For Fv'/Fm', although both negative and positive g values were obtained, the absolute g values were in many cases smaller than 0.5 (|g value| < 0.5), suggesting a small effect of waterlogging on this measurement. The largest effects were observed for varieties #239 and #274 for negative g values (-0.52 and -0.63, respectively), and for variety #283 for the positive g values (+0.63). For ΦII, both positive and negative g values were obtained and varieties #261 and #418 were the most affected (g values of -1.23 and -1.21, respectively). Finally, because NPQt estimates the excess energy dissipated as heat, for this measurement, varieties with positive g values would be considered as being more affected by waterlogging. Effect size analysis with NPQt yielded both negative and positive values, with most being small, however, variety #229 displayed the biggest ratio in this parameter (0.69), followed by variety #274 (0.6).

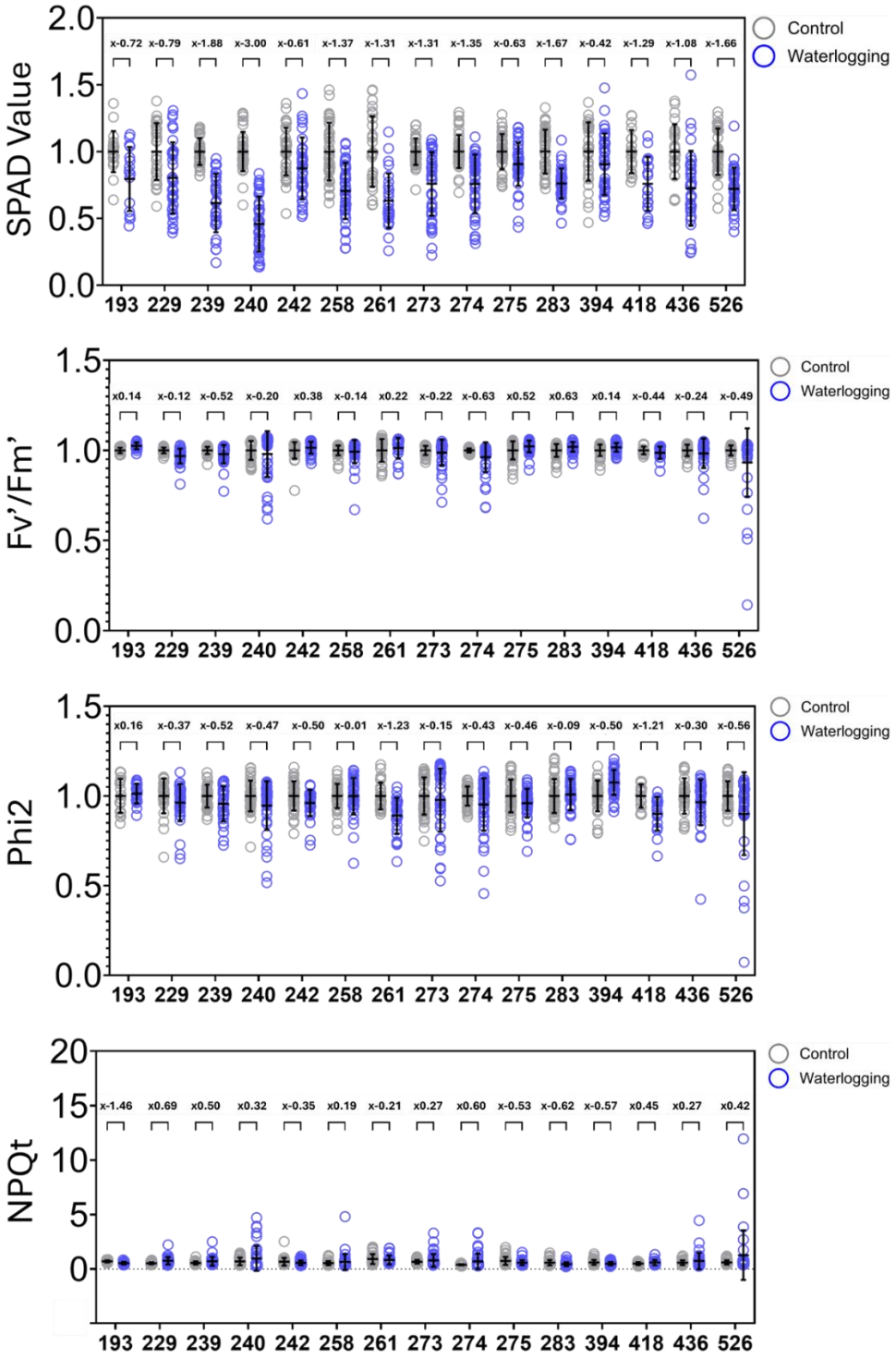

Figure 4.4. Waterlogging effects different in rapeseed varieties. Photosynthetic parameters were derived from measurements taken from the 3rd leaf of rapeseed plants using MultispeQ (SPAD, ΦII, Fv'/Fm', NPQt) at 15 days of waterlogging (blue circles) and control (grey circles) conditions. Results are means ± standard deviation (SD) of 3 biological replicates (n = 3). Statistical analysis: two-way ANOVA with Tukey's test ($p < 0.05$), effect sizes were calculated following Hedge's g formula (Hedges, 1981; Ialongo, 2016).

Both physiological parameters (leaf area and shoot fresh weight (FW)) consistently showed negative g values, corresponding to waterlogging having a negative effect on the growth of all 15 varieties (**Figure 4.5**). The absolute g values obtained tended to be larger compared to those calculated for photosynthetic parameters (except for SPAD measurements) and suggested that varieties #240, #242, #436 and #526 were among the most strongly affected by waterlogging treatment, and hence potentially more sensitive. In contrast, variety #418 seemed less sensitive compared to the others.

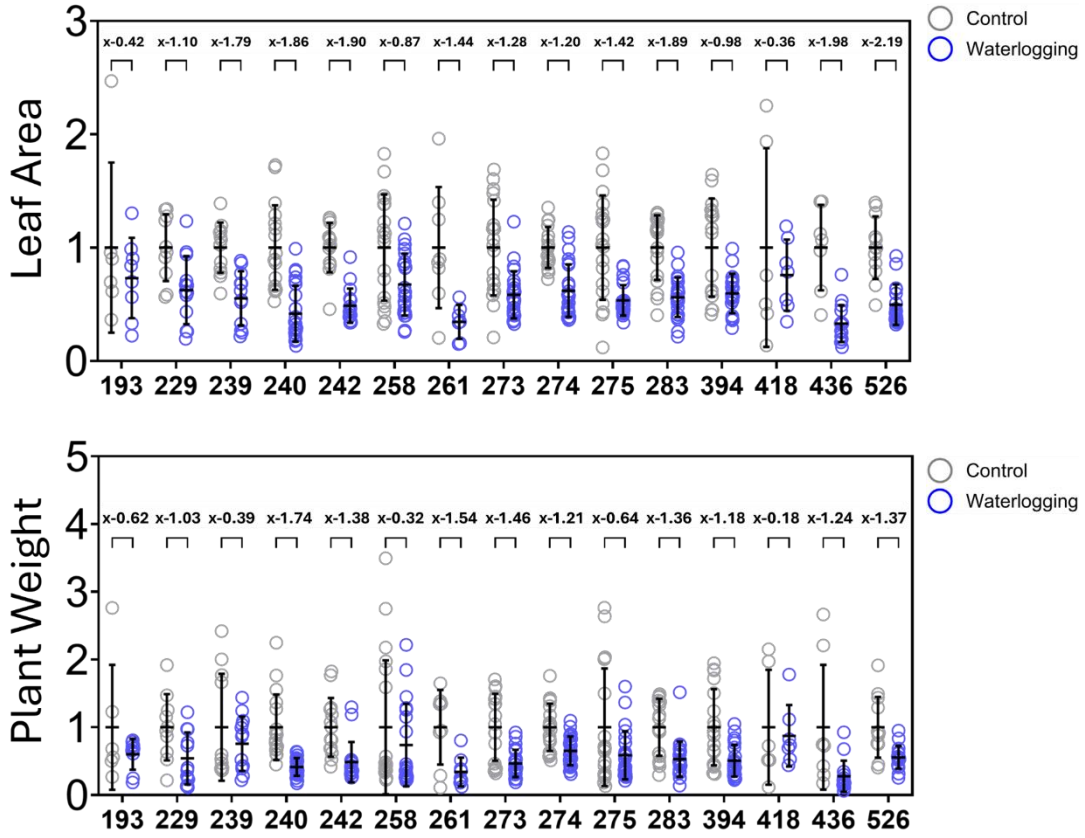

Figure 4.5. Waterlogging affects differently physiological measurements. Physiological parameters (plant weight and leaf area) taken at day 15 of waterlogging (blue circles) and control (grey circles) treatment. Results are means ± standard deviation (SD) of 3 biological replicates (n = 3). Statistical analysis: two-way ANOVA with Tukey's test ($p < 0.05$), effect sizes were calculated following Hedge's g formula (Hedges, 1981; Ialongo, 2016).

Altogether, this pilot experiment with 15 different rapeseed varieties suggested that the chosen experimental conditions could be suitable to distinguish between rapeseed varieties that may be sensitive to waterlogging. Moreover, when put together (**Figure 4.6**), these results allowed

the selection of two varieties that could serve as internal controls across the multiple batches and replicates that could be used to screen the whole population of approximately 100 varieties. This will be important at later stages, to account for batch-specific and environmental-dependent effects, to monitor the performance of the experiment and to improve statistical analyses. Specifically, we selected varieties #240 and #229 as internal controls, as #240 seemed to be consistently more sensitive to waterlogging with a particularly strong effect on SPAD and leaf area measurements, while variety #229 showed a stronger response for NPQt and plant weight. An additional factor for choosing these two varieties was that they rapidly produced large amounts of seeds, which would ensure enough material for the large-scale screening.

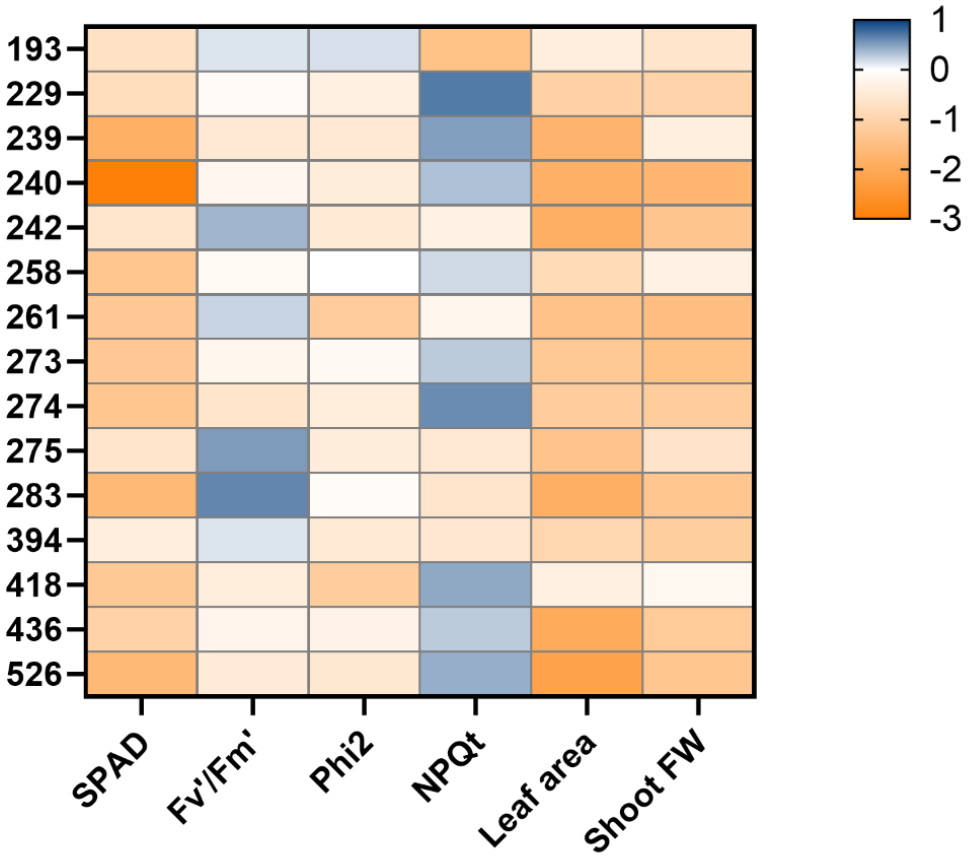

Figure 4.6. Waterlogging response differs among rapeseed varieties. Heatmap summarising the effect sizes calculates in **Figure 4.3**. Warmer colours indicate stronger sensitivity to waterlogging, whereas cooler colours denote less sensitivity.

4.3.2. Overview of the experimental approach to the screen and of data obtained

4.3.2.1. Experimental design for the screen

As outlined in the Introduction, this project aims to identify rapeseed varieties that are tolerant/sensitive to waterlogging, as well as resilient to the combination of waterlogging and *S. sclerotiorum*. To this end, the 100 rapeseed varieties subset of the BRAVO collection of commercial rapeseed varieties (kindly provided by collaborators at the John Innes Centre: Dr. Rachel Wells, Prof. Chris Ridout and Prof. Lars Østergaard) was screened for waterlogging tolerance, and subsequent infection with the necrotrophic fungal pathogen *S. sclerotiorum*. As this aspect of my PhD work was part of a larger project funded by Research Ireland, I shared the work with a postdoctoral researcher in the lab, Dr. Shreenivas Singh, who carried out the *S. sclerotiorum* pathogen assays, while I focused on the waterlogging treatments. The screen resulted in a large dataset that required complex statistical methods for analysis and correction. This statistical analysis was performed by our collaborator Prof. Rafael de Andrade Moral (Maynooth University), who also provided advice for the experimental set up of the screen.

As the ~100 rapeseed varieties could not be handled at the same time, the screen was carried out in batches. Each batch contained four randomly selected varieties and two internal controls (varieties #240 and #229) that could be used to identify and correct for batch-dependent effects, ensuring robust statistical comparisons across batches and biological replicates. In addition to having batches, 3 biological (independent) replicates were completed sequentially over a period of two years, so that all varieties were tested in batches in the first replicate, before initiating the second replicate. The batches also contained of different varieties (apart for the #240 and #229 controls) in each biological replicate. Trays were randomly distributed in the greenhouse, and plants corresponding to each variety were grown and waterlogged in individual trays to avoid potential effects of one variety on another (**Figure 4.7**). To ensure enough statistical power for analysis, we aimed at having 8 plants/variety/experimental condition/biological replicate. Due to germination problems, however, this was not always the case, and in such situations, the available plants were equally split between each of the treatments.

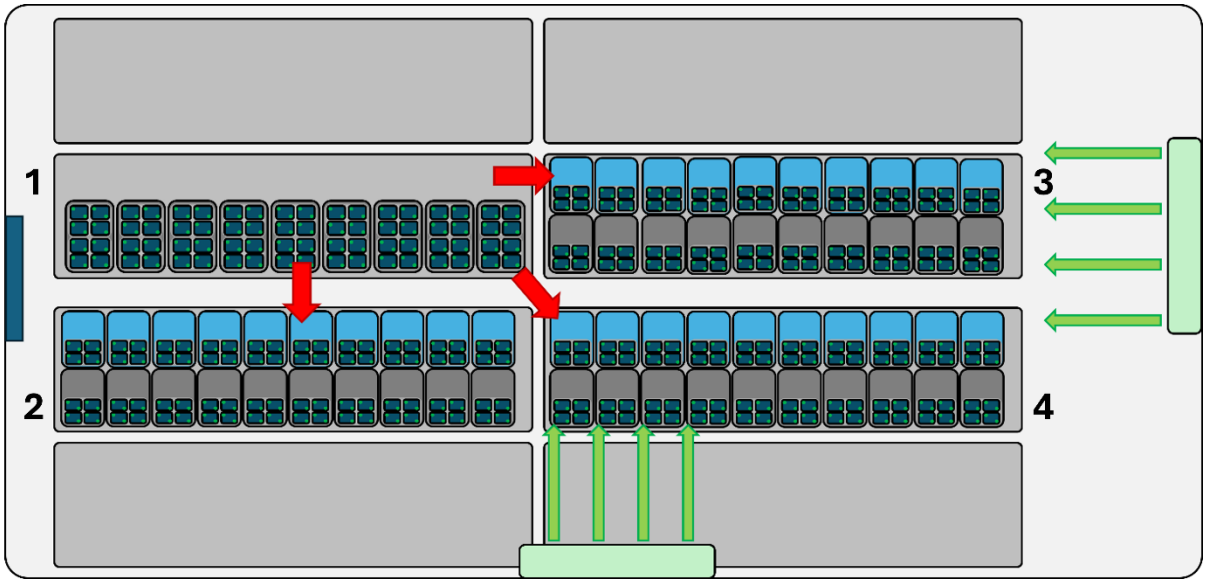

Figure 4.7. Plant arrangement during waterlogging screening in the greenhouse. Plants were grown for 3 weeks on **Table 1**, then they were moved to **Tables 2, 3, or 4** as they face waterlogging or control conditions for 15 days. Green arrows represent the air currents given by the AC units (green squares). Blue squares represent plants undergoing waterlogging treatment

Plants responses to waterlogging were measured using the same photosynthetic (on the 3rd leaf) and physiological parameters as those outlined in **Table 4.1**. For multispeQ measurements, two independent measurements were taken close to the tip of each leaf and on each side of the mid vein. The average of these measurements was calculated and treated as a single representative value for that leaf. This approach reduced the variability of the measurements and the influence of physiological variability within the leaf, providing a more robust estimate of the different photosynthetic measurements. In addition, the multispeQ device measured environmental variables such as Photosynthetically Active Radiation (PAR), ambient humidity and ambient temperature. Other variables that were recorded included (i) location of each batch in the greenhouse to account for the airflows present in different areas, (ii) age and type of lamps (this was necessary, because of an upgrade that had to be scheduled at the end of the first replicate and which resulted in a change of lighting system in the greenhouse), and (iii) light intensity of the lamps, which was regularly adjusted during autumn and spring to account for decreased and increased natural light. The systematic recording of these environmental parameters together with the presence of the internal controls within every batch allowed correction of the data for batch-dependent environmental factors to ensure that the observed

differences were caused by genetic diversity instead of environmental variation in the greenhouse.

In order to determine the effect of waterlogging on plant *S. sclerotinia* infection, after 15 days of waterlogging (or for control plants, 15 days of normal watering), the third leaf (used for multispeQ measurements) was infected with *S. sclerotiorum* using a detached leaf assay (Zamani-Noor and Jedryczka, 2025). The lesion size caused by *S. sclerotiorum* infection was then measured at 24 and 48 hours post inoculation (hpi). The pathogen inoculations, as well as lesion size measurements were performed by Dr. Shreenivas Singh.

Altogether, our screen resulted in a large dataset of 14 parameters that were measured (columns) and 5,990 rows (number of individual plants used).

4.3.2.2. Overview of the raw data obtained

To obtain an overview of the results, all averages and standard deviations calculated from the raw data were plotted, both for control and waterlogged plants. Examination of the plots indicated that some traits were markedly different between control and waterlogged populations, such as for example Fm', ΦII or SPAD, while other measurement such as leaf thickness, and lesion sizes at 24 and 48 hpi did not show clear differences between control and waterlogged populations (**Figure 4.8**). Overall, there also appeared to be differences between varieties, especially within the plant populations that experienced waterlogging. However, without a statistical model that accounts for environmental factors, it is difficult to further identify differences that may be linked to genotype within the population.

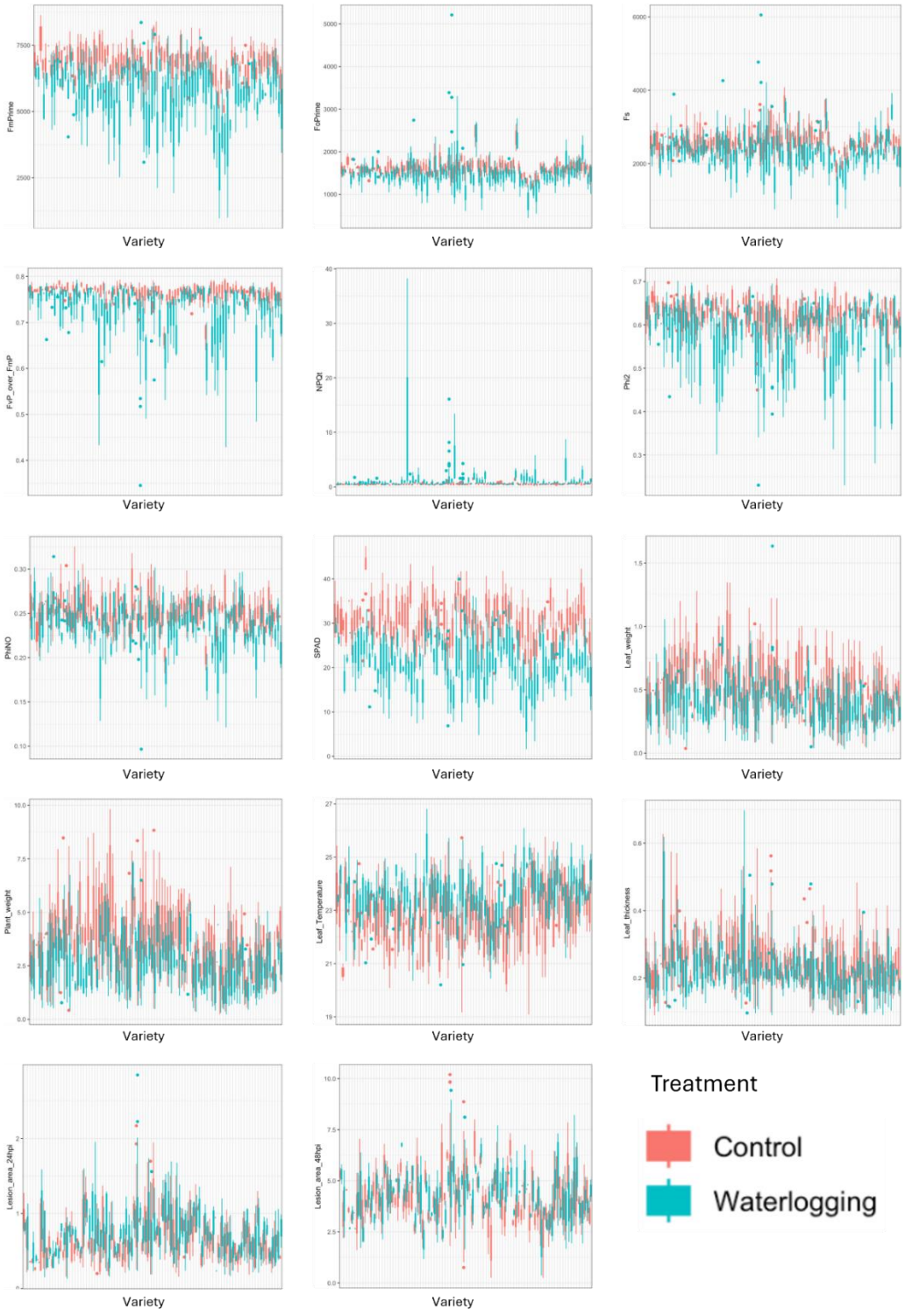

Figure 4.8. Overview of the raw data obtained. Different measurements made for each variety and treatment are shown, including Fm', Fo', Fs, Fv'/Fm', SPAD, ΦII, ΦNO, NPQt, leaf temperature, leaf thickness, leaf weight, plant weight, and lesion size at 24 and 48 hpi. The X-Axis corresponds to the different varieties, which are arranged so that for a given variety, the data for control (red) and waterlogged (blue) are shown next to each other. Results are means ± standard deviation (SD) of 3 biological replicates (n = 3).

4.3.3. Statistical analysis of the dataset

To identify genetically determined differences between rapeseed varieties in terms of waterlogging tolerance/sensitivity and for resilience to the combination of waterlogging + *S. sclerotiorum*, we analysed the data using two different approaches:

(i) identifying differences between varieties in control conditions, and separately in waterlogged conditions. For example, in this analysis, after data normalisation, we compared all varieties to each other after waterlogging and determined those that behaved differently from the entire population of waterlogged varieties. This analysis is outlined in **section 4.3.3.1 below**.

(ii) Identifying differences in the varieties' ability to respond to waterlogging and maintain photosynthetic capacity and growth. For this analysis, for each variety and for each type of measurement, ratios of waterlogged:control were calculated and considered to rank the varieties after data normalisation. The results of this analysis are explained in **section 4.3.3.2 below**.

Considering the complexity of the dataset and of the corrections needed, this statistical analysis was performed by our collaborator Prof. Rafael de Andrade Moral. The results and their interpretation are presented below.

4.3.3.1. Comparison of varieties within either waterlogged or control populations

First, the raw MultispeQ measurements were analysed using a mixed-effects model including treatment variable (control vs. waterlogging), together with environmental covariates (batch location, light intensity, lamp age, ambient humidity, ambient temperature, and time of day when the measurement was taken) as fixed effects. These covariates allow for the quantification and correction for environmental changes that might influence photosynthetic and physiological performance individually (per measurement). In addition, batch number and variety name were included as random factors, as these parameters introduce structured variability that needs to be accounted for. The variety itself was treated as a random effect to estimate the variability between rapeseed varieties, accounting for the effect of genetic diversity on waterlogging responses. Biologically, this model quantifies both the global impact of waterlogging on photosynthetic, physiological and pathogenesis-related measurements, while accounting for how individual varieties diverge from the population's mean under either control or waterlogged conditions, as well as with/without the *S. sclerotiorum* pathogen. For clarity, we

refer to this as the "*absolute"* approach below. For all response variables we assumed a normal distribution, except ΦII and ΦNO, which are continuous proportions between 0 and 1, and therefore a beta distribution was assumed.

To determine the overall effect of waterlogging on each measured parameter, the regression coefficients of the absolute analysis approach were analysed (**Table 4.2**). These coefficients indicate by how much and in which direction the different parameters measured change depending on the environmental covariates. In the case of waterlogging treatment, all photosynthetic-related parameters were reduced except for NPQt and leaf temperature, suggesting that the waterlogging treatment negatively affects photosynthetic capacity (**Table 4.2**) (Tietz et al., 2017). Because an increase in NPQt suggests loss of photosynthesis efficiency (i.e. more energy is dissipated as heat), the results obtained for this measurement are in line with the other photosynthetic ones. Waterlogging treatment also negatively affected the physiological parameters recorded (*e.g*. plant weight), suggesting a negative effect of waterlogging on growth (**Table 4.2**). In terms of plant resistance/susceptibility to *S. sclerotiorum*, the model could not predict with sufficient confidence that the effect was different from zero for the lesion size measurements at 24 hpi and 48 hpi, suggesting a lack of influence of waterlogging treatment in the progression of *S. sclerotiorum* infection in detached leaves (**Table 4.2**).

Table 4.2. Regression coefficients accounting for waterlogging effect on all the varieties for each parameter measured in the screen. Values represent the estimated regression coefficients (Estimate) with their corresponding standard errors (Std. Error) and 95% credible intervals (l-95% CI and u-95% CI). Negative estimates indicate a decrease in the parameter value upon waterlogging relative to control, whereas positive estimates indicate an increase. Effects are considered statistically significant when the 95% confidence interval does not include zero, indicating that waterlogging had a meaningful impact on that parameter.

Parameter	Estimate	Std. Error	l-95% CI	u-95% CI
Fm'	-1070.72	90.73	-1252.92	-891.85
Fo'	-117.96	27.45	-171.49	-65.49
Fs	-253.18	43.86	-339.76	-167.4
Fv'/Fm'	-0.03	< 0.01	-0.04	-0.02
NPQt	0.56	0.18	0.2	0.9
ΦII	-0.16	0.03	-0.21	-0.11

ΦNO	-0.09	0.01	-0.12	-0.07
SPAD	-9.09	0.56	-10.16	-7.99
Leaf Temp.	0.64	0.09	0.47	0.81
Leaf Thickness	-0.04	0.01	-0.05	-0.03
Leaf Weight	-0.15	0.02	-0.18	-0.11
Plant Weight	-1.02	0.13	-1.26	-0.77
Lesion Area (24h)	0.05	0.03	< 0.01	0.1
Lesion Area (48h)	0.11	0.11	-0.11	0.32

Having determined the global impact of waterlogging treatment on photosynthetic and physiological parameters, the next question was whether this impact was different depending on the rapeseed variety considered. The variety-dependent random effects (*i.e.* a prediction of the effect of the variety on the response to the stress after data normalisation) were used to answer this question. When comparing variety-dependent variation between control and waterlogged conditions, we found increased variation in photosynthesis-related parameters upon waterlogging, suggesting that there are intrinsic differences in the manner individual rapeseed varieties respond to waterlogging in the whole population (**Table 4.3**). In contrast, physiological parameters show a decrease in variability upon waterlogging, suggesting that, even though the waterlogging treatment negatively affects growth, differences fall within a narrower range after waterlogging (**Table 4.3**). A similar observation was made for the lesion size at 24 and 48 hpi.

Table 4.3. Variance of the random effects and confidence intervals for each measured parameter. Values represent the estimated variances (Estimate) with their corresponding standard errors (Std. Error).

Parameter	Treatment	Estimate	Std. Error
Fm'	Control	106.07	68.18
	Waterlog.	631.94	70.26
Fo'	Control	51.02	28.02
	Waterlog.	171.21	22.78
Fs	Control	120.3	40.16
	Waterlog.	275.13	33.33
Fv'/Fm'	Control	< 0.01	< 0.01

	Waterlog.	0.03	< 0.01
NPQt	Control	0.07	0.05
	Waterlog.	1.28	0.14
ΦII	Control	0.02	0.01
	Waterlog.	0.17	0.02
ΦNO	Control	0.01	0.01
	Waterlog.	0.08	0.01
SPAD	Control	2.21	0.41
	Waterlog.	3.11	0.41
Leaf Temp.	Control	0.26	0.11
	Waterlog.	0.26	0.11
Leaf Thickness	Control	0.02	0.01
	Waterlog.	0.01	0.01
Leaf Weight	Control	0.08	0.02
	Waterlog.	0.02	0.01
Plant Weight	Control	0.5	0.13
	Waterlog.	0.15	0.11
Lesion Area (24h)	Control	0.06	0.03
	Waterlog.	0.03	0.02
Lesion Area (48h)	Control	0.25	0.14
	Waterlog.	0.15	0.1

Random effects were subjected to a Principal Component Analysis (PCA) as a quality-control overview before formal statistics. This analysis allows the (i) visualization of how samples group by treatment (control vs waterlogging), (ii) spotting of trait modules (e.g., ΦII / Fv'/Fm' vs NPQt) and redundancy from mathematically linked indices, and (iii) quantification of the traits driving separation (loadings).

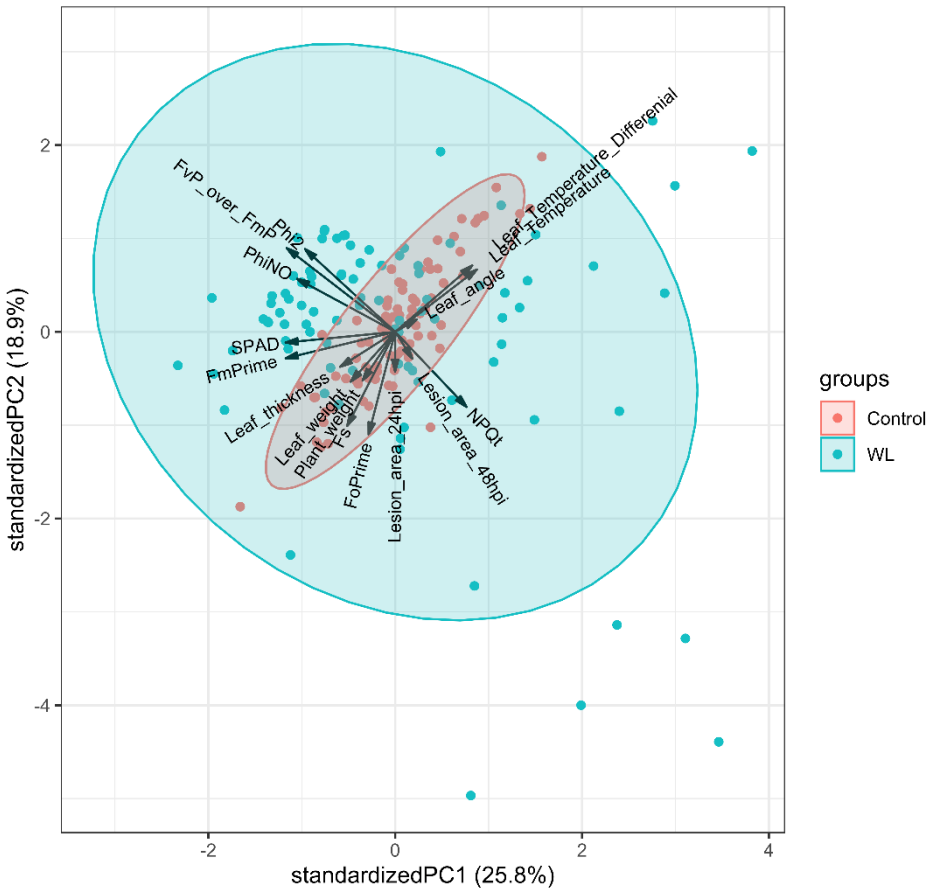

Figure 4.9. Principal Component Analysis (PCA) of physiological and phenotypic traits in control and waterlogged (WL) *Brassica napus* plants. PCA biplot illustrating the distribution of rapeseed cultivars grown under control (red dots) and waterlogged (blue dots) conditions based on standardised physiological and phenotypic parameters. Arrows indicate the loading vectors of each variable, each point represents a cultivar, and 95% confidence ellipses indicate the multivariate spread of each treatment group. The first two components (PC1 = 25.8%, PC2 = 18.9%) together explain 44.7% of the total variance.

PCA analysis accounts for 44.7% of the total variance, explained by the first two components (PC1 = 25.8%, PC2 = 18.9%) (**Figure 4.9**). PC1 separates traits in the stress-responsive traits in the positive values, such as lesion area caused by *S. sclerotiorum* at 48 hpi, NPQt or leaf temperature, and physiological and photosynthetic efficiency-related traits in the negative values, such as ΦII, Fv'/Fm' or SPAD. However, it is not clear what PC2 accounts for by looking at the trait positioning along this axis (**Figure 4.9**). Taking into account the vector lengths and directions, ΦII, ΦNO, Fv'/Fm', NPQt, or SPAD explain more variation than other

measurements such as leaf thickness or leaf angle, therefore indicating that these traits are suitable for GWAS analysis.

Blue dots indicate cultivars measured in waterlogged conditions and form a cloud that is shifted slightly to the positive values of PC1, suggesting that plants experiencing waterlogging show higher stress-responsive trait values and lower physiological and photosynthetic efficiency-related trait values (**Figure 4.9**). On the contrary, cultivars measured in control conditions (red dots), cluster more towards the centre and slightly to the left, suggesting more homogeneous physiological responses under non-stressed conditions (**Figure 4.9**). However, there is a substantial overlap between both groups, which comes from the different responses given by the different rapeseed cultivars, which can maintain photosynthetic efficiency and pigment status instead of activating photoprotective mechanisms, which indicates tolerance when dealing with waterlogging conditions; or increase photoprotective mechanisms in response to lower photosynthetic efficiency of waterlogged plants.

In addition, several photosynthetic traits are also mathematically linked by definition (**Table 4.10**), and therefore, can mislead our interpretations of the data from the large-scale screening. Therefore we plotted a correlation matrix to have a visual image of this correlation between photosynthetic parameters. Some of these relationships include NPQt negative correlation with ΦNO, ΦII and Fv'/Fm' or the positive correlation between Fv'/Fm' and ΦII (**Figure 4.10),** as expected.

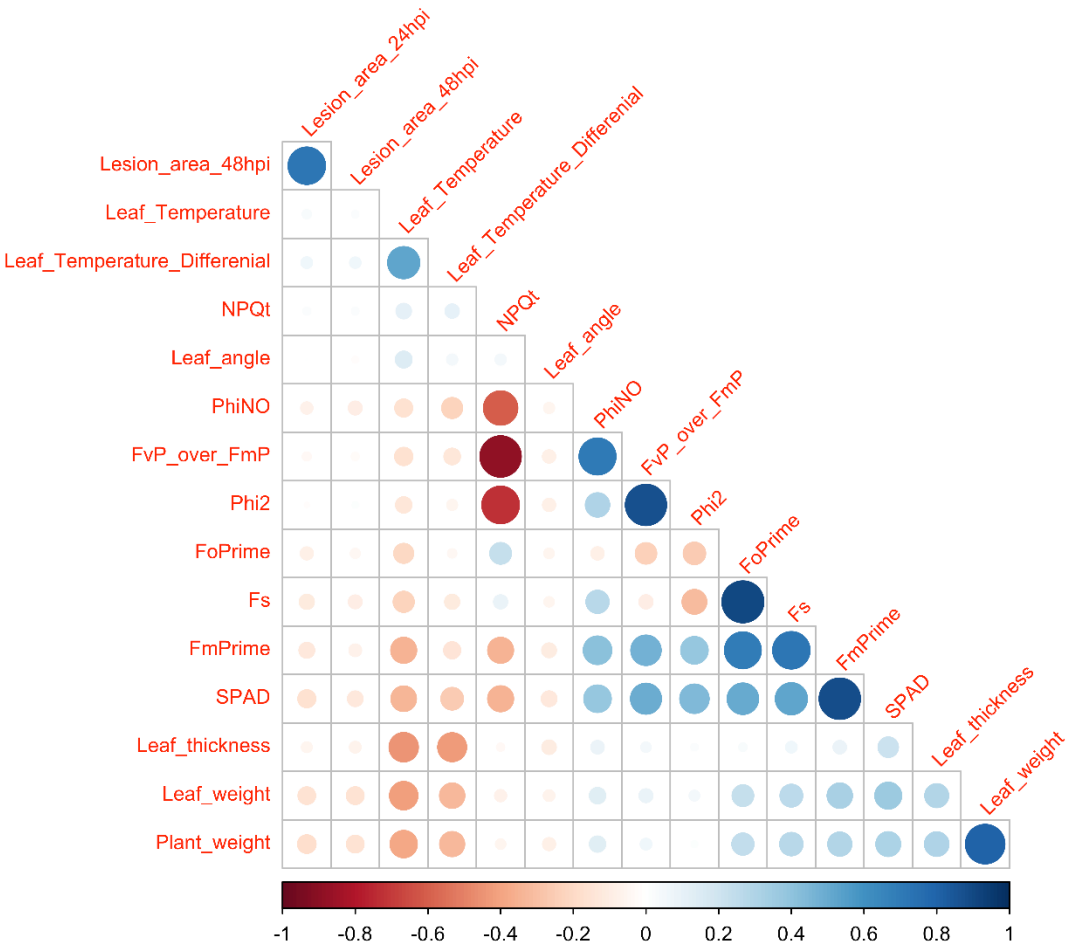

Figure 4.10. Correlation structure of photosynthetic traits in *Brassica napus* under waterlogging followed by *S. sclerotiorum* infection. Heatmap shows pairwise correlations among the different traits evaluated in the large-scale screening. Cells display Pearson's r (two-tailed tests; Benjamini–Hochberg–adjusted *P* values). Rows/columns are ordered by average-linkage hierarchical clustering to reveal trait modules. Colour scale indicates correlation magnitude (blue, positive; white, zero; red, negative).

Next, we considered the random effects for each variety and each parameter measured within the population for both control and waterlogged conditions separately. Thereby, we can determine by how much each variety deviates from the population mean (predicted random effects) in each treatment conditions, with a range (credible intervals) showing the uncertainty of the model estimate. The plotted predicted random effects take into account environmental and batch effects, thus showing the performance of each variety as a deviation from the population mean caused by genetic differences. Therefore, these graphs indicate which varieties perform

better than the population average (i.e. waterlogging tolerance; in blue except for NPQt), or below the population average (waterlogging sensitivity; in red, except for NPQt).

For example, for Fm' (see **Table 4.1** for definition), there were statistically significant differences between the varieties under waterlogging conditions, so that varieties #414, #436, #401, #438, #418, #230, #258, #448, #203, #237 and #411 could potentially be sensitive to waterlogging treatment, whereas varieties #99, #121, #221, #105, #242 and #96 were identified as potentially tolerant (**Figure 4.11**).

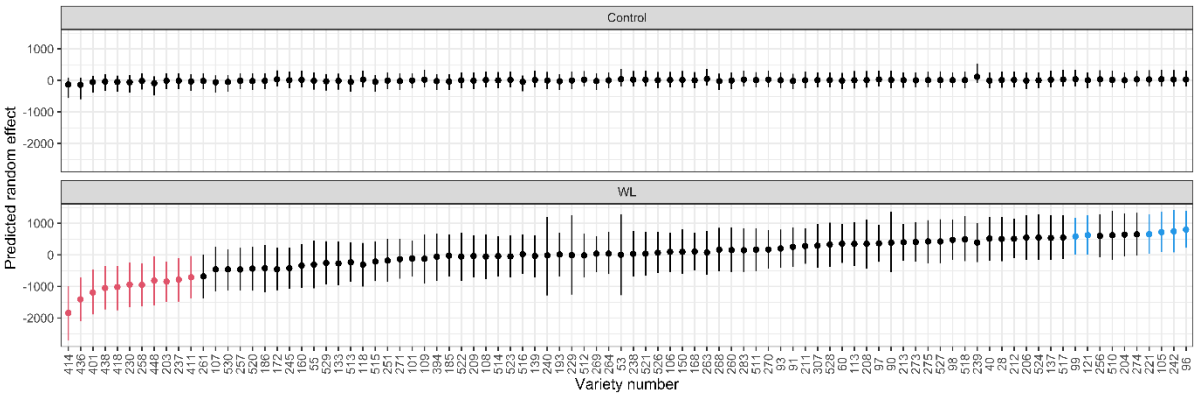

Figure 4.11. Predicted random effects of rapeseed varieties for Fm' under control and waterlogged conditions. Predicted random effects ± credible intervals are shown for each individual rapeseed variety. The varieties are identified based on their 3-digit identifier on the X-Axis.

The same analysis was repeated for each of the photosynthetic parameters that were measured. Each of the plots are presented in **Figures 4.12 - 4.19**. Throughout the analysis, we could observe no significant deviations from specific varieties in control conditions across the parameters, except for the SPAD measurements, for which we observed statistically significant differences between some varieties grown in control conditions. In the waterlogged population, varietal differences were observed for Fo', Fs, Fv'/Fm', NPQt, ΦII, ΦNO and SPAD. The summary of the potentially waterlogging sensitive or tolerant varieties for each of the measured parameters is presented in **Table 4.4** below.

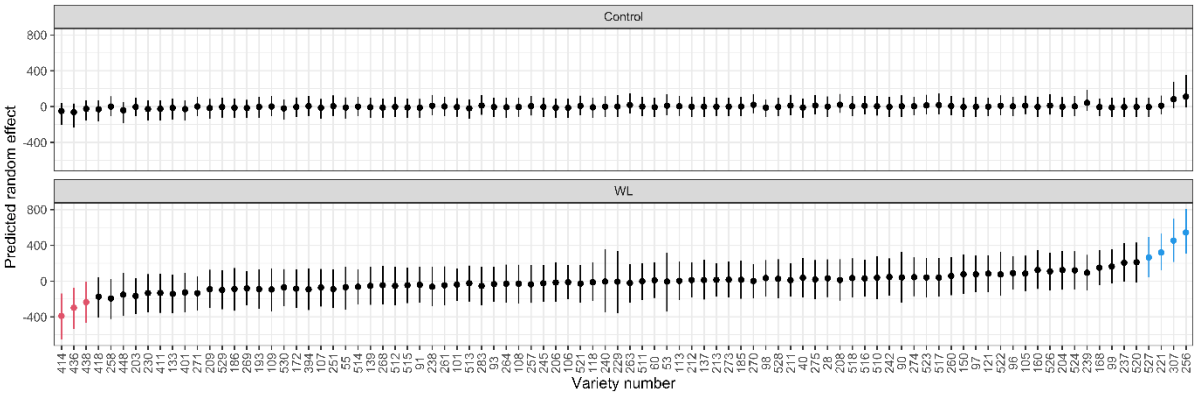

Figure 4.12. Predicted random effects of rapeseed varieties for Fo' under control and waterlogged conditions. Predicted random effects ± credible intervals are shown for each individual rapeseed variety. The varieties are identified based on their 3-digit identifier on the X-Axis.

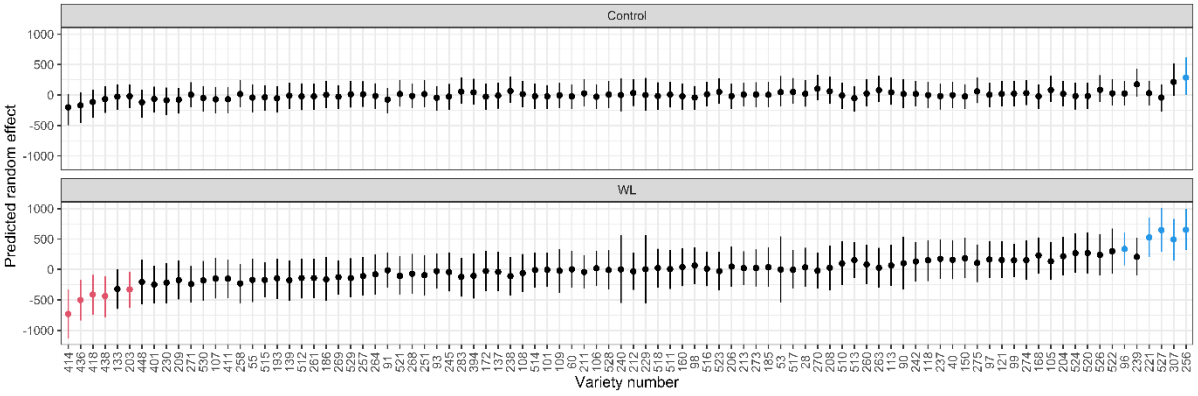

Figure 4.13. Predicted random effects of rapeseed varieties for Fs under control and waterlogged conditions. Predicted random effects ± credible intervals are shown for each individual rapeseed variety. The varieties are identified based on their 3-digit identifier on the X-Axis.

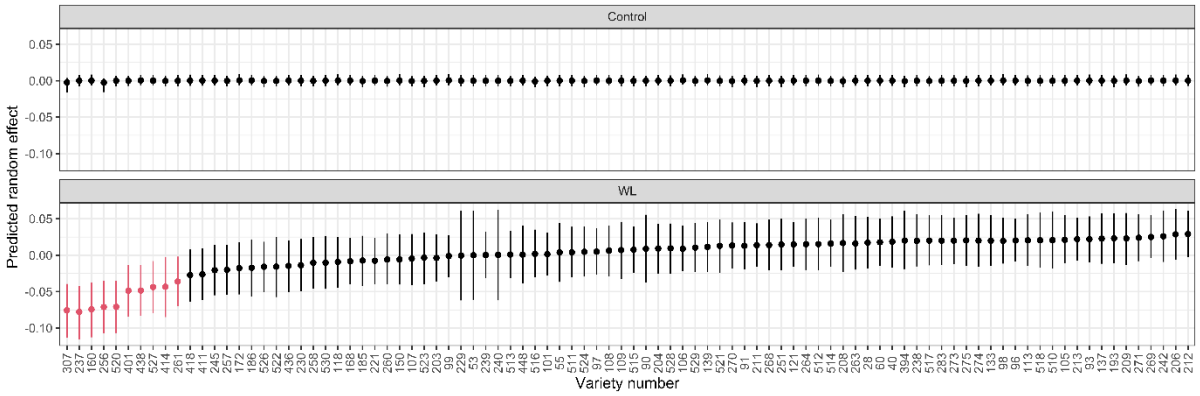

Figure 4.14. Predicted random effects of rapeseed varieties for Fv'/Fm' under control and waterlogged conditions. Predicted random effects ± credible intervals are shown for each individual rapeseed variety. The varieties are identified based on their 3-digit identifier on the X-Axis.

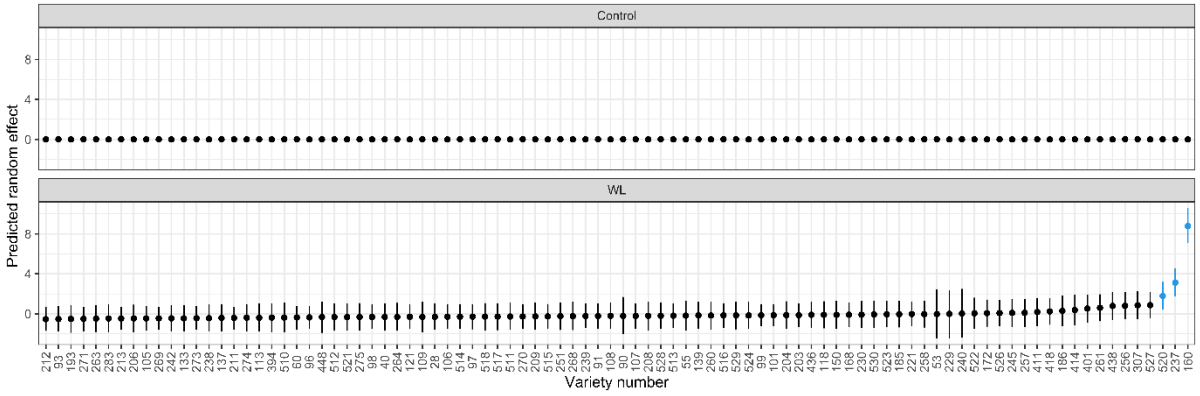

Figure 4.15. Predicted random effects of rapeseed varieties for NPQt under control and waterlogged conditions. Predicted random effects ± credible intervals are shown for each individual rapeseed variety. The varieties are identified based on their 3-digit identifier on the X-Axis.

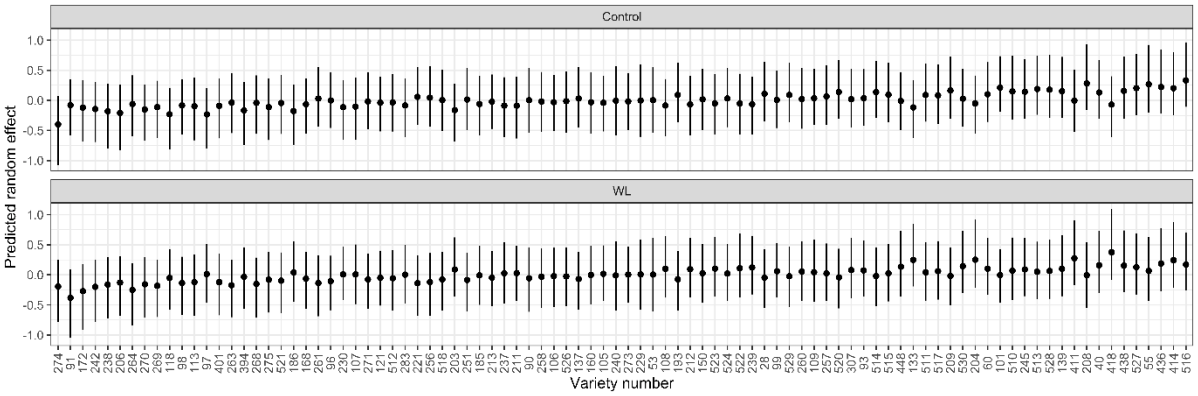

Figure 4.16. Predicted random effects of rapeseed varieties for Leaf Temperature under control and waterlogged conditions. Predicted random effects ± credible intervals are shown for each individual rapeseed variety. The varieties are identified based on their 3-digit identifier on the X-Axis.

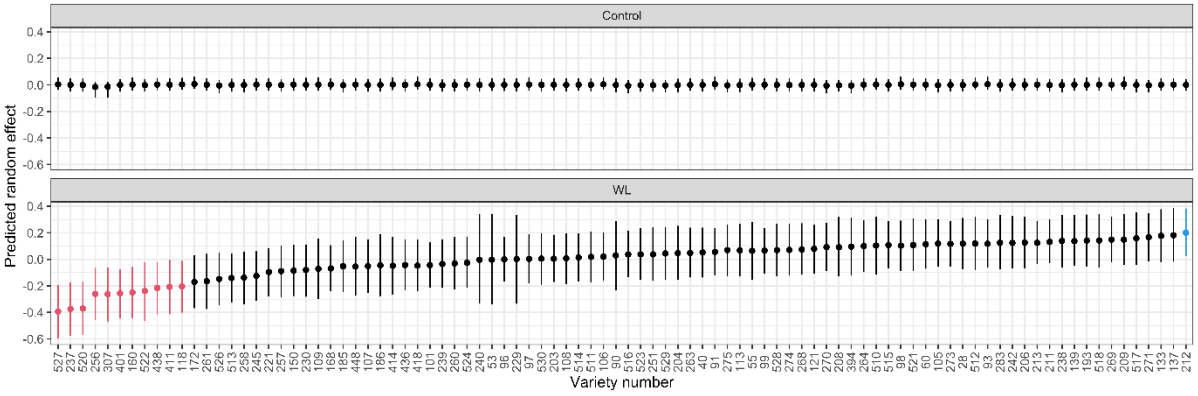

Figure 4.17. Predicted random effects of rapeseed varieties for ΦII under control and waterlogged conditions. Predicted random effects ± credible intervals are shown for each individual rapeseed variety. The varieties are identified based on their 3-digit identifier on the X-Axis.

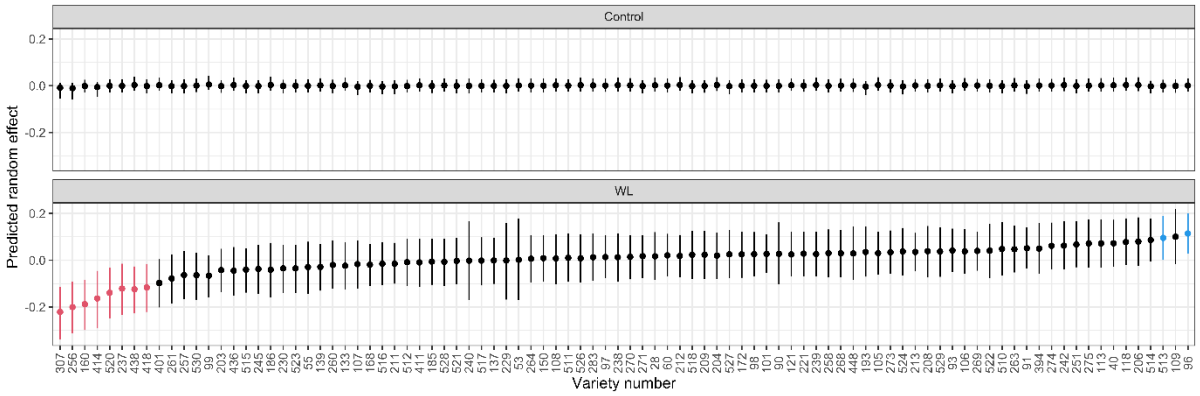

Figure 4.18. Predicted random effects of rapeseed varieties for ΦNO under control and waterlogged conditions. Predicted random effects ± credible intervals are shown for each individual rapeseed variety. The varieties are identified based on their 3-digit identifier on the X-Axis.

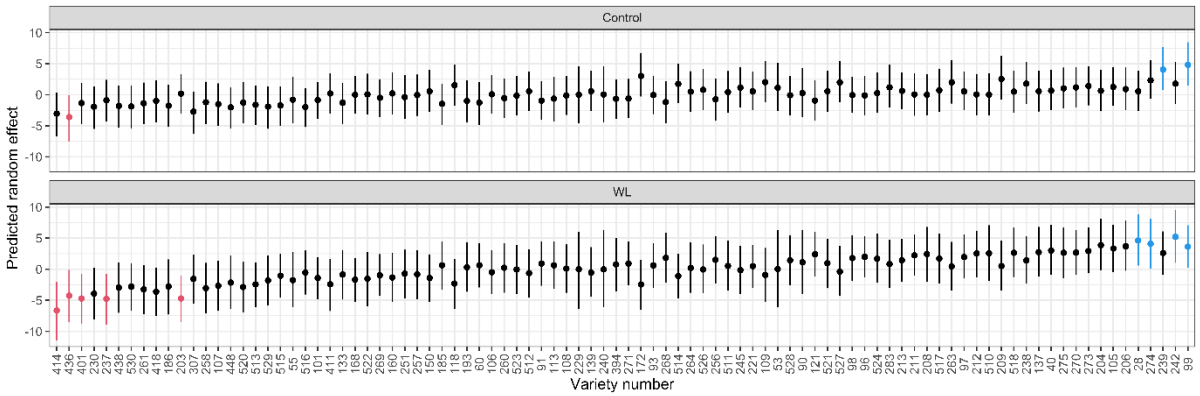

Figure 4.19. Predicted random effects of rapeseed varieties for SPAD under control and waterlogged conditions. Predicted random effects ± credible intervals are shown for each individual rapeseed variety. The varieties are identified based on their 3-digit identifier on the X-Axis.

When considering the physiological traits, 'leaf weight' corresponds to the weight of the 3rd leaf (on which multispeQ measurements were made), whereas 'plant weight' is the weight of the aerial part of the plant. The analysis of the predicted random effects based on these two types of measurements did not observe any varieties that behaved differently from the population in either treatment (**Figures 4.20**).

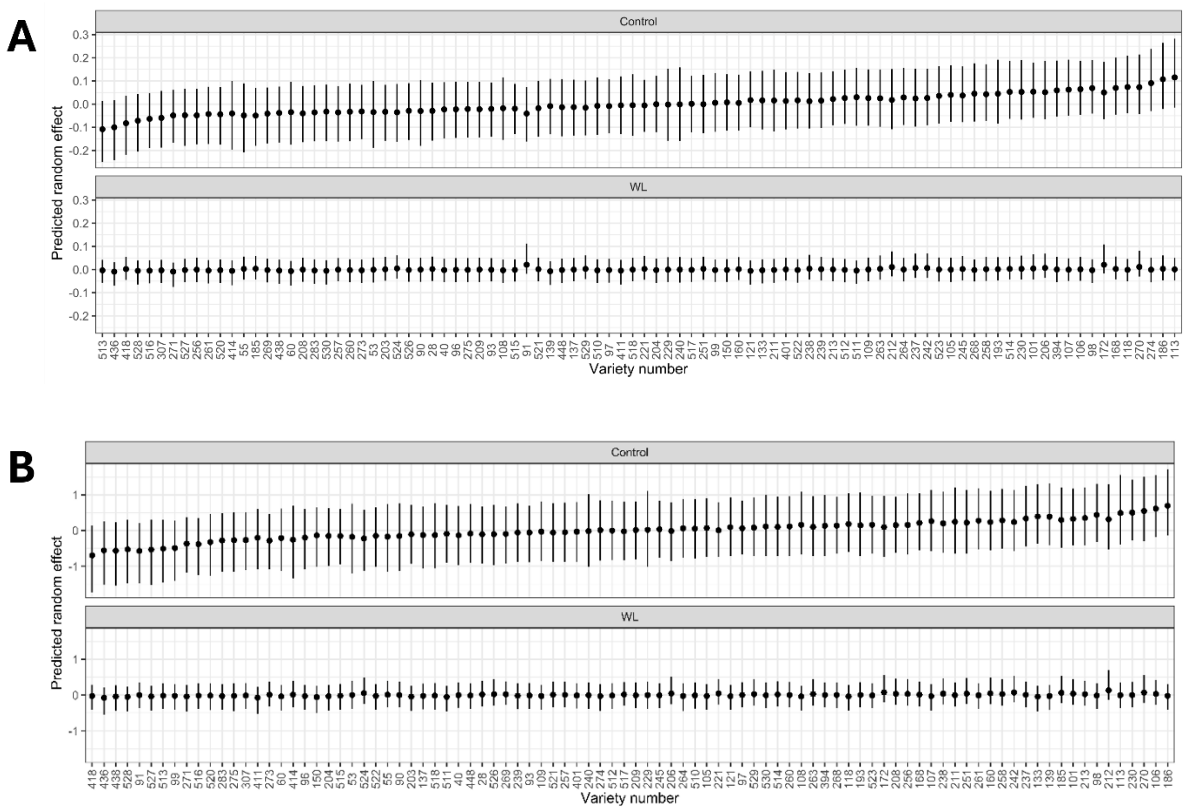

Figure 4.20. Predicted random effects of rapeseed varieties for leaf and plant weight under control and waterlogged conditions. Predicted random effects ± credible intervals are shown for each individual rapeseed variety. The varieties are identified based on their 3-digit identifier on the X-Axis.

Similarly to plant and leaf weight, analysis the leaf thickness parameter captured by the multispeQ did not allow for the identification of varieties that may be either sensitive or tolerant to waterlogging (**Figure 4.21**).

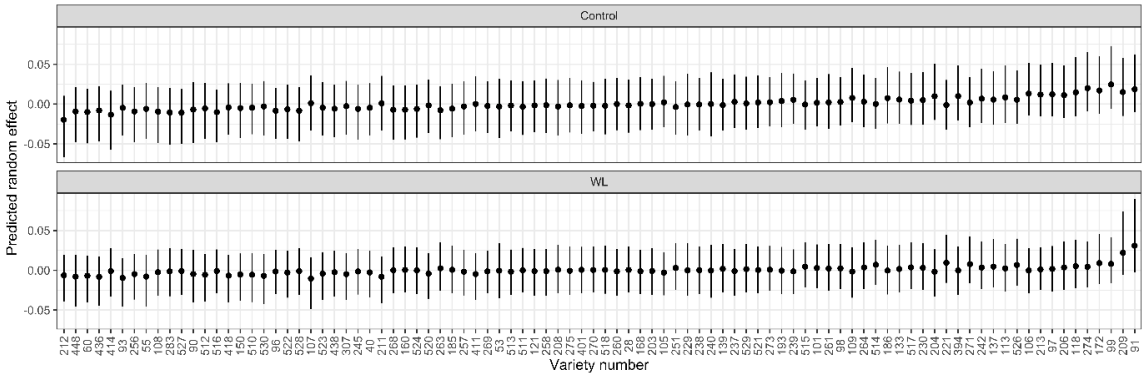

Figure 4.21. Predicted random effects of rapeseed varieties for leaf thickness under control and waterlogged conditions. Predicted random effects ± credible intervals are shown for each individual rapeseed variety. The varieties are identified based on their 3-digit identifier on the X-Axis.

Finally, analysis of the lesion size caused by *S. sclerotiorum* infection at 24 and at 48 hpi did not allow us to identify varieties that behaved differently in the control or in the waterlogged populations (**Figure 4.22**).

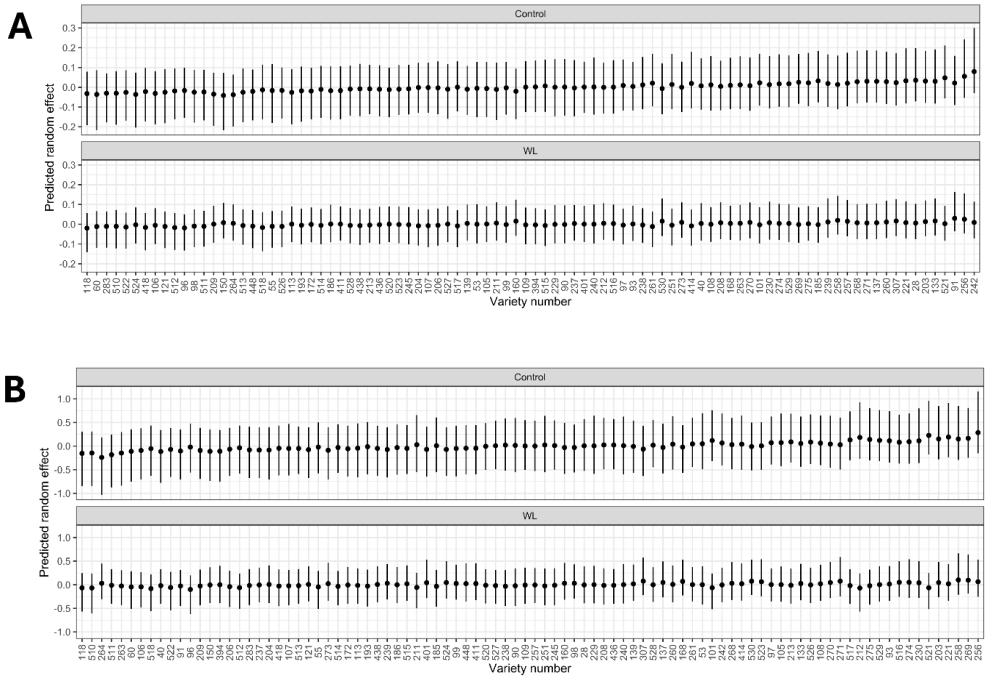

Figure 4.22. Predicted random effects of rapeseed varieties for lesion size of *S. sclerotiorum* infection under control and waterlogging conditions. Predicted random effects ± credible intervals are shown for each individual rapeseed variety at *S. sclerotiorum* infection at 24 hpi (A) and 48 hpi (B). The varieties are identified based on their 3-digit identifier on the X-Axis.

As indicated above, **Table 4.4** summarises the information gathered through the analysis of the random effects, listing for each measured parameter the varieties that could potentially be tolerant or sensitive.

Table 4.4. Putative tolerant and sensitive varieties based on the analysis of random effects for each measured parameter.

Parameter	Tolerant	Sensitive
Fm'	#96, #99, #105, #121, #221, #242	#203, #230, 237, #258, #401, #411, #414, #418, #436, #438, 448
Fo'	#221, #256, #307, #520, #527	#414, #436, #438
Fs	#96, #221, #256, #307, #527	#133, #203, #414, #418, #436, #438
Fv'/Fm'	-	#160, #237, #256, #261, #307, #401, #414, #438, #520, #527
NPQt	-	#160, #237, #520
ΦII	#212	#118, #160, #237, #256, #307, #401, #411, #438, #520, #522, #527
ΦNO	#96, #513	#160, #237, #256, #307, #414, #418, #438, #520
SPAD	#28, #99, #204, #242	#237, #401, #414, #436

Based on the aggregated data presented in **Table 4.4**, it is difficult to identify with confidence varieties that may be either tolerant or sensitive to waterlogging +/- *S. sclerotiorum*, because the different parameters measured do not consistently predict the same varieties as being tolerant or sensitive to the different treatments. In order to identify with more confidence candidate tolerant/sensitive varieties that could be studied in more detail, we sought to determine the overlap between the predictions of each of the measured parameters, presuming that a variety that is predicted as tolerant (or as sensitive) across a higher number of measured parameters is indeed more likely to perform better (or worse) under stress conditions. To this end,

we represented the data from **Table 4.4** as UpSet plots (**Figure 4.23**). Interestingly, varieties #237, #414 and #438 were predicted as sensitive to waterlogging in 6 out of the 8 parameters measured. Varieties #160, #401, #436 and #520 were predicted as sensitive to waterlogging in 4 out of the 8 traits analysed (**Figure 4.19**). Altogether, we concluded that these seven varieties were the most likely to be more sensitive to waterlogging. In contrast, the identification of varieties that could be predicted as tolerant to waterlogging across multiple measure parameters was more difficult, suggesting that this may be a less frequent trait in the population. The highest degree of overlap was observed with varieties #96 and #221, which displayed above-average performance in 3 out of 6 traits (Fv'/Fm' and NPQt did not identify any tolerant varieties) in response to waterlogging (**Figure 4.23**).

Intriguingly, we observed a set of varieties that were identified as potentially tolerant for some traits, but sensitive for others, for example, (i) variety #527 was identified as possibly sensitive to waterlogging for Fv'/Fm' and ΦII parameters, but maybe tolerant for Fo' and Fs; (ii) varieties #307 and #256 were identified as potentially sensitive for Fv'/Fm', ΦII and ΦNO, but tolerant for Fo' and Fs; and (iii) variety #520 was identified as possibly sensitive for Fv'/Fm', NPQt, ΦII and ΦNO, but tolerant for Fo' (**Figure 4.23**).

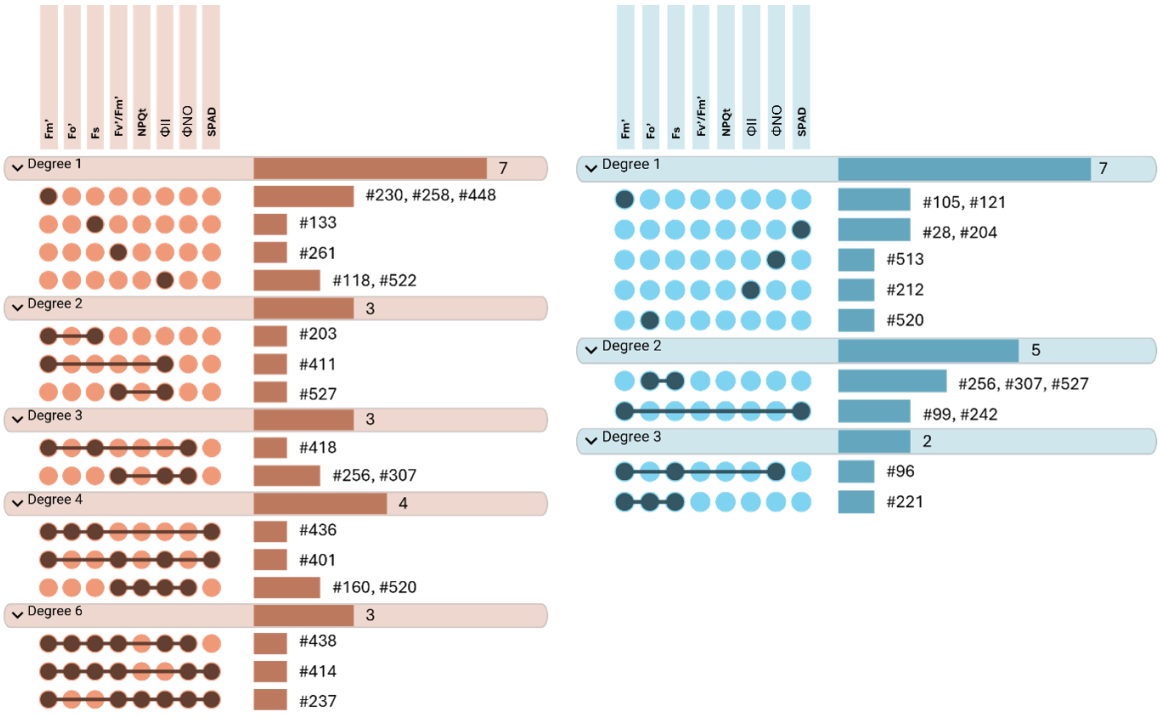

Figure 4.23. UpSet plots for predicted sensitive and tolerant rapeseed varieties. UpSet plot representation of the overlap between different measured parameters for varieties predicted to be sensitive (red plot) tolerant (blue plot) to waterlogging. UpSet plots were created by using Multinet (https://multinet.app).

4.3.3.2. Analysis of the impact of waterlogging relative to control conditions per variety

To complement the analysis of the variation with control or waterlogged population and to consolidate the identification of tolerant or sensitive genotypes to waterlogging + *S. sclerotiorum*, we also modelled, for each measured parameter, the ratio between waterlogged and control conditions (waterlogging/control) for each rapeseed variety. This approach was additionally motivated by the fact that the "absolute" approach did not identify any variety with a significantly response to *S. sclerotiorum* according to whether plants had faced control or waterlogging conditions prior to infection. This approach also corrects for intrinsic varietal differences, as the ones observed by the deviations from the population mean in SPAD values in control conditions (**Figure 4.19**), and environmental effects within a given batch. By analysing the ratios with a simpler mixed-effects model, we focused on the relative performance of each genotype in response to waterlogging compared to control conditions (also with/without *S. sclerotiorum*), providing another indicator of tolerance or sensitivity. For example, in this analysis, waterlogging-sensitive varieties can be identified because the ratios will be consistently low, whereas more waterlogging-tolerant varieties will have ratios closer to 1 or higher. It is also possible to compare the relative behaviour of each variety to that of the population. This is visualised by plotting predicted random effects and credible intervals. For brevity, we refer to this analysis as the "*relative*" approach.

Compared to the "absolute" approach outlined in **section 4.3.3.1 above**, this analysis resulted in few varietal differences for most of the measured parameters. For photosynthesis-related traits, only two varieties were identified as sensitive to waterlogging in two different traits - variety #527 for ΦII and variety #160 with NPQt (**Figure 4.24**).

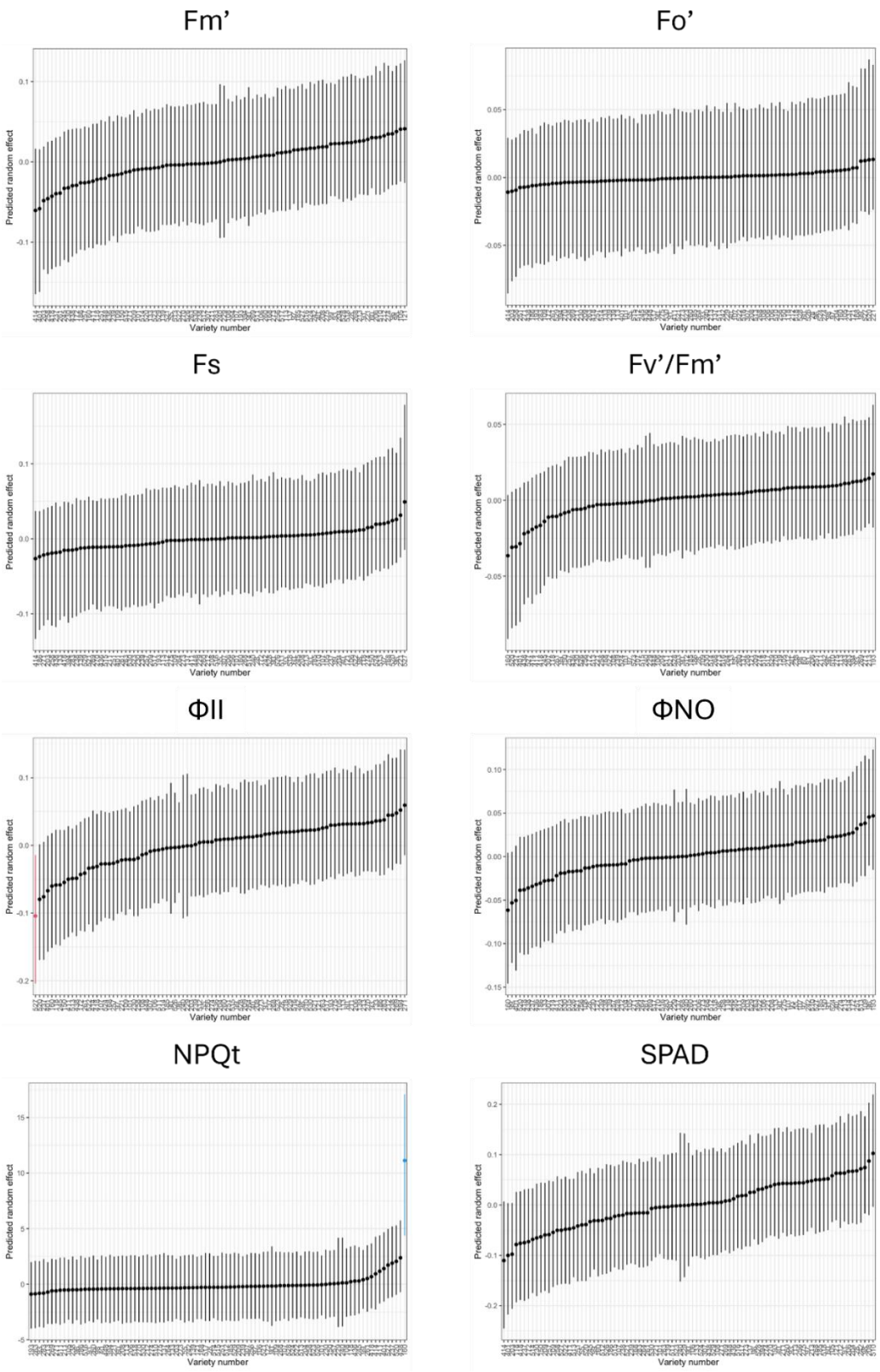

Figure 4.24. Predicted random effects of rapeseed varieties for photosynthetic-related traits under waterlogged conditions normalised for control conditions. Predicted random effects ± credible intervals are shown for each individual rapeseed variety. The varieties are identified based on their 3-digit identifier on the X-Axis.

For the physiological parameters, only variety #160 was identified as potentially tolerant to waterlogging with regards to leaf weight (**Figure 4.25**).

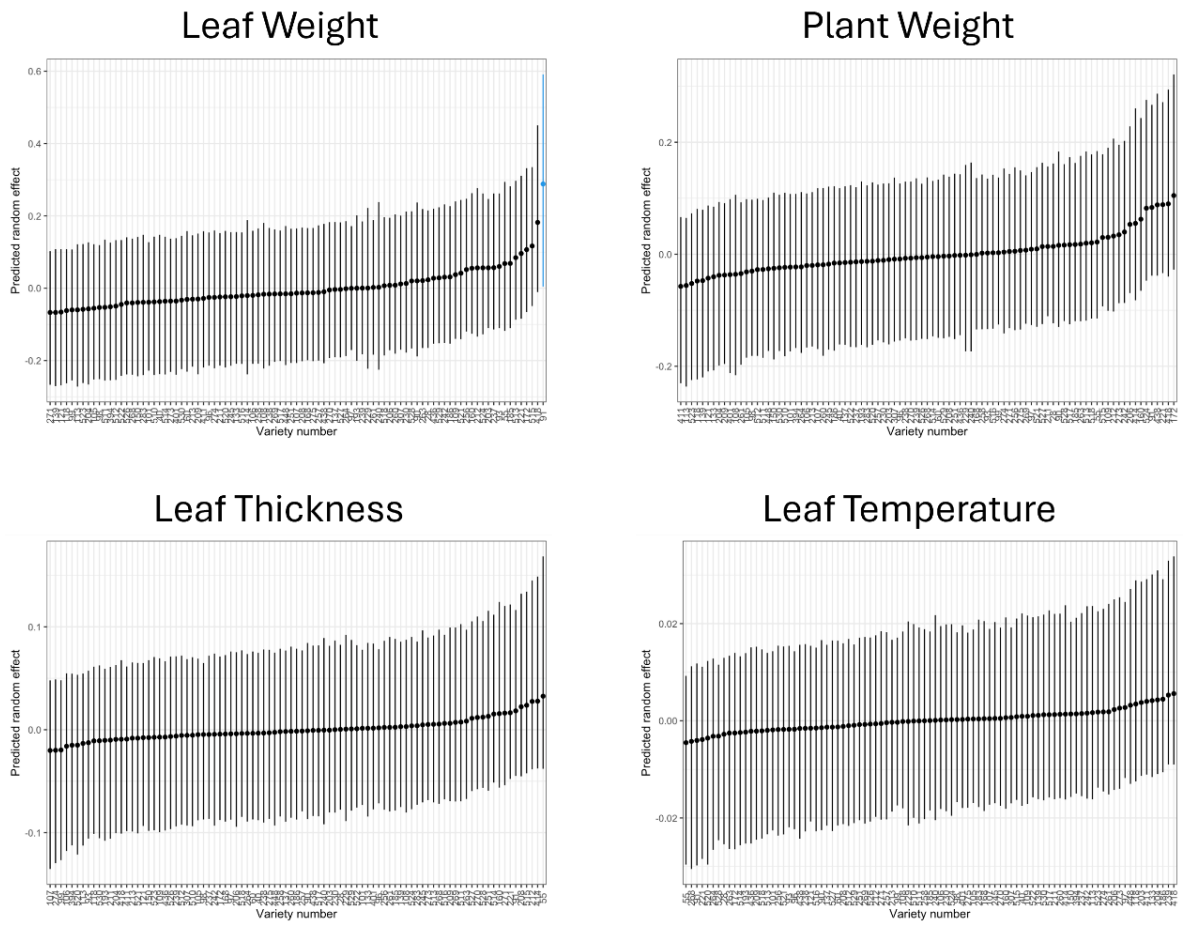

Figure 4.25. Predicted random effects of rapeseed varieties for physiological traits under waterlogging conditions normalised for control conditions. Predicted random effects ± credible intervals are shown for each individual rapeseed variety. The varieties are identified based on their 3-digit identifier on the X-Axis.

In terms of *S. sclerotiorum* resistance, this relative analysis only allowed us to identify varieties #511 and #264 as being potentially more tolerant to *S. sclerotiorum* infection (48 hpi) when plants faced waterlogging treatment just before infection (**Figure 4.26**).

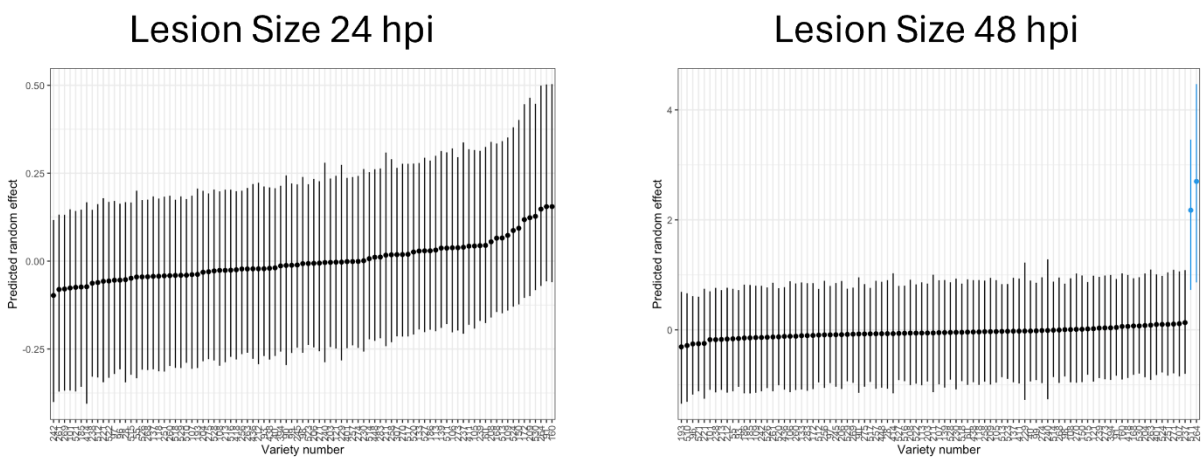

Figure 4.26. Predicted random effects of rapeseed varieties for lesion size at 24 and 48 hpi of *S. sclerotiorum* infection under waterlogged conditions normalised for control conditions. Predicted random effects ± credible intervals are shown for each individual rapeseed variety. The varieties are identified based on their 3-digit identifier on the X-Axis.

Although this analysis yielded very few varieties that could potentially be considered as tolerant or sensitive compared to the population mean, we used the predicted random effects as a method of ranking the varieties, so that we considered the 10 varieties with the lowest predicted random effects (i.e. predicted most sensitive varieties) and the 10 varieties with the highest predicted random effects (i.e. predicted 10 best varieties). For NPQt, the reasoning is reversed, as outlined previously. This ranking was used for every measured parameter. We then generated an UpSet plot to visualise the overlaps between the different rankings for each of the measured parameters (**Figure 4.27**). For varieties ranked as potentially sensitive, some appeared in 7 out of the 14 measured parameters (#401, #414 and #418), others appeared in 6/14 parameters (#118 and #438) and others in 5/14 parameters (#203, #237, #411 and #520). These varieties were therefore considered as higher confidence sensitive ones to waterlogging. In addition, for potential tolerant varieties to waterlogging, one appeared in 7/14 parameters (#221), one in 6/14 parameters (#91) and two in 5/14 parameters (#172 and #271) (**Figure 4.27**), and these would be the higher confidence tolerant varieties.

In terms of pathogen resistance, 4 varieties were ranked as potentially susceptible at 24 hpi (#185, #242, #269 and #512) and 5 at 48 hpi (#55, #96, #212, #213 and #510). When analysing varieties ranked for resilience to waterlogging + *S. sclerotiorum* infection, a lower number of potentially resilient varieties were found at 24 hpi (#209 and #530) and at 48 hpi (#307 and #401). Intriguingly, a number of varieties were ranked as potentially susceptible to *S. sclerotiorum*

infection at both 24 and 48 hpi (#101, #221, #238 and #521), suggesting that these varieties become more susceptible to *S. sclerotiorum* when experiencing waterlogging (because ratios of waterlogged:control are being considered here). However, there were no varieties ranked as potentially resistant for both timepoints when comparing lesion as a ratio of waterlogged:control. Interestingly, 2 varieties ranked as performing better against *S. sclerotiorum* upon waterlogging and for parameters measured for waterlogging response (#264 together with leaf temperature, and #524 together with Fs and plant weight). These two varieties may be particularly interesting to further examine for resilience.

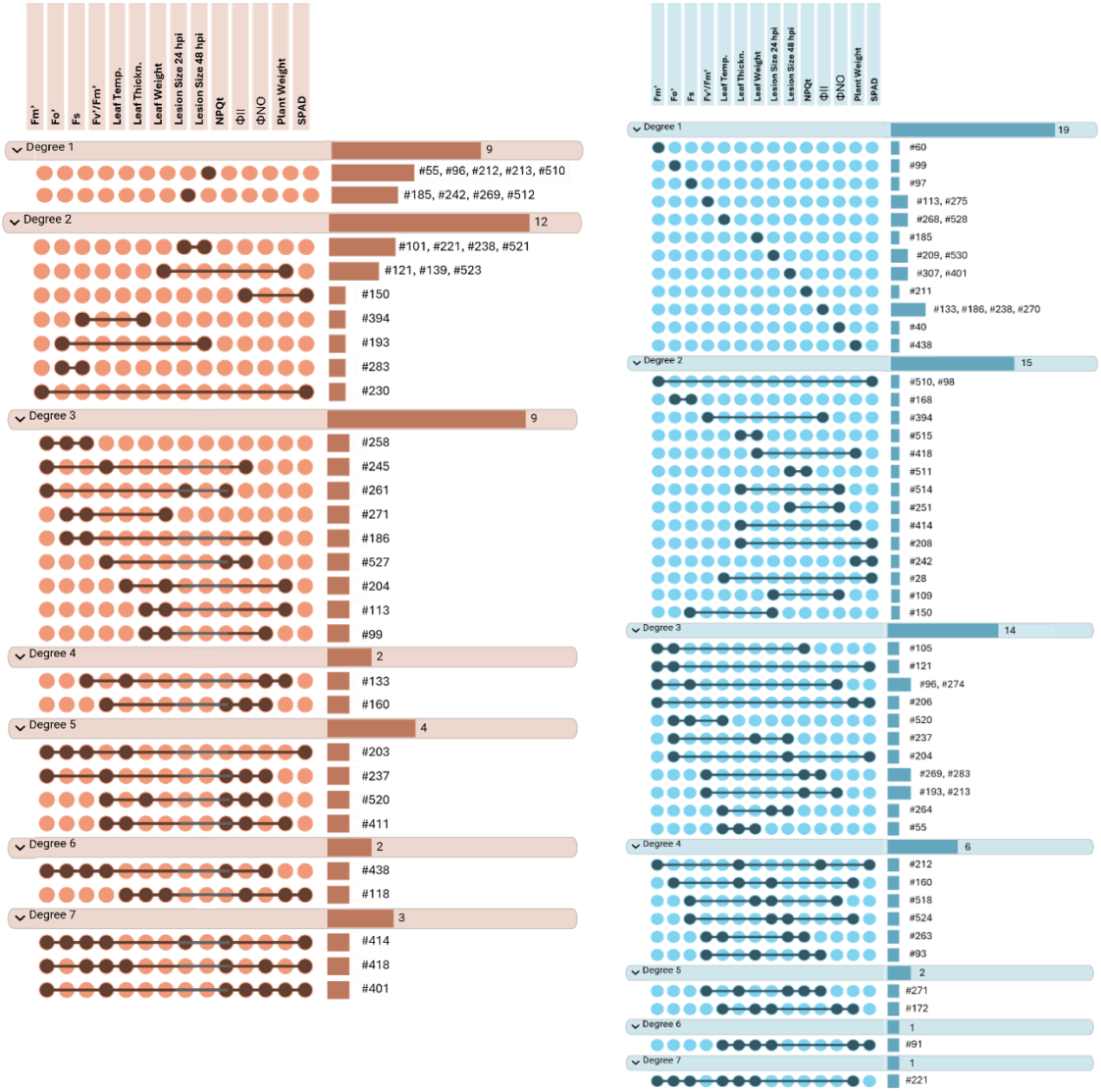

Figure 4.27. UpSet plots for the 10 most sensitive and tolerant rapeseed varieties under waterlogged conditions normalised for control conditions. UpSet plot representation of overlaps in traits for comparison of sensitive (red plot) and tolerant (blue plot). The vertical bar chart gives the traits measured in the screening, and the horizontal bar chart the number of overlapping rapeseed varieties in the intersects indicated by connected dots.

4.3.3.3. Analysis combination

Examining which varieties were consistently identified as tolerant or susceptible across both the absolute and relative approaches allowed the identification of genotypes whose classification was robust to the analytical framework used (**Table 4.5**). By using both approaches, we can capture how environmental covariates such as waterlogging conditions modulate photosynthetic and pathogen defence traits by using the absolute model, and we can study the ability of each variety to maintain physiological function relative to its own control by using the relative model. As only one of the approaches identifies varieties with significant behaviours in response to *S.sclerotiorum* infection, this analysis was performed to spot varieties supported that are likely to represent biologically meaningful and stable responses to waterlogging, whereas those identified by only one approach may reflect model-specific sensitivity to baseline varietal differences or relative stress effects.

Table 4.5. Identified tolerant and sensitive varieties for each measured parameter in the 'absolute' analysis that were present in the 10 most tolerant and sensitive varieties in the 'relative' analysis.

Parameter	Tolerant	Sensitive
Fm'	#96, #105, #121, #221	#203, #230, #237, #258, #401, #414, #418, #438
Fo'	#221, #520, #527	#414, #438
Fs	#96, #221, #527	#133, #203 , #414, #418, #438
Fv'/Fm'	-	#160, #237, #401, #414, #438, #520, #527
NPQt	-	#160, #237
ΦII	#212	#118, #160, #237, #401, #411, #520, #527
ΦNO	#96, #513	#160, #237, #438, #418, #520
SPAD	#28, #204, #242	# 401, #414

Altogether, these results allowed us to identify tolerant varieties, such as variety #221, identified as tolerant in Fm', Fo' and Fs parameters, variety 96, identified as tolerant in Fm', Fs and ΦNO parameters, and other identified in only 1 or 2 parameters (**Table 4.5**). Furthermore, we identified sensitive varieties, such as variety #414, identified as sensitive in Fm', Fo', Fs, Fv'/Fm', ΦII, ΦNO, SPAD parameters, variety #401, identified as sensitive in Fm', Fv'/Fm', ΦII, SPAD

parameters, variety #438, identified as sensitive in *Fm'*, Fo', Fs, Fv'/Fm', ΦNO, or other varieties such as #237, #160 and #520, identified as sensitive 4 or 5 parameters (**Table 4.5**). Moreover, varieties #520 and #527 are identified as both sensitive and tolerant to waterlogging for different parameters, underscoring that waterlogging tolerance in rapeseed is a multifaceted trait, where different parameters function individually across varieties.

4.3.4. Conclusions

Although we cannot conclude that waterlogging affects *S. sclerotiorum* resistance across this collection of varieties (**Table 4.2**), the reduced cultivar-dependent variability in lesion size at 24 and 48 hpi following waterlogging suggests that prior waterlogging stress may constrain the genotypic differences in pathogen response among varieties (**Table 4.3**). We can nevertheless conclude that varieties exhibit different responses to the sequential combination of waterlogging stress and *S. sclerotiorum* infection as we could identify varieties #511 and #264 as tolerant to waterlogging + *S. sclerotiorum* infection at 48 hpi (**Figure 4.26**). Intriguingly, as these varieties exhibited tolerance to waterlogging + *S. sclerotiorum* infection, there are other varieties (#221) that were tolerant to waterlogging alone in Fm' and Fo' parameters but were ranked as potentially sensitive to waterlogging + *S. sclerotiorum* infection at both 24 and 48 hpi (**Figure 4.23 and Table 4.5**).

Taken together, these results allowed for the identification of a representative set of traits to further investigate the genetic basis of waterlogging tolerance through a genome-wide association study (GWAS). This set of traits accounts for (i) pigment status (SPAD), (ii) photochemistry and photosynthetic efficiency (Fv'/Fm', ΦII, ΦNO), (iii) photoprotective mechanisms (NPQt), (iv) biomass generation (plant weight) and (v) progress of pathogen infection by *S. sclerotiorum* (lesion area at 24 hpi).

4.4. Discussion

This chapter established an experimental and analytical framework to investigate how prior waterlogging influences rapeseed performance, both in the absence and after subsequent challenge with *S. sclerotiorum*. This framework included measurements that fell in two categories – photosynthesis-related ones and physiological measurements. Measuring these parameters in 15 varieties allowed us to identify two rapeseed varieties (#229 and #240) as

internal controls that could be included in all batches of the large-scale screen to account for environmental and batch-specific variations in the statistical analysis of the dataset, which increases the robustness of the subsequent mixed-model analysis (**Figures 4.1-6**).

At the population level, after completing the large screen, the mixed-model analysis showed that waterlogging influenced each of the measured traits (**Table 4.2**), although the magnitude of the effect differed among parameters. This agrees with previous evidence showing that waterlogging affected the photosynthetic capacity and that such parameters can be used in screens for waterlogging tolerance/sensitivity (Lee et al., 2014; Li et al., 2023; Nabloussi et al., 2019; Song et al., 2025; Zhou and Lin, 1995). We also analysed the variance of the random effects and confidence intervals for each measured parameter (**Table 4.3**) which indicated which parameters triggered the most conserved responses across the varieties in the population. Interestingly, we observed that waterlogging altered the distribution of variability within the population in a trait-dependent manner. Photosynthesis-related parameters became more variable under stress (**Table 4.3**), suggesting that the photosynthetic capacity may be differently regulated across varieties in response to waterlogging. This indicates that not only all measured traits contribute equally to the identification of tolerant genotypes, but the increased variability observed in photosynthetic parameters under waterlogging specifically supports their use as discriminatory traits in future screenings. In contrast, physiological-related traits exhibited reduced variability upon waterlogging (**Table 4.3**), suggesting conserved biomass changes across the rapeseed population, even if photosynthetic capacity diverges. Lesion sizes following *S. sclerotiorum* inoculation showed a similar reduction in variability at 24–48 hpi, suggesting that waterlogging conditions prior to the inoculation may compress phenotypic spread in early infection dynamics even if it does not uniformly shift mean disease progression. Intriguingly, a recent study pinpointed that maintaining chlorophyll levels correlates with Sclerotinia stem rot resistance (Chawade et al., 2024). However, although waterlogging significantly changes chlorophyll content on rapeseed leaves, lesion size at 24–48 hpi was not affected by waterlogging at the population level, suggesting that the relation between physiological status and disease outcome is likely dependent on genotype-specific regulatory mechanisms. (**Table 4.2**).

Next, the dataset obtained from the large-scale screen was analysed by our collaborator, Prof. Rafael de Andrade Moral, through two different approaches. First, the "raw" measurements were used to estimate treatment effects while adjusting for environmental covariates (termed 'absolute' approach). Second, we normalised waterlogging to control measurements to analyse the data as a fold-change behaviour of each rapeseed variety upon waterlogging compared to the respective control (termed 'relative' approach). This second approach was important as it

reduced the influence of intrinsic varietal differences in baseline trait values, such as those observed for SPAD under control conditions. Additionally, the absolute approach did not identify any variety whose response to *S. sclerotiorum* differed significantly depending on whether plants had previously faced control or waterlogging conditions. These two approaches are complementary, in that each of them captured different biological questions, the absolute approach identifies sensitive or tolerant rapeseed varieties to waterlogging within the whole population, while the 'relative' approach asked how strongly each variety responded to waterlogging relative to its own baseline. By combining the results from both analyses, we thought to identify varieties that are consistently predicted as sensitive or tolerant to waterlogging, or that are susceptible/resistant to *S. sclerotiorum* in the presence or absence of waterlogging pre-treatment.

From the waterlogging point of view, the combination of both approaches identified putative tolerant varieties such as #221 (based on Fm', Fo', Fs) and #96 (based on Fm', Fs, ΦNO) together with candidate sensitive varieties including #414 (based on Fm', Fo', Fs, Fv'/Fm', ΦII, ΦNO, SPAD), #401 (based on Fm', Fv'/Fm', ΦII, SPAD), and #438 (based on Fm', Fo', Fs, Fv'/Fm', ΦNO) (**Table 4.5**). These classifications suggest that waterlogging tolerance in this panel is associated primarily with the ability to preserve PSII-related function rather than with a generalised maintenance of all physiological traits. Tolerant varieties such as #221, have a PSII that remains stable under waterlogging, preserving thylakoid function and sustaining electron transport with adequate metabolic sinks, allowing variety #221 to keep photochemistry operating despite waterlogging stress. In contrast, sensitive varieties like variety #401 fail to maintain PSII function and pigment integrity under waterlogging, leading to reduced carbon assimilation and likely growth penalties, which is visible in the relative approach which predicts #401 as sensitive to waterlogging based on the plant weight parameter. Thus, the combined approach was useful for figuring out which physiological parameters of performance were associated with waterlogging tolerance (**Figure 4.21 and Table 4.5**).

A note of caution is that several chlorophyll fluorescence parameters are mathematically related, and therefore significant changes across multiple such traits should not be over-counted as independent evidence. Nevertheless, this analysis has indicated that fewer potential tolerant varieties are identified and that in general they are classified as potentially tolerant based on a lower number of parameters, which might suggest that from a biological point of view, waterlogging tolerance within the different genotypes of commercial varieties is not a common trait. This could be linked to the fact there has been no selection for this trait in breeding programmes. Another possibility for the seemingly easier identification of candidate

waterlogging-sensitive varieties is that traits like Fv'/Fm', ΦII have a limited range of possible values (between 0 and 1 in the case of ΦII, and between 0 and a theorical limit of 0.84 for Fv'/Fm'), making it easier to detect declines rather than increases. This would make negative shifts in sensitive lines more easily identifiable, while tolerant lines have limited room to "overperform."

Several varieties showed trait-dependent discordance, being identified as tolerant for some parameters and sensitive for others: #527 was sensitive for Fv'/Fm' and ΦII, but tolerant for Fo' and Fs; #307 and #256 were sensitive for Fv'/Fm', ΦII and ΦNO, yet tolerant for Fo' and Fs; and #520 was sensitive for Fv'/Fm', NPQt, ΦII and ΦNO, but tolerant for Fo'. This trait-specific discordance is the result of waterlogging perturbation of multiple and partly independent layers of PSII function, which include PSII efficiency (Fv'/Fm', ΦII), energy dissipation (NPQt, ΦNO), pigment status (SPAD), and biomass generation. These layers allow for the different varieties to stabilise one layer (Fo' and Fs) while failing in another (e.g., Fv'/Fm' and ΦII). From this data, we can conclude that varietal performance under waterlogging cannot always be reduced to a simple tolerant-versus-sensitive binary. For example, these varieties appear to maintain their antenna and PSII reaction centres intact, evidenced by their tolerance in Fo' and Fs, however, the operational efficiency of PSII is compromised, evidenced by their susceptibility in Fv'/Fm' and ΦII. These results indicate a decoupling between structural stability and functional yield, consistent with bottlenecks in downstream electron sinks (Baker, 2008; Genty et al., 1989). This suggests that different ways of waterlogging resilience may exist, each regulated by partially distinct physiological mechanisms, which is important for breeding efforts and the identification of novel regulators of stress responses.

With respect to the first aim of the chapter, at the population level prior waterlogging did not significantly alter lesion size in the detached-leaf assay. However, this does not mean that waterlogging has no effect on disease outcome. The absolute approach was unable to identify any variety that would be considered as either resistant or susceptible, but the relative approach successfully identified varieties #511 and #264 as potentially less susceptible to *S. sclerotinia* infection at 48 hpi (but not at 24 hpi) following waterlogging, suggesting a time-dependent tolerance that emerges during lesion expansion. This finding also indicates that waterlogging may influence a rapeseed ability to fight off *S. sclerotiorum* infection, but this effect is genotype-dependent and may become apparent only during later stages of lesion expansion. One possibility to explain this finding is that waterlogging of the roots elicits a cross-priming response in the aerial parts of the plant that boosts the plant's ability to defend itself against pathogens. Such cross-priming mechanisms have been identified with other crop/pathogen combinations (e.g. Fukushima et al., 2016; Keswani et al., 2022; Martínez et al., 2019) or with different

combinations of abiotic and biotic stresses (e.g. Hilker et al., 2016). Interestingly, it also resembles observation made in *A. thaliana*, in which it was shown that waterlogging pre-treatment could induce increases resistance to the bacterial pathogen *Pseudomonas syringae* pv. tomato (Hsu et al., 2013).

This framework not only produced a classification of all varieties in terms of waterlogging tolerance but also established itself as a robust framework for identifying informative contrasts of waterlogging responses. The screen demonstrated that waterlogging responses can be resolved effectively at the varietal level, particularly through photosynthesis-related traits, and that combining absolute and relative analytical approaches strengthens confidence in the resulting classifications. Taken together, the results show that the framework was effective for capturing varietal responses to waterlogging, but that the effect of prior waterlogging on *S. sclerotiorum* infection was more subtle, more genotype-dependent, and less consistently detectable than the effect of waterlogging alone. These conclusions directly support the next stage of the thesis, in which we investigate the molecular basis of waterlogging tolerance, disease resistance, or resilience to the combined waterlogging and *S. sclerotorium* infection. In this respect, the framework achieved the third aim of the chapter: it identifies the phenotypic structure necessary to guide subsequent gene discovery.

5. Identifying candidate genes for rapeseed resilience to waterlogging and/or Sclerotinia using GWAS approaches

5.1. Introduction

5.1.1. Background Information

Most of the studies regarding waterlogging stress in *Brassica napus* involve the identification of tolerant and susceptible varieties to waterlogging, to then perform transcriptomic analyses on those varieties to identify transcriptionally up or downregulated genes in response to waterlogging (Hong et al., 2023; Lee et al., 2014; Li et al., 2021; Zou et al., 2015). However, these studies overlook allelic diversity, focusing on what may be only line-specific waterlogging responses and the outcomes of the stress responses, instead of identifying the genetic basis for the stress tolerance/susceptibility. In contrast, Genome Wide Association Studies (GWAS) allowed for the identification of genomic regions and/or specific gene(s) that could be responsible for stress tolerance by detecting loci whose allelic variation correlates with phenotypic variation. In addition, it accounts for relatedness (through kinship corrections) and population structure, minimising the line-specific waterlogging false positive associations. GWAS studies have, however, their own limitations. *Brassica napus* (genome AACC, n=19) arose ~7500 years ago after hybridisation between ancestors of *B. rapa* (Asian cabbage or turnip, genome AA, n=10) and *B. oleracea* (Mediterranean cabbage, genome CC, n=9), followed by chromosome doubling (allopolyploidy) (Chalhoub et al., 2014; Rousseau-Gueutin et al., 2021). This genome complexity results in gene duplication and redundancy, which could allow for differential expression of homoeologs under waterlogging or pathogen infection, thus contributing to new gene functions and to plant survival to stresses. However, the same genome complexity complicates GWAS-based dissection of tolerance mechanisms, as gene redundancy, or ambiguous, context-specific expression patterns challenges the gene-level validation of tolerance to waterlogging and to *S. sclerotiorum*.

Genome-Wide Association Studies (GWAS) and complementary QTL analyses have significantly advanced the understanding of waterlogging tolerance in *B. napus*. Examples include (i) using advanced Unnamed Aerial Vehicule (UAV)-based field phenotyping, followed by GWAS, which identified hundreds of associated loci, defining 40 candidate genes related to known stress response pathways, such as *CIPK15* and 2-oxoglutarate-dependent dioxygenases (Li et al., 2022); (ii) studies focusing on Seedling Death Rate (SDR), which identified 26 significant

Single Nucleotide Polymorphisms (SNPs) associations and 17 consensus QTLs for the SDR trait (X. Wang et al., 2020); (iii) the identification of *BnaA04g14070D* (*BnaA04.BAK7*), a RLK, which acts as a crucial positive regulator of submergence tolerance by forming a conserved positive feedback loop with the TEOSINTE BRANCHED1, CYCLOIDEA, PROLIFERATING CELL FACTOR 1 and 2 (TCP) transcription factor TCP21 (Guo et al., 2025); and (iv) the identification of an elite haplotype (HAP1) in the *BnaA04.BAK7* region, associated with improved tolerance, alongside consistent QTL clusters (like the six associated with relative root/hypocotyl length and fresh weight) that involve genes dedicated to oxidation-reduction processes and protein/RNA degradation (Ding et al., 2020).

These techniques have also been used to study Sclerotinia Stem Rot (SSR) resistance in *B. napus*. These examples concluded that resistance to SSR is controlled by multiple minor QTLs whose identification serves as a valuable resource for future breeding. Examples of identified marker genes for *S. sclerotiorum* resistance include (i) novel loci on A05, A09, and C01 chromosomes, identifying candidate genes such as *BnROS1 or BnMED15A*, whose homologues regulate disease resistance also in *A. thaliana* (Newman et al., 2023); (ii) three major loci (DSRC4, DSRC6, DSRC8) located on the C sub-genome gathering 39 candidate genes (Wu et al., 2016); (iii) a significant QTL located on chromosome A03 identified on a field study (Khan et al., 2023); or (iv) 133 significant SNPs corresponding with 123 loci for disease traits (Roy et al., 2021).

Individual regulatory components are particularly important in plant stress responses because stress-response networks are frequently organised around key regulators that connect multiple signalling pathways and thereby determine the strength, timing, and specificity of downstream stress responses. In this context, proteins pinpointed as convergence points in hypoxia and flg22 responses in *A. thaliana* have similar but separated roles in *B. napus*. For example, *BnRBOHD* was found to be transcriptionally induced in response to *S. sclerotiorum* downstream of *B. napus* GDSL LIPASE-LIKE 1 (BnaC07.GLIP1) (Ding et al., 2024). In addition, *BnWRKY33* was found to enhance resistance to *Sclerotinia sclerotiorum* by driving antimicrobial/phytoalexin and hormone-responsive defences after MPK3/MPK4 signalling activation, while also being a target of negative regulatory pathways as the one displayed by the regulatory module formed by the WRKY transcription factor BnWRKY28 and the VQ-motif protein BnVQ12. These proteins physically interact and, in the context of Sclerotinia sclerotiorum infection, the induced VQ12–WRKY28 complex which dampens WRKY33 expression by outcompetition at later infection stages of infection (Hu et al., 2021; Wang et al., 2014; Zhang et al., 2022). However, these components have not yet been demonstrated to have a role in the waterlogging response in *B. napus*. Given their well-established roles in hypoxia responses in *A.*

thaliana, they are strong candidates as points of convergence that contribute to waterlogging tolerance in rapeseed, and therefore, have a potential role in the cross-tolerance between waterlogging and *S. sclerotiorum* infection.

In summary, Sclerotinia stem rot (SSR) and waterlogging stress have been widely studied individually, but no study has tested how waterlogging influences rapeseed defences to *S. sclerotiorum* infection in a diverse rapeseed population such as the one used here.

5.1.2. Aims of this chapter

In chapter 4, we identified sensitive and tolerant candidate rapeseed varieties to waterlogging stress, together with susceptible and resistant rapeseed varieties to *S. sclerotiorum* infection with and without waterlogging conditions prior to the infection. However, the genetic basis, molecular mechanisms and regulatory pathways responsible for this tolerance to individual and combined stresses need to be examined. Therefore, the aim of this work was to apply GWAS to identify candidate genes that contribute to individual stress tolerance to waterlogging and *S. sclerotiorum* infection in addition to the combination of waterlogging and *S. sclerotiorum* infection.

5.2. GWAS and GEM analyses to identify SNPs relevant to the traits of interest

To investigate the genetic basis for the different responses to waterlogging and *S. sclerotiorum* infection identified in the rapeseed screen detailed in Chapter 4, our collaborators Dr. Rachel Wells and Dr. Emmanuel Solomon (John Innes Centre; UK) performed associative transcriptomics (Harper et al., 2012; Havlickova et al., 2018) combining genome-wide SNPs and gene expression marker (GEM) association analysis to reveal SNPs and genes that might be linked to the observed behaviours in the screen. These two analyses were performed on the data obtained when trait values under both control and waterlogging conditions were normalised to the corresponding control measurement for each variety (i.e. the ratios of waterlogged/control were considered, noted for example $SPAD^{w}/SPAD^{c}$; **see section 4.3.3.2 above**).

GWAS use samples from natural populations and cultivars to identify associations between genetic variants and traits, revealing the genetic basis of stress response traits, understanding the interaction between genetic variation and environments, and pinpointing targets for selective breeding (Clauw et al., 2025). These studies calculate an association

between a SNP and a single phenotype for each SNP. The GWAS analysis of the large-scale rapeseed screening presented in Chapter 4 was performed by our collaborators using the Genome Association and Prediction Integrated Tool (GAPIT) (Lipka et al., 2012; Tang et al., 2016). By using this software, different statistical models are used to analyse the data, including Generalized Linear Model (GLM), Mixed Linear Model (single-locus; MLM), Fixed and Random Model Circulating Probability Unification (FarmCPU), Bayesian-information and Linkage-disequilibrium Iteratively Nested Keyway (Blink), the multi-locus mixed model (MLMM) and the Compressed Mixed Linear Model (CMLM) (compared in **Table 5.1**). All these models account for population structure, reducing baseline allele-frequency differences unrelated to the trait caused by systematic ancestry differences within the population (distinct subpopulations/breeding pools), avoiding false trait-SNP associations. Furthermore, pairwise genomic relatedness arising from shared recent ancestry (kinship) was considered, as it can also inflate SNP–trait associations if unmodeled. However, not all the models used account for kinship (GLM does not), but also not all the models that account for it, do it in the same way (MLM/CMLM/MLMM incorporate a K matrix while FarmCPU and Blink use selected marker covariates (plus PCs/Q)).

Table 5.1. Summary of GWAS models used for the detection of SNP/trait associations in rapeseed.

Model	Model type	Key features and statistical framework	Advantages Limitations
GLM	Single-locus, mixed effects	Tests each SNP independently using a fixed-effect model. Incorporates population structure *via* covariates.	Suitable for large datasets with simple structure. High false-positive rate Ignores relatedness among individuals.
MLM		Extends GLM by including both fixed (population) and random (kinship) effects.	Robust across diverse populations. May miss small-effect loci.
CMLM		Simplifies MLM by clustering individuals into groups.	Faster than MLM; maintains statistical rigor. Compression may obscure fine-scale relatedness.
MLMM	Multi-locus, mixed effects	Incorporates multiple significant loci as cofactors.	Increases power to detect small-effect loci; controls confounding. Model selection can be complex.

FarmCPU	Multi-locus, iterative fixed/random effects	Separates testing and model optimization steps by fitting fixed and random effects.	High power and low false-positive rate Efficient for complex polygenic traits.
			May overfit when marker density is low or sample size is limited.
Blink	Multi-locus, LD-based mixed model	Builds on FarmCPU by replacing bin-based marker selection with LD-based clustering and BIC for model optimization.	Computationally efficient; Improved power by exploiting LD structure.
			Sensitive to LD threshold and uneven marker distribution.

In addition, Dr. R. Wells and Dr. E. Solomon performed GEM analyses that treat expression levels as markers, running regression analyses to test whether the variation in expression of a gene explains some of the variation in the trait (Lin et al., 2017).

In sum, Dr. R. Wells and Dr. E. Solomon performed the analyses with high-density SNP and GEM markers to identify loci and gene expression patterns that are statistically associated with the selected traits. Multiple testing was controlled at FDR = 0.05 using the qvalue package (v2.40.0) in R, which estimates q-values following Storey's procedure (Storey and Bass, 2025). The results were visualized using Manhattan plots to highlight candidate genomic regions associated with a specific trait. This analysis was carried out by using the ratios of waterlogged/control for the seven measured parameters (or traits) for which there were statistically significant differences in the 'absolute' analysis (i.e. SPAD, Fv'/Fm', ΦII, ΦNO, NPQt, plant weight and lesion size at 24 hpi). For each of these traits, the FitScores that indicate the best-fit models, as well as the global Manhattan plots obtained with all statistical models used are presented in the Appendix. In contrast, GWAS analysis with the normalised values of Fv'/Fm' and NPQt, identified several SNPs that could be relevant to waterlogging tolerance. The data obtained for these two traits and candidate SNPs are presented in more detail below. The GEM analysis that was performed with Fv'/Fm' and NPQt did not reveal any GEMs that could contribute to the traits observed. All the Manhattan plots obtained are presented in the Appendix.

5.2.1. GWAS analysis with Fv'/Fm'

To investigate the genetic basis of PSII efficiency upon waterlogging conditions, we carried out a GWAS on the normalised Fv'/Fm' measurements (i.e. $(Fv'/Fm')^{w}/(Fv'/Fm')^{c}$) and identified Blink as the most adequate model to carry out this analysis due to the lower FitScore value (**Table 5.2**). The Manhattan plots obtained for each of the models are also presented in **Appendix A**.

Table 5.2. FitScores to assess the relative goodness-of-fit of each model for Fv'/Fm'. Lower FitScore values indicate a better fit between the model and the observed phenotypic data.

Models	FitScore
GLM	115.4128
MLM	115.4125
FarmCPU	158.9913
Blink	10.53026
MLMM	31.13719
CMLM	115.4209

Using the Blink model, two novel SNPs located on chromosomes A07 and C07 were significantly associated with the trait (**Figure 5.1 and Table 5.3**). Other models also identified these two SNPs as significant (Chr. A07 observed in CMLM and MLMM models; Chr.C07 observed in FarmCPU) (**Figure 5.1 and Table 5.3**).

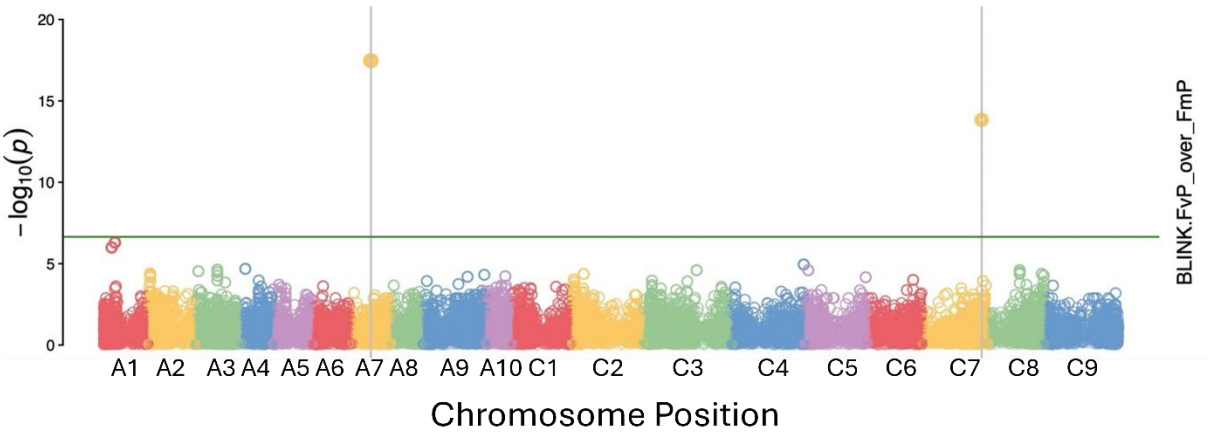

Figure 5.1. Manhattan plots obtained for normalised Fv'/Fm' using Blink. Chromosomes are designated with different colours. Multiple testing was controlled at FDR = 0.05 using the qvalue package (v2.40.0) in R, which estimates q-values following Storey's procedure (Storey and Bass, 2025). The model used is indicated on the right. Candidate genes and quantitative trait nucleotides (QTNs) are marked with grey vertical lines.

Significant associations were detected at markers Cab008997.1:363 on chromosome C07 (P = 9.45 × 10^{-22}) and at Bo7g110390.1:257 on C17 (P = 4.69 × 10^{-15}) (**Table 5.3**). Cab008997.1:363 has no *A. thaliana* homologue, but it is located close to a disease resistance

cluster, while Bo7g110390.1:257 is a rapeseed homologue of *A. thaliana INVOLVED IN RRNA PROCESSING 9* (*At_IRP9;* At4g25550) - a gene identified by Palm et al., 2019 as being involved in pre-rRNA maturation, with heterozygous mutants for *At_IRP9* being sensitive to high salt and sugar stresses. This finding points to a possible regulatory role of the rapeseed *IRP9* homologue, or any other gene in linkage with this marker, in maintaining ribosomal function and cellular homeostasis during waterlogging stress. However, the phenotypic variance explained (PVE) value obtained for both models was 0, suggesting that these two SNPs may not explain the variation observed for this trait (PVE = 0), suggesting these SNPs reside in linkage disequilibrium (LD) with other explanatory loci. The minor allele frequencies (maf) of these SNPs were 0.02 and 0.46, respectively, which is very low and suggests that one is very rare within the population, whereas the other is present in nearly half of the population (**Table 5.3**). The positive values of the effect sizes (0.155 and 0.058 respectively) further suggest that these two SNPs may contribute to higher Fv'/Fm' values, which would correlate with a better ability to maintain photosynthesis upon waterlogging stress (**Table 5.3**).

Table 5.3. Significant SNPs associated with the normalised Fv'/Fm' ratio using the Blink model. The table reports each SNP identifier, chromosome location (Chr.), physical position, p-value of association, minor allele frequency (maf), estimated allelic effect on the trait, and the percentage of phenotypic variance explained (PVE) by each SNP. Abbr: abbreviation given to specific SNP; At homolog.: corresponding *A. thaliana* homologue.

Abbr. / At homolog.	SNP	Chr.	Position	P.value	maf	Effect	PVE(%)
$SNP1^{Fv'/Fm'}$ / *At_IRP9*	Bo7g110390.1:257:A	C07	43764934	4.69e-15	0.46226	0.05762	0
$SNP2^{Fv'/Fm'}$ / -	Cab008997.1:363:T	A07	13827406	9.45e-22	0.02830	0.15474	0

In addition, to visualise how the phenotype differed depending on the SNP, plots with the different genotypic variants in the population and their respective values for $(Fv'/Fm')^{w}/(Fv'/Fm')^{c}$ were generated. For the Cab008997.1:363:T SNP, varieties carrying C/C homozygotes at this SNP showed higher Fv'/Fm' values than entries recorded as "N"; however, because "N" denotes a missing/low confidence call rather than a true alternative allele (**Figure 5.2**). Furthermore, varieties carrying the A/G (R) genotype at Bo7g110390.1:257 showed higher normalized Fv'/Fm'

than A/A homozygotes, indicating higher photosynthetic efficiency under waterlogging (**Figure 5.2**).

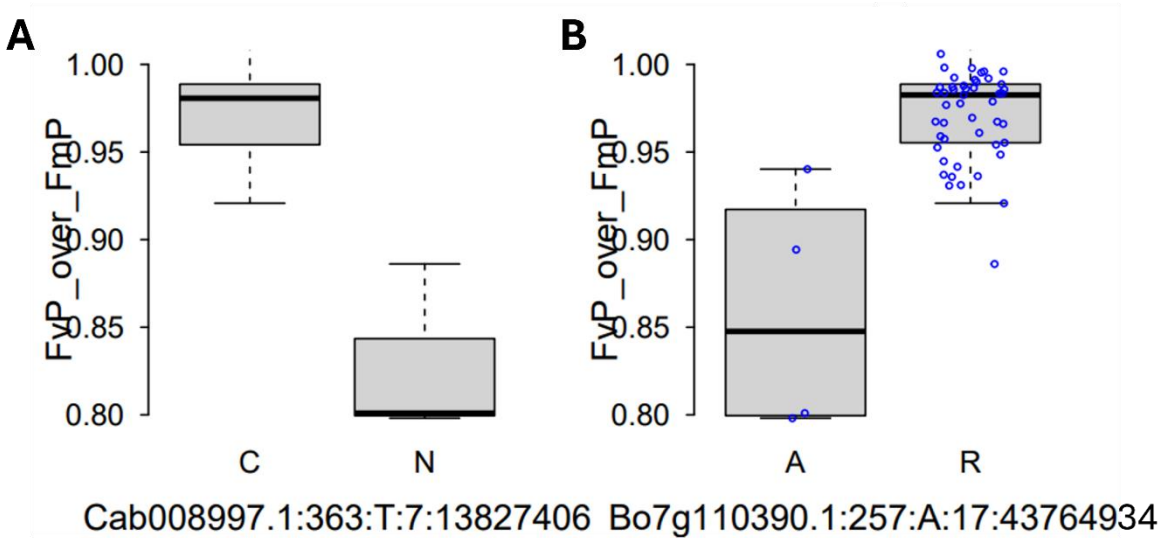

Figure 5.2. Differences in normalised Fv'/Fm' performance by genotype of associated SNP in the Blink model. Each panel displays the distribution of the normalized Fv'/Fm' ratios (Fv'/Fm'^{W} / Fv'/Fm'^{C}; Y-Axis, blue dots) across different haplotypes of the SNP markers associated with Fv'/Fm' (X-Axis).

Although FarmCPU had the worst FitScore for this trait, its associated SNPs were still examined, as this model can detect true associations with complex trait architectures overlooked by other approaches. By using this model, four additional SNPs associated with normalised Fv'/Fm' performance were identified, in addition to Bo7g110390.1:257, which had also been identified with the Blink model (**Figure 5.2**). The most significant SNP was Bo6rg112170.1:1269 on Chromosome C06 (P=5.71x10^{-10}), followed by Bo3g007450.1:528 on chromosome C03 (P=9.78x10^{-8}), Bo4g195600.1:618 on chromosome C04 (P=6.69x10^{-8}), and Cab007205.1:3648 on chromosome A10 (P=5.41x10^{-8}) (**Table 5.4**).

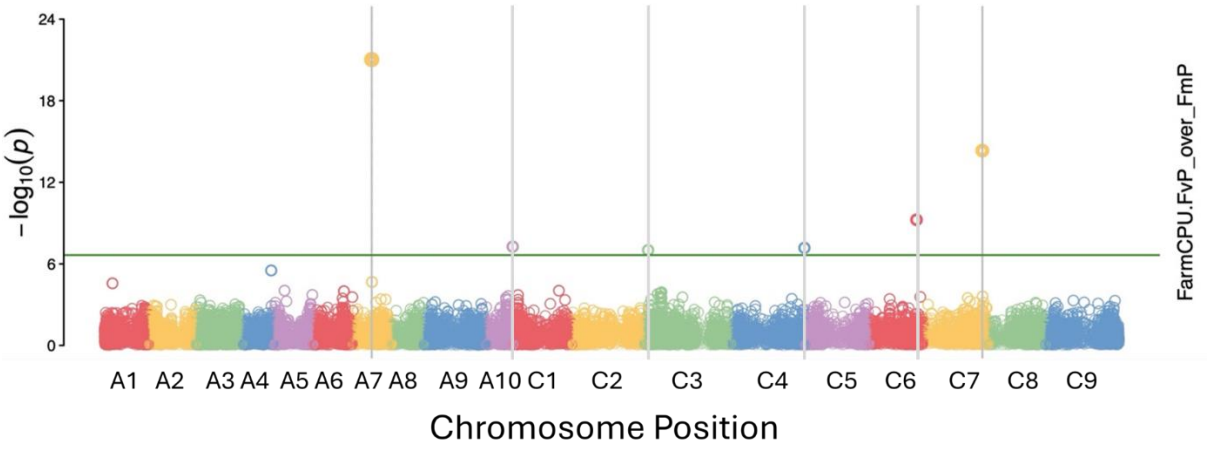

Figure 5.4. Manhattan plots obtained for normalised Fv'/Fm' using FarmCPU. Chromosomes are designated with different colours. Multiple testing was controlled at FDR = 0.05 using the qvalue package (v2.40.0) in R, which estimates q-values following Storey's procedure (Storey and Bass, 2025). The model used is indicated on the right. Candidate genes and quantitative trait nucleotides (QTNs) are marked with grey vertical lines.

The *A. thaliana* homologue for Bo6rg112170.1 is *ALANINE-2-OXOGLUTARATE AMINOTRANSFERASE 2* (At_*AOAT2;* At1g70580), which encodes a peroxisomal aminotransferase that catalyses the reversible transamination reaction essential in photorespiration (Igarashi et al., 2006, 2003; Liepman and Olsen, 2003). This gene is functionally redundant with At_*AOAT1* (At1g23310), and both genes are part of the Alanine aminotransferase (AlaAT) family, whose member, At_AlaAT1has been shown to be regulated in low-oxygen conditions (Loreti et al., 2005; Miyashita et al., 2007). Bo3g007450.1 has no *A. thaliana* homologue. Bo4g195600.1 is annotated as being the homologue of a protein annotated in *A. thaliana* as being an AAA-type ATPase (At2g45500), but its function has not been experimentally characterised. In contrast, Cab007205.1:3648 is the rapeseed homologue of the well-known *A. thaliana* ethylene receptor EIN2, which has been widely linked to hypoxia and pathogen stress responses, and has been proposed as a convergence point for the crosstalk between these two stresses in combined stress conditions (**see also section 1.4.3.2 above**).

Table 5.4. Significant SNPs associated with the normalised Fv'/Fm' ratio using the FarmCPU model. The table reports each SNP identifier, chromosome location (Chr.), physical position, p-value of association, minor allele frequency (maf), estimated allelic effect on the trait, and the percentage of phenotypic variance explained (PVE) by each SNP. Abbr: abbreviation given to specific SNP; At homolog.: corresponding *A. thaliana* homologue.

Abbr. / At homolog.	SNP	Chr.	Position	P.value	maf	effect	PVE (%)
SNP3$^{Fv'/Fm'}$ / *At_EIN2*	Cab007205.1:3648:A	A10	19690994	5.41e-08	0.18868	-0.0135	0.91451
SNP4 $^{Fv'/Fm'}$ / -	Bo3g007450.1:528:C	C03	2699737	9.78e-08	0.33962	-0.01044	4.16545
SNP5 $^{Fv'/Fm'}$ / At2g45500	Bo4g195600.1:618:G	C04	52966968	6.69e-08	0.34908	0.01551	2.33424
SNP6 $^{Fv'/Fm'}$ / At_*AOAT2*	Bo6rg112170.1:1269:G	C06	35025428	5.71e-10	0.40566	-0.02693	0.03646

In contrast with the SNPs identified by using the Blink model, the FarmCPU SNPs have PVE values ranging from 0.03% to 4.17% (**Table 5.4**). Furthermore, the maf values of these SNPs ranged from 0.19 to 0.41, indicating that these SNPs were present at intermediate frequencies within the population (**Table 5.4**). Nevertheless, these SNPs accounted for little effect on the normalised Fv'/Fm' as their effect values ranged from -0.027 to 0.016 (**Table 5.4**). This is further evidenced by the phenotype distribution as a function of genotype variation across the population, where Bo6rg112170.1:1269 SNP (i.e. homologue of At*_AOAT2;* At1g70580) displayed higher values for Fv'/Fm' in G/G plants than C/C plants, indicating G is the favourable allele for waterlogging tolerance (**Figure 5.5**). However, at Cab007205.1:3648, no haplotype displayed significantly different normalized Fv'/Fm' values. At Bo4g195600.1:618, A/G (R) shows a higher median than G/G, although with a few low outliers (**Figure 5.5**). However, this should not be interpreted as a true heterozygote effect, as these calls can represent hemiSNPs arising from the collapse of highly similar A- and C-genome sequences during read mapping (Trick et al., 2009). In such cases the "R" call likely reflects different bases on the two subgenomes rather than a single-locus heterozygote. Similarly, at Bo3g007450.1:528, C/T (Y) and C/C outperform T/T, implying C is favourable to waterlogging tolerance (**Figure 5.5**).

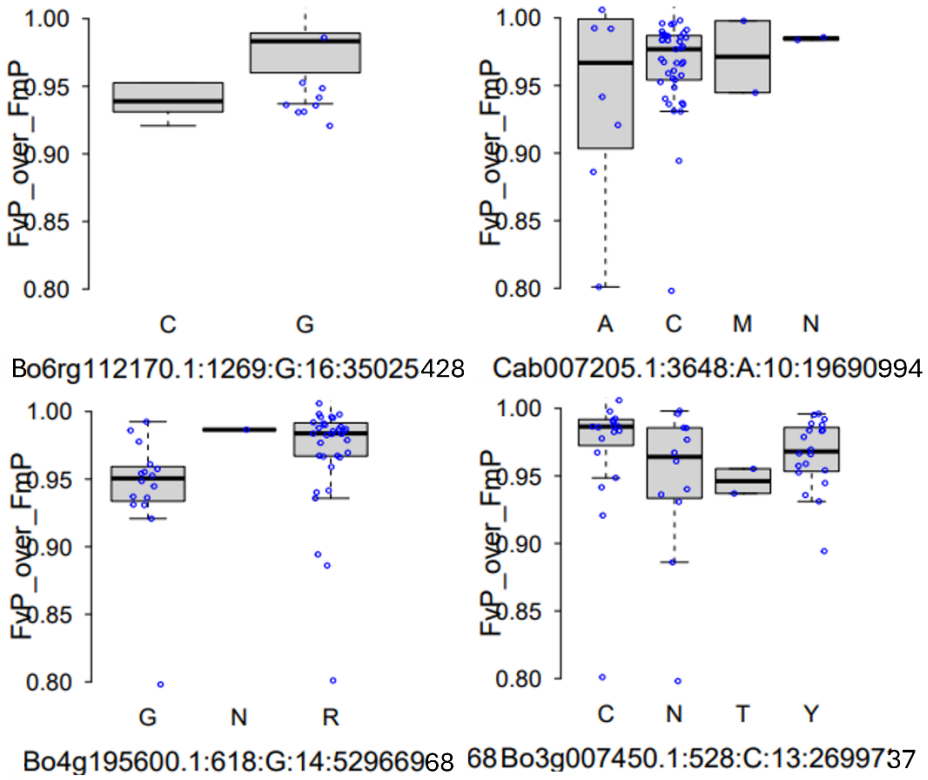

Figure 5.5. Differences in normalised Fv'/Fm' performance by genotype of associated SNP in the FarmCPU model. Each panel displays the distribution of the normalized Fv'/Fm' ratios (Fv'/Fm'^{W} / Fv'/Fm'^{C}; Y-Axis, blue dots) across different haplotypes of the SNP markers associated with Fv'/Fm' (X-Axis).

Altogether, these results provide six candidate genes to further explore their role in waterlogging response.

5.2.2. GWAS analysis with NPQt

The FitScores obtained when conducting the GWAS analysis with NPQt suggest that FarmCPU was the most adequate model, followed by Blink (**Table 5.5**). Hence our analysis focused on the SNPs identified by these two models.

Table 5.5. FitScores for the six GWAS models to assess the relative goodness-of-fit of each model for NPQt. Lower FitScore values indicate a better fit between the model and the observed phenotypic data.

Models	FitScore
GLM	2815.202
MLM	2815.164
FarmCPU	1.558636
Blink	9.390185
MLMM	132.6971
CMLM	2815.164

By using the FarmCPU model, three novel SNPs located in chromosomes A04, C06 and C08 associated with the trait were identified (**Figure 5.6 and Table 5.6**). Other models also identified two out of these three SNPs as significantly associated with NPQt (i.e. the SNP on chromosome 4 was identified with the MLMM model; the SNP on chromosome 16 was also identified with GLM, MLM, Blink and CMLM models) (**Figure 5.6 and Table 5.6**). The most significant association was at genomic position Bo6rg118020.1:963 on chromosome C06 (P = 9.39× 10^{-58}), followed by Cab026024.1:300 on chromosome A04 (P = 1.44 × 10^{-31}), and Bo8g091950.1:1272 on chromosome C08 (P = 2.47 × 10^{-8}) (**Figure 5.6**).

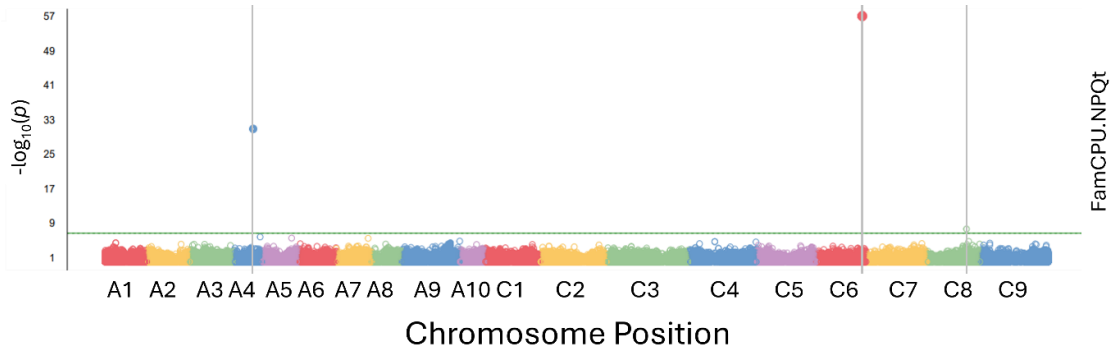

Figure 5.6. Manhattan plots obtained for normalised NPQt using FarmCPU. Chromosomes are designated with different colours. Multiple testing was controlled at FDR = 0.05 using the qvalue package (v2.40.0) in R, which estimates q-values following Storey's procedure (Storey and Bass, 2025). The model used is indicated on the right. Candidate genes and quantitative trait nucleotides (QTNs) are marked with grey vertical lines.

Bo6rg118020.1 is a rapeseed homologue of *A. thaliana SUPPRESSORS OF MEC-8 AND UNC-52 1* (*At_SMU1; At1g73720*), which functions primarily as a splicing factor within the spliceosome. It acts together with its partner At_SMU2 during the transition from the pre-catalytic to activated spliceosome, stabilising RNA–protein interactions and ensuring accurate splice site recognition (Chung et al., 2009; Kanno et al., 2017). In addition, *At_SMU1* can also contribute to environmental responses, as it is involved in low-magnesium tolerance and proper co-transcriptional splicing during cold stress (Feng et al., 2020; Long et al., 2024).

Cab026024.1 is a rapeseed homologue of *A. thaliana UDP-D-AOPIOSE/UDP-D-XYLOSE SYNTHASE 1* (*At_AXS1*), which functions as an enzyme that catalyses the conversion of UDP-D-glucuronate to a mixture of UDP-D-apiose and UDP-D-xylose in a NAD+-dependent way (Choi et al., 2012; Mølhøj et al., 2003). D-Apiose serves as the binding site for borate cross-linking of rhamnogalacturonan II (RG-II) in the plant cell wall, influencing cell-wall architecture and plant growth (Mølhøj et al., 2003; Zhao et al., 2020). Mutants for this gene display growth arrest, leaf yellowing and cell death symptoms, including cell lysis and disintegration of cellular organelles and compartments which was accompanied by excessive formation of ROS and by induction of various protease genes (Zhao et al., 2020). Furthermore, abnormal wall structure of the affected cells was evident including excessive cell wall thickening and wall gaps (Ahn et al., 2006; X. Zhao et al., 2020).

Bo8g091950.1 is a rapeseed homologue of *A. thaliana CALCIUM-DEPENDENT PROTEIN KINASE 32* (*At_CPK32; At3g57530*), which functions as a Ca^{2+} sensor. Although *CPK32* has not been studied in the context of hypoxic conditions, it has been shown to be transcriptionally upregulated within 30 minutes of flooding in a Ca^{2+}-dependent way (Bakshi et al., 2023). In addition, *CPK32* acts as a positive regulator of ammonium (NH_4^+) uptake in roots via phosphorylation of serine residue S450 in the C-terminus of AMT1;1 (Qin et al., 2020). Furthermore, submergence triggers rapid accumulation of this NH_4^+ transporter AtAMT1;1, and other Ca^{2+} sensor (CIPK15) suppresses AMT activity through its phosphorylation (Chen and Ho, 2023).

Among these three SNPs, Bo6rg118020.1:963 has the largest PVE (18.47%), whereas the other two have a PVE of 0%, indicating that this SNP is likely the primary contributor to the variance explained in our model. The maf of these variants ranged from 0.028 to 0.491, indicating that both rare and intermediate-frequency alleles contributed to the trait variation (**Table 5.6**). Furthermore, the values of the positive effect sizes for two SNPs are negative (-0.59 and -3.28),

suggesting a positive influence on waterlogging tolerance, whereas Bo6rg118020.1:963 has a large positive effect (27.88), suggesting a negative influence on waterlogging tolerance (**Table 5.6**).

Table 5.6. Significant SNPs associated with the NPQt ratio under waterlogging conditions in Brassica napus identified using the FarmCPU model. The table reports each SNP identifier, chromosome location (Chr.), physical position, p-value of association, minor allele frequency (maf), estimated allelic effect on the trait, and the percentage of phenotypic variance explained (PVE). Abbr: abbreviation given to specific SNP; At homolog.: corresponding *A. thaliana* homologue.

Abbr. / AT Homolog.	SNP	Chr.	Position	P.value	maf	effect	PVE (%)
$SNP1^{NPQt}$ / *At_SMU1*	Bo6rg118020.1:963:G	C06	36724185	9.38e-58	0.49057	27.88449	18.478
$SNP2^{NPQt}$ / *At_AXS1*	Cab026024.1:300:T	A04	15280679	1.44e-31	0.02830	-3.27865	0
$SNP3^{NPQt}$ / *At_CPK32*	Bo8g091950.1:1272:C	C08	31218633	2.47e-08	0.45283	-0.59001	0

In addition, to visualise how the $NPQt^{w}/NPQt^{C}$ ratios differed depending on the SNP genotype, we generated plots corresponding to the different genotypes observed among the rapeseed population and their respective values for $NPQt^{w}/NPQt^{C}$. For the Bo6rg118020.1:963 SNP, varieties with A/A genotype for this SNP displayed bigger $NPQt^{w}/NPQt^{C}$ values (**Figure 5.7 A**). For Cab026024.1:300 SNP, varieties carrying C/C at this location were associated with a higher $NPQt^{w}/NPQt^{C}$, whereas varieties carrying T/T (or uracyl) had lower $NPQt^{w}/NPQt^{C}$ values (**Table 5.6 and Figure 5.7 B**). Varieties carrying C/C genotype at Bo8g091950.1:1272 SNP displayed slightly higher $NPQt^{w}/NPQt^{C}$ values than varieties carrying C/T (**Table 5.6 and Figure 5.7 C**).

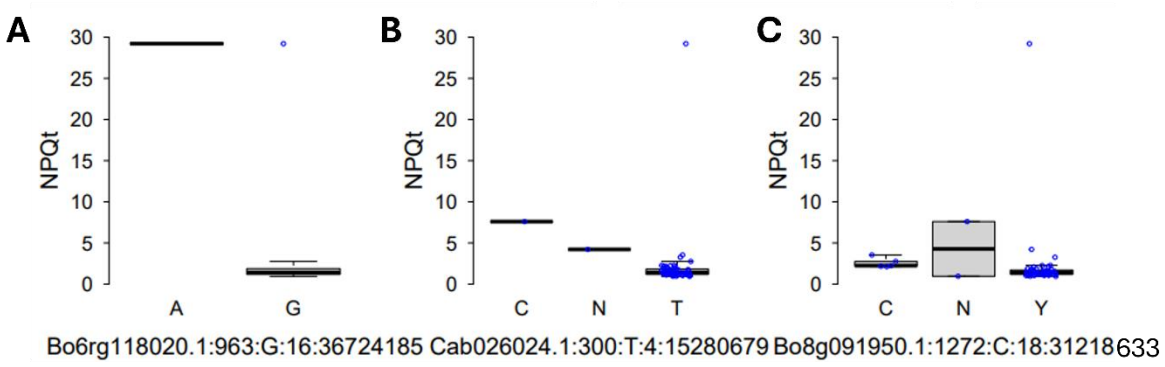

Figure 5.7. Differences in normalised NPQt performance by genotype of associated SNP in the FarmCPU model. Each panel displays the distribution of the normalized NPQt ratios ($NPQt^{W}$ / $NPQt^{C}$; Y-Axis, blue dots) across different haplotypes of the SNP markers associated with NPQt (X-Axis).

We repeated the same analysis with Blink, which was the second best-fit model (**Table 5.5**) and could provide complementary insights into the genetic basis for high or low $NPQt^{W}/NPQt^{C}$ ratios. By using this model, we identified novel SNPs associated with $NPQt^{W}/NPQt^{C}$ performance in addition to one also identified with FarmCPU (Bo6rg118020.1:963) (**Figure 5.8**). The most significantly associated SNP was Cab008997.1:363 located in chromosome A07 (P=5.28x10^{-19}), followed by BnaC09g43910D:231 on chromosome C09 (P=2.45x10^{-8}), Cab043190.1:141 on chromosome A04 (P=1.91x10^{-7}), and Bo3g040620.1:802 on chromosome C03 (P=1.29x10^{-7}) (**Table 5.7**).

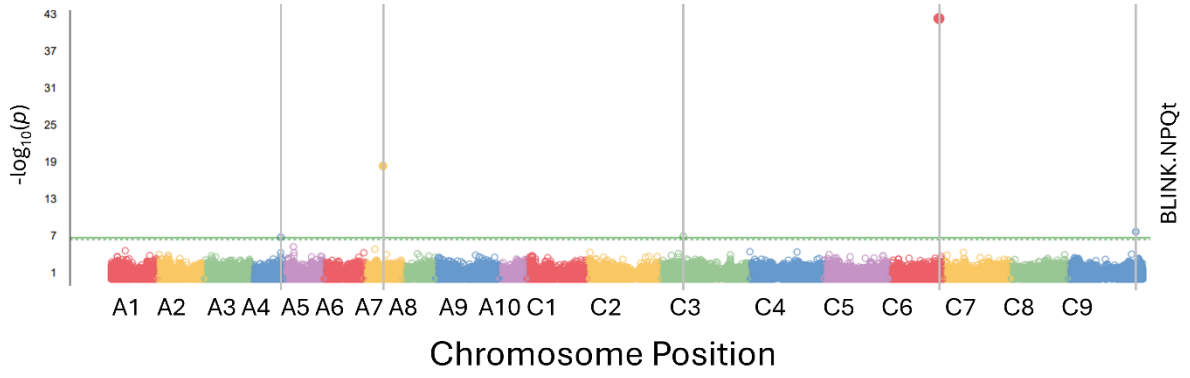

Figure 5.8. Manhattan plots obtained for normalised NPQt using BLINK. Chromosomes are designated with different colours. Multiple testing was controlled at FDR = 0.05 using the qvalue package (v2.40.0) in R, which estimates q-values following Storey's procedure (Storey and Bass,

2025). The model used is indicated on the right. Candidate genes and quantitative trait nucleotides (QTNs) are marked with grey vertical lines.

BnaC09g43910D is a rapeseed homologue of *BETA-GALACTOSIDASE 13* (At_*BGAL13; At2g16730*), a member of the glycosyl hydrolase family 35 (GH35) with β-galactosidase activity, that likely functions in cell wall remodelling, seed mucilage modification, and carbohydrate metabolism (Becker et al., 2003; Chandrasekar and Van Der Hoorn, 2016; Hrubá et al., 2005).

The homologues of Cab043190.1 is *At2g41250*, an *A. thaliana* gene encoding a Haloacid Dehalogenase (HAD)-like hydrolase superfamily protein, predicted to localise to the mitochondrion. The protein contains conserved HAD domains characteristic of Mg^{2+}-dependent phosphatases and other hydrolases, suggesting a role in dephosphorylation or small molecule metabolism (Burroughs et al., 2006; Du et al., 2021; Rawat et al., 2011).

Bo3g040620.1 is a rapeseed homologue of *A. thaliana* SECOND SUBUNIT (B2) of the DNA POLYMERASE EPSILON (POLε) complex (*At_DPB2; At5g22110*), a key enzyme responsible for leading-strand DNA synthesis during replication ensuring replication fidelity and coordination with cell-cycle progression. Moreover, it has been shown to be linked to epigenetic regulation, and responses to DNA damage and abiotic stress (García et al., 2017; Pedroza-Garcia et al., 2016; Ronceret et al., 2005; Yin et al., 2009).

Interestingly, Cab008997.1 was identified in the GWAS analysis with $NPQt^{W}/NPQt^{C}$ and had also been identified with $Fv'/Fm'^{W}/Fv'/Fm'^{C}$, indicating that this SNP may potentially be involved in multiple traits response to waterlogging stress. In comparison to Fv'/Fm', Cab008997.1:363 had a large negative effect on $NPQt^{w}/NPQt^{C}$ (-3.59) and accounts for intermediate unique components of phenotypic variation (PVE=2.82%) (**Table 5.7**).

For the remaining three SNPs mentioned above, only Bo3g040620.1:802:C displayed a significant maf value (0.47 compared to 0.028 for Cab008997.1:363:T, 0.075 for Cab043190.1:141:C, or 0.094 for BnaC09g43910D:231:G) (**Table 5.7**). The effects of the SNPs identified with Blink were negative for Bo3g040620.1:802:C (-1.21), indicating potential association with a low $NPQt^{w}/NPQt^{C}$ ratio, and positive for Cab043190.1:141:C (0.54) and BnaC09g43910D:231:G (0.59), albeit with low values (**Table 5.7**). In addition, these three SNPs displayed low PVE values of 0.17%, 0.38% and 0.1% for Cab043190.1:141:C, Bo3g040620.1:802:C and BnaC09g43910D:231:G, respectively, indicating that each associated SNPs individually contributes only to a small proportion of the overall phenotypic variance for $NPQt^{w}/NPQt^{C}$ ratio (**Table 5.7**).

Table 5.7. Significant SNPs associated with the $NPQt^{w}/NPQt^{C}$ ratio using the Blink model. The table reports each SNP identifier, chromosome location (Chr.), physical position, p-value of association, minor allele frequency (maf), estimated allelic effect on the trait, and the percentage of phenotypic variance explained (PVE) by each SNP. Abbr: abbreviation given to specific SNP; At homolog.: corresponding *A. thaliana* homologue.

Abbr. / At homolog.	SNP	Chr.	Position	P.value	maf	effect	PVE (%)
$SNP4^{NPQt}$ / At2g41250	Cab043190.1:141:C	A04	20791047	1.91e-07	0.07547	0.53624	0.17131
$SNP5^{NPQt}$ / -	Cab008997.1:363:T	A07	13827406	5.28e-19	0.02830	-3.59027	2.82128
$SNP6^{NPQt}$ / *At_DPB2*	Bo3g040620.1:802:C	C03	16777757	1.29e-07	0.47170	-1.20735	0.38460
$SNP7^{NPQt}$ / At_*BGAL13*	BnaC09g43910D:231:G	C09	49621951	2.45e-08	0.09434	0.58836	0.09942

Phenotype distribution visualisation of these SNPs indicated that for Bo3g040620.1:802, varieties displaying T/T (or uracyl) displayed higher values of $NPQt^{w}/NPQt^{C}$ (i.e. likely waterlogging sensitivity) than varieties carrying C/T genotypes (**Figure 5.9**). Although Cab043190.1:141and Cab008997.1:363 had missing entries, varieties containing C/C genotype displayed lower values of $NPQt^{w}/NPQt^{C}$ ratio (i.e. likely better tolerance to waterlogging), although at Cab008997.1:363 SNP it can only be compared to entries recorded as "N" (missing data) (**Figure 5.9**). For BnaC09g43910D:231, varieties carrying G/G genotypes displayed lower values of $NPQt^{w}/NPQt^{C}$ ratio (i.e. likely better tolerance to waterlogging) than varieties carrying A/G genotypes.

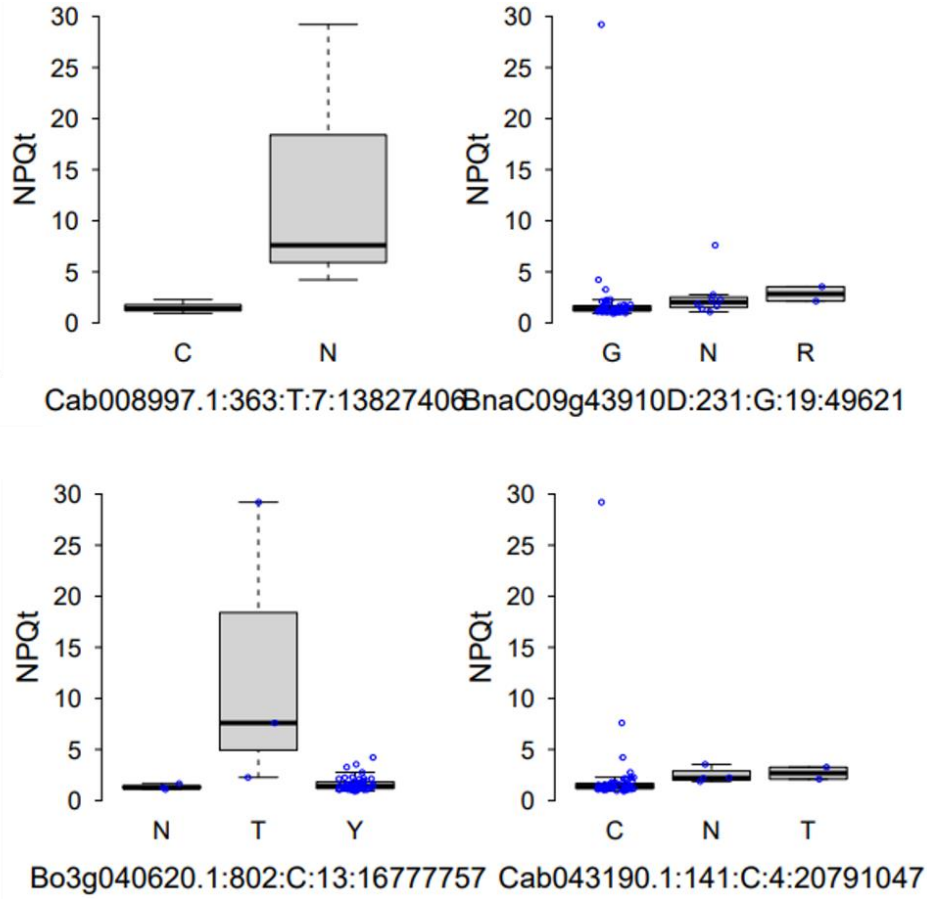

Figure 5.9. Differences in normalised $NPQt^{W}/NPQt^{C}$ performance by genotype of associated SNP in the Blink model. Each panel displays the distribution of the normalised NPQt ratios ($NPQt^{W}$ / $NPQt^{C}$; Y-Axis, blue dots) across different haplotypes of the SNP markers associated with NPQt (X-Axis).

5.2.3. GWAS analysis with Lesion Size at 24 hpi

The FitScores obtained when conducting the GWAS analysis with Lesion size at 24 hpi suggest that FarmCPU was the most adequate model, followed by Blink (**Table 5.8**). Only SNPs were associated with Lesion size at 24 hpi in the blink model, hence our analysis focused on the SNPs identified by this model.

Table 5.8. FitScores for the six GWAS models to assess the relative goodness-of-fit of each model for NPQt. Lower FitScore values indicate a better fit between the model and the observed phenotypic data.

models	FitScore
GLM	117.0684
MLM	117.0739
FarmCPU	10.02098
Blink	11.27736
MLMM	101.376
CMLM	118.6929

By using the Blink model, three novel SNPs located in chromosome A01 were associated with the trait were identified (**Figure 5.10 and Table 5.9**). The most significant association was at genomic position Cab044960.1:2889 (P = 9.34× 10^{-7}), followed by Cab042243.1:550 (P = 7.04 × 10^{-31}), and Cab044960.1:2229 (P = 6.67 × 10^{-8}) (**Table 5.9**). Intriguingly, all the SNP peaks were located in a region of linkage disequilibrium.

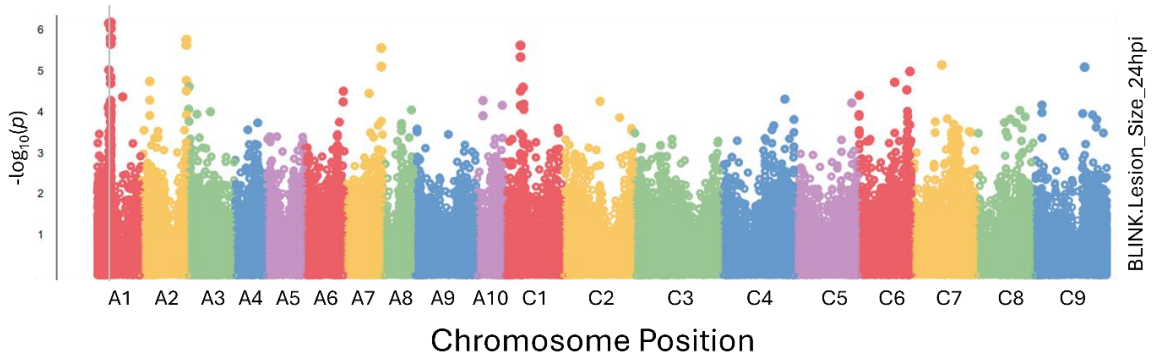

Figure 5.10. Manhattan plots obtained for normalised Lesion Size 24 hpi using BLINK. Chromosomes are designated with different colours. Multiple testing was controlled at FDR = 0.05 using the qvalue package (v2.40.0) in R, which estimates q-values following Storey's procedure (Storey and Bass, 2025). The model used is indicated on the right. Candidate genes and quantitative trait nucleotides (QTNs) are marked with grey vertical lines.

Cab042243.1 is a rapeseed homologue of *A. thaliana MAGNESIUM-PROTOPRPHYRIN IX METHYLTRANSFERASE (CHLM)* (*At_CHLM; At4g25080*), which encodes a protein with methyltransferase activity responsible for the methylation of magnesium protoporphyrin IX, a

essential step for chlorophyll biosynthesis (Block et al., 2002; Tanaka et al., 2011). *At_CHLM* locates to both the envelope and thylakoid chloroplast membranes (Block et al., 2002). Its activity is tightly regulated by chloroplast redox state and by folate-dependent one-carbon metabolism (Richter et al., 2016; Van Wilder et al., 2009). Intriguingly, null mutations of this gene impair photosystem accumulation and activates chloroplast-to-nucleus retrograde signalling (Pontier et al., 2007), whereas missense mutation (G to A transition) is suggested to disrupt membrane association of *At_CHLM* and triggers O_2^- accumulation together with hypersensitivity to salt-stress and down-regulation of multiple stress response genes (Huang et al., 2020). Furthermore, genetic evidence indicates that this gene has also been involved in guard-cell ABA signalling (Tomiyama et al., 2014).

Cab044960.1 is a rapeseed homologue of *A. thaliana COP1-INTERACTING PROTEIN 7 (CIP7)* (*At_CIP7; At4g27430*), which encodes for a light-responsive protein that binds COP1 and functions as a transcriptional co-activator (Yamamoto et al., 1998). The protein encoded by this gene has been shown to locate in the nucleus and, recently, to be associated with microtubules (Arico et al., 2024). In this same study, Ser-195 phosphorylation was shown to promote hypocotyl elongation and favours transverse MTs orientation in etiolated seedlings (Arico et al., 2024). However, direct roles in response to environmental stresses have not been demonstrated yet, though its canonical placement in light/anthocyanin programs suggests indirect connections to photoprotection pathways (Araguirang and Richter, 2022). Intriguingly, two different SNPs were located in this gene (Cab044960.1:2229 and Cab044960.1:2889) (**Table 5.9**).

These three SNPs have very low minor allele frequencies (0.056 to 0.122), indicating that these alleles are rare in our population. In addition, these SNPs have moderate effects on the trait (-0.28 to 0.57), intriguingly, the two SNPs located to the same gene have different effects, one positive (Cab044960.1:2229:A) and one negative (Cab044960.1:2889:C), suggesting that different haplotypes have opposite effects on infection progression.

Table 5.9. Significant SNPs associated with the NPQt ratio under waterlogging conditions in Brassica napus identified using the FarmCPU model. The table reports each SNP identifier, chromosome location (Chr.), physical position, p-value of association, minor allele frequency (maf), estimated allelic effect on the trait, and the percentage of phenotypic variance explained (PVE). Abbr: abbreviation given to specific SNP; At homolog.: corresponding *A. thaliana* homologue.

Abbr. / AT Homolog.	SNP	Chr.	Position	P.value	maf	effect
SNP1^{24hpi} / *At_CIP7*	Cab044960.1:2229:A	A01	10147554	6.67e-07	0.06604	0.46131
SNP2^{24hpi} / *At_CIP7*	Cab044960.1:2889:C	A01	10147554	9.34e-07	0.12264	-0.28009
SNP3^{24hpi} / *At_CHLM*	Cab042243.1:550:G	A01	8817524	7.04e-07	0.05660	0.57040

5.2.4. Conclusions

The GWAS analysis identified potential marker-trait associations for three measured parameters that are associated with photosynthetic capacity and infection progression following 2 weeks of waterlogging. The identified candidates have plausible roles in DNA synthesis, RNA processing, Ca^{2+} and ethylene signalling, as well as cell wall metabolism and light signalling. The obtained results demonstrate that this study provides a promising approach to study waterlogging tolerance and the crosstalk between waterlogging and *S. sclerotiorum* in rapeseed.

5.3. Discussion

This chapter aimed to identify the genetic basis underlying the stress response of rapeseed (*Brassica napus*) to waterlogging, *Sclerotinia sclerotiorum* infection and their combination. To do so, we used GWAS and GEM analyses together with the dataset generated in Chapter 4 to move from varietal contrasts to candidate loci and regulatory processes that may contribute to tolerance or susceptibility under individual and combined stress conditions. Overall, the results support the view that these traits are genetically complex and polygenic, they also highlight several candidate loci that point to different biological processes, particularly

translation and RNA processing, ethylene and Ca2+ signalling, and photosynthesis-associated regulation.

To do so, we focused specifically on the ratios of waterlogged to control for each variety. Our first conclusion is that the ability to detect significant associations depended strongly on the trait analysed, as no significant SNPs or GEMs were identified for several of the traits, including SPAD, ΦNO, ΦII and plant weight. This may be in line with the fact that the statistical analysis presented in chapter 4 using the 'relative' approach also did not reveal varieties with a behaviour that was significantly different for those same traits. The absence of significant SNPs could indicate that these traits are under control of multiple genes (polygenic control) or that they are heavily influenced by environmental factors, thus requiring different experimental approaches for genetic dissection. In contrast, the 'absolute' statistical analysis presented in Chapter 4 could be used to distinguish between varieties that performed better or worse than the population upon waterlogging treatment. These results implicate two main things, (i) future analyses using absolute values for control and waterlogged conditions separately may recover additional loci and (ii) traits with significant loci detected in the ratio-based analysis are likely to be particularly relevant for understanding the genetic basis of stress responses.

Two traits relate to how PSII performance is maintained under stress allowed us to identify SNPs that may be relevant to waterlogging tolerance/sensitivity. For $(Fv'/Fm')^{W}/(Fv'/Fm')^{C}$ ratios, six novel SNPs were identified using the two best-fit models – Blink and FarmCPU. Several of the genes associated with the SNPs identified could be relevant to waterlogging response. Bo7g110390.1 (**Table 5.4**) is a homologue of *At_IRP9*, a gene involved in ribosomal RNA processing. As outlined in **chapter 3** (**section 3.6**), translational regulation is a key layer of control during combined hypoxia and immune signalling (Branco-Price et al., 2008; Lee and Bailey-Serres, 2019; Mustroph et al., 2009; Sorenson and Bailey-Serres, 2014). This association extends that concept by suggesting that natural variation in the machinery supporting RNA maturation and ribosome function may contribute to variation in photosynthetic resilience under waterlogging. Nonetheless, the low phenotypic variance attributed to this SNP indicates that, although it may be associated with waterlogging tolerance, it is not sufficient to explain the differences observed within the population. This may indicate the participation of additional and unidentified loci that require further study. In that context, a more careful analysis of the GWAS results may be needed, such as for example examining more carefully the genomic regions neighbouring the SNP or identifying regions in which SNPs cluster albeit without them being above the threshold for statistical significance. Nonetheless, the identification of this SNP is still important because it points to a regulatory layer that is rarely considered in crop waterlogging

studies. In previous studies in mammals there is evidence that hypoxia reprograms rRNA 2'-O-methylation, increasing heterogeneity in ribosomes (Metge et al., 2021). This diversity in the mixture of rRNAs and protein composition of ribosomes has been hypothesised to produce "specialised ribosomes'' that differentially regulate translation upon hypoxia (Metge et al., 2021).

Although not the best model, the FarmCPU model identified that Bo6rg112170.1 (**Table 5.4**), a homologue of *At_AOA2*. Although this locus was identified in a weaker model, it is notable because alanine aminotransferase-related metabolism has long been associated with low-oxygen acclimation. The At_AOA2 enzyme catalyses the glutamate:glyoxylate aminotransferase (GGAT) reaction as part of the photorespiration process, and is part of the AlaAT family, whose members include *At_AlaAT1*, which is known to be transcriptionally responsive to low-oxygen availability (Loreti et al., 2005; Miyashita et al., 2007). This family of proteins canonically catalyzes L-alanine + 2-oxoglutarate ⇌ pyruvate + L-glutamate, which is a key reaction in anaerobic metabolism and contributes to store carbon-nitrogen in the form alanine during hypoxia and reconvert alanine to pyruvate upon re-oxygenation (Miyashita et al., 2007). However, this role has only been confirmed for *At_AlaAT1*, and further study for additional alanine aminotransferases needs to be done to further define whether *At_AOAT2* and other isoforms contribute to alanine accumulation and catabolism during hypoxia and re-oxygenation.

This model also associated Cab007205.1 (**Table 5.4**) to the $(Fv'/Fm')^{W}/(Fv'/Fm')^{C}$ ratio. Although its effect and PVE values indicated that the variation of this SNP has a small effect on the trait and does not fully explain the variation observed in the population, its *A. thaliana* homologue is *At_EIN2*, a well-known TF involved in ethylene signalling. This TF has been proposed as a convergent point between hypoxia and pathogen responses (**see also section 1.4.3.2 above**) as it is involved in the transcriptional regulation of genes involved in both hypoxia and pathogen responses (e.g. regulation of At_*FLS2*, At_*ACS2/6*, At_*FRK1*, At_*HRE1*...) (Boutrot et al., 2010; Gravino et al., 2015; Hess et al., 2011; Mersmann et al., 2010; X. Wang et al., 2022; Yang, 2014). Intriguingly, At_EIN2 has been recently involved in the modulation of translation together with GENERAL CONTROL NONDEREPRESSIBLE 2 (At_GCN2). Both genes were activated by entrapped ethylene during submergence to regulate the reduction in polysome loading and translational enhancement of specific mRNAs (Cho et al., 2022). Taken together, the identification of these SNPs associated with $(Fv'/Fm')^{W}/(Fv'/Fm')^{C}$ highlight the role of translation control observed in Chapter 3 during hypoxia response. In addition, these SNPs support a model in which translation control and peroxisomal C–N flux regulate PSII performance upon waterlogging. Although individual SNP effects on the trait performance are small, together they are consistent with a polygenic regulation for Fv'/Fm' under waterlogging.

The NPQt results expand this picture and suggest that natural variation in rapeseed responses to waterlogging also involves spliceosome function, cell wall organisation, and Ca2+-dependent signalling. Intriguingly, Cab008997.1:363:T (no homologue in *A. thaliana*) was associated with both Fv'/Fm' and NPQt ratios, indicating that this SNP is potentially involved in multiple traits response to waterlogging stress. The lack of *A. thaliana* homologue suggests that this gene may be rapeseed-specific, but this requires more careful analysis using BLAST. The association with multiple traits indicates that this SNP constitutes a candidate pleiotropic locus, which does not act on isolated outputs but instead affect broader physiological states that influence several photosynthetic parameters simultaneously. This SNP has a large effect on NPQt and a minor effect on Fv'/Fm' under waterlogging. Because NPQt is a photoprotective valve, a negative effect could mean reduced photoprotection (risking more PSII stress) or less need for energy dissipation.

Among the SNPs associated exclusively with NPQt, Bo6rg118020.1 (homologue of *At_SMU1*) on chromosome C06, explained a big portion of the phenotypic variance and was associated with a large negative effect on waterlogging tolerance (**Table 5.6**). At_SMU1 is involved in the transition from the pre-catalytic to activated spliceosome, stabilising RNA–protein interactions and ensuring accurate splice site recognition and has been linked to co-transcriptional splicing under cold/low Mg (Chung et al., 2009; Feng et al., 2020; Kanno et al., 2017; Long et al., 2024). Hypoxia limits cellular ATP and perturbs co-transcriptional RNA processing (Gibbs et al., 2025), conditions under which spliceosome activation is especially vulnerable. By facilitating the activation step, SMU1 is potentially well placed to maintain splicing fidelity when oxygen is scarce, thereby reducing hypoxia-induced intron retention and mis-splicing in stress-response transcripts (Juntawong et al., 2014).

Additional SNPs associated exclusively with NPQt include Cab026024.1:300:T (*At_AXS1*) and BnaC09g43910D (homologue of At_*BGAL13*). Both candidates implicate carbohydrate and cell wall metabolism growth (Mølhøj et al., 2003; Zhao et al., 2020; Becker et al., 2003; Chandrasekar and Van Der Hoorn, 2016; Hrubá et al., 2005) and although their individual effects are modest, they point towards variation in how plants remodel structural components under stress. This is plausible in the context of waterlogging, which affects growth, cellular integrity, and turgor-related processes.

The identification of a CPK32-like locus within the NPQt dataset is also noteworthy. Although this SNP has a negative effect on little waterlogging tolerance and explains little variation across the population it is mechanistically attractive because Ca2+ signalling is a well-

established component of both hypoxia and immune responses. In *A. thaliana*, At_CPK32 is a Ca^{2+}-sensor which is induced and potentially involved in hypoxia through the regulation of AMT1;1 (Bakshi et al., 2023; Chen and Ho, 2023; Qin et al., 2020). *At_CPK32* has been shown to have a role in plant immunity in response to AtPep1, as mutants for CPK32 display enhanced ROS production by RBOHD, higher activation of MAPK cascades, transcript abundance of PDF1.2 and reduced *Pst* DC3000 growth and *B. cinerea* lesion area (Wang, 2018). In addition, *At_CPK32* is one plausible candidate to regulate the trade-off between waterlogging and *S. sclerotiorum* infection in combined stress conditions, given the role of Ca^{2+} as a convergent point in hypoxia and flg22 (**see also section 1.3.1 above**), and the Ca2+-linked regulation role as a plausible determinant of RBOHD behaviour under combined hypoxia and flg22 treatment (**see Chapter 3**).

Taken together, the identification of these SNPs associated with NPQt highlight the role of Ca^{2+} signalling, spliceosome control and cell wall metabolism, regulate non-photochemical quenching upon waterlogging. Together these SNPs contribute to the polygenic regulation for NPQt under waterlogging.

By contrast, the associations identified for *S. sclerotiorum* lesion size at 24 hpi suggest that the influence of prior waterlogging on pathogen responses may involve somewhat different regulatory layers, particularly those linked to light signalling, chloroplast function, and growth–defence coordination. Among the SNPs associated with *S. sclerotiorum* lesion size at 24 hpi, Cab044960.1 (rapeseed homologue of *At_CIP7*) was associated with two haplotypes, which suggests either allelic complexity or multiple functional variants within the same genomic region. Based on At_CIP7 role in hypocotyl elongation, we propose that this gene has a role in the switch that plants experience between growth and immune programs when the plant detects a pathogen. Other plausible explanation for the association is that waterlogging responses affect microtubule layout through the movement of tolerance materials to the cell wall, and handling of ROS, and therefore affect this protein, and downstream *S. sclerotiorum* lesion sizes. However, the identification of two opposite effects given by two different haplotypes needs further investigation with future fine mapping of the region where these SNPs are located.

Cab042243.1:550 was also associated with *S. sclerotiorum* lesion size at 24 hpi. Cab042243.1 is the rapeseed homologue of *At_CHLM*, an enzyme catalysing an essential step in chlorophyll biosynthesis (Block et al., 2002; Tanaka et al., 2011). This is consistent with its role in chloroplast-to-nucleus retrograde signalling (Pontier et al., 2007), which has been previously known to interact with mitochondrial retrograde signalling (Shapiguzov et al., 2019). In addition, chloroplast produced ROS upon flg22 in a weaker and slower way compared to cytosol, activating

retrograde signalling and contributing to plant immunity (Arnaud et al., 2023; Nomura et al., 2012). It is also consistent with the idea that light-dependent photosynthetic electron flow helps determine the strength of flg22-responsive gene expression (Sano et al., 2014). This gene also sets a precedent for future studies to use photosynthetic parameters to study the crosstalk between hypoxia and plant immunity and evaluate the outcome of pathogen infections in plants who have previously faced hypoxic conditions.

Taken together, these associated SNPs highlight the role of light signalling and photosynthesis in pathogen infection of plants previously subjected to waterlogging conditions. As seen in Chapter 4, waterlogging disturbs photosynthesis, therefore the identification of these SNPs highlights the role of maintaining photosynthetic efficiency for immunity responses. For future breeding programs selecting varieties that maintain a better photosynthetic efficiency during waterlogging could result in better pathogen resistant variants in combined stress conditions.

At the same time, several limitations should be considered when interpretating this data. First, the ratio-based GWAS approach may have reduced power to detect loci affecting constitutive trait values. Second, for several loci the PVE was low, meaning that these markers should be considered entry points rather than definitive causal determinants. Third, some candidate associations remain provisional and require better characterisation of neighbouring genes and local linkage structure. Finally, the present study identifies associations rather than mechanisms. Functional validation will therefore be an essential step to carry out in the future.

Overall, this chapter advances the aims of the thesis by showing that GWAS can identify plausible regulatory loci associated with waterlogging tolerance and with the influence of prior waterlogging on pathogen outcome. It also elucidates that the genetic architecture of responses to waterlogging and combined waterlogging–*S. sclerotiorum* stress is distributed and polygenic, with only a minority of loci showing moderate explanatory power. Interestingly, the candidate loci identified here converge on a limited number of biologically plausible processes not just isolated "stress genes". These loci now provide a tractable set of candidates for future functional work and breeding programs, providing a starting point for future research to understand the molecular mechanisms underlying waterlogging tolerance, and those regulating the influence of waterlogging on pathogen resistance in rapeseed. For this purpose, functional approaches, such as gene editing and overexpression studies, could provide further insights into the regulatory pathways controlled by these loci, which could then be targeted for crop improvement strategies. Alternatively, mutant *A. thaliana* plants for these candidate genes could be characterised for their

tolerance to waterlogging and to the combined waterlogging/immunity stress, or to hypoxia and combined hypoxia/immunity.

6. Chapter 6: Conclusions

Plants live in a complex environment, where they can face multiple stresses at once, however, how plants respond to these stress combinations is poorly understood. In this thesis, the crosstalk between low O_2 levels (hypoxia) and immune responses that plants trigger during the combination of flooding and pathogen attack were studied by using model species *Arabidopsis thaliana* and the crop *Brassica napus*.

6.1. RBOHD as a convergence point in combined hypoxia/flg22 treatments

In *A. thaliana*, combined hypoxia and flg22 treatments were used to study the role of RBOHD in the crosstalk between hypoxia responses and PTI. The results obtained show that RBOHD plays a role under combined hypoxia/flg22 treatments, with *ERFVII*s, *WRKY33*, and *CPK28* converging on the regulation of *RBOHD*, both at transcriptional and post-transcriptional levels. The crosstalk depended on developmental stage and light availability, thus adding additional levels of complexity to RBOHD regulation. Hypoxic conditions allow stabilisation of the ERFVII TFs, which contribute to the hyper-induction of *RBOHD* when flg22 treatment is combined with hypoxia. This is in line with the known interaction of ERFVIIs with the *RBOHD* promoter (Yao et al., 2017), and could be the result of the co-activation of oxygen-sensing and immune pathways at the same time, especially considering the emerging roles of the ERFVIIs in plant defences against pathogens (Gravot et al., 2016; Kerpen et al., 2019; Valeri et al., 2021). Consistent with their differential regulation through development, ERFVIIs exerted their strongest influence on *RBOHD* expression in HF conditions in seedlings, whereas in 4-week old plants, they only contributed to baseline levels of RBOHD protein. This points to a potential developmental regulation of the hypoxia/immunity crosstalk. Another transcriptional regulator of *RBOHD* identified here under combined treatment is WRKY33. This TF is known to bind the *RBOHD* promoter (Zhao et al., 2020), our data shows that *WRKY33* expression mirrors *RBOHD* transcriptional dynamics under combined and single stresses.

Results also showed that *RBOHD* mRNA and RBOHD protein levels do not correlate. Under HF in the light, RBOHD protein levels declined compared to those in NF, while transcript levels increased in HF compared to NF. This inversion implicates translational and/or post-translational (e.g. protein stability) regulatory mechanisms for RBOHD. Here, negative regulator

of plant immunity, and previously characterised interactor to RBOHD, CPK28 emerged as a candidate regulator of RBOHD protein levels in HF conditions (Bakshi et al., 2023; Monaghan et al., 2014; Yu et al., 2024), potentially through direct phosphorylation or *via* indirect phosphorylation cascades that could involve with BIK1 and E3 ligases. The latter remains to be experimentally explored.

Based on these results we propose the following model: when plants face hypoxia prior to flg22 treatment present active ERFVIIs which regulate transcriptional and post-transcriptional dynamics of RBOHD in seedlings. However, in 4-week old plants, the ERFVIIs only control basal levels of RBOHD protein abundance, and other elements of the hypoxia stress response (CPK28) control RBOHD transcription and protein levels in a light-dependent manner, possibly due to a stronger activation of hypoxia responses in the dark (**Figure 3.19**).

6.2. Genetic basis for rapeseed resilience to waterlogging and *S. sclerotiorum*

Despite the insights gained from the experiments conducted in *Arabidopsis*, sole reliance on this model plant to investigate the crosstalk between hypoxia and immunity naturally limits the acquisition and implementation of new knowledge suitable for translation to crop species. As well as being a species of economic and societal value, (**see also sections 1.5.2.2 and 4.1.1 above**), rapeseed (*Brassica napus*) is closely related to *Arabidopsis*. To bridge this gap between fundamental research using *Arabidopsis* and more applied research with agronomical relevance, I completed a screen (together with Dr. Shreenivas Singh) to determine the impact of waterlogging on a set of ~100 commercial rapeseed varieties and on their defence capabilities against the necrotrophic fungal pathogen *Sclerotinia sclerotiorum*. Specifically, I monitored how waterlogging affected photosynthetic capacity and biomass accumulation, together with its effect on early timepoints of *Sclerotinia sclerotiorum* infection.

Across the panel, chlorophyll-fluorescence and other photosynthetic parameters differed between genotypes after waterlogging, indicating that photochemical control is genotype-specific. By contrast, physiological traits, showed decreased variance, suggesting a conserved adjustment of growth after waterlogging despite the genotype-specific control of photosynthesis. This reduction in variance was also observed in early timepoints of *S. sclerotiorum* infection (24 and 48 hpi). Therefore, this trait-type split (diversification in photosynthesis, conservation in biomass generation and early disease progress) indicates that

multiple solutions exist for maintaining electron transport and energy dissipation under low O_2, while downstream growth and early pathogen outcomes are restricted at the population level.

These patterns enabled the identification of tolerant and sensitive varieties using both absolute (absolute waterlogging values) and relative (waterlogging to control) approaches. Intriguingly, some varieties displayed tolerance for some photosynthetic parameters and sensitivity for others, highlighting the complexity of the regulation of photosynthesis by waterlogging. This experimental approach allowed the identification of two varieties tolerant to *S. sclerotiorum* infection at 48 hpi after previously facing waterlogging conditions, however, no susceptible genotypes were identified, suggesting that waterlogging could have a genotype-specific priming of pathogen infection.

Genomic association studies (GWAS) focusing on waterlogged:control ratios (to capture stress responsiveness) revealed a broadly polygenic architecture in which many small-effect loci shape performance of specific traits (i.e. Fv'/Fm', NPQt and lesion size at 24 hpi) after waterlogging and *S. sclerotiorum* infection after waterlogging, but the SNP-associated loci converge on a few processes. For example, rapeseed homologues of splicing activators and other RNA-processing candidates were associated with higher NPQt and Fv'/Fm' ratios – i.e. with potential resilience to the stress (Branco-Price et al., 2008; Lee and Bailey-Serres, 2019; Mustroph et al., 2009; Sorenson and Bailey-Serres, 2014). Another example includes Ca^{2+} signalling, as a rapeseed homologue for *At_CPK32* was associated with tolerant NPQt ratios. In addition, cell-wall/carbohydrate enzymes (e.g., homologues for *Arabidopsis At_AXS1* or *At_BGAL13*) were associates with better photosynthetic performance upon waterlogging, consistent with cell wall integrity serving as both mechanical buffer in hypoxia and a key factor impeding the entrance of the pathogen (Ambros et al., 2022; Zou et al., 2013). Additional marker genes identified point to ethylene (*At_EIN2-like*) and photorespiration/peroxisome links (*At_AOA2-like*), tying hormonal signalling pathways and redox balance to photochemical stability. Analysis of lesion size ratios, allowed for the identification of genes associated with light status (rapeseed homologue of *At_CIP7*) and photosynthesis (*At_CHLM-like*) as modulators of *S. sclerotiorum* infection after waterlogging.

6.3. Common regulators of the crosstalk between hypoxia and immunity

This thesis aimed to understand how plants regulate immune activation upon low oxygen conditions, and how the crosstalk between hypoxia and immunity programs translates from molecular regulation in *Arabidopsis thaliana* to population-level phenotypes and allelic variation in *Brassica napus*. Across chapters, three modulators are present in the regulation of this crosstalk: (i) Ca^{2+} signalling, (ii) light-dependent control over hypoxia and immunity/defence crosstalk (also through photosynthesis), and (iii) decoupling between mRNA and protein levels (**Figure 6.1**).

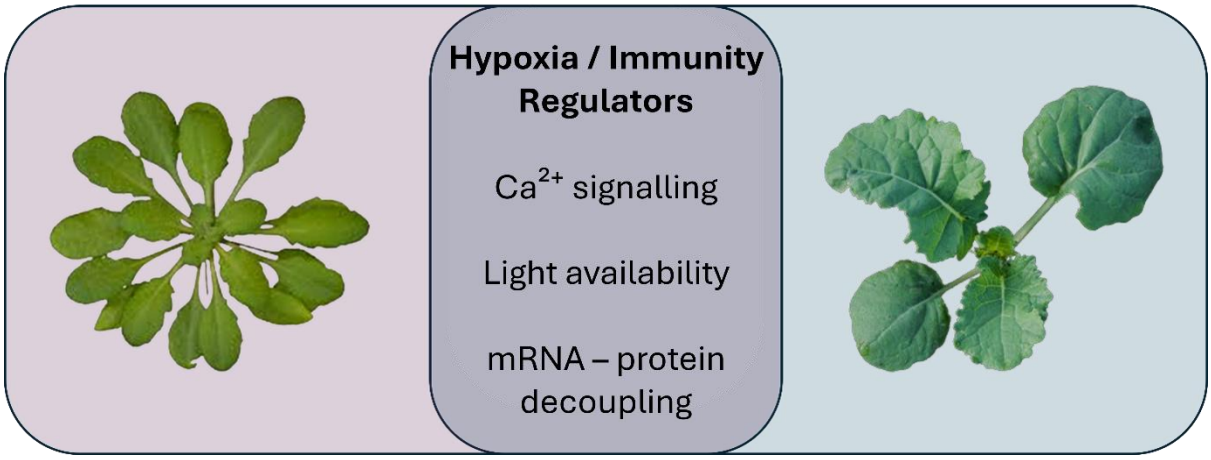

Figure 6.1. Model of common elements in *A. thaliana* and *B. napus* regulating hypoxia and immunity crosstalk. Recurrent elements regulating both RBOHD in *Arabidopsis thaliana* (purple circle) and waterlogging/ *S. sclerotiorum* in *Brassica napus* (blue circle).

Across the thesis, Ca^{2+} signalling emerged as a common regulator of immunity under low O_2 conditions. In *A. thaliana*, combined hypoxia/flg22 revealed a role of the Ca^{2+}-dependent kinase CPK28 in the regulation of RBOHD at the protein level, suggested by a potential activation of CPK28 upon hypoxia (Bakshi et al., 2023; Yu et al., 2024), ensuring increased RBOHD protein abundance in dark HF conditions. In *Brassica napus*, GWAS associated a rapeseed homologue of *At_CPK32* as a candidate gene for tuning NPQt and photochemical resilience under waterlogging. Together these findings position Ca^{2+}-responsive kinases as convergence points that integrate hypoxia and immune signalling programs, and as practical targets for validation and marker development.

A second recurring regulator of hypoxia/flg22 combination is the decoupling between mRNA and protein levels. In *A. thaliana, RBOHD* transcripts can be hyper-induced during light HF conditions while RBOHD protein levels decline. This is in line with translation, protein modification, and turnover control of RBOHD protein when oxygen levels and energy status are limited. In *B. napus* we observe a similar trend, as we detected SNPs in genes such as a homologue of the splicing factor *At_SMU1* and a rapeseed homologue of *At_EIN2*, which controls translation upon submergence in an ethylene-dependent way (Cho et al., 2022). These genes were associated with photosynthetic performance of *B. napus* upon waterlogging, and could potentially also influence the response to combined waterlogging and *S. sclerotiorum* infection. Across chapters, the data suggest that regulating defence responses under waterlogged conditions is at the level of ribosome engagement, RNA processing, and proteostasis on points of convergence such as RBOHD or other common regulators of stress responses.

Waterlogging consistently perturbed photosynthetic function, which partially explains downstream susceptibility to *S. sclerotiorum*. In *B. napus*, photosynthetic traits (e.g., Fv'/Fm', NPQt, SPAD) showed large genotype-specific diversity upon waterlogging. Loci linked with photochemistry and light signalling (homologues of *At_CHLM* and *At_CIP7*) were associated with disease progression subsequent to waterlogging conditions. These associations potentially connects chlorophyll/retrograde pathways and photoregulation to early disease dynamics after flooding. In *A. thaliana*, light availability also reprogrammed the immune network state in hypoxic conditions around RBOHD, hyper-inducing its transcript levels, and differentially regulating its protein levels. Together, these results establish light availability as a central hub in the crosstalk between hypoxia and pathogen responses by a regulating hypoxia/flg22 control over RBOHD, and establishes photosynthesis as a practical phenotyping indicator for selecting lines that maintain both photochemical efficiency under waterlogging and disease resilience after waterlogging.

6.4. Future directions

Regarding *A. thaliana*, future work should be done to elucidate the mechanism by which CPK28 regulates RBOHD transcript and protein levels under simultaneous hypoxia/flg22, whether if it is by direct phosphorylation of by indirect regulation through BIK1 or additional E3 ligases. Furthermore, future work on CPK28 activation during hypoxic conditions could potentially explain mechanisms by which hypoxia represses PTI, as previously proposed by Mooney et al., 2024. Furthermore, additional assays to quantify RBOHD activity should be carried

out in the future. Due to technical difficulties, such measurements in the different mutant backgrounds could not be completed.

Regarding *B. napus*, future work should focus on the validation of the genes identified by GWAS (e.g., homologues for *At_SMU1, At_CPK32, At_AOAT2, At_CHLM, At_CIP7* or *Cab008997.1*) in their role as regulators of waterlogging tolerance or pathogen resistance in waterlogging followed by *S. sclerotorium* infection. Due to time constrains, specific location of SNPs in their corresponding genes and genome could not be performed. Once SNPs are located within their corresponding genes, expression assays across genotypes including RT-qPCRs or promoter–reporter assays (using transient expression systems in rapeseed (Mooney and Graciet, 2020) could be performed. Specifically, for intronic/splice-site SNPs, check splicing assays, specifically for coding SNPs, check protein function. Additionally, future work could knock-in the allele swap, or knock-out the candidate gene followed by adequate testing for predicted phenotypic shifts. However, the latter is complicated considering that rapeseed is an allotetraploid. Other model systems could therefore be used, such as *Arabidopsis thaliana*. In the long term, field or multi-environment validation should be performed to confirm the allele contributes to waterlogging tolerance or pathogen resistance in waterlogging followed by *S. sclerotorium* infection.

Finally, these strands should be unified in a predictive, testable model where three mechanisms (Ca^{2+} signalling, light/energy status, and mRNA-protein decoupling), jointly regulate defence outputs during simultaneous hypoxia and flg22 or waterlogging/*S.sclerotorium* in both *A. thaliana* and *B. napus* species.

7. References

Abbas, M., Berckhan, S., Rooney, D.J., Gibbs, D.J., Vicente Conde, J., Sousa Correia, C., Bassel, G.W., Marín-De La Rosa, N., León, J., Alabadí, D., Blázquez, M.A., Holdsworth, M.J., 2015. Oxygen sensing coordinates photomorphogenesis to facilitate seedling survival. Current Biology 25 (11): 1483–1488. https://doi.org/10.1016/j.cub.2015.03.060

Adachi, H., Nakano, T., Miyagawa, N., Ishihama, N., Yoshioka, M., Katou, Y., Yaeno, T., Shirasu, K., Yoshioka, H., 2015. WRKY transcription factors phosphorylated by MAPK regulate a plant immune NADPH oxidase in *nicotiana benthamiana*. Plant Cell 27 (9): 2645–2663. https://doi.org/10.1105/tpc.15.00213

Ahn, J.W., Verma, R., Kim, M., Lee, J.Y., Kim, Y.K., Bang, J.W., Reiter, W.D., Pai, H.S., 2006. Depletion of UDP-D-apiose/UDP-D-xylose synthases results in rhamnogalacturonan-II deficiency, cell wall thickening, and cell death in higher plants. Journal of Biological Chemistry 281 (19): 13708–13716. https://doi.org/10.1074/jbc.M512403200

Akter, S., Perri, M., Lavilla-Puerta, M., Ferretti, B., Dalle Carbonare, L., Shukla, V., Telara, Y., Zhang, D., Gunawardana, D.M., Myers, W.K., Giuntoli, B., Flashman, E., Licausi, F., 2024. H2O2 repurposes the plant oxygen-sensing machinery to control the transcriptional response to oxidative stress. bioRxiv. https://doi.org/10.1101/2024.10.21.619351

Al-Shehbaz, I.A., 2012. A generic and tribal synopsis of the Brassicaceae (Cruciferae). Taxon 61 (5): 931–954. https://doi.org/10.1002/tax.615002

Ambros, S., Kotewitsch, M., Wittig, P.R., Bammer, B., Mustroph, A., 2022. Transcriptional Response of Two Brassica napus Cultivars to Short-Term Hypoxia in the Root Zone. Front. Plant Sci. 13. https://doi.org/10.3389/fpls.2022.897673

Andreasson, E., Jenkins, T., Brodersen, P., Thorgrimsen, S., Petersen, N.H.T., Zhu, S., Qiu, J.L., Micheelsen, P., Rocher, A., Petersen, M., Newman, M.A., Nielsen, H.B., Hirt, H., Somssich, I., Mattsson, O., Mundy, J., 2005. The MAP kinase substrate MKS1 is a regulator of plant defense responses. EMBO Journal 24 (14): 2579–2589. https://doi.org/10.1038/sj.emboj.7600737

Araguirang, G.E., Richter, A.S., 2022. Activation of anthocyanin biosynthesis in high light – what is the initial signal? New Phytologist 236 (6): 2037–2043. https://doi.org/10.1111/nph.18488

Arico, D.S., Burachik, N.B., Wengier, D.L., Mazzella, M.A., 2024. Arabidopsis hypocotyl growth in darkness requires the phosphorylation of a microtubule-associated protein. Plant Journal 118 (6): 1815–1831. https://doi.org/10.1111/tpj.16711

Arnaud, D., Deeks, M.J., Smirnoff, N., 2023. Organelle-targeted biosensors reveal distinct oxidative events during pattern-triggered immune responses. Plant Physiol. 191 (4): 2551–2569. https://doi.org/10.1093/plphys/kiac603

Arthur, J.S.C., Ley, S.C., 2013. Mitogen-activated protein kinases in innate immunity. Nat Rev Immunol 13 (9): 679–692 https://doi.org/10.1038/nri3495

Asai, T., Tena, G., Plotnikova, J., Willmann, M.R., Chiu, W.-L., Gómez-Gómez, L., Boller, T., Ausubel, F.M., Sheen, J., 2002. MAP kinase signalling cascade in *Arabidopsis* innate immunity. Nature 415 (6875): 977–983. https://doi.org/10.1038/415977a

Ashraf, M., Mehmood, S., 1990. Effects of waterlogging on growth and some physiological parameters of four Brassica species. Plant Soil 121 (2): 203–209. https://doi.org/10.1007/BF00012313

Atkinson, N.J., Urwin, P.E., 2012. The interaction of plant biotic and abiotic stresses: fromgenes to the field. J. Exp. Bot. 63 (2): 3523–3544. https://doi.org/10.1093/jxb/err313

Baena-González, E., Sheen, J., 2008. Convergent energy and stress signaling. Trends in Plant Science, 13 (9): 474-482. https://doi.org/10.1016/j.tplants.2008.06.006

Bai, J., Zhou, Y., Sun, J., Chen, K., Han, Y., Wang, R., Zou, Y., Du, M., Lu, D., 2023. BIK1 protein homeostasis is maintained by the interplay of different ubiquitin ligases in immune signaling. Nat. Commun. 14 (1): 4624. https://doi.org/10.1038/s41467-023-40364-0

Baker, N.R., 2008. Chlorophyll fluorescence: A probe of photosynthesis in vivo. Annu. Rev. Plant Biol. 59, 89-113. https://doi.org/10.1146/annurev.arplant.59.032607.092759

Baker, N.R., Rosenqvist, E., 2004. Applications of chlorophyll fluorescence can improve crop production strategies: An examination of future possibilities. J. Exp. Bot. 55 (403): 1607–1621. https://doi.org/10.1093/jxb/erh196

Bakshi, A., Choi, W.G., Kim, S.H., Gilroy, S., 2023. The vacuolar Ca2+ transporter CATION EXCHANGER 2 regulates cytosolic calcium homeostasis, hypoxic signaling, and response to flooding in Arabidopsis thaliana. New Phytologist 240 (5): 1830–1847. https://doi.org/10.1111/nph.19274

Barreto, P., Dambire, C., Sharma, G., Vicente, J., Osborne, R., Yassitepe, J., Gibbs, D.J., Maia, I.G., Holdsworth, M.J., Arruda, P., 2022. Mitochondrial retrograde signaling through UCP1-mediated inhibition of the plant oxygen-sensing pathway. Current Biology 32 (6): 1403-1411.e4. https://doi.org/10.1016/j.cub.2022.01.037

Baxter-Burrell, A., Yang, Z., Springer, P.S., Bailey-Serres, J., 2002. RopGAP4-dependent Rop GTPase rheostat control of Arabidopsis oxygen deprivation tolerance. Science. 296, 2026–2028. https://doi.org/10.1126/science.1071505

Beck, M., Zhou, J., Faulkner, C., Mac, D.L., Robatzek, S., 2012. Spatio-temporal cellular dynamics of the Arabidopsis flagellin receptor reveal activation status-dependent endosomal sorting. Plant Cell 24 (10): 4205–4219. https://doi.org/10.1105/tpc.112.100263

Becker, J.D., Boavida, L.C., Carneiro, J., Haury, M., Feijó, J.A., 2003. Transcriptional Profiling of Arabidopsis Tissues Reveals the Unique Characteristics of the Pollen Transcriptome. Plant Physiol. 133 (2): 713–725. https://doi.org/10.1104/pp.103.028241

Berriri, S., Garcia, A.V., dit Frey, N.F., Rozhon, W., Pateyron, S., Leonhardt, N., Montillet, J.L., Leung, J., Hirt, H., Colcombet, J., 2012. Constitutively active mitogen-activated protein kinase versions reveal functions of Arabidopsis MPK4 in pathogen defense signaling. Plant Cell 24 (10): 4281–4293. https://doi.org/10.1105/tpc.112.101253

Berrocal-Lobo, M., Molina, A., Solano, R., 2002. Constitutive expression of Ethylene-Response-Factor1 in arabidopsis confers resistance to several necrotrophic fungi. Plant Journal 29 (1): 23–32. https://doi.org/10.1046/j.1365-313x.2002.01191.x

Bethke, G., Pecher, P., Eschen-Lippold, L., Tsuda, K., Katagiri, F., Glazebrook, J., Scheel, D., Lee, J., 2012. Activation of the *Arabidopsis thaliana* mitogen-activated protein kinase MPK11 by the flagellin-derived elicitor peptide flg22. Molecular Plant-Microbe Interactions 25 (4): 471–480. https://doi.org/10.1094/MPMI-11-11-0281

Bethke, G. , Unthan, T., Uhrig, J.F., Pöschl, Y., Gust, A.A., Scheel, D. , Lee, J., 2009. Flg22 regulates the release of an ethylene response factor substrate from MAP kinase 6 in *Arabidopsis thaliana* via ethylene signaling. *Proc. Natl. Acad. Sci. U.S.A.* 106 (19): 8067-8072, https://doi.org/10.1073/pnas.0810206106

Bhardwaj, V., Meier, S., Petersen, L.N., Ingle, R.A., Roden, L.C., 2011. Defence responses of arabidopsis thaliana to infection by pseudomonas syringae are regulated by the circadian clock. PLoS One 6 (10): e26968. https://doi.org/10.1371/journal.pone.0026968

Bi, G., Zhou, Z., Wang, W., Li, L., Rao, S., Wu, Y., Zhang, X., Menke, F.L.H., Chen, S., Zhou, J.M., 2018. Receptor-like cytoplasmic kinases directly link diverse pattern recognition receptors to the activation of mitogen-activated protein kinase cascades in arabidopsis. Plant Cell 30 (7): 1543–1561. https://doi.org/10.1105/tpc.17.00981

Binder, B.M., 2020. Ethylene signaling in plants. Journal of Biological Chemistry 295 (22): 7710–7725. https://doi.org/10.1074/jbc.REV120.010854

Birkenbihl, R.P., Diezel, C., Somssich, I.E., 2012. Arabidopsis WRKY33 is a key transcriptional regulator of hormonal and metabolic responses toward Botrytis cinerea infection. Plant Physiol. 159 (1): 266–285. https://doi.org/10.1104/pp.111.192641

Birkenbihl, R.P., Kracher, B., Somssich, I.E., 2017. Induced genome-wide binding of three arabidopsis WRKY transcription factors during early MAMP-triggered immunity. Plant Cell 29 (1): 20–38. https://doi.org/10.1105/tpc.16.00681

Bisceglia, N., Gravino, M., Savatin, D., 2015. Luminol-based Assay for Detection of Immunity Elicitor-induced Hydrogen Peroxide Production in Arabidopsis thaliana Leaves. Bio. Protoc. 5 (24): e1685. https://doi.org/10.21769/bioprotoc.1685

Bleecker, A.B., Estelle, M.A., Somerville, C., Kende, H., 1988. Insensitivity to Ethylene Conferred by a Dominant Mutation in *Arabidopsis thaliana*. *Science* 241 (4869): 1086–1089. https://doi.org/10.1126/science.241.4869.1086

Block, M.A., Tewari, A.K., Albrieux, C., Maréchal, E., Joyard, J., 2002. The plant S-adenosyl-L-methionine:Mg-protoporphyrin IX methyltransferase is located in both envelope and thylakoid chloroplast membranes. Eur. J. Biochem. 269 (1): 240–248. https://doi.org/10.1046/j.0014-2956.2001.02643.x

Borrowman, S., Kapuganti, J.G., Loake, G.J., 2023. Expanding roles for S-nitrosylation in the regulation of plant immunity. Free Radic. Biol. Med. 194, 357-368. https://doi.org/10.1016/j.freeradbiomed.2022.12.009

Boudsocq, M., Willmann, M.R., McCormack, M., Lee, H., Shan, L., He, P., Bush, J., Cheng, S.H., Sheen, J., 2010. Differential innate immune signalling via Ca2+-sensor protein kinases. Nature 464 (7287): 418–422. https://doi.org/10.1038/nature08794

Boutrot, F., Segonzac, C., Chang, K.N., Qiao, H., Ecker, J.R., Zipfel, C., Rathjen, J.P., 2010. Direct transcriptional control of the Arabidopsis immune receptor FLS2 by the ethylene-dependent transcription factors EIN3 and EIL1. Proc. Natl. Acad. Sci. U.S.A. 107 (32): 14502–14507. https://doi.org/10.1073/pnas.1003347107

Branco-Price, C., Kaiser, K.A., Jang, C.J.H., Larive, C.K., Bailey-Serres, J., 2008. Selective mRNA translation coordinates energetic and metabolic adjustments to cellular oxygen deprivation and reoxygenation in Arabidopsis thaliana. Plant Journal 56 (5): 743–755. https://doi.org/10.1111/j.1365-313X.2008.03642.x

Brazel, A.J., Graciet, E. (2023). Complexity of Abiotic Stress Stimuli: Mimicking Hypoxic Conditions Experimentally on the Basis of Naturally Occurring Environments. Plant Abiotic Stress Signaling. Methods in Molecular Biology, 2642. https://doi.org/10.1007/978-1-0716-3044-0_2

Brodersen, P., Petersen, M., Nielsen, H.B., Zhu, S., Newman, M.A., Shokat, K.M., Rietz, S., Parker, J., Mundy, J., 2006. Arabidopsis MAP kinase 4 regulates salicylic acid- and jasmonic acid/ethylene-dependent responses via EDS1 and PAD4. Plant Journal 47 (4): 532–546. https://doi.org/10.1111/j.1365-313X.2006.02806.x

Brunello, L., Kunkowska, A.B., Olmi, E., Triozzi, P.M., Castellana, S., Perata, P., Loreti, E., 2024. The transcription factor ORA59 represses hypoxia responses during Botrytis cinerea infection and reoxygenation. Plant Physiol. 197 (1): kiae677. https://doi.org/10.1093/plphys/kiae677

Bui, L.T., Giuntoli, B., Kosmacz, M., Parlanti, S., Licausi, F., 2015. Constitutively expressed ERF-VII transcription factors redundantly activate the core anaerobic response in Arabidopsis thaliana. Plant Science 236, 37–43. https://doi.org/10.1016/j.plantsci.2015.03.008

Bui, L.T., Shukla, V., Giorgi, F.M., Trivellini, A., Perata, P., Licausi, F., Giuntoli, B., 2020. Differential submergence tolerance between juvenile and adult Arabidopsis plants involves the ANAC017 transcription factor. Plant Journal 104 (4): 979–994. https://doi.org/10.1111/tpj.14975

Burroughs, A.M., Allen, K.N., Dunaway-Mariano, D., Aravind, L., 2006. Evolutionary Genomics of the HAD Superfamily: Understanding the Structural Adaptations and Catalytic Diversity in a Superfamily of Phosphoesterases and Allied Enzymes. J. Mol. Biol. 361 (5): 1003–1034. https://doi.org/10.1016/j.jmb.2006.06.049

Cai, H., Huang, Y., Chen, F., Liu, L., Chai, M., Zhang, M., Yan, M., Aslam, M., He, Q., Qin, Y., 2021. ERECTA signaling regulates plant immune responses via chromatin-mediated promotion of WRKY33 binding to target genes. New Phytologist 230 (2): 737–756. https://doi.org/10.1111/nph.17200

Cao, F.Y., DeFalco, T.A., Moeder, W., Li, B., Gong, Y., Liu, X.M., Taniguchi, M., Lumba, S., Toh, S., Shan, L., Ellis, B., Desveaux, D., Yoshioka, K., 2018. Arabidopsis ETHYLENE RESPONSE FACTOR 8 (ERF8) has dual functions in ABA signaling and immunity. BMC Plant Biol. 18 (1): 211. https://doi.org/10.1186/s12870-018-1402-6

Cao, L., Wang, W., Zhang, W., Staiger, C.J., 2022. Lipid Signaling Requires ROS Production to Elicit Actin Cytoskeleton Remodeling during Plant Innate Immunity. Int. J. Mol. Sci. 23 (5): 2447. https://doi.org/10.3390/ijms23052447

Cao, X., Huang, J., Zhou, G., Deng, N., 2025. A review of rice–rapeseed cropping system in China: towards sustainable development. Crop and Environment 4 (3): 192-202. https://doi.org/10.1016/j.crope.2025.06.003

Cao, Y., Aceti, D.J., Sabat, G., Song, J., Makino, S. ichi, Fox, B.G., Bent, A.F., 2013. Mutations in FLS2 Ser-938 Dissect Signaling Activation in FLS2-Mediated Arabidopsis Immunity. PLoS Pathog. 9 (4): e1003313. https://doi.org/10.1371/journal.ppat.1003313

Caspersen, M.B., Qiu, J.L., Zhang, X., Andreasson, E., Næsted, H., Mundy, J., Svensson, B., 2007. Phosphorylation sites of Arabidopsis MAP kinase substrate 1 (MKS1). Biochim. Biophys. Acta Proteins Proteom. 1774 (9): 1156–1163. https://doi.org/10.1016/j.bbapap.2007.07.002

Castellana, S., Triozzi, P.M., Dell'Acqua, M., Loreti, E., Perata, P., 2024. Environmental genome-wide association studies across precipitation regimes reveal that the E3 ubiquitin ligase MBR1 regulates plant adaptation to rainy environments. Plant Commun. 5 (12). https://doi.org/10.1016/j.xplc.2024.101074

Castro, B., Baik, S., Tran, M., Zhu, J., Li, T., Tang, A., Aoun, N., Blundell, A.C., Gomez, M., Zhang, E., Cho, M.J., Lowe-Power, T., Siddique, S., Staskawicz, B., Coaker, G., 2025. Gene editing of the E3 ligase PIRE1 fine-tunes reactive oxygen species production for enhanced bacterial disease resistance in tomato. Plant Cell 37 (5). https://doi.org/10.1093/plcell/koaf049

Chalhoub, B., Denoeud, F., Liu, S., Parkin, I.A.P., Tang, H., Wang, Xiyin, Chiquet, J., Belcram, H., Tong, C., Samans, B., Corréa, M., Da Silva, C., Just, J., Falentin, C., Koh, C.S., Le Clainche, I., Bernard, M., Bento, P., Noel, B., Labadie, K., Alberti, A., Charles, M., Arnaud, D., Guo, H., Daviaud, C., Alamery, S., Jabbari, K., Zhao, M., Edger, P.P., Chelaifa, H., Tack, D., Lassalle, G., Mestiri, I., Schnel, N., Le Paslier, M.-C., Fan, G., Renault, V., Bayer, P.E., Golicz, A.A., Manoli, S., Lee, T.-H., Ha, V., Thi, D., Chalabi, S., Hu, Q., Fan, C., Tollenaere, R., Lu, Y., Battail, C., Shen, J., Sidebottom, C.H.D., Wang, Xinfa, Canaguier, A., Chauveau, A., Bérard, A., Deniot, G., Guan, M., Liu, Z., Sun, F., Lim, Y.P., Lyons, E., Town, C.D., Bancroft, I., Wang, Xiaowu, Meng, J., Ma, J., Pires, J.C., King, G.J., Brunel, D., Delourme, R., Renard, M., Aury, J.-M., Adams, K.L., Batley, J., Snowdon, R.J., Tost, J., Edwards, D., Zhou, Y., Hua, W., Sharpe, A.G., Andrew, †, Paterson, H., Guan, C., Patrick Wincker, †, Science, S.O., 2014. Early allopolyploid evolution in the post-Neolithic Brassica napus oilseed genome. *Science.* 345 (6199): 950-953. https://doi.org/10.1126/science.1253435

Chaloner, T.M., Gurr, S.J., Bebber, D.P., 2020. Plant pathogen infection risk tracks global crop yields under climate change. Nat. Clim. Chang. 11 (8): 710–715. https://doi.org/10.1038/s41558-021-01104-8

Chandrasekar, B., Van Der Hoorn, R.A.L., 2016. Beta galactosidases in Arabidopsis and tomato - A mini review. Biochem. Soc. Trans. 44 (1): 150–158. https://doi.org/10.1042/BST20150217

Chang, C., Kwok, S.F., Bleecker, A.B., Meyerowitz, E.M., 1993. Arabidopsis Ethylene-Response Gene ETR1: Similarity of Product to Two-Component Regulators The present address of. Science. 262 (5133): 539–544. https://doi.org/10.1126/science.8211181

Chang, R., Jang, C.J.H., Branco-Price, C., Nghiem, P., Bailey-Serres, J., 2012. Transient MPK6 activation in response to oxygen deprivation and reoxygenation is mediated by mitochondria and aids seedling survival in Arabidopsis. Plant Mol. Biol. 78 (1): 109–122. https://doi.org/10.1007/s11103-011-9850-5

Chawade, A., Thuraga, V., Sepp, S.S., Ghosh, S., Ghadamgahi, F., Odilbekov, F., Muthusamy, S., Vetukuri, R.R., Abreha, K.B., 2024. Genomic loci for sclerotinia stem rot resistance and chlorophyll stability in Brassica napus: integrating GWAS with microbiome insights. Plant-Environment Interactions 6 (5). https://doi.org/10.1002/pei3.70092

Chen, D., Cao, Y., Li, H., Kim, D., Ahsan, N., Thelen, J., Stacey, G., 2017. Extracellular ATP elicits DORN1-mediated RBOHD phosphorylation to regulate stomatal aperture. Nat. Commun. 8 (1): 2265. https://doi.org/10.1038/s41467-017-02340-3

Chen, H., Xue, L., Chintamanani, S., Germain, H., Lin, H., Cui, H., Cai, R., Zuo, J., Tang, X., Li, X., Guo, H., Zhou, J.M., 2009. ETHYLENE INSENSITIVE3 and ETHYLENE INSENSITIVE3-LIKE1 repress SALICYLIC ACID INDUCTION DEFICIENT2 expression to negatively regulate plant innate immunity in Arabidopsis. Plant Cell 21 (8): 2527–2540. https://doi.org/10.1105/tpc.108.065193

Chen, J., Tan, C., Zhu, M., Zhang, C., Wang, Z., Ni, X., Liu, Y., Wei, T., Wei, X.F., Fang, X., Xu, Y., Huang, X., Qiu, J., Liu, H., 2024. CropGS-Hub: a comprehensive database of genotype and phenotype resources for genomic prediction in major crops. Nucleic Acids Res. 52 (D1), D1519–D1529. https://doi.org/10.1093/nar/gkad1062

Chen, R.S., Wang, J.Y., Sarwar, R., Tan, X.L., 2023. Genetic breakthroughs in the Brassica napus–Sclerotinia sclerotiorum interactions. Front. Plant Sci. 14. https://doi.org/10.3389/fpls.2023.1276055

Chen, X., Zhang, T., Wang, H., Zhao, W., Guo, Z., 2025. Transcription factor WRKY complexes in plant signaling pathways. Phytopathology Research 7 (1): 54. https://doi.org/10.1186/s42483-025-00349-x

Chen, Y., Zhang, J., 2024. Multiple functions and regulatory networks of WRKY33 and its orthologs. Gene 931. https://doi.org/10.1016/j.gene.2024.148899

Chen, Y.N., Ho, C.H., 2023. CIPK15-mediated inhibition of NH4+ transport protects Arabidopsis from submergence. Heliyon 9 (9). https://doi.org/10.1016/j.heliyon.2023.e20235

Chi, Y., Wang, C., Wang, M., Wan, D., Huang, F., Jiang, Z., Crawford, B.M., Vo-Dinh, T., Yuan, F., Wu, F., Pei, Z.M., 2021. Flg22-induced Ca2+ increases undergo desensitization and resensitization. Plant Cell Environ. 44 (12): 3563–3575. https://doi.org/10.1111/pce.14186

Chinchilla, D., Bauer, Z., Regenass, M., Boller, T., Felix, G., 2006. The Arabidopsis receptor kinase FLS2 binds flg22 and determines the specificity of flagellin perception. Plant Cell 18 (2): 465–476. https://doi.org/10.1105/tpc.105.036574

Chinchilla, D., Zipfel, C., Robatzek, S., Kemmerling, B., Nürnberger, T., Jones, J.D.G., Felix, G., Boller, T., 2007. A flagellin-induced complex of the receptor FLS2 and BAK1 initiates plant defence. Nature 448 (7152): 497–500. https://doi.org/10.1038/nature05999

Cho, H.-Y., Chou, M.-Y., Ho, H.-Y., Chen, W.-C., Shih, M.-C., 2022. Ethylene modulates translation dynamics in Arabidopsis under submergence via GCN2 and EIN2, Sci. Adv. 8 (22). https://doi.org/10.1126/sciadv.abm7863

Choi, S.H., Mansoorabadi, S.O., Liu, Y.N., Chien, T.C., Liu, H.W., 2012. Analysis of UDP-D-apiose/UDP-D-xylose synthase-catalyzed conversion of UDP-D-apiose phosphonate to UDP-D-xylose phosphonate: Implications for a retroaldol-aldol mechanism. J. Am. Chem. Soc. 134 (34): 13946–13949. https://doi.org/10.1021/ja305322x

Choi, W.G., Toyota, M., Kim, S.H., Hilleary, R., Gilroy, S., 2014. Salt stress-induced Ca2+ waves are associated with rapid, long-distance root-to-shoot signaling in plants. Proc. Natl. Acad. Sci. U.S.A. 111 (17): 6497–6502. https://doi.org/10.1073/pnas.1319955111

Chung, H., Kim, S., Kim, K.T., Hwang, B.G., Kim, H.J., Lee, S.J., Lee, Y.H., 2019. A novel approach to investigate hypoxic microenvironment during rice colonization by Magnaporthe oryzae. Environ. Microbiol. 21 (3): 1151–1169. https://doi.org/10.1111/1462-2920.14563

Chung, T., Wang, D., Kim, C.S., Yadegari, R., Larkins, B.A., 2009. Plant SMU-1 and SMU-2 homologues regulate Pre-mRNA splicing and multiple aspects of development. Plant Physiol. 151 (3): 1498–1512. https://doi.org/10.1104/pp.109.141705

Clauw, P., Ellis, T.J., Liu, H.J., Sasaki, E., 2025. Beyond the Standard GWAS - A Guide for Plant Biologists. Plant Cell Physiol 66 (4): 431–443. https://doi.org/10.1093/pcp/pcae079

Clifton, R., Lister, R., Parker, K.L., Sappl, P.G., Elhafez, D., Millar, A.H., Day, D.A., Whelan, J., 2005. Stress-induced co-expression of alternative respiratory chain components in Arabidopsis thaliana. Plant Mol. Biol. 58 (2): 193–212. https://doi.org/10.1007/s11103-005-5514-7

Cui, B., Pan, Q., Cui, W., Wang, Y., P Loake, V.I., Yuan, S., Liu, F., Loake, G.J., 2024. S-nitrosylation of a receptor-like cytoplasmic kinase regulates plant immunity, Sci. Adv. 10 (11). https://doi.org/10.1126/sciadv.adk3126

Cui, Y., Qian, H., Yin, J., Xu, C., Luo, P., Zhang, X., Yu, M., Su, B., Li, X., Lin, J., 2023. Single-molecule analysis reveals the phosphorylation of FLS2 governs its spatiotemporal dynamics and immunity 12. https://doi.org/10.7554/eLife.91072.3

Czechowski, T., Stitt, M., Altmann, T., Udvardi, M.K., Scheible, W.-R., 2005. Genome-wide identification and testing of superior reference genes for transcript normalization in Arabidopsis. Plant Physiology 139 (1): 5–17. https://doi.org/10.1104/pp.105.063743

D'Ambrosio, J.M., Couto, D., Fabro, G., Scuffi, D., Lamattina, L., Munnik, T., Andersson, M.X., Álvarez, M.E., Zipfel, C., Laxalt, A.M., 2017. Phospholipase C2 affects MAMP-triggered immunity by modulating ROS production. Plant Physiol. 175 (2): 970–981. https://doi.org/10.1104/pp.17.00173

Datta, R., Kumar, D., Sultana, A., Hazra, S., Bhattacharyya, D., Chattopadhyay, S., 2015. Glutathione regulates ACC synthase transcription via WRKY33 and ACC oxidase by modulating mRNA stability to induce ethylene synthesis during stress. Plant Physiol. 169 (4): 2963–2981. https://doi.org/10.1104/pp.15.01543

Daudi, A., Cheng, Z., O'Brien, J.A., Mammarella, N., Khan, S., Ausubel, F.M., Paul Bolwell, G., 2012. The apoplastic oxidative burst peroxidase in Arabidopsis is a major component of

pattern-triggered immunity. Plant Cell 24 (1): 275–287. https://doi.org/10.1105/tpc.111.093039

Davletova, S., Rizhsky, L., Liang, H., Shengqiang, Z., Oliver, D.J., Coutu, J., Shulaev, V., Schlauch, K., Mittler, R., 2005a. Cytosolic ascorbate peroxidase 1 is a central component of the reactive oxygen gene network of Arabidopsis. Plant Cell 17 (1): 268–281. https://doi.org/10.1105/tpc.104.026971

Davletova, S., Schlauch, K., Coutu, J., Mittler, R., 2005b. The zinc-finger protein Zat12 plays a central role in reactive oxygen and abiotic stress signaling in Arabidopsis. Plant Physiol. 139 (2): 847–856. https://doi.org/10.1104/pp.105.068254

De Clercq, I., Vermeirssen, V., Van Aken, O., Vandepoele, K., Murcha, M.W., Law, S.R., Inzé, A., Ng, S., Ivanova, A., Rombaut, D., van de Cotte, B., Jaspers, P., Van de Peer, Y., Kangasjärvi, J., Whelan, J., Van Breusegem, F., 2013. The membrane-bound NAC transcription factor ANAC013 functions in mitochondrial retrograde regulation of the oxidative stress response in Arabidopsis. Plant Cell 25 (9): 3472–3490. https://doi.org/10.1105/tpc.113.117168

De Marchi, R., Sorel, M., Mooney, B., Fudal, I., Goslin, K., Kwaśniewska, K., Ryan, P.T., Pfalz, M., Kroymann, J., Pollmann, S., Feechan, A., Wellmer, F., Rivas, S., Graciet, E., 2016. The N-end rule pathway regulates pathogen responses in plants. Sci. Rep. 6 (1): 26020. https://doi.org/10.1038/srep26020

de Torres Zabela, M., Fernandez-Delmond, I., Niittylä, T., Sanchez, P., Grant, M., 2002. Differential expression of genes encoding Arabidopsis phospholipases after challenge with virulent or avirulent *Pseudomonas* isolates. Molecular Plant-Microbe Interactions 15, 808–816. https://doi.org/10.1094/MPMI.2002.15.8.808

Della Coletta, R., Qiu, Y., Ou, S., Hufford, M.B., Hirsch, C.N., 2021. How the pan-genome is changing crop genomics and improvement. Genome Biol 22, (1). https://doi.org/10.1186/s13059-020-02224-8

Derbyshire, M.C., Denton-Giles, M., 2016. The control of sclerotinia stem rot on oilseed rape (Brassica napus): current practices and future opportunities. Plant Pathol. 65 (6): 859-877. https://doi.org/10.1111/ppa.12517

Dhatterwal, P., Sharma, N., Prasad, M., 2024. Decoding the functionality of plant transcription factors. J. Exp. Bot. 75 (16): 4745–4759. https://doi.org/10.1093/jxb/erae231

Ding, L.N., Hu, Y.H., Li, T., Li, M., Li, Y.T., Wu, Y.Z., Cao, J., Tan, X.L., 2024. A GDSL motif-containing lipase modulates Sclerotinia sclerotiorum resistance in Brassica napus. Plant Physiol. 196 (4): 2973–2988. https://doi.org/10.1093/plphys/kiae500

Ding, L.N., Li, T., Guo, X.J., Li, M., Liu, X.Y., Cao, J., Tan, X.L., 2021. Sclerotinia Stem Rot Resistance in Rapeseed: Recent Progress and Future Prospects. J. Agric. Food Chem. 69 (10): 2965–2978. https://doi.org/10.1021/acs.jafc.0c07351

Ding, X. yu, XU, J. song, HUANG, H., QIAO, X., SHEN, M. zhen, CHENG, Y., ZHANG, X. kun, 2020. Unraveling waterlogging tolerance-related traits with QTL analysis in reciprocal intervarietal introgression lines using genotyping by sequencing in rapeseed (Brassica napus L.). J. Integr. Agric. 19 (8): 1974–1983. https://doi.org/10.1016/S2095-3119(19)62783-8

Ding, Z.J., Xu, C., Yan, J.Y., Wang, Y.X., Cui, M.Q., Yuan, J.J., Wang, Y.N., Li, G.X., Wu, J.X., Wu, Y.R., Xu, J.M., Li, C.X., Shi, Y.Z., Mao, C.Z., Guo, J.T., Zhou, J.M., Benhamed, M., Harberd, N.P., Zheng, S.J., 2024. The LRR receptor-like kinase ALR1 is a plant aluminum ion sensor. Cell Res. 34 (4): 281–294. https://doi.org/10.1038/s41422-023-00915-y

dit Frey, N.F., Mbengue, M., Kwaaitaal, M., Nitsch, L., Altenbach, D., Häweker, H., Lozano-Duran, R., Njo, M.F., Beeckman, T., Huettel, B., Borst, J.W., Panstruga, R., Robatzek, S., 2012. Plasma membrane calcium ATPases are important components of receptor-mediated signaling in plant immune responses and development. Plant Physiol. 159 (2): 798–809. https://doi.org/10.1104/pp.111.192575

Djamei, A., Pitzschke, A., Nakagami, H., Rajh, I., Hirt, H., 2007. Trojan Horse Strategy in *Agrobacterium* Transformation: Abusing MAPK Defense Signaling. *Science* 318 (5849): 450-453. https://doi.org/10.1126/science.1145718

Donahue, R.A., Poulson, M.E., Edwards, G.E., 1997. A method for measuring whole plant photosynthesis in Arabidopsis thaliana, Photosynthesis Research. 52 (3): 263–269. https://doi.org/10.1023/A:1005834327441

Du, H., Chen, J., Zhan, H., Li, S., Wang, Y., Wang, W., Hu, X., 2023. The Roles of CDPKs as a Convergence Point of Different Signaling Pathways in Maize Adaptation to Abiotic Stress. Int. J. Mol. Sci. 24 (3): 2325. https://doi.org/10.3390/ijms24032325

Du, Z., Deng, S., Wu, Z., Wang, C., 2021. Genome-wide analysis of haloacid dehalogenase genes reveals their function in phosphate starvation responses in rice. PLoS One 16 (1): e0245600. https://doi.org/10.1371/journal.pone.0245600

Dubiella, U., Seybold, H., Durian, G., Komander, E., Lassig, R., Witte, C.P., Schulze, W.X., Romeis, T., 2013. Calcium-dependent protein kinase/NADPH oxidase activation circuit is required for rapid defense signal propagation. Proc. Natl. Acad. Sci. U.S.A. 110 (21): 8744–8749. https://doi.org/10.1073/pnas.1221294110

Dynowski, M., Schaaf, G., Loque, D., Moran, O., Ludewig, U., 2008. Plant plasma membrane water channels conduct the signalling molecule H2O2. Biochemical Journal 414 (1): 53–61. https://doi.org/10.1042/BJ20080287

Edwards, K., Johnstone, C., Thompson, C., 1991. A simple and rapid method for the preparation of plant genomic DNA for PCR analysis, Nucleic Acids Research. 19 (6): 1349. https://doi.org/10.1093/nar/19.6.1349

Ekanayake, G., Smith, J.M., Jones, K.B., Stiers, H.M., Robinson, S.J., LaMontagne, E.D., Kostos, P.H., Cornish, P. V., Bednarek, S.Y., Heese, A., 2021. Dynamin-related protein drp1a functions with drp2b in plant growth, flg22-immune responses, and endocytosis. Plant Physiol. 185 (4): 1986–2002. https://doi.org/10.1093/plphys/kiab024

Erayya, Sarkhel, S., Managanvi, K., Kumar, S., Alipatra, A., 2023. Emerging Diseases of Vegetables Due to Changing Climate. 2, 323–340. https://doi.org/10.1007/978-3-031-20840-9_15

Evans, M.J., Choi, W.G., Gilroy, S., Morris, R.J., 2016. A ROS-assisted calcium wave dependent on the AtRBOHD NADPH oxidase and TPC1 cation channel propagates the systemic response to salt stress. Plant Physiol. 171 (3): 1771–1784. https://doi.org/10.1104/pp.16.00215

Exposito-Rodriguez, M., Laissue, P.P., Yvon-Durocher, G., Smirnoff, N., Mullineaux, P.M., 2017. Photosynthesis-dependent H2O2 transfer from chloroplasts to nuclei provides a high-light signalling mechanism. Nat. Commun. 8: 49. https://doi.org/10.1038/s41467-017-00074-w

Eysholdt-Derzsó, E., Renziehausen, T., Frings, S., Frohn, S., von Bongartz, K., Igisch, C.P., Mann, J., Häger, L., Macholl, J., Leisse, D., Hoffmann, N., Winkels, K., Wanner, P., De Backer, J., Luo, X., Sauter, M., De Clercq, I., van Dongen, J.T., Schippers, J.H.M., Schmidt-Schippers, R.R., 2023. Endoplasmic reticulum–bound ANAC013 factor is cleaved by RHOMBOID-LIKE 2 during the initial response to hypoxia in Arabidopsis thaliana. Proc. Natl. Acad. Sci. U.S.A. 120 (11): e2221308120. https://doi.org/10.1073/pnas.2221308120

Fan, B., Liao, K., Wang, L.N., Shi, L.L., Zhang, Y., Xu, L.J., Zhou, Y., Li, J.F., Chen, Y.Q., Chen, Q.F., Xiao, S., 2023. Calcium-dependent activation of CPK12 facilitates its cytoplasm-to-nucleus translocation to potentiate plant hypoxia sensing by phosphorylating ERF-VII transcription factors. Mol. Plant 16 (6): 979–998. https://doi.org/10.1016/j.molp.2023.04.002

FAO, 2021. Food Outlook – Biannual Report on Global Food Markets, Food Outlook – Biannual Report on Global Food Markets. FAO. https://doi.org/10.4060/cb4479en

Feechan, A., Kwon, E., Yun, B.-W., Wang, Y., Pallas, J.A., Loake, G.J., 2005. A central role for S-nitrosothiols in plant disease resistance. Proceedings of the National Academy of Sciences of the United States of America 102 (22): 8054–8059. https://doi.org/10.1073/pnas.0501456102

Felle, H.H., 2006. Apoplastic pH during low-oxygen stress in barley. Ann. Bot. 98 (5): 1085–1093. https://doi.org/10.1093/aob/mcl193

Feng, Z., Nagao, H., Li, B., Sotta, N., Shikanai, Y., Yamaguchi, K., Shigenobu, S., Kamiya, T., Fujiwara, T., 2020. An SMU Splicing Factor Complex within Nuclear Speckles Contributes to Magnesium Homeostasis in Arabidopsis. Plant Physiol. 184 (1): 428–442. https://doi.org/10.1104/PP.20.00109

Fichman, Y., Miller, G., Mittler, R., 2019. Whole-Plant Live Imaging of Reactive Oxygen Species. Mol. Plant 12 (9): 1203–1210. https://doi.org/10.1016/j.molp.2019.06.003

Fichman, Y., Myers, R.J., Grant, D.G., Mittler, R., 2021. Plasmodesmata-localized proteins and ROS orchestrate light-induced rapid systemic signaling in Arabidopsis, *Sci. Signal.*14 (671): eabf032. https://doi.org/10.1126/scisignal.abf0322

Fichman, Y., Zandalinas, S.I., Peck, S., Luan, S., Mittler, R., 2022a. HPCA1 is required for systemic reactive oxygen species and calcium cell-to-cell signaling and plant acclimation to stress. Plant Cell 34 (11): 4453–4471. https://doi.org/10.1093/plcell/koac241

Fichman, Y., Zandalinas, S.I., Peck, S., Luan, S., Mittler, R., 2022b. HPCA1 is required for systemic reactive oxygen species and calcium cell-to-cell signaling and plant acclimation to stress. Plant Cell 34 (11): 4453–4471. https://doi.org/10.1093/plcell/koac241

Forzani, C., Carreri, A., De La Fuente Van Bentem, S., Lecourieux, D., Lecourieux, F., Hirt, H., 2011. The Arabidopsis protein kinase Pto-interacting 1-4 is a common target of the oxidative signal-inducible 1 and mitogen-activated protein kinases. FEBS Journal 278 (7): 1126–1136. https://doi.org/10.1111/j.1742-4658.2011.08033.x

Frungillo, L., Skelly, M.J., Loake, G.J., Spoel, S.H., Salgado, I., 2014. S-nitrosothiols regulate nitric oxide production and storage in plants through the nitrogen assimilation pathway. Nat. Commun. 5 (1): 5401. https://doi.org/10.1038/ncomms6401

Fukushima, S., Mori, M., Sugano, S., Takatsuji, H., 2016. Transcription factor WRKY62 plays a role in pathogen defense and hypoxia-responsive gene expression in rice. Plant Cell Physiol. 57 (12): 2541–2551. https://doi.org/10.1093/pcp/pcw185

Gao, M., Liu, J., Bi, D., Zhang, Z., Cheng, F., Chen, S., Zhang, Y., 2008. MEKK1, MKK1/MKK2 and MPK4 function together in a mitogen-activated protein kinase cascade to regulate innate immunity in plants. Cell Res. 18 (12): 1190–1198. https://doi.org/10.1038/cr.2008.300

Gao, M., Wang, X., Wang, D., Xu, F., Ding, X., Zhang, Z., Bi, D., Cheng, Y.T., Chen, S., Li, X., Zhang, Y., 2009. Regulation of Cell Death and Innate Immunity by Two Receptor-like Kinases in Arabidopsis. Cell Host Microbe 6 (1): 34–44. https://doi.org/10.1016/j.chom.2009.05.019

Gao, X., Chen, X., Lin, W., Chen, S., Lu, D., Niu, Y., Li, L., Cheng, C., McCormack, M., Sheen, J., Shan, L., He, P., 2013a. Bifurcation of Arabidopsis NLR Immune Signaling via Ca2+-Dependent Protein Kinases. PLoS Pathog. 9 (1). https://doi.org/10.1371/journal.ppat.1003127

García, J.A.P., Mazubert, C., del Olmo, I., Bourge, M., Domenichini, S., Bounon, R., Tariq, Z., Delannoy, E., Piñeiro, M., Jarillo, J.A., Bergounioux, C., Benhamed, M., Raynaud, C., 2017. Function of the plant DNA polymerase epsilon in replicative stress sensing, a genetic analysis. Plant Physiol. 173 (3): 1735–1749. https://doi.org/10.1104/pp.17.00031

García, P., Singh, S., Graciet, E., 2024. New Insights into the Connections between Flooding/Hypoxia Response and Plant Defenses against Pathogens. Plants. 13 (16): 2176. https://doi.org/10.3390/plants13162176

Garcion, C., Lohmann, A., Lamodière, E., Catinot, J., Buchala, A., Doermann, P., Métraux, J.P., 2008. Characterization and biological function of the Isochorismate Synthase2 gene of Arabidopsis. Plant Physiol. 147 (3): 1279–1287. https://doi.org/10.1104/pp.108.119420

Garrett, K.A., Nita, M., De Wolf, E.D., Esker, P.D., Gomez-Montano, L., Sparks, A.H., 2016. Plant Pathogens as Indicators of Climate Change, in: Climate Change: Observed Impacts on Planet Earth: Second Edition. Elsevier Inc., 325–338. https://doi.org/10.1016/B978-0-444-63524-2.00021-X

Garzón, M., Eifler, K., Faust, A., Scheel, H., Hofmann, K., Koncz, C., Yephremov, A., Bachmair, A., 2007. PRT6/At5g02310 encodes an Arabidopsis ubiquitin ligase of the N-end rule pathway with arginine specificity and is not the CER3 locus. FEBS Lett. 581 (17): 3189–3196. https://doi.org/10.1016/j.febslet.2007.06.005

Gasch, P., Fundinger, M., Müller, J.T., Lee, T., Bailey-Serres, J., Mustropha, A., 2016. Redundant ERF-VII transcription factors bind to an evolutionarily conserved cis-motif to regulate hypoxia-responsive gene expression in arabidopsis. Plant Cell 28 (1): 160–180. https://doi.org/10.1105/tpc.15.00866

Geigenberger, P., 2003. Response of plant metabolism to too little oxygen. Curr. Opin. Plant Biol. 6 (3): 247-256. https://doi.org/10.1016/S1369-5266(03)00038-4

Genty, B., Briantais, J.M., Baker, N.R., 1989. The relationship between the quantum yield of photosynthetic electron transport and quenching of chlorophyll fluorescence. Biochim. Biophys. Acta Gen. Subj. 990 (1): 87–92. https://doi.org/10.1016/S0304-4165(89)80016-9

George, J., Stegmann, M., Monaghan, J., Bailey-Serres, J., Zipfel, C., 2023. Arabidopsis translation initiation factor binding protein CBE1 negatively regulates accumulation of the NADPH oxidase respiratory burst oxidase homolog D. Journal of Biological Chemistry 299 (8): 105018. https://doi.org/10.1016/j.jbc.2023.105018

Gibbs, D.J., Conde, J.V., Berckhan, S., Prasad, G., Mendiondo, G.M., Holdsworth, M.J., 2015. Group VII ethylene response factors coordinate oxygen and nitric oxide signal transduction and stress responses in plants. Plant Physiol. 169 (1): 23–31. https://doi.org/10.1104/pp.15.00338

Gibbs, D.J., Lee, S.C., Md Isa, N., Gramuglia, S., Fukao, T., Bassel, G.W., Correia, C.S., Corbineau, F., Theodoulou, F.L., Bailey-Serres, J., Holdsworth, M.J., 2011. Homeostatic response to hypoxia is regulated by the N-end rule pathway in plants. Nature 479 (7373): 415–418. https://doi.org/10.1038/nature10534

Gibbs, D.J., MdIsa, N., Movahedi, M., Lozano-Juste, J., Mendiondo, G.M., Berckhan, S., Marín-delaRosa, N., VicenteConde, J., SousaCorreia, C., Pearce, S.P., Bassel, G.W., Hamali, B., Talloji, P., Tomé, D.F.A., Coego, A., Beynon, J., Alabadí, D., Bachmair, A., León, J., Gray, J.E., Theodoulou, F.L., Holdsworth, M.J., 2014a. Nitric Oxide Sensing in Plants Is Mediated by Proteolytic Control of Group VII ERF Transcription Factors. Mol. Cell 53 (3): 369–379. https://doi.org/10.1016/j.molcel.2013.12.020

Gibbs, D.J., MdIsa, N., Movahedi, M., Lozano-Juste, J., Mendiondo, G.M., Berckhan, S., Marín-delaRosa, N., VicenteConde, J., SousaCorreia, C., Pearce, S.P., Bassel, G.W., Hamali, B., Talloji, P., Tomé, D.F.A., Coego, A., Beynon, J., Alabadí, D., Bachmair, A., León, J., Gray, J.E., Theodoulou, F.L., Holdsworth, M.J., 2014b. Nitric Oxide Sensing in Plants Is Mediated by Proteolytic Control of Group VII ERF Transcription Factors. Mol. Cell 53 (3), 369–379. https://doi.org/10.1016/j.molcel.2013.12.020

Gibbs, D.J., Theodoulou, F.L., Bailey-Serres, J., 2025. Primed to persevere: Hypoxia regulation from epigenome to protein accumulation in plants. Plant Physiol. 197 (1): kiae584. https://doi.org/10.1093/plphys/kiae584

Giuntoli, B., Lee, S.C., Licausi, F., Kosmacz, M., Oosumi, T., van Dongen, J.T., Bailey-Serres, J., Perata, P., 2014. A Trihelix DNA Binding Protein Counterbalances Hypoxia-Responsive Transcriptional Activation in Arabidopsis. PLoS Biol. 12 (9): e1001950. https://doi.org/10.1371/journal.pbio.1001950

Giuntoli, B., Shukla, V., Maggiorelli, F., Giorgi, F.M., Lombardi, L., Perata, P., Licausi, F., 2017. Age-dependent regulation of ERF-VII transcription factor activity in Arabidopsis thaliana. Plant Cell Environ. 40 (10): 2333–2346. https://doi.org/10.1111/pce.13037

Gkizi, D., Lehmann, S., L'Haridon, F., Serrano, M., Paplomatas, E.J., Métraux, J.-P., Tjamos, S.E., 2016. The innate immune signaling system as a regulator of disease resistance and induced systemic resistance activity against *Verticillium dahliae*. Molecular Plant-Microbe Interactions 29 (4): 313–323. https://doi.org/10.1094/MPMI-11-15-0261-R

Gómez-Gómez, L., Boller, T., 2000. FLS2: An LRR Receptor-like Kinase Involved in the Perception of the Bacterial Elicitor Flagellin in Arabidopsis. Mol. Cell 5 (6): 1003–1011. https://doi.org/10.1016/S1097-2765(00)80265-8

Gonzali, S., Loreti, E., Cardarelli, F., Novi, G., Parlanti, S., Pucciariello, C., Bassolino, L., Banti, V., Licausi, F., Perata, P., 2015. Universal stress protein HRU1 mediates ROS homeostasis under anoxia. Nat. Plants 1 (11): 15151. https://doi.org/10.1038/nplants.2015.151

Goodspeed, D., Chehab, E.W., Min-Venditti, A., Braam, J., Covington, M.F., 2012. Arabidopsis synchronizes jasmonate-mediated defense with insect circadian behavior. Proc. Natl. Acad. Sci. U. S. A. 109 (12): 4674–4677. https://doi.org/10.1073/pnas.1116368109

Goto, Y., Kadota, Y., Mbengue, M., Lewis, J.D., Matsui, H., Maki, N., Ngou, B.P.M., Sklenar, J., Derbyshire, P., Shibata, A., Ichihashi, Y., Guttman, D.S., Nakagami, H., Suzuki, T., Menke, F.L.H., Robatzek, S., Desveaux, D., Zipfel, C., Shirasu, K., 2024. The leucine-rich repeat receptor kinase QSK1 regulates PRR-RBOHD complexes targeted by the bacterial effector HopF2 *Pto*. Plant Cell 36 (12): 4932–4951. https://doi.org/10.1093/plcell/koae267

Goto, Y., Maki, N., Sklenar, J., Derbyshire, P., Menke, F.L.H., Zipfel, C., Kadota, Y., Shirasu, K., 2024. The phagocytosis oxidase/Bem1p domain-containing protein PB1CP negatively regulates the NADPH oxidase RBOHD in plant immunity. New Phytologist 241 (4): 1763–1779. https://doi.org/10.1111/nph.19302

Gravino, M., Savatin, D.V., MacOne, A., De Lorenzo, G., 2015. Ethylene production in Botrytis cinerea- and oligogalacturonide-induced immunity requires calcium-dependent protein kinases. Plant Journal 84 (6): 1073–1086. https://doi.org/10.1111/tpj.13057

Gravot, A., Richard, G., Lime, T., Lemarié, S., Jubault, M., Lariagon, C., Lemoine, J., Vicente, J., Robert-Seilaniantz, A., Holdsworth, M.J., Manzanares-Dauleux, M.J., 2016a. Hypoxia response in Arabidopsis roots infected by Plasmodiophora brassicae supports the development of clubroot. BMC Plant Biol. 16 (1): 1–10. https://doi.org/10.1186/s12870-016-0941-y

Gravot, A., Richard, G., Lime, T., Lemarié, S., Jubault, M., Lariagon, C., Lemoine, J., Vicente, J., Robert-Seilaniantz, A., Holdsworth, M.J., Manzanares-Dauleux, M.J., 2016b. Hypoxia response in Arabidopsis roots infected by Plasmodiophora brassicae supports the development of clubroot. BMC Plant Biol. 16 (1): 251. https://doi.org/10.1186/s12870-016-0941-y

Gschwend, F., Aregger, K., Gramlich, A., Walter, T., Widmer, F., 2020. Periodic waterlogging consistently shapes agricultural soil microbiomes by promoting specific taxa. Applied Soil Ecology 155, 103623. https://doi.org/10.1016/j.apsoil.2020.103623

Guo, F.-Q., Okamoto, M., Crawford, N.M., 2003. Identification of a plant nitric oxide synthase gene involved in hormonal signaling. Science 302 (5642): 100–103. https://doi.org/10.1126/science.1086770

Guo, Y., Chen, J., Kuang, L., Wang, N., Zhang, G., Jiang, L., Wu, D., 2020. Effects of waterlogging stress on early seedling development and transcriptomic responses in Brassica napus. Molecular Breeding 40 (9): 85. https://doi.org/10.1007/s11032-020-01167-z

Guo, Y., Zhang, Y., Li, Y., Liu, J., Hu, Y., Jiang, J., Li, Q., Chen, Y., Hu, W., Jiang, L., Pan, R., Wu, D., Dong, J., 2025. BKK1/BAK7 and TCP21 form a positive feedback loop to facilitate

submergence tolerance in plants. Cell Rep. 44 (6): 115788. https://doi.org/10.1016/j.celrep.2025.115788

Gupta, K.J., Fernie, A.R., Kaiser, W.M., van Dongen, J.T., 2011. On the origins of nitric oxide. Trends Plant Sci. 16 (3): 160-168. https://doi.org/10.1016/j.tplants.2010.11.007

Gupta, K.J., Mur, L.A.J., Wany, A., Kumari, A., Fernie, A.R., Ratcliffe, R.G., 2020. The role of nitrite and nitric oxide under low oxygen conditions in plants. New Phytologist 225 (3): 1143–1151. https://doi.org/10.1111/nph.15969

Halter, T., Imkampe, J., Mazzotta, S., Wierzba, M., Postel, S., Bücherl, C., Kiefer, C., Stahl, M., Chinchilla, D., Wang, X., Nürnberger, T., Zipfel, C., Clouse, S., Borst, J.W., Boeren, S., De Vries, S.C., Tax, F., Kemmerling, B., 2014. The leucine-rich repeat receptor kinase BIR2 is a negative regulator of BAK1 in plant immunity. Current Biology 24 (2): 134–143. https://doi.org/10.1016/j.cub.2013.11.047

Han, L., Li, G.J., Yang, K.Y., Mao, G., Wang, R., Liu, Y., Zhang, S., 2010. Mitogen-activated protein kinase 3 and 6 regulate Botrytis cinerea-induced ethylene production in Arabidopsis. Plant Journal 64 (1): 114–127. https://doi.org/10.1111/j.1365-313X.2010.04318.x

Hanson, M.C., Petch, G.M., Ottosen, T.B., Skjøth, C.A., 2022. Climate change impact on fungi in the atmospheric microbiome. Science of the Total Environment 830, 154491. https://doi.org/10.1016/j.scitotenv.2022.154491

Hao, H., Fan, L., Chen, T., Li, R., Li, X., He, Q., Botella, M.A., Lin, J., 2014. Clathrin and membrane microdomains cooperatively regulate RbohD dynamics and activity in Arabidopsis. Plant Cell 26 (4): 1729–1745. https://doi.org/10.1105/tpc.113.122358

Hao, X., Wang, S., Fu, Y., Liu, Y., Shen, H., Jiang, L., McLamore, E.S., Shen, Y., 2024. The WRKY46–MYC2 module plays a critical role in E-2-hexenal-induced anti-herbivore responses by promoting flavonoid accumulation. Plant Commun. 5 (2): 100734. https://doi.org/10.1016/j.xplc.2023.100734

Hao, Y., Zeng, Z., Yuan, M., Li, H., Guo, S., Yang, Y., Jiang, S., Hawara, E., Li, J., Zhang, P., Wang, J., Xin, X., Ma, W., Liu, H., 2025. The blue-light receptor CRY1 serves as a switch to balance photosynthesis and plant defense. Cell Host Microbe 33 (1): 137-150. https://doi.org/10.1016/j.chom.2024.12.003

Harper, A.L., Trick, M., Higgins, J., Fraser, F., Clissold, L., Wells, R., Hattori, C., Werner, P., Bancroft, I., 2012. Associative transcriptomics of traits in the polyploid crop species Brassica napus. Nat. Biotechnol. 30 (8): 798–802. https://doi.org/10.1038/nbt.2302

Hartman, K., Tringe, S.G., 2019. Interactions between plants and soil shaping the root microbiome under abiotic stress. Biochemical Journal 476 (19): 2705–2724. https://doi.org/10.1042/BCJ20180615

Hartman, S., Liu, Z., van Veen, H., Vicente, J., Reinen, E., Martopawiro, S., Zhang, H., van Dongen, N., Bosman, F., Bassel, G.W., Visser, E.J.W., Bailey-Serres, J., Theodoulou, F.L., Hebelstrup, K.H., Gibbs, D.J., Holdsworth, M.J., Sasidharan, R., Voesenek, L.A.C.J., 2019. Ethylene-mediated nitric oxide depletion pre-adapts plants to hypoxia stress. Nat. Commun. 10 (1): 4020. https://doi.org/10.1038/s41467-019-12045-4

Hartman, S., Sasidharan, R., Voesenek, L.A.C.J., 2021. The role of ethylene in metabolic acclimations to low oxygen. New Phytologist. 229 (1): 64-70. https://doi.org/10.1111/nph.16378

Hashimoto, K., Kudla, J., 2011. Calcium decoding mechanisms in plants. Biochimie. 93 (12): 2054-2059. https://doi.org/10.1016/j.biochi.2011.05.019

Hass, C., Lohrmann, J., Albrecht, V., Sweere, U., Hummel, F., Yoo, S.D., Hwang, I., Zhu, T., Schäfer, E., Kudla, J., Harter, K., 2004. The response regulator 2 mediates ethylene signalling and hormone signal integration in Arabidopsis. EMBO Journal 23 (16): 3290–3302. https://doi.org/10.1038/sj.emboj.7600337

Havlickova, L., He, Z., Wang, L., Langer, S., Harper, A.L., Kaur, H., Broadley, M.R., Gegas, V., Bancroft, I., 2018. Validation of an updated Associative Transcriptomics platform for the polyploid crop species Brassica napus by dissection of the genetic architecture of erucic acid and tocopherol isoform variation in seeds. Plant Journal 93 (1): 181–192. https://doi.org/10.1111/tpj.13767

He, C., Liew, L.C., Yin, L., Lewsey, M.G., Whelan, J., Berkowitz, O., 2022. The retrograde signaling regulator ANAC017 recruits the MKK9–MPK3/6, ethylene, and auxin signaling pathways to balance mitochondrial dysfunction with growth. Plant Cell 34 (9): 3460–3481. https://doi.org/10.1093/plcell/koac177

He, X., Jiang, J., Wang, C.Q., Dehesh, K., 2017. ORA59 and EIN3 interaction couples jasmonate-ethylene synergistic action to antagonistic salicylic acid regulation of PDF expression. J. Integr. Plant Biol. 59 (4): 275–287. https://doi.org/10.1111/jipb.12524

Hebelstrup, K.H., Østergaard-Jensen, E., Hill, R.D., 2008. Bioimaging Techniques for Subcellular Localization of Plant Hemoglobins and Measurement of Hemoglobin-Dependent Nitric Oxide Scavenging In Planta, in: Methods in Enzymology. Academic Press Inc. 437, 595–604. https://doi.org/10.1016/S0076-6879(07)37030-4

Hedges, L. V, 1981. Distribution Theory for Glass's Estimator of Effect Size and Related Estimators. Journal of Educational Statistics. 6 (2): 107-128. https://doi.org/10.2307/1164588

Hee Nam, K., Li, J., 2002. BRI1/BAK1, a Receptor Kinase Pair Mediating Brassinosteroid Signaling, Cell. 110 (2): 203-212. https://doi.org/10.1016/S0092-8674(02)00814-0

Henry, E., Fung, N., Liu, J., Drakakaki, G., Coaker, G., 2015. Beyond Glycolysis: GAPDHs Are Multi-functional Enzymes Involved in Regulation of ROS, Autophagy, and Plant Immune Responses. PLoS Genet. 11 (4): e1005199. https://doi.org/10.1371/journal.pgen.1005199

Hess, D.T., Matsumoto, A., Kim, S.O., Marshall, H.E., Stamler, J.S., 2005. Protein S-nitrosylation: Purview and parameters. Nat. Rev. Mol. Cell Biol. 6 (2): 150–166. https://doi.org/10.1038/nrm1569

Hess, N., Klode, M., Anders, M., Sauter, M., 2011. The hypoxia responsive transcription factor genes ERF71/HRE2 and ERF73/HRE1 of Arabidopsis are differentially regulated by ethylene. Physiol. Plant. 143 (1): 41–49. https://doi.org/10.1111/j.1399-3054.2011.01486.x

Hilker, M., Schwachtje, J., Baier, M., Balazadeh, S., Bäurle, I., Geiselhardt, S., Hincha, D.K., Kunze, R., Mueller-Roeber, B., Rillig, M.C., Rolff, J., Romeis, T., Schmülling, T., Steppuhn, A.,

van Dongen, J., Whitcomb, S.J., Wurst, S., Zuther, E., Kopka, J., 2016. Priming and memory of stress responses in organisms lacking a nervous system. Biological Reviews 91 (4): 1118–1133. https://doi.org/10.1111/brv.12215

Hilleary, R., Paez-Valencia, J., Vens, C.S., Toyota, M., Palmgren, M., Gilroy, S., 2020. Tonoplast-localized Ca2+ pumps regulate Ca2+ signals during pattern-triggered immunity in Arabidopsis thaliana. Proceedings of the National Academy of Sciences of the United States of America 117 (31): 18849–18857. https://doi.org/10.1073/pnas.2004183117

Hirabayashi, Y., Mahendran, R., Koirala, S., Konoshima, L., Yamazaki, D., Watanabe, S., Kim, H., Kanae, S., 2013. Global flood risk under climate change. Nat. Clim. Chang. 3 (9): 816–821. https://doi.org/10.1038/nclimate1911

Hofmann, A., Wienkoop, S., Harder, S., Bartlog, F., Lüthje, S., 2020. Hypoxia-responsive class iii peroxidases in maize roots: Soluble and membrane-bound isoenzymes. Int. J. Mol. Sci. 21 (22): 1–23. https://doi.org/10.3390/ijms21228872

Holdsworth, M.J., Vicente, J., Sharma, G., Abbas, M., Zubrycka, A., 2020. The plant N-degron pathways of ubiquitin-mediated proteolysis. J. Integr. Plant Biol. 62 (1): 70-89. https://doi.org/10.1111/jipb.12882

Hong, B., Zhou, B., Peng, Z., Yao, M., Wu, J., Wu, X., Guan, C., Guan, M., 2023. Tissue-Specific Transcriptome and Metabolome Analysis Reveals the Response Mechanism of Brassica napus to Waterlogging Stress. Int. J. Mol. Sci. 24 (7): 6015. https://doi.org/10.3390/ijms24076015

Hong, B., Zhou, B., Zhao, D., Liao, L., Chang, T., Wu, X., Wu, J., Yao, M., Chen, H., Mao, J., Guan, C., Guan, M., 2024. Yield, cell structure and physiological and biochemical characteristics of rapeseed under waterlogging stress. BMC Plant Biol. 24 (1): 941. https://doi.org/10.1186/s12870-024-05599-z

Hong, X., Qi, F., Wang, R., Jia, Z., Lin, F., Yuan, M., Xin, X.F., Liang, Y., 2023. Ascorbate peroxidase 1 allows monitoring of cytosolic accumulation of effector-triggered reactive oxygen species using a luminol-based assay. Plant Physiol. 191 (2): 1416–1434. https://doi.org/10.1093/plphys/kiac551

Hrubá, P., Honys, D., Twell, D., Čapková, V., Tupý, J., 2005. Expression of β-galactosidase and β-xylosidase genes during microspore and pollen development. Planta 220 (6): 931–940. https://doi.org/10.1007/s00425-004-1409-0

Hsu, F.C., Chou, M.Y., Chou, S.J., Li, Y.R., Peng, H.P., Shih, M.C., 2013. Submergence confers immunity mediated by the WRKY22 transcription factor in Arabidopsis. Plant Cell 25 (7): 2699–2713. https://doi.org/10.1105/tpc.113.114447

Hsu, F.C., Chou, M.Y., Peng, H.P., Chou, S.J., Shih, M.C., 2011. Insights into hypoxic systemic responses based on analyses of transcriptional regulation in arabidopsis. PLoS One 6 (12): e28888. https://doi.org/10.1371/journal.pone.0028888

Hu, H., Tang, Y., Wu, J., Chen, F., Yang, Y., Pan, X., Dong, X., Jin, X., Liu, S., Du, X., 2021. Brassica napus Mediator Subunit16 Induces BnMED25- and BnWRKY33-Activated Defense Signaling to Confer Sclerotinia sclerotiorum Resistance. Front. Plant Sci. 12. https://doi.org/10.3389/fpls.2021.663536

Hu, L., Yang, L., 2019. Time to fight: Molecular mechanisms of age-related resistance. Phytopathology. 109 (9): 1500–1508. https://doi.org/10.1094/PHYTO-11-18-0443-RVW

Hu, Y., Dong, Q., Yu, D., 2012. Arabidopsis WRKY46 coordinates with WRKY70 and WRKY53 in basal resistance against pathogen Pseudomonas syringae. Plant Science 185–186, 288–297. https://doi.org/10.1016/j.plantsci.2011.12.003

Hua, J., Chang, C., Sun, Q., Meyerowizt, E.M., 1995. Ethylene Insensitivity Conferred by Arabidopsis ERS Gene. Science 269 (5231): 1712–1714. https://doi.org/10.1126/science.7569898

Hua, J., Sakai, H., Nourizadeh, S., Chen, Q.G., Bleecker, A.B., Ecker, J.R., Meyerowitz, E.M., 1998. EIN4 and ERS2 Are Members of the Putative Ethylene Receptor Gene Family in Arabidopsis. Plant Cell 10 (8): 1321–1332. https://doi.org/10.1105/tpc.10.8.1321

Huang, C., David, M.P., Cao, Z.L., Xiao, L.T., 2020. Mutation of chloroplast CHLM contributes to down-regulation of multiple stress response genes in Arabidopsis. Plant Growth Regul. 91 (2): 209–219. https://doi.org/10.1007/s10725-020-00600-9

Ialongo, C., 2016. Understanding the effect size and its measures. Biochem. Med. (Zagreb). 26 (2): 150–163. https://doi.org/10.11613/BM.2016.015

Ichimura, K., Casais, C., Peck, S.C., Shinozaki, K., Shirasu, K., 2006. MEKK1 is required for MPK4 activation and regulates tissue-specific and temperature-dependent cell death in Arabidopsis. Journal of Biological Chemistry 281 (48): 36969–36976. https://doi.org/10.1074/jbc.M605319200

Igarashi, D., Miwa, T., Seki, M., Kobayashi, M., Kato, T., Tabata, S., Shinozaki, K., Ohsumi, C., 2003. Identification of photorespiratory glutamate:glyoxylate aminotransferase (GGAT) gene in Arabidopsis. Plant Journal 33 (6): 975–987. https://doi.org/10.1046/j.1365-313X.2003.01688.x

Igarashi, D., Tsuchida, H., Miyao, M., Ohsumi, C., 2006. Glutamate:Glyoxylate aminotransferase modulates amino acid content during photorespiration. Plant Physiol. 142 (3): 901–910. https://doi.org/10.1104/pp.106.085514

Imkampe, J., Halter, T., Huang, S., Schulze, S., Mazzotta, S., Schmidt, N., Manstretta, R., Postel, S., Wierzba, M., Yang, Y., van Dongen, W.M.A.M., Stahl, M., Zipfel, C., Goshe, M.B., Clouse, S., de Vries, S.C., Tax, F., Wang, X., Kemmerling, B., 2017. The arabidopsis leucine-rich repeat receptor kinase BIR3 negatively regulates BAK1 receptor complex formation and stabilizes BAK1. Plant Cell 29 (9): 2285–2303. https://doi.org/10.1105/tpc.17.00376

Ishikawa, A., 2009. The arabidopsis G-protein β-subunit is required for defense response against Agrobacterium tumefaciens. Biosci. Biotechnol. Biochem. 73 (1): 47–52. https://doi.org/10.1271/bbb.80449

Jahnová, J., Luhová, L., Petřivalský, M., 2019. S-nitrosoglutathione reductase-the master regulator of protein S-nitrosation in plant NO signaling. Plants. 8 (2): 48. https://doi.org/10.3390/plants8020048

Jeong, R.D., Chandra-Shekara, A.C., Barman, S.R., Navarre, D., Klessig, D.F., Kachroo, A., Kachroo, P., 2010. Cryptochrome 2 and phototropin 2 regulate resistance protein-

mediated viral defense by negatively regulating an E3 ubiquitin ligase. Proc. Natl. Acad. Sci. U.S.A. 107 (30): 13538–13543. https://doi.org/10.1073/pnas.1004529107

Jethva, J., Lichtenauer, S., Schmidt-Schippers, R., Steffen-Heins, A., Poschet, G., Wirtz, M., van Dongen, J.T., Eirich, J., Finkemeier, I., Bilger, W., Schwarzländer, M., Sauter, M., 2023. Mitochondrial alternative NADH dehydrogenases NDA1 and NDA2 promote survival of reoxygenation stress in Arabidopsis by safeguarding photosynthesis and limiting ROS generation. New Phytologist 238 (1): 96–112. https://doi.org/10.1111/nph.18657

Jia, W., Ma, M., Chen, J., Wu, S., 2021. Plant morphological, physiological and anatomical adaption to flooding stress and the underlying molecular mechanisms. Int. J. Mol. Sci. 22 (3): 1088. https://doi.org/10.3390/ijms22031088

Jiang, X., Hoehenwarter, W., Scheel, D., Lee, J., 2020. Phosphorylation of the CAMTA3 transcription factor triggers its destabilization and nuclear export. Plant Physiol. 184 (2): 1056–1071. https://doi.org/10.1104/pp.20.00795

Jiang, Y., Yue, Y., Lu, C., Latif, M.Z., Liu, H., Wang, Z., Yin, Z., Li, Y., Ding, X., 2024. AtSNU13 modulates pre-mRNA splicing of RBOHD and ALD1 to regulate plant immunity. BMC Biol. 22 (1): 153. https://doi.org/10.1186/s12915-024-01951-9

John Markwell, John C. Osterman, Jennifer L. Mitchell, 1995. Calibration of the Minolta SPAD-502 leaf chlorophyll meter. Photosynth. Res. 46 (3): 467–472. https://doi.org/10.1007/BF00032301

Joo, S., Liu, Y., Lueth, A., Zhang, S., 2008. MAPK phosphorylation-induced stabilization of ACS6 protein is mediated by the non-catalytic C-terminal domain, which also contains the cis-determinant for rapid degradation by the 26S proteasome pathway. Plant Journal 54 (1): 129–140. https://doi.org/10.1111/j.1365-313X.2008.03404.x

Juntawong, P., Girke, T., Bazin, J., Bailey-Serres, J., 2014. Translational dynamics revealed by genome-wide profiling of ribosome footprints in Arabidopsis. Proc. Natl. Acad. Sci. U.S.A. 111 (1): E203-E212. https://doi.org/10.1073/pnas.1317811111

Kabbage, M., Yarden, O., Dickman, M.B., 2015. Pathogenic attributes of Sclerotinia sclerotiorum: Switching from a biotrophic to necrotrophic lifestyle. Plant Science. 233, 53-60. https://doi.org/10.1016/j.plantsci.2014.12.018

Kadota, Y., Shirasu, K., Zipfel, C., 2015. Regulation of the NADPH Oxidase RBOHD during Plant Immunity. Plant Cell Physiol. 56 (8): 1472–1480. https://doi.org/10.1093/pcp/pcv063

Kadota, Y., Sklenar, J., Derbyshire, P., Stransfeld, L., Asai, S., Ntoukakis, V., Jones, J.D., Shirasu, K., Menke, F., Jones, A., Zipfel, C., 2014. Direct Regulation of the NADPH Oxidase RBOHD by the PRR-Associated Kinase BIK1 during Plant Immunity. Mol. Cell 54 (1): 43–55. https://doi.org/10.1016/j.molcel.2014.02.021

Kalachova, T., Skrabálková, E., Pateyron, S., Soubigou-Taconnat, L., Djafi, N., Collin, S., Sekereš, J., Burketová, L., Potocký, M., Pejchar, P., Ruelland, E., 2022. DIACYLGLYCEROL KINASE 5 participates in flagellin-induced signaling in Arabidopsis. Plant Physiol. 190 (3): 1978–1996. https://doi.org/10.1093/plphys/kiac354

Kanno, T., Lin, W.-D., Fu, J.L., Matzke, A.J.M., Matzke, M., 2017. A genetic screen implicates a CWC16/Yju2/CCDC130 protein and SMU1 in alternative splicing in Arabidopsis thaliana. RNA. 23, 1068–1079. https://doi.org/10.1261/rna.060517.116

Kdidi, S., Vaca-Medina, G., Peydecastaing, J., Oukarroum, A., Fayoud, N., Barakat, A., 2019a. Electrostatic separation for sustainable production of rapeseed oil cake protein concentrate: Effect of mechanical disruption on protein and lignocellulosic fiber separation. Powder Technol. 344, 10–16. https://doi.org/10.1016/j.powtec.2018.11.107

Kdidi, S., Vaca-Medina, G., Peydecastaing, J., Oukarroum, A., Fayoud, N., Barakat, A., 2019b. Electrostatic separation for sustainable production of rapeseed oil cake protein concentrate: Effect of mechanical disruption on protein and lignocellulosic fiber separation. Powder Technol. 344, 10–16. https://doi.org/10.1016/j.powtec.2018.11.107

Keinath, N.F., Waadt, R., Brugman, R., Schroeder, J.I., Grossmann, G., Schumacher, K., Krebs, M., 2015. Live Cell Imaging with R-GECO1 Sheds Light on flg22- and Chitin-Induced Transient [Ca2+]cyt Patterns in Arabidopsis. Mol. Plant 8 (8): 1188–1200. https://doi.org/10.1016/j.molp.2015.05.006

Keller, T., Damude, H.G., Werner, D., Doerner, P., Dixon, R.A., Lamb, C., 1998. A Plant Homolog of the Neutrophil NADPH Oxidase gp91 phox Subunit Gene Encodes a Plasma Membrane Protein with Ca2+ Binding Motifs, The Plant Cell. 10 (2): 255–266. https://doi.org/10.1105/tpc.10.2.255

Kerpen, L., Niccolini, L., Licausi, F., van Dongen, J.T., Weits, D.A., 2019. Hypoxic conditions in crown galls induce plant anaerobic responses that support tumor proliferation. Front. Plant Sci. 10. https://doi.org/10.3389/fpls.2019.00056

Keswani, C., Raghuwanshi, R., Mukherjee, A., Gawande, S., 2022. Concurrent waterlogging and anthracnose-twister disease in rainy-season onions (Allium cepa): Impact and management. Front. Microbiol. 13. https://doi.org/10.3389/fmicb.2022.1063472

Khan, M.A., Cowling, W.A., Banga, S.S., Barbetti, M.J., Cantila, A.Y., Amas, J.C., Thomas, W.J.W., You, M.P., Tyagi, V., Bharti, B., Edwards, D., Batley, J., 2023. Genetic and molecular analysis of stem rot (Sclerotinia sclerotiorum) resistance in Brassica napus (canola type). Heliyon 9 (9): e19237. https://doi.org/10.1016/j.heliyon.2023.e19237

Kiep, V., Vadassery, J., Lattke, J., Maaß, J.P., Boland, W., Peiter, E., Mithöfer, A., 2015. Systemic cytosolic Ca2+ elevation is activated upon wounding and herbivory in Arabidopsis. New Phytologist 207 (4): 996–1004. https://doi.org/10.1111/nph.13493

Kim, N.Y., Jang, Y.J., Park, O.K., 2018. AP2/ERF family transcription factors ORA59 and RAP2.3 interact in the nucleus and function together in ethylene responses. Front. Plant Sci. 871, 1–12. https://doi.org/10.3389/fpls.2018.01675

Kim, W., Iizumi, T., Hosokawa, N., Tanoue, M., Hirabayashi, Y., 2023. Flood impacts on global crop production: advances and limitations. Environmental Research Letters 18 (5): 054007. https://doi.org/10.1088/1748-9326/accd85

Kimura, S., Hunter, K., Vaahtera, L., Tran, H.C., Citterico, M., Vaattovaara, A., Rokka, A., Stolze, S.C., Harzen, A., Meißner, L., Wilkens, M.M.T., Hamann, T., Toyota, M., Nakagami, H., Wrzaczek, M., 2020. CRK2 and C-terminal phosphorylation of NADPH oxidase RBOHD

regulate reactive oxygen species production in arabidopsis. Plant Cell 32 (4): 1063–1080. https://doi.org/10.1105/tpc.19.00525

Kimura, S., Kaya, H., Kawarazaki, T., Hiraoka, G., Senzaki, E., Michikawa, M., Kuchitsu, K., 2012. Protein phosphorylation is a prerequisite for the Ca 2+-dependent activation of Arabidopsis NADPH oxidases and may function as a trigger for the positive feedback regulation of Ca 2+ and reactive oxygen species. Biochim. Biophys. Acta Mol. Cell Res. 1823 (2): 398–405. https://doi.org/10.1016/j.bbamcr.2011.09.011

Kissoudis, C., van de Wiel, C., Visser, R.G.F., van der Linden, G., 2014. Enhancing crop resilience to combined abiotic and biotic stress through the dissection of physiological and molecular crosstalk. Front. Plant Sci. 5 :207. https://doi.org/10.3389/fpls.2014.00207

Kong, L., Ma, X., Zhang, C., Kim, S. Il, Li, B., Xie, Y., Yeo, I.C., Thapa, H., Chen, S., Devarenne, T.P., Munnik, T., He, P., Shan, L., 2024. Dual phosphorylation of DGK5-mediated PA burst regulates ROS in plant immunity. Cell 187 (3): 609-623.e21. https://doi.org/10.1016/j.cell.2023.12.030

Koo, D., Lee, H.G., Bae, S.H., Lee, K., Seo, P.J., 2024. Callus proliferation-induced hypoxic microenvironment decreases shoot regeneration competence in Arabidopsis. Mol. Plant 17 (3): 395–408. https://doi.org/10.1016/j.molp.2024.01.009

Korneli, C., Danisman, S., Staiger, D., 2014. Differential control of pre-invasive and post-invasive antibacterial defense by the Arabidopsis circadian clock. Plant Cell Physiol. 55 (9): 1613–1622. https://doi.org/10.1093/pcp/pcu092

Kosmacz, M., Parlanti, S., Schwarzländer, M., Kragler, F., Licausi, F., Van Dongen, J.T., 2015. The stability and nuclear localization of the transcription factor RAP2.12 are dynamically regulated by oxygen concentration. Plant Cell Environ. 38 (6): 1094–1103. https://doi.org/10.1111/pce.12493

Koussevitzky, S., Suzuki, N., Huntington, S., Armijo, L., Sha, W., Cortes, D., Shulaev, V., Mittler, R., 2008. Ascorbate peroxidase 1 plays a key role in the response of Arabidopsis thaliana to stress combination. Journal of Biological Chemistry 283 (49): 34197–34203. https://doi.org/10.1074/jbc.M806337200

Köster, P., He, G., Liu, C., Dong, Q., Hake, K., Schmitz-Thom, I., Heinkow, P., Eirich, J., Wallrad, L., Hashimoto, K., Schültke, S., Finkemeier, I., Romeis, T., Kudla, J., 2025. A bi-kinase module sensitizes and potentiates plant immune signaling. Science Advances 11 (4): eadt9804. https://doi.org/10.1126/sciadv.adt9804

Kuai, J., Li, X., Xie, Y., Li, Z., Wang, B., Zhou, G., 2020. Leaf characteristics at recovery stage affect seed oil and protein content under the interactive effects of nitrogen and waterlogging in rapeseed. Agriculture (Switzerland) 10 (6): 1–16. https://doi.org/10.3390/agriculture10060207

Kubo, A., Saji, H., Tanaka, Kiyoshi, Tanaka, Kunisuke, Kondo, N., 1992. Cloning and sequencing of a cDNA encoding ascorbate peroxidase from Arabidopsis thaliana, Plant Molecular Biology. 18 (4): 691–701. https://doi.org/10.1007/BF00020011

Kuhlgert, S., Austic, G., Zegarac, R., Osei-Bonsu, I., Hoh, D., Chilvers, M.I., Roth, M.G., Bi, K., TerAvest, D., Weebadde, P., Kramer, D.M., 2016. MultispeQ Beta: A tool for large-scale

plant phenotyping connected to the open photosynQ network. R. Soc. Open Sci. 3 (10): 160592. https://doi.org/10.1098/rsos.160592

Kumar, K., Raina, S.K., Sultan, S.M., 2020. Arabidopsis MAPK signaling pathways and their cross talks in abiotic stress response. J. Plant Biochem. Biotechnol. 29 (4): 700–714. https://doi.org/10.1007/s13562-020-00596-3

Kunkowska, A.B., Fontana, F., Betti, F., Soeur, R., Beckers, G.J.M., Meyer, C., De Jaeger, G., Weits, D.A., Loreti, E., Perata, P., 2023. Target of rapamycin signaling couples energy to oxygen sensing to modulate hypoxic gene expression in Arabidopsis. Proc. Natl. Acad. Sci. U.S.A. 120 (3): e2212474120. https://doi.org/10.1073/pnas.2212474120

Kuzmin, E. V., Karpova, O. V., Elthon, T.E., Newton, K.J., 2004. Mitochondrial respiratory deficiencies signal up-regulation of genes for heat shock proteins. Journal of Biological Chemistry 279 (20): 20672–20677. https://doi.org/10.1074/jbc.M400640200

Kwak, J.M., Mori, I.C., Pei, Z.-M., Leonhardt, N., Torres, M.A., Dangl, J.L., Bloom, R.E., Bodde, S., Jones, J.D.G., Schroeder, J.I., 2003. NADPH oxidase AtrbohD and AtrbohF genes function in ROS-dependent ABA signaling in *Arabidopsis*. EMBO Journal 22 (11): 2623–2633. https://doi.org/10.1093/emboj/cdg277

Lahlali, R., Taoussi, M., Laasli, S.E., Gachara, G., Ezzouggari, R., Belabess, Z., Aberkani, K., Assouguem, A., Meddich, A., El Jarroudi, M., Barka, E.A., 2024. Effects of climate change on plant pathogens and host-pathogen interactions. Crop and Environment. 3 (3): 159-170. https://doi.org/10.1016/j.crope.2024.05.003

Lai, A.G., Doherty, C.J., Mueller-Roeber, B., Kay, S.A., Schippers, J.H.M., Dijkwel, P.P., 2012. Circadian Clock-Associated 1 regulates ROS homeostasis and oxidative stress responses. Proc. Natl. Acad. Sci. U.S.A. 109 (42): 17129–17134. https://doi.org/10.1073/pnas.1209148109

Lamichhane, J.R., Barbetti, M.J., Chilvers, M.I., Pandey, A.K., Steinberg, C., 2024. Exploiting root exudates to manage soil-borne disease complexes in a changing climate. Trends Microbiol. 32 (1): 27-37. https://doi.org/10.1016/j.tim.2023.07.011

Lecourieux, D., Mazars, C., Pauly, N., Ranjeva, R., Pugin, A., 2002. Analysis and effects of cytosolic free calcium increases in response to elicitors in Nicotiana plumbaginifolia cells. Plant Cell 14 (10): 2627–2641. https://doi.org/10.1105/tpc.005579

Lee, D.H., Lal, N.K., Lin, Z.J.D., Ma, S., Liu, J., Castro, B., Toruño, T., Dinesh-Kumar, S.P., Coaker, G., 2020. Regulation of reactive oxygen species during plant immunity through phosphorylation and ubiquitination of RBOHD. Nat. Commun. 11 (1): 1838. https://doi.org/10.1038/s41467-020-15601-5

Lee, T.A., Bailey-Serres, J., 2019. Integrative Analysis from the Epigenome to Translatome Uncovers Patterns of Dominant Nuclear Regulation during Transient Stress. Plant Cell 31 (11): 2573–2595. https://doi.org/10.1105/tpc.19.00463

Lee, U., Wie, C., Fernandez, B.O., Feelisch, M., Vierling, E., 2008. Modulation of nitrosative stress by S-nitrosoglutathione reductase is critical for thermotolerance and plant growth in Arabidopsis. Plant Cell 20 (3): 786–802. https://doi.org/10.1105/tpc.107.052647

Lee, Y.H., Kim, K.S., Jang, Y.S., Hwang, J.H., Lee, D.H., Choi, I.H., 2014. Global gene expression responses to waterlogging in leaves of rape seedlings. Plant Cell Rep. 33 (2): 289–299. https://doi.org/10.1007/s00299-013-1529-8

Lew, T.T.S., Koman, V.B., Silmore, K.S., Seo, J.S., Gordiichuk, P., Kwak, S.Y., Park, M., Ang, M.C.Y., Khong, D.T., Lee, M.A., Chan-Park, M.B., Chua, N.H., Strano, M.S., 2020. Real-time detection of wound-induced H2O2 signalling waves in plants with optical nanosensors. Nat. Plants 6 (4): 404–415. https://doi.org/10.1038/s41477-020-0632-4

Li, G., Meng, X., Wang, R., Mao, G., Han, L., Liu, Y., Zhang, S., 2012. Dual-level regulation of ACC synthase activity by MPK3/MPK6 cascade and its downstream WRKY transcription factor during ethylene induction in arabidopsis. PLoS Genet. 8 (6): e1002767. https://doi.org/10.1371/journal.pgen.1002767

Li, J., Brader, G., Kariola, T., Tapio Palva, E., 2006. WRKY70 modulates the selection of signaling pathways in plant defense. Plant Journal 46 (3): 477–491. https://doi.org/10.1111/j.1365-313X.2006.02712.x

Li, J., Iqbal, S., Zhang, Y., Chen, Y., Tan, Z., Ali, U., Guo, L., 2021. Transcriptome analysis reveals genes of flooding-tolerant and flooding-sensitive rapeseeds differentially respond to flooding at the germination stage. Plants 10 (4): 693. https://doi.org/10.3390/plants10040693

Li, J., Wen, J., Lease, K.A., Doke, J.T., Tax, F.E., Walker, J.C., 2002. BAK1, an Arabidopsis LRR Receptor-like Protein Kinase, Interacts with BRI1 and Modulates Brassinosteroid Signaling, Cell. 110 (2): 213-222. https://doi.org/10.1016/S0092-8674(02)00812-7

Li, J., Xie, T., Chen, Y., Zhang, Y., Wang, C., Jiang, Z., Yang, W., Zhou, G., Guo, L., Zhang, J., 2022. High-throughput unmanned aerial vehicle-based phenotyping provides insights into the dynamic process and genetic basis of rapeseed waterlogging response in the field. J. Exp. Bot. 73 (15): 5264–5278. https://doi.org/10.1093/jxb/erac242

Li, J., Zhang, Y., Chen, Y., Wang, Y., Zhou, Z., Tu, J., Guo, L., Yao, X., 2024. The roles of cell wall polysaccharides in response to waterlogging stress in Brassica napus L. root. BMC Biol. 22 (1): 191. https://doi.org/10.1186/s12915-024-01972-4

Li, J., Zhong, R., Palva, E.T., 2017. WRKY70 and its homolog WRKY54 negatively modulate the cell wall-associated defenses to necrotrophic pathogens in Arabidopsis. PLoS One 12 (8): e0183731. https://doi.org/10.1371/journal.pone.0183731

Li, L., Li, M., Yu, L., Zhou, Z., Liang, X., Liu, Z., Cai, G., Gao, L., Zhang, X., Wang, Y., Chen, S., Zhou, J.M., 2014. The FLS2-associated kinase BIK1 directly phosphorylates the NADPH oxidase RbohD to control plant immunity. Cell Host Microbe 15 (3): 329–338. https://doi.org/10.1016/j.chom.2014.02.009

Li, L., Zhang, L., Tang, J., Xing, H., Zhao, L., Jie, H., Jie, Y., 2023. Waterlogging increases greenhouse gas release and decreases yield in winter rapeseed (Brassica napus L.) seedlings. Sci. Rep. 13 (1): 18673. https://doi.org/10.1038/s41598-023-46156-2

Li, N., Han, X., Feng, D., Yuan, D., Huang, L.J., 2019. Signaling crosstalk between salicylic acid and ethylene/Jasmonate in plant defense: Do we understand what they are whispering? Int. J. Mol. Sci. 20 (3): 671. https://doi.org/10.3390/ijms20030671

Li, Y., Liu, K., Tong, G., Xi, C., Liu, J., Zhao, H., Wang, Y., Ren, D., Han, S., 2022. MPK3/MPK6-mediated phosphorylation of ERF72 positively regulates resistance to Botrytis cinerea through directly and indirectly activating the transcription of camalexin biosynthesis enzymes. J. Exp. Bot. 73 (1): 413–428. https://doi.org/10.1093/jxb/erab415

Liang, X., Ding, P., Lian, K., Wang, J., Ma, M., Li, L., Li, L., Zhang, X., Chen, S., Zhang, Y., Zhou, J.-M., 2016. Arabidopsis heterotrimeric G proteins regulate immunity by directly coupling to the FLS2 receptor. eLife 5: e13568. https://doi.org/10.7554/eLife.13568.001

Liang, X., Ma, M., Zhou, Z., Wang, J., Yang, X., Rao, S., Bi, G., Li, L., Zhang, X., Chai, J., Chen, S., Zhou, J.M., 2018. Ligand-triggered de-repression of Arabidopsis heterotrimeric G proteins coupled to immune receptor kinases. Cell Res. 28 (5): 529–543. https://doi.org/10.1038/s41422-018-0027-5

Liang, Y., Strelkov, S.E., Kav, N.N.V., 2009. Oxalic acid-mediated stress responses in Brassica napus L. Proteomics 9 (11): 3156–3173. https://doi.org/10.1002/pmic.200800966

Licausi, F., Kosmacz, M., Weits, D.A., Giuntoli, B., Giorgi, F.M., Voesenek, L.A.C.J., Perata, P., Van Dongen, J.T., 2011. Oxygen sensing in plants is mediated by an N-end rule pathway for protein destabilization. Nature 479 (7373): 419–422. https://doi.org/10.1038/nature10536

Licausi, F., Van Dongen, J.T., Giuntoli, B., Novi, G., Santaniello, A., Geigenberger, P., Perata, P., 2010a. HRE1 and HRE2, two hypoxia-inducible ethylene response factors, affect anaerobic responses in Arabidopsis thaliana. Plant Journal 62 (2): 302–315. https://doi.org/10.1111/j.1365-313X.2010.04149.x

Licausi, F., Weits, D.A., Pant, B.D., Scheible, W.R., Geigenberger, P., van Dongen, J.T., 2011c. Hypoxia responsive gene expression is mediated by various subsets of transcription factors and miRNAs that are determined by the actual oxygen availability. New Phytologist 190 (2): 442–456. https://doi.org/10.1111/j.1469-8137.2010.03451.x

Liepman, A.H., Olsen, L.J., 2003. Alanine aminotransferase homologs catalyze the glutamate:Glyoxylate aminotransferase reaction in peroxisomes of Arabidopsis. Plant Physiol. 131 (1): 215–227. https://doi.org/10.1104/pp.011460

Lin, H., Wang, M., Chen, Y., Nomura, K., Hui, S., Gui, J., Zhang, X., Wu, Y., Liu, J., Li, Q., Deng, Y., Li, L., Yuan, M., Wang, S., Yang He, S., He, Z., 2022. An MKP-MAPK protein phosphorylation cascade controls vascular immunity in plants, Sci. Adv. 8 (10): eabg8723. https://doi.org/10.1126/sciadv.abg8723

Lin, H. ying, Liu, Q., Li, X., Yang, J., Liu, S., Huang, Y., Scanlon, M.J., Nettleton, D., Schnable, P.S., 2017. Substantial contribution of genetic variation in the expression of transcription factors to phenotypic variation revealed by eRD-GWAS. Genome Biol. 18 (1): 192. https://doi.org/10.1186/s13059-017-1328-6

Lin, W., Li, B., Lu, D., Chen, S., Zhu, N., He, P., Shan, L., 2014. Tyrosine phosphorylation of protein kinase complex BAK1/BIK1 mediates Arabidopsis innate immunity. Proc. Natl. Acad. Sci. U.S.A. 111 (9): 3632–3637. https://doi.org/10.1073/pnas.1318817111

Lindsey, B.E., Rivero, L., Calhoun, C.S., Grotewold, E., Brkljacic, J., 2017. Standardized method for high-throughput sterilization of Arabidopsis seeds. Journal of Visualized Experiments. 128: e56587. https://doi.org/10.3791/56587

Lipka, A.E., Tian, F., Wang, Q., Peiffer, J., Li, M., Bradbury, P.J., Gore, M.A., Buckler, E.S., Zhang, Z., 2012. GAPIT: Genome association and prediction integrated tool. Bioinformatics 28 (18): 2397–2399. https://doi.org/10.1093/bioinformatics/bts444

Liu, B., Sun, L., Ma, L., Hao, F.S., 2017. Both AtrbohD and AtrbohF are essential for mediating responses to oxygen deficiency in Arabidopsis. Plant Cell Rep. 36 (6): 947–957. https://doi.org/10.1007/s00299-017-2128-x

Liu, F., VanToai, T., Moy, L.P., Bock, G., Linford, L.D., Quackenbush, J., 2005. Global transcription profiling reveals comprehensive insights into hypoxic response in Arabidopsis. Plant Physiol. 137 (3): 1115–1129. https://doi.org/10.1104/pp.104.055475

Liu, K., Harrison, M.T., Yan, H., Liu, D.L., Meinke, H., Hoogenboom, G., Wang, B., Peng, B., Guan, K., Jaegermeyr, J., Wang, E., Zhang, F., Yin, X., Archontoulis, S., Nie, L., Badea, A., Man, J., Wallach, D., Zhao, J., Benjumea, A.B., Fahad, S., Tian, X., Wang, W., Tao, F., Zhang, Z., Rötter, R., Yuan, Y., Zhu, M., Dai, P., Nie, J., Yang, Y., Zhang, Y., Zhou, M., 2023. Silver lining to a climate crisis in multiple prospects for alleviating crop waterlogging under future climates. Nat. Commun. 14 (1): 765. https://doi.org/10.1038/s41467-023-36129-4

Liu, M., Tan, X., Sun, X., Zwiazek, J.J., 2020. Properties of root water transport in canola (Brassica napus) subjected to waterlogging at the seedling, flowering and podding growth stages. Plant Soil 454 (1): 431–445. https://doi.org/10.1007/s11104-020-04669-z

Liu, M., Zwiazek, J.J., 2022. Transcriptomic Analysis of Distal Parts of Roots Reveals Potentially Important Mechanisms Contributing to Limited Flooding Tolerance of Canola (Brassica napus) Plants. Int. J. Mol. Sci. 23 (24): 15469. https://doi.org/10.3390/ijms232415469

Liu, P., Zhao, Z., Tang, Yaqi, Zhou, Y., Liu, J., Xu, K., Chen, Y., Li, X., Tang, Yaru, Yang, L., 2025. The HY5-NPR1 module governs light-dependent virulence of a plant bacterial pathogen. Cell Host Microbe. 33 (9): 1606-1622.e10. https://doi.org/10.1016/j.chom.2025.08.007

Liu, X., Zhou, Y., Chen, K., Xiao, Z., Liang, X., Lu, D., 2023. Phosphorylation status of CPK28 affects its ubiquitination and protein stability. New Phytologist 237 (4): 1270–1284. https://doi.org/10.1111/nph.18596

Liu, X., Zhou, Y., Du, M., Liang, X., Fan, F., Huang, G., Zou, Y., Bai, J., Lu, D., 2022. The calcium-dependent protein kinase CPK28 is targeted by the ubiquitin ligases ATL31 and ATL6 for proteasome-mediated degradation to fine-tune immune signaling in Arabidopsis. Plant Cell 34 (1): 679–697. https://doi.org/10.1093/plcell/koab242

Liu, Y., Gong, T., Kong, X., Sun, J., Liu, L., 2024. XYLEM CYSTEINE PEPTIDASE 1 and its inhibitor CYSTATIN 6 regulate pattern-triggered immunity by modulating the stability of the NADPH oxidase RESPIRATORY BURST OXIDASE HOMOLOG D. Plant Cell 36 (2): 471–488. https://doi.org/10.1093/plcell/koad262

Liu, Y., Zhang, S., 2004. Phosphorylation of 1-aminocyclopropane-1-carboxylic acid synthase by MPK6, a stress-responsive mitogen-activated protein kinase, induces ethylene biosynthesis in arabidopsis. Plant Cell 16 (12): 3386–3399. https://doi.org/10.1105/tpc.104.026609

Liu, Z., Guo, C., Wu, R., Hu, Y., Zhou, Y., Wang, J., Yu, X., Zhang, Y., Bawa, G., Sun, X., 2022. FLS2–RBOHD–PIF4 Module Regulates Plant Response to Drought and Salt Stress. Int. J. Mol. Sci. 23 (3): 1080. https://doi.org/10.3390/ijms23031080

Liu, Z., Zhou, Y., Liu, Y., Qin, A., Sun, S., Liu, H., Yang, J., Hu, M., Xie, Y., Song, X., Gao, P., Guo, E., Wang, S., Herrera-Estrella, L., Tran, L.-S.P., Sun, X., 2023. Single-cell RNA-sequencing reveals the generation of new immune response-induced cells with novel role in *Arabidopsis thaliana* response to the bacterial flagellin epitope flg22. Cell Press Sneak Peek. http://dx.doi.org/10.2139/ssrn.4548674

Long, X., Cai, Y., Wang, H., Liu, Y., Huang, X., Xuan, H., Li, W., Zhang, X., Zhang, H., Fang, X., He, H., Xu, G., Dean, C., Yang, H., 2024. Cotranscriptional splicing is required in the cold to produce COOLAIR isoforms that repress Arabidopsis FLC. Proc. Natl. Acad. Sci. U.S.A. 121 (47): e2407628121. https://doi.org/10.1073/pnas.2407628121

Lorenzo, O., Piqueras, R., Sánchez-Serrano, J.J., Solano, R., 2003. ETHYLENE RESPONSE FACTOR1 integrates signals from ethylene and jasmonate pathways in plant defense. Plant Cell 15 (1): 165–178. https://doi.org/10.1105/tpc.007468

Loreti, E., Perata, P., 2023. ERFVII transcription factors and their role in the adaptation to hypoxia in Arabidopsis and crops. Front. Genet. 14 :1213839. https://doi.org/10.3389/fgene.2023.1213839

Loreti, E., Poggi, A., Novi, G., Alpi, A., Perata, P., 2005. A genome-wide analysis of the effects of sucrose on gene expression in arabidopsis seedlings under anoxia. Plant Physiol. 137 (3): 1130–1138. https://doi.org/10.1104/pp.104.057299

Lou, S., Guo, X., Liu, L., Song, Y., Zhang, Lei, Jiang, Y., Zhang, Lushui, Sun, P., Liu, B., Tong, S., Chen, N., Liu, M., Zhang, H., Liang, R., Feng, X., Zheng, Y., Liu, H., Holdsworth, M.J., Liu, J., 2022. Allelic shift in cis-elements of the transcription factor RAP2.12 underlies adaptation associated with humidity in Arabidopsis thaliana, Sci. Adv. 8 (18): eabn8281. https://doi.org/10.1126/sciadv.abn8281

Lu, D., Lin, W., Gao, X., Wu, S., Cheng, C., Avila, J., Heese, A., Devarenne, T.P., He, P., Shan, L., 2011. Direct ubiquitination of pattern recognition receptor FLS2 attenuates plant innate immunity. Science (1979). 332 (6036): 1439–1442. https://doi.org/10.1126/science.1204903

Lu, D., Wu, S., Gao, X., Zhang, Y., Shan, L., He, P., 2010. A receptor-like cytoplasmic kinase, BIK1, associates with a flagellin receptor complex to initiate plant innate immunity. Proc. Natl. Acad. Sci. U.S.A. 107 (1): 496–501. https://doi.org/10.1073/pnas.0909705107

Luis A. J. Mur, Anushen Sivakumaran, Julien Mandon, Simona M. Cristescu, Frans J. M. Harren, Kim H. Hebelstrup, 2012. Haemoglobin modulates salicylate and jasmonate/ethylene-mediated resistance mechanisms against pathogens. J. Exp. Bot. 63 (2): 695–709. https://doi.org/10.1093/jxb/err313

Luo, X., Dai, Y., Zheng, C., Yang, Y., Chen, W., Wang, Q., Chandrasekaran, U., Du, J., Liu, W., Shu, K., 2021. The ABI4-RbohD/VTC2 regulatory module promotes reactive oxygen species (ROS) accumulation to decrease seed germination under salinity stress. New Phytologist 229 (2): 950–962. https://doi.org/10.1111/nph.16921

Ma, C., Liu, Y., Bai, B., Han, Z., Tang, J., Zhang, H., Yaghmaiean, H., Zhang, Y., Chai, J., 2017. Structural basis for BIR1-mediated negative regulation of plant immunity. Cell Res. 27 (12): 1521–1524. https://doi.org/10.1038/cr.2017.123

Ma, Haigang, Gao, Y., Wang, Y., Dai, Y., Ma, Hongxiang, 2022. Regulatory Mechanisms of Mitogen-Activated Protein Kinase Cascades in Plants: More than Sequential Phosphorylation. Int. J. Mol. Sci. 23 (7): 3572. https://doi.org/10.3390/ijms23073572

Ma, M., Wang, P., Chen, R., Bai, M., He, Z., Xiao, D., Xu, G., Wu, H., Zhou, J.M., Dou, D., Bi, G., Liang, X., 2024. The OXIDATIVE SIGNAL-INDUCIBLE1 kinase regulates plant immunity by linking microbial pattern-induced reactive oxygen species burst to MAP kinase activation. Plant Cell 37 (1): koae311. https://doi.org/10.1093/plcell/koae311

Ma, Y., Flückiger, I., Nicolet, J., Pang, J., Dickinson, J.B., De Bellis, D., Emonet, A., Fujita, S., Geldner, N., 2024. Comparisons of two receptor-MAPK pathways in a single cell-type reveal mechanisms of signalling specificity. Nat. Plants. 10 (9): 1343–1362. https://doi.org/10.1038/s41477-024-01768-y

Ma, Y., Zhao, Y., Walker, R.K., Berkowitz, G.A., 2013. Molecular steps in the immune signaling pathway evoked by plant elicitor peptides: Ca2+-dependent protein kinases, nitric oxide, and reactive oxygen species are downstream from the early Ca2+ signal. Plant Physiol. 163 (3): 1459–1471. https://doi.org/10.1104/pp.113.226068

Macho, A.P., Boutrot, F., Rathjen, J.P., Zipfel, C., 2012. ASPARTATE OXIDASE plays an important role in Arabidopsis stomatal immunity. Plant Physiol. 159 (4): 1845–1856. https://doi.org/10.1104/pp.112.199810

Madsen, H., Lawrence, D., Lang, M., Martinkova, M., Kjeldsen, T.R., 2014. Review of trend analysis and climate change projections of extreme precipitation and floods in Europe. J. Hydrol. (Amst). 519, 3634–3650. https://doi.org/10.1016/j.jhydrol.2014.11.003

Manish Kumar Maurya, Vikash Kumar Yadav, Sumant Pratap Singh, Rajender Jatoth, Hemant Kumar Singh, Dinesh Singh, 2022. Impact of Climate Change on Diseases of Crops and Their Management—A Review. J. Agric. Sci. Technol. B 12, 1-15. https://doi.org/10.17265/2161-6264/2022.01.001

Mao, G., Meng, X., Liu, Y., Zheng, Z., Chen, Z., Zhang, S., 2011. Phosphorylation of a WRKY transcription factor by two pathogen-responsive MAPKs drives phytoalexin biosynthesis in Arabidopsis. Plant Cell 23 (4): 1639–1653. https://doi.org/10.1105/tpc.111.084996

Martínez, M., Arata, A.F., Lázaro, L., Stenglein, S.A., Dinolfo, M.I., 2019. Effects of waterlogging stress on plant-pathogen interaction between Fusarium poae and wheat/ barley. Acta Sci. Agron. 41 (1): e42629. https://doi.org/10.4025/actasciagron.v41i1.42629

Martínez-Arias, C., Witzell, J., Solla, A., Martin, J.A., Rodríguez-Calcerrada, J., 2022. Beneficial and pathogenic plant-microbe interactions during flooding stress. Plant Cell Environ. 45 (10): 2875–2897. https://doi.org/10.1111/pce.14403

Mbengue, M., Bourdais, G., Gervasi, F., Beck, M., Zhou, J., Spallek, T., Bartels, S., Boller, T., Ueda, T., Kuhn, H., Robatzek, S., 2016. Clathrin-dependent endocytosis is required for immunity mediated by pattern recognition receptor kinases. Proc. Natl. Acad. Sci. U.S.A. 113 (39): 11034–11039. https://doi.org/10.1073/pnas.1606004113

McAinsh, M.R., Pittman, J.K., 2009. Shaping the calcium signature. New Phytologist. 181 (2): 275-294. https://doi.org/10.1111/j.1469-8137.2008.02682.x

Mei, J., Qian, L., Disi, J.O., Yang, X., Li, Q., Li, J., Frauen, M., Cai, D., Qian, W., 2011. Identification of resistant sources against Sclerotinia sclerotiorum in Brassica species with emphasis on B. oleracea. Euphytica 177 (3): 393–399. https://doi.org/10.1007/s10681-010-0274-0

Men, S., Chen, H., Chen, S., Zheng, S., Shen, X., Wang, C., Yang, Z., Liu, D., 2020. Effects of supplemental nitrogen application on physiological characteristics, dry matter and nitrogen accumulation of winter rapeseed (Brassica napus L.) under waterlogging stress. Sci. Rep. 10 (1): 10201. https://doi.org/10.1038/s41598-020-67260-7

Meng, X., Xu, J., He, Y., Yang, K.Y., Mordorski, B., Liu, Y., Zhang, S., 2013. Phosphorylation of an ERF transcription factor by Arabidopsis MPK3/MPK6 regulates plant defense gene induction and fungal resistance. Plant Cell 25 (3): 1126–1142. https://doi.org/10.1105/tpc.112.109074

Merkouropoulos, G., Andreasson, E., Hess, D., Boller, T., Peck, S.C., 2008. An Arabidopsis protein phosphorylated in response to microbial elicitation, AtPHOS32, is a substrate of MAP kinases 3 and 6. Journal of Biological Chemistry 283 (16): 10493–10499. https://doi.org/10.1074/jbc.M800735200

Mersmann, S., Bourdais, G., Rietz, S., Robatzek, S., 2010. Ethylene signaling regulates accumulation of the FLS2 receptor and is required for the oxidative burst contributing to plant immunity. Plant Physiol. 154 (1): 391–400. https://doi.org/10.1104/pp.110.154567

Metge, B.J., Kammerud, S.C., Pruitt, H.C., Shevde, L.A., Samant, R.S., 2021. Hypoxia re-programs 2'-O-Me modifications on ribosomal RNA. iScience 24 (1): 102010. https://doi.org/10.1016/j.isci.2020.102010

Miller, G., Mittler, R., 2006. Could heat shock transcription factors function as hydrogen peroxide sensors in plants? Ann. Bot. 98 (2): 279-288. https://doi.org/10.1093/aob/mcl107

Miller, G., Schlauch, K., Tam, R., Cortes, D., Torres, M.A., Shulaev, V., Dangl, J.L., Mittler, R., 2009. The plant NADPH oxidase RBOHD mediates rapid systemic signaling in response to diverse stimuli. Sci. Signal. 2 (84): ra45-ra45. https://doi.org/10.1126/scisignal.2000448

Miricescu, A., Byrne, T., Doorly, C.M., Ng, C.K.Y., Barth, S., Graciet, E., 2021. Experimental comparison of two methods to study barley responses to partial submergence. Plant Methods 17 (1): 40. https://doi.org/10.1186/s13007-021-00742-5

Miricescu, A., Goslin, K., Graciet, E., 2018. Ubiquitylation in plants: Signaling hub for the integration of environmental signals. J. Exp. Bot. 69 (19): 4511–4527. https://doi.org/10.1093/jxb/ery165

Mittler, R., 2017. ROS Are Good. Trends Plant Sci. 22 (1): 11-19. https://doi.org/10.1016/j.tplants.2016.08.002

Mittler, R., 2006. Abiotic stress, the field environment and stress combination. Trends Plant Sci. 11 (1): 15–19. https://doi.org/10.1016/j.tplants.2005.11.002

Mittler, R., Zandalinas, S.I., Fichman, Y., Van Breusegem, F., 2022. Reactive oxygen species signalling in plant stress responses. Nat. Rev. Mol. Cell Biol. 23 (10): 663–679. https://doi.org/10.1038/s41580-022-00499-2

Miyashita, Y., Dolferus, R., Ismond, K.P., Good, A.G., 2007. Alanine aminotransferase catalyses the breakdown of alanine after hypoxia in Arabidopsis thaliana. Plant Journal 49 (6): 1108–1121. https://doi.org/10.1111/j.1365-313X.2006.03023.x

Mølhøj, M., Verma, R., Reiter, W.D., 2003. The biosynthesis of the branched-chain sugar d-apiose in plants: Functional cloning and characterization of a UDP-D-apiose/UDP-D-xylose synthase from Arabidopsis. Plant Journal 35 (6): 693–703. https://doi.org/10.1046/j.1365-313X.2003.01841.x

Møller, I.M., 2001. PLANT MITOCHONDRIA AND OXIDATIVE STRESS: Electron Transport, NADPH Turnover, and Metabolism of Reactive Oxygen Species, Annu. Rev. Plant Physiol. Plant Mol. Biol. 52, 561-591. https://doi.org/10.1146/annurev.arplant.52.1.561

Monaghan, J., Matschi, S., Shorinola, O., Rovenich, H., Matei, A., Segonzac, C., Malinovsky, F.G., Rathjen, J.P., Maclean, D., Romeis, T., Zipfel, C., 2014. The calcium-dependent protein kinase CPK28 buffers plant immunity and regulates BIK1 turnover. Cell Host Microbe 16 (5): 605–615. https://doi.org/10.1016/j.chom.2014.10.007

Mooney, B.C., Doorly, C.M., Mantz, M., García, P., Huesgen, P.F., Graciet, E., 2024. Hypoxia represses pattern-triggered immune responses in Arabidopsis. Plant Physiol. 196 (3): 2064–2077. https://doi.org/10.1093/plphys/kiae432

Mooney, B.C., Graciet, E., 2020. A simple and efficient *Agrobacterium*-mediated transient expression system to dissect molecular processes in *Brassica rapa* and *Brassica napus*. Plant Direct. 4 (7): 1–12. https://doi.org/10.1002/pld3.237

Morales, J., Kadota, Y., Zipfel, C., Molina, A., Torres, M.A., 2016. The Arabidopsis NADPH oxidases RbohD and RbohF display differential expression patterns and contributions during plant immunity. J. Exp. Bot. 67 (6): 1663–1676. https://doi.org/10.1093/jxb/erv558

Moreau, M., Gyu, I.L., Wang, Y., Crane, B.R., Klessig, D.F., 2008. AtNOS/AtNOA1 is a functional Arabidopsis thaliana cGTPase and not a nitric-oxide synthase. Journal of Biological Chemistry 283 (47): 32957–32967. https://doi.org/10.1074/jbc.M804838200

Morten Petersen, Peter Brodersen, Henrik Naested, Erik Andreasson, Ursula Lindhart, Bo Johansen, Henrik B. Nielsen, Michelle Lacy, Mark J. Austin, Jane E. Parker, Sashi B. Sharma, Daniel F. Klessig, Rob Martienssen, Ole Mattsson, Anders B. Jensen, John Mundy, 2000. Arabidopsis MAP Kinase 4 Negatively Regulates Systemic Acquired Resistance. Cell 103 (7): 1111–1120. https://doi.org/10.1016/S0092-8674(00)00213-0

Mousavi, S.A.R., Chauvin, A., Pascaud, F., Kellenberger, S., Farmer, E.E., 2013. GLUTAMATE RECEPTOR-LIKE genes mediate leaf-to-leaf wound signalling. Nature 500 (7463): 422–426. https://doi.org/10.1038/nature12478

Mullins, E., Quinlan, C., Jones, P., 1999. Isolation of mutants exhibiting altered resistance to Sclerotinia sclerotiorum from small M 2 populations of an oilseed rape (Brassica napus) variety, European Journal of Plant Pathology. 105 (5): 465–475. https://doi.org/10.1023/A:1008729316161

Mur, L.A.J., Prats, E., Pierre, S., Hall, M.A., Hebelstrup, K.H., 2013. Integrating nitric oxide into salicylic acid and jasmonic acid/ethylene plant defense pathways. Front. Plant Sci. 4: 215. https://doi.org/10.3389/fpls.2013.00215

Murchie, E.H., Lawson, T., 2013. Chlorophyll fluorescence analysis: A guide to good practice and understanding some new applications. J. Exp. Bot. 64 (13): 3983–3998. https://doi.org/10.1093/jxb/ert208

Mustroph, A., 2018. Improving flooding tolerance of crop plants. Agronomy. 8 (9): 160. https://doi.org/10.3390/agronomy8090160

Mustroph, A., Zanetti, M.E., Jang, C.J.H., Holtan, H.E., Repetti, P.P., Galbraith, D.W., Girke, T., Bailey-Serres, J., 2009. Profiling translatomes of discrete cell populations resolves altered cellular priorities during hypoxia in Arabidopsis. PNAS 106 (44): 18843–18848. https://doi.org/10.1073/pnas.0906131106

Nabloussi, A., Bahri, H., Lakbir, M., Moukane, H., Kajji, A., El Fechtali, M., 2019. Assessment of a set of rapeseed (Brassica napus L.) varieties under waterlogging stress at different plant growth stages . OCL 26. https://doi.org/10.1051/ocl/2019033

Nakagami, H., Soukupová, H., Schikora, A., Žárský, V., Hirt, H., 2006. A mitogen-activated protein kinase kinase kinase mediates reactive oxygen species homeostasis in Arabidopsis. Journal of Biological Chemistry 281 (50): 38697–38704. https://doi.org/10.1074/jbc.M605293200

Neik, T.X., Barbetti, M.J., Batley, J., 2017. Current status and challenges in identifying disease resistance genes in brassica napus. Front. Plant Sci. 8: 1788. https://doi.org/10.3389/fpls.2017.01788

Newman, T.E., Khentry, Y., Leo, A., Lindbeck, K.D., Kamphuis, L.G., Derbyshire, M.C., 2023. Association Mapping Combined with Whole Genome Sequencing Data Reveals Candidate Causal Variants for Sclerotinia Stem Rot Resistance in Brassica napus. Phytopathology 113 (5): 800–811. https://doi.org/10.1094/PHYTO-06-22-0217-FI

Ng, S., Ivanova, A., Duncan, O., Law, S.R., Van Aken, O., De Clercq, I., Wang, Y., Carrie, C., Xu, L., Kmiec, B., Walker, H., Van Breusegem, F., Whelan, J., Giraud, E., 2013. A membrane-bound NAC transcription factor, ANAC017, mediates mitochondrial retrograde signaling in Arabidopsis. Plant Cell 25 (9): 3450–3471. https://doi.org/10.1105/tpc.113.113985

Nguyen, C.T., Kurenda, A., Stolz, S., Chételat, A., Farmer, E.E., 2018. Identification of cell populations necessary for leaf-toleaf electrical signaling in a wounded plant. Proc. Natl. Acad. Sci. U.S.A. 115 (40): 10178–10183. https://doi.org/10.1073/pnas.1807049115

Nguyen, X.C., Kim, S.H., Lee, K., Kim, K.E., Liu, X.M., Han, H.J., Hoang, M.H.T., Lee, S.W., Hong, J.C., Moon, Y.H., Chung, W.S., 2012. Identification of a C2H2-type zinc finger transcription factor (ZAT10) from Arabidopsis as a substrate of MAP kinase. Plant Cell Rep. 31 (4): 737–745. https://doi.org/10.1007/s00299-011-1192-x

Nobori, T., Monell, A., Lee, T.A., Sakata, Y., Shirahama, S., Zhou, J., Nery, J.R., Mine, A., Ecker, J.R., 2025. A rare PRIMER cell state in plant immunity. Nature. 638 (8049): 197–205. https://doi.org/10.1038/s41586-024-08383-z

Nolan, P., O'Sullivan, J., McGrath, R., 2017. Impacts of climate change on mid-twenty-first-century rainfall in Ireland: a high-resolution regional climate model ensemble approach. International Journal of Climatology 37 (12): 4347–4363. https://doi.org/10.1002/joc.5091

Nomura, H., Komori, T., Uemura, S., Kanda, Y., Shimotani, K., Nakai, K., Furuichi, T., Takebayashi, K., Sugimoto, T., Sano, S., Suwastika, I.N., Fukusaki, E., Yoshioka, H., Nakahira, Y., Shiina, T., 2012. Chloroplast-mediated activation of plant immune signalling in Arabidopsis. Nat. Commun. 3 (1): 926. https://doi.org/10.1038/ncomms1926

Ogasawara, Y., Kaya, H., Hiraoka, G., Yumoto, F., Kimura, S., Kadota, Y., Hishinuma, H., Senzaki, E., Yamagoe, S., Nagata, K., Nara, M., Suzuki, K., Tanokura, M., Kuchitsu, K., 2008. Synergistic activation of the arabidopsis NADPH oxidase AtrbohD by Ca 2+ and phosphorylation. Journal of Biological Chemistry 283 (14): 8885–8892. https://doi.org/10.1074/jbc.M708106200

Oldham, K.E.A., Mabbitt, P.D., 2024. Ubiquitin E3 ligases in the plant Arg/N-degron pathway. Biochemical Journal. 481 (24): 1949–1965. https://doi.org/10.1042/BCJ20240132

Palm, D., Streit, D., Shanmugam, T., Weis, B.L., Ruprecht, M., Simm, S., Schleiff, E., 2019. Plant-specific ribosome biogenesis factors in Arabidopsis thaliana with essential function in rRNA processing. Nucleic Acids Res. 47 (4): 1880–1895. https://doi.org/10.1093/nar/gky1261

Palma, F.R., Gantner, B.N., Sakiyama, M.J., Kayzuka, C., Shukla, S., Lacchini, R., Cunniff, B., Bonini, M.G., 2024. ROS production by mitochondria: function or dysfunction? Oncogene 43 (5): 295–303. https://doi.org/10.1038/s41388-023-02907-z

Pandey, P., Ramegowda, V., Senthil-Kumar, M., 2015. Shared and unique responses of plants to multiple individual stresses and stress combinations: Physiological and molecular mechanisms. Front. Plant Sci. 6: 723. https://doi.org/10.3389/fpls.2015.00723

Papalexiou, S.M., Montanari, A., 2019. Global and Regional Increase of Precipitation Extremes Under Global Warming. Water Resour. Res. 55 (6): 4901–4914. https://doi.org/10.1029/2018WR024067

Papdi, C., Pérez-Salamõ, I., Joseph, M.P., Giuntoli, B., Bögre, L., Koncz, C., Szabados, L., 2015. The low oxygen, oxidative and osmotic stress responses synergistically act through the ethylene response factor VII genes RAP2.12, RAP2.2 and RAP2.3. Plant Journal 82 (5): 772–784. https://doi.org/10.1111/tpj.12848

Park, H.Y., Seok, H.Y., Woo, D.H., Lee, S.Y., Tarte, V.N., Lee, E.H., Lee, C.H., Moon, Y.H., 2011. AtERF71/HRE2 transcription factor mediates osmotic stress response as well as hypoxia response in Arabidopsis. Biochem. Biophys. Res. Commun. 414 (1): 135–141. https://doi.org/10.1016/j.bbrc.2011.09.039

Pattyn, J., Vaughan-Hirsch, J., Van de Poel, B., 2021. The regulation of ethylene biosynthesis: a complex multilevel control circuitry. New Phytologist. 229 (2): 770-782. https://doi.org/10.1111/nph.16873

Pecher, P., Eschen-Lippold, L., Herklotz, S., Kuhle, K., Naumann, K., Bethke, G., Uhrig, J., Weyhe, M., Scheel, D., Lee, J., 2014. The Arabidopsis thaliana mitogen-activated protein kinases MPK3 and MPK6 target a subclass of 'VQ-motif'-containing proteins to regulate immune responses. New Phytologist 203 (2): 592–606. https://doi.org/10.1111/nph.12817

Pedersen, O., Colmer, T.D., Garcia-Robledo, E., Revsbech, N.P., 2018. CO2 and O2 dynamics in leaves of aquatic plants with C3 or CAM photosynthesis-application of a novel CO2 microsensor. Ann. Bot. 122 (4): 605–615. https://doi.org/10.1093/aob/mcy095

Pedroza-Garcia, J.A., Domenichini, S., Mazubert, C., Bourge, M., White, C., Hudik, E., Bounon, R., Tariq, Z., Delannoy, E., Del Olmo, I., Piñeiro, M., Jarillo, J.A., Bergounioux, C., Benhamed, M., Raynaud, C., 2016. Role of the Polymerase ϵ sub-unit DPB2 in DNA replication, cell cycle regulation and DNA damage response in Arabidopsis. Nucleic Acids Res. 44 (15): 7251–7266. https://doi.org/10.1093/nar/gkw449

Peláez-Vico, M.Á., Tukuli, A., Singh, P., Mendoza-Cózatl, D.G., Joshi, T., Mittler, R., 2023. Rapid systemic responses of Arabidopsis to waterlogging stress. Plant Physiol. 193 (3): 2215–2231. https://doi.org/10.1093/PLPHYS/KIAD433

Peláez-Vico, M.Á., Zandalinas, S.I., Devireddy, A.R., Sinha, R., Mittler, R., 2024. Systemic stomatal responses in plants: Coordinating development, stress, and pathogen defense under a changing climate. Plant Cell Environ. 47 (4): 1171–1184. https://doi.org/10.1111/pce.14797

Peng, H.P., Lin, T.Y., Wang, N.N., Shih, M.C., 2005. Differential expression of genes encoding 1-aminocyclopropane-1-carboxylate synthase in Arabidopsis during hypoxia. Plant Mol. Biol. 58 (1): 15–25. https://doi.org/10.1007/s11103-005-3573-4

Penninckx, I.A.M.A., Thomma, B.P.H.J., Buchala, A., Métraux, J.-P., Broekaert, W.F., 1998. Concomitant Activation of Jasmonate and Ethylene Response Pathways Is Required for Induction of a Plant Defensin Gene in Arabidopsis, The Plant Cell. 10 (12): 2103–2113. https://doi.org/10.1105/tpc.10.12.2103

Pittman, J.K., Shigaki, T., Marshall, J.L., Morris, J.L., Cheng, N.-H., Hirschi, K.D., 2004. Functional and regulatory analysis of the Arabidopsis thaliana CAX2 cation transporter. Plant Mol Biol. 56 (6): 959–971. https://doi.org/10.1007/s11103-004-6446-3

Ploschuk, R.A., Miralles, D.J., Colmer, T.D., Ploschuk, E.L., Striker, G.G., 2018. Waterlogging of winter crops at early and late stages: Impacts on leaf physiology, growth and yield. Front. Plant Sci. 9: 1863. https://doi.org/10.3389/fpls.2018.01863

Pokhrel, B., 2021. Plant Pathology & Microbiology Effects of Environmental Factors on Crop Diseases Development. J Plant Pathol Microbiol 12 (5): 553. https://doi.org/10.35248/2157-7471.21.12.553

Pontier, D., Albrieux, C., Joyard, J., Lagrange, T., Block, M.A., 2007. Knock-out of the magnesium protoporphyrin IX methyltransferase gene in Arabidopsis: Effects on chloroplast development and on chloroplast-to-nucleus signaling. Journal of Biological Chemistry 282 (4): 2297–2304. https://doi.org/10.1074/jbc.M610286200

Popescu, S.C., Popescu, G. V., Bachan, S., Zhang, Z., Gerstein, M., Snyder, M., Dinesh-Kumar, S.P., 2009. MAPK target networks in Arabidopsis thaliana revealed using functional protein microarrays. Genes Dev. 23, 80–92. https://doi.org/10.1101/gad.1740009

Prasch, C.M., Sonnewald, U., 2013. Simultaneous application of heat, drought, and virus to Arabidopsis plants reveals significant shifts in signaling networks. Plant Physiol. 162 (4): 1849–1866. https://doi.org/10.1104/pp.113.221044

Pré, M., Atallah, M., Champion, A., De Vos, M., Pieterse, C.M.J., Memelink, J., 2008. The AP2/ERF domain transcription factor ORA59 integrates jasmonic acid and ethylene signals in plant defense. Plant Physiol. 147 (3): 1347–1357. https://doi.org/10.1104/pp.108.117523

Premkumar, A., Lindberg, S., Lager, I., Rasmussen, U., Schulz, A., 2019. Arabidopsis PLDs with C2-domain function distinctively in hypoxia. Physiol. Plant. 167 (1): 90–110. https://doi.org/10.1111/ppl.12874

Provart, N.J., Alonso, J., Assmann, S.M., Bergmann, D., Brady, S.M., Brkljacic, J., Browse, J., Chapple, C., Colot, V., Cutler, S., Dangl, J., Ehrhardt, D., Friesner, J.D., Frommer, W.B., Grotewold, E., Meyerowitz, E., Nemhauser, J., Nordborg, M., Pikaard, C., Shanklin, J., Somerville, C., Stitt, M., Torii, K.U., Waese, J., Wagner, D., Mccourt, P., 2016. 50 years of Arabidopsis research: Highlights and future directions. New Phytologist 209 (3): 921–944. https://doi.org/10.1111/nph.13687

Pucciariello, C., Parlanti, S., Banti, V., Novi, G., Perata, P., 2012. Reactive oxygen species-driven transcription in Arabidopsis under oxygen deprivation. Plant Physiol. 159 (1): 184–196. https://doi.org/10.1104/pp.111.191122

Qi, F., Li, J., Ai, Y., Shangguan, K., Li, P., Lin, F., Liang, Y., 2024. DGK5β-derived phosphatidic acid regulates ROS production in plant immunity by stabilizing NADPH oxidase. Cell Host Microbe 32 (3): 425-440.e7. https://doi.org/10.1016/j.chom.2024.01.011

Qi, F., Li, J., Hong, X., Jia, Z., Wu, B., Lin, F., Liang, Y., 2023. Overexpression of an Antioxidant Enzyme APX1 in cpr5 Mutant Restores its Pleiotropic Growth Phenotype. Antioxidants 12 (2): 301. https://doi.org/10.3390/antiox12020301

Qiao, H., Chang, K.N., Yazaki, J., Ecker, J.R., 2009. Interplay between ethylene, ETP1/ETP2 F-box proteins, and degradation of EIN2 triggers ethylene responses in Arabidopsis. Genes Dev. 23, 512–521. https://doi.org/10.1101/gad.1765709

Qin, D. Bin, Liu, M.Y., Yuan, L., Zhu, Y., Li, X.D., Chen, L.M., Wang, Yi, Chen, Y.F., Wu, W.H., Wang, Yang, 2020. Calcium-dependent protein kinase 32-mediated phosphorylation is essential for the ammonium transport activity of AMT1;1 in Arabidopsis roots. J. Exp. Bot. 71 (16): 5087–5097. https://doi.org/10.1093/jxb/eraa249

Qiu, J.L., Fiil, B.K., Petersen, K., Nielsen, H.B., Botanga, C.J., Thorgrimsen, S., Palma, K., Suarez-Rodriguez, M.C., Sandbech-Clausen, S., Lichota, J., Brodersen, P., Grasser, K.D., Mattsson, O., Glazebrook, J., Mundy, J., Petersen, M., 2008. Arabidopsis MAP kinase 4 regulates gene expression through transcription factor release in the nucleus. EMBO Journal 27 (16): 2214–2221. https://doi.org/10.1038/emboj.2008.147

Qiu, J.L., Zhou, L., Yun, B.W., Nielsen, H.B., Fiil, B.K., Petersen, K., MacKinlay, J., Loake, G.J., Mundy, J., Morris, P.C., 2008c. Arabidopsis mitogen-activated protein kinase kinases MKK1 and MKK2 have overlapping functions in defense signaling mediated by MEKK1, MPK4, and MKS1. Plant Physiol. 148 (1): 212–222. https://doi.org/10.1104/pp.108.120006

Qu, Z.L., Zhong, N.Q., Wang, H.Y., Chen, A.P., Jian, G.L., Xia, G.X., 2006. Ectopic expression of the cotton non-symbiotic hemoglobin gene GhHbd1 triggers defense responses and increases disease tolerance in Arabidopsis. Plant Cell Physiol. 47 (8): 1058–1068. https://doi.org/10.1093/pcp/pcj076

Rao, S., Zhou, Z., Miao, P., Bi, G., Hu, M., Wu, Y., Feng, F., Zhang, X., Zhou, J.M., 2018. Roles of receptor-like cytoplasmic kinase VII members in pattern-triggered immune signaling. Plant Physiol. 177 (4): 1679–1690. https://doi.org/10.1104/pp.18.00486

Rawat, R., Sandoval, F.J., Wei, Z., Winkler, R., Roje, S., 2011. An FMN hydrolase of the haloacid dehalogenase superfamily is active in plant chloroplasts. Journal of Biological Chemistry 286 (49): 42091–42098. https://doi.org/10.1074/jbc.M111.260885

Ren, D., Liu, Y., Yang, K.-Y., Han, L., Mao, G., Glazebrook, J., Zhang, S., 2008. A fungal-responsive MAPK cascade regulates phytoalexin biosynthesis in Arabidopsis. 105 (14): 5638-5643, https://doi.org/10.1073/pnas.0711301105

Ren, D., Yang, H., Zhang, S., 2002. Cell death mediated by MAPK is associated with hydrogen peroxide production in Arabidopsis. Journal of Biological Chemistry 277 (1): 559–565. https://doi.org/10.1074/jbc.M109495200

Richter, A.S., Wang, P., Grimm, B., 2016. Arabidopsis Mg-protoporphyrin IX methyltransferase activity and redox regulation depend on conserved cysteines. Plant Cell Physiol. 57 (3): 519–527. https://doi.org/10.1093/pcp/pcw007

Robatzek, S., Chinchilla, D., Boller, T., 2006. Ligand-induced endocytosis of the pattern recognition receptor FLS2 in Arabidopsis. Genes Dev. 20, 537–542. https://doi.org/10.1101/gad.366506

Roeder, A.H.K., Argueso, C.T., Williams, M., Auge, G., Li, X., Strader, L., Uauy, C., Wu, S., 2025. Focus on Translational Research from Arabidopsis to Crop Plants and Beyond. Plant Cell. 37 (5): koaf119. https://doi.org/10.1093/plcell/koaf119

Ronceret, A., Guilleminot, J., Lincker, F., Gadea-Vacas, J., Delorme, V., Bechtold, N., Pelletier, G., Delseny, M., Chabouté, M.E., Devic, M., 2005. Genetic analysis of two Arabidopsis DNA polymerase epsilon subunits during early embryogenesis. Plant Journal 44 (2): 223–236. https://doi.org/10.1111/j.1365-313X.2005.02521.x

Rossel, J.B., Wilson, P.B., Hussain, D., Woo, N.S., Gordon, M.J., Mewett, O.P., Howell, K.A., Whelan, J., Kazan, K., Pogsona, B.J., 2007. Systemic and intracellular responses to photooxidative stress in Arabidopsis. Plant Cell 19 (12): 4091–4110. https://doi.org/10.1105/tpc.106.045898

Rousseau-Gueutin, M., Belser, C., Silva, C. Da, Richard, G., Istace, B., Cruaud, C., Falentin, C., Boideau, F., Boutte, J., Delourme, R., Deniot, G., Engelen, S., De Carvalho, J.F., Lemainque, A., Maillet, L., Morice, J., Wincker, P., Denoeud, F., Chèvre, A.M., Aury, J.M., 2021. Long-read assembly of the Brassica napus reference genome Darmor-bzh. Gigascience 9 (12): giaa137. https://doi.org/10.1093/gigascience/giaa137

Roy, J., Shaikh, T.M., del Río Mendoza, L., Hosain, S., Chapara, V., Rahman, M., 2021. Genome-wide association mapping and genomic prediction for adult stage sclerotinia stem rot resistance in Brassica napus (L) under field environments. Sci. Rep. 11 (1): 21773. https://doi.org/10.1038/s41598-021-01272-9

Ruonan Wang, 2018. The Role of Calcium Dependent Protein Kinase in the Triggered Immune Responses of Arabidopsis thaliana. PhD Thesis. UC San Diego.

Rushton, P.J., Somssich, I.E., Ringler, P., Shen, Q.J., 2010. WRKY transcription factors. Trends Plant Sci. 15 (5): 247-258. https://doi.org/10.1016/j.tplants.2010.02.006

Rushton, P.J., Torres, J.T., Parniske, M., Wernert, P., Hahlbrock, K., Somssich, E., 1996. Interaction of elicitor-induced DNA-binding proteins with elicitor response elements in the

promoters of parsley PR1 genes, The EMBO Journal. 15 (20): 5690-5700. https://doi.org/10.1002/j.1460-2075.1996.tb00953.x

Ryan, C., Curley, M., Walsh, S., Murphy, C., 2022. Long-term trends in extreme precipitation indices in Ireland. International Journal of Climatology 42 (7): 4040–4061. https://doi.org/10.1002/joc.7475

Saini, H., Devrani, A., Synrem, G., Priyanka, 2025. Application of CRISPR Technology in Plant Improvement: An Update Review. Advances in Agriculture. 2025 (1): 4578877. https://doi.org/10.1155/aia/4578877

Sakai, H., Hua, J., Chen, Q.G., Chang, C., Medrano, L.J., Bleecker, A.B., Meyerowitz, E.M., 1998. ETR2 is an ETR1-like gene involved in ethylene signaling in Arabidopsis, Plant Biology. Proc. Natl. Acad. Sci. U.S.A. 95 (10): 5812-5817. https://doi.org/10.1073/pnas.95.10.5812

Sakamoto, A., Ueda, M., Morikawa, H., 2002. Arabidopsis glutathione-dependent formaldehyde dehydrogenase is an S-nitrosoglutathione reductase. Elsevier Science. 515 (1-3): 20-24. https://doi.org/10.1016/S0014-5793(02)02414-6

Salvador-Recatalà, V., 2016. New roles for the GLUTAMATE RECEPTOR-LIKE 3.3, 3.5, and 3.6 genes as on/off switches of wound-induced systemic electrical signals. Plant Signal. Behav. 11 (4): e1161879. https://doi.org/10.1080/15592324.2016.1161879

Salvador-Recatalà, V., Tjallingii, W.F., Farmer, E.E., 2014. Real-time, in vivo intracellular recordings of caterpillar-induced depolarization waves in sieve elements using aphid electrodes. New Phytologist 203 (2): 674–684. https://doi.org/10.1111/nph.12807

Sanders, D., Pelloux, J., Brownlee, C., Harper, J.F., 2002. Calcium at the crossroads of signaling. Plant Cell 14 (suppl_1): S401–S417. https://doi.org/10.1105/tpc.002899

Sano, S., Aoyama, M., Nakai, K., Shimotani, K., Yamasaki, K., Sato, M.H., Tojo, D., Suwastika, I.N., Nomura, H., Shiina, T., 2014. Light-dependent expression of flg22-induced defense genes in Arabidopsis. Front. Plant Sci. 5: 531. https://doi.org/10.3389/fpls.2014.00531

Sara I. Zandalinas, Yosef Fichman, Amith R. Devireddy, Soham Sengupta, Rajeev K. Azad, Ron Mittler, 2020. Systemic signaling during abiotic stress combination in plants 117 (24): 13810-13820. https://doi.org/10.1073/pnas.2005077117

Sasidharan, R., Bailey-Serres, J., Ashikari, M., Atwell, B.J., Colmer, T.D., Fagerstedt, K., Fukao, T., Geigenberger, P., Hebelstrup, K.H., Hill, R.D., Holdsworth, M.J., Ismail, A.M., Licausi, F., Mustroph, A., Nakazono, M., Pedersen, O., Perata, P., Sauter, M., Shih, M.C., Sorrell, B.K., Striker, G.G., van Dongen, J.T., Whelan, J., Xiao, S., Visser, E.J.W., Voesenek, L.A.C.J., 2017. Community recommendations on terminology and procedures used in flooding and low oxygen stress research. New Phytologist. 214 (4): 1403-1407. https://doi.org/10.1111/nph.14519

Scharein, B., Voet-van-Vormizeele, J., Harter, K., Groth, G., 2008. Ethylene signaling: Identification of a putative ETR1-AHP1 phosphorelay complex by fluorescence spectroscopy. Anal. Biochem. 377 (1): 72–76. https://doi.org/10.1016/j.ab.2008.03.015

Schippers, J.H.M., von Bongartz, K., Laritzki, L., Frohn, S., Frings, S., Renziehausen, T., Augstein, F., Winkels, K., Sprangers, K., Sasidharan, R., Vertommen, D., Van Breusegem, F., Hartman, S., Beemster, G.T.S., Mhamdi, A., van Dongen, J.T., Schmidt-Schippers, R.R., 2024. ERFVII-

controlled hypoxia responses are in part facilitated by MEDIATOR SUBUNIT 25 in Arabidopsis thaliana. Plant Journal. 120 (2): 748-768. https://doi.org/10.1111/tpj.17018

Schmidt, R.R., Fulda, M., Paul, M. V., Anders, M., Plum, F., Weits, D.A., Kosmacz, M., Larson, T.R., Graham, I.A., Beemster, G.T.S., Licausi, F., Geigenberger, P., Schippers, J.H., van Dongen, J.T., 2018. Low-oxygen response is triggered by an ATP-dependent shift in oleoyl-CoA in Arabidopsis. Proc. Natl. Acad. Sci. U.S.A. 115 (51): E312101–E12110. https://doi.org/10.1073/pnas.1809429115

Schulze, B., Mentzel, T., Jehle, A.K., Mueller, K., Beeler, S., Boller, T., Felix, G., Chinchilla, D., 2010. Rapid heteromerization and phosphorylation of ligand-activated plant transmembrane receptors and their associated kinase BAK1. Journal of Biological Chemistry 285 (13): 9444–9451. https://doi.org/10.1074/jbc.M109.096842

Schwarzländer, M., Fricker, M.D., Sweetlove, L.J., 2009. Monitoring the in vivo redox state of plant mitochondria: Effect of respiratory inhibitors, abiotic stress and assessment of recovery from oxidative challenge. Biochim. Biophys. Acta Bioenerg. 1787 (5): 468–475. https://doi.org/10.1016/j.bbabio.2009.01.020

Schwessinger, B., Roux, M., Kadota, Y., Ntoukakis, V., Sklenar, J., Jones, A., Zipfel, C., 2011. Phosphorylation-dependent differential regulation of plant growth, cell death, and innate immunity by the regulatory receptor-like kinase BAK1. PLoS Genet. 7 (4): e1002046. https://doi.org/10.1371/journal.pgen.1002046

Sew, Y.S., Harvey Millar, A., Stroeher, E., 2015. Micro-respiratory measurements in plants, in: Plant Mitochondria: Methods and Protocols. Methods in Molecular Biology 1305: 187-196. https://doi.org/10.1007/978-1-4939-2639-8_13

Shahoveisi, F., Markell, S., Del, L.E., Mendoza, R., Kandel, H., 2020. Canola Diseases: Sclerotinia Stem Rot (PP1989).

Shapiguzov, A., Vainonen, J.P., Hunter, K., Tossavainen, H., Tiwari, A., Järvi, S., Hellman, M., Aarabi, F., Alseekh, S., Wybouw, B., van der Kelen, K., Nikkanen, L., Krasensky-Wrzaczek, J., Sipari, N., Keinänen, M., Tyystjärvi, E., Rintamäki, E., De Rybel, B., Salojärvi, J., van Breusegem, F., Fernie, A.R., Brosché, M., Permi, P., Aro, E.M., Wrzaczek, M., Kangasjärvi, J., 2019. Arabidopsis RCD1 coordinates chloroplast and mitochondrial functions through interaction with ANAC transcription factors. Elife 8:e43284. https://doi.org/10.7554/eLife.43284

Sheikh, A.H., Eschen-Lippold, L., Pecher, P., Hoehenwarter, W., Sinha, A.K., Scheel, D., Lee, J., 2016. Regulation of WRKY46 transcription factor function by mitogen-activated protein kinases in Arabidopsis thaliana. Front. Plant Sci. 7: 61. https://doi.org/10.3389/fpls.2016.00061

Shekhawat, K., Fröhlich, K., García-Ramírez, G.X., Trapp, M.A., Hirt, H., 2023. Ethylene: A Master Regulator of Plant–Microbe Interactions under Abiotic Stresses. Cells. 12 (1): 31. https://doi.org/10.3390/cells12010031

Shen, J., Zhang, J., Zhou, M., Zhou, H., Cui, B., Gotor, C., Romero, L.C., Fu, L., Yang, J., Foyer, C.H., Pan, Q., Shen, W., Xie, Y., 2020. Persulfidation-based modification of cysteine desulfhydrase and the NADPH oxidase RBOHD controls guard cell abscisic acid signaling. Plant Cell 32 (4): 1000–1017. https://doi.org/10.1105/tpc.19.00826

Shukla, V., Lombardi, L., Pencik, A., Novak, O., Weits, D.A., Loreti, E., Perata, P., Giuntoli, B., Licausi, F., 2020. Jasmonate signalling contributes to primary root inhibition upon oxygen deficiency in arabidopsis thaliana. Plants 9 (8): 1046. https://doi.org/10.3390/plants9081046

Simmons, C.R., Lafitte, H.R., Reimann, K.S., Brugière, N., Roesler, K., Albertsen, M.C., Greene, T.W., Habben, J.E., 2021. Successes and insights of an industry biotech program to enhance maize agronomic traits. Plant Science. 307: 110899. https://doi.org/10.1016/j.plantsci.2021.110899

Smith, J.M., Heese, A., 2014. Rapid bioassay to measure early reactive oxygen species production in Arabidopsis leaf tissue in response to living Pseudomonas syringae. Plant Methods 10 (1): 6. https://doi.org/10.1186/1746-4811-10-6

Smith, J.M., Leslie, M.E., Robinson, S.J., Korasick, D.A., Zhang, T., Backues, S.K., Cornish, P. V., Koo, A.J., Bednarek, S.Y., Heese, A., 2014a. Loss of Arabidopsis thaliana Dynamin-Related Protein 2B Reveals Separation of Innate Immune Signaling Pathways. PLoS Pathog. 10 (12): e1004578. https://doi.org/10.1371/journal.ppat.1004578

Smith, J.M., Salamango, D.J., Leslie, M.E., Collins, C.A., Heese, A., 2014. Sensitivity to Flg22 Is modulated by ligand-induced degradation and de novo synthesis of the endogenous flagellin-receptor FLAGELLIN-SENSING2. Plant Physiol. 164 (1): 440–454. https://doi.org/10.1104/pp.113.229179

Solano, R., Stepanova, A., Chao, Q., Ecker, J.R., 1998. Nuclear events in ethylene signaling: a transcriptional cascade mediated by ETHYLENE-INSENSITIVE3 and ETHYLENE-RESPONSE-FACTOR1. Genes and Development 12, 3703–3714. https://doi.org/10.1101/gad.12.23.3703

Son, G.H., Wan, J., Kim, H.J., Nguyen, X.C., Chung, W.S., Hong, J.C., Stacey, G., 2012. Ethylene-Responsive Element-Binding Factor 5, ERF5, Is Involved in Chitin-Induced Innate Immunity Response. Mol. Plant. Microbe. Interact. 25 (1): 48–60. https://doi.org/10.1094/MPMI -06-11-0165

Song, S., Huang, H., Gao, H., Wang, J., Wu, D., Liu, X., Yang, S., Zhai, Q., Li, C., Qi, T., Xie, D., 2014. Interaction between MYC2 and ETHYLENE INSENSITIVE3 modulates antagonism between jasmonate and ethylene signaling in Arabidopsis. Plant Cell 26 (1): 263–279. https://doi.org/10.1105/tpc.113.120394

Song, X., Ge, L., Wang, K., Wang, N., Wang, X., 2025. Transcriptome and Small-RNA Sequencing Reveals the Response Mechanism of Brassica napus to Waterlogging Stress. Plants 14 (9): 1340. https://doi.org/10.3390/plants14091340

Sorenson, R., Bailey-Serres, J., 2014. Selective mRNA sequestration by OLIGOURIDYLATEBINDING PROTEIN 1 contributes to translational control during hypoxia in Arabidopsis. Proc. Natl. Acad. Sci. U.S.A. 111 (6): 2373–2378. https://doi.org/10.1073/pnas.1314851111

Spallek, T., Beck, M., Ben Khaled, S., Salomon, S., Bourdais, G., Schellmann, S., Robatzek, S., 2013. ESCRT-I Mediates FLS2 Endosomal Sorting and Plant Immunity. PLoS Genet. 9 (12): e1004035. https://doi.org/10.1371/journal.pgen.1004035

Stary, S., Yin, X.J., Potuschak, T., Schlögelhofer, P., Nizhynska, V., Bachmair, A., 2003. PRT1 of Arabidopsis Is a Ubiquitin Protein Ligase of the Plant N-End Rule Pathway with Specificity for Aromatic Amino-Terminal Residues. Plant Physiol. 133 (3): 1360–1366. https://doi.org/10.1104/pp.103.029272

Storey, J.D., Bass, A.J., 2025. Bioconductor's qvalue package Version 2.40.0.

Striker, G.G., 2012. Flooding Stress on Plants: Anatomical, Morphological and Physiological Responses. Botany. IntechOpen, London, chapter 1. https://doi.org/10.5772/32922

Suarez-Rodriguez, M.C., Adams-Phillips, L., Liu, Y., Wang, H., Su, S.H., Jester, P.J., Zhang, S., Bent, A.F., Krysan, P.J., 2007. MEKK1 is required for flg22-induced MPK4 activation in arabidopsis plants. Plant Physiol. 143 (2): 661–669. https://doi.org/10.1104/pp.106.091389

Subbaiah, C.C., Douglas, ', Bush, S., Sachs, M.M., 1994. Elevation of Cytosolic Calcium Precedes Anoxic Gene Expression in Maize Suspension-Cultured Cells, The Plant Cell. 6 (12): 1747–1762. https://doi.org/10.1105/tpc.6.12.1747

Sudhamsu, J., Gyu, I.L., Klessig, D.F., Crane, B.R., 2008. The structure of YqeH: An AtNOS1/AtNOA1 ortholog that couples gtp hydrolysis to molecular recognition. Journal of Biological Chemistry 283 (47): 32968–32976. https://doi.org/10.1074/jbc.M804837200

Sulaiman, Y., Knight, M.R., Kataky, R., 2012. Non-invasive monitoring of temperature stress in Arabidopsis thaliana roots, using ion amperometry. Analytical Methods 4 (6): 1656–1661. https://doi.org/10.1039/c2ay05747f

Sun, L., Qin, J., Wu, X., Zhang, Jinghan, Zhang, Jie, 2022. TOUCH 3 and CALMODULIN 1/4/6 cooperate with calcium-dependent protein kinases to trigger calcium-dependent activation of CAM-BINDING PROTEIN 60-LIKE G and regulate fungal resistance in plants. Plant Cell 34 (10): 4088–4104. https://doi.org/10.1093/plcell/koac209

Sun, T., Nitta, Y., Zhang, Q., Wu, D., Tian, H., Lee, J.S., Zhang, Y., 2018. Antagonistic interactions between two MAP kinase cascades in plant development and immune signaling . EMBO Rep. 19 (7): EMBR201745324. https://doi.org/10.15252/embr.201745324

Sun, Y., Li, L., Macho, A.P., Han, Z., Hu, Z., Zipfel, C., Zhou, J.M., Chai, J., 2013. Structural basis for flg22-induced activation of the Arabidopsis FLS2-BAK1 immune complex. Science. 342 (6158): 624–628. https://doi.org/10.1126/science.1243825

Tada, T., Kato, M., Tanaka, C., Shiraiwa, T., 2021. Effects of Phytophthora sojae inoculation under flooded conditions on growth of soybean seedlings. Plant Prod. Sci. 24 (4): 433–439. https://doi.org/10.1080/1343943X.2021.1881408

Tagliani, A., Tran, A.N., Novi, G., Di Mambro, R., Pesenti, M., Sacchi, G.A., Perata, P., Pucciariello, C., 2020. The calcineurin β-like interacting protein kinase CIPK25 regulates potassium homeostasis under low oxygen in Arabidopsis. J. Exp. Bot. 71 (9): 2678–2689. https://doi.org/10.1093/jxb/eraa004

Tamura, K., Bono, H., 2022. Meta-Analysis of RNA Sequencing Data of Arabidopsis and Rice under Hypoxia. Life 12 (7): 1079. https://doi.org/10.3390/life12071079

Tanaka, R., Kobayashi, K., Masuda, T., 2011. Tetrapyrrole Metabolism in Arabidopsis thaliana . Arabidopsis Book 9, e0145. https://doi.org/10.1199/tab.0145

Tang, H., Bi, H., Liu, B., Lou, S., Song, Y., Tong, S., Chen, N., Jiang, Y., Liu, J., Liu, H., 2021. WRKY33 interacts with WRKY12 protein to up-regulate RAP2.2 during submergence induced hypoxia response in Arabidopsis thaliana. New Phytologist 229 (1): 106–125. https://doi.org/10.1111/nph.17020

Tang, Y., Liu, X., Wang, J., Li, M., Wang, Q., Tian, F., Su, Z., Pan, Y., Liu, D., Lipka, A.E., Buckler, E.S., Zhang, Z., 2016. GAPIT Version 2: An Enhanced Integrated Tool for Genomic Association and Prediction. Plant Genome 9 (2): plantgenome2015.11.0120. https://doi.org/10.3835/plantgenome2015.11.0120

Terrón-Camero, L.C., Molina-Moya, E., Peláez-Vico, M.Á., Sandalio, L.M., Romero-Puertas, M.C., 2023. Nitric Oxide and Globin Glb1 Regulate Fusarium oxysporum Infection of Arabidopsis thaliana. Antioxidants 12 (7): 1321. https://doi.org/10.3390/antiox12071321

Thor, K., Peiter, E., 2014. Cytosolic calcium signals elicited by the pathogen-associated molecular pattern flg22 in stomatal guard cells are of an oscillatory nature. New Phytologist 204 (4): 873–881. https://doi.org/10.1111/nph.13064

Tian, H., Wu, Z., Chen, S., Ao, K., Huang, W., Yaghmaiean, H., Sun, T., Xu, F., Zhang, Yanjun, Wang, S., Li, X., Zhang, Yuelin, 2021. Activation of TIR signalling boosts pattern-triggered immunity. Nature 598 (7881): 500–503. https://doi.org/10.1038/s41586-021-03987-1

Tian, W., Hou, C., Ren, Z., Wang, C., Zhao, F., Dahlbeck, D., Hu, S., Zhang, L., Niu, Q., Li, L., Staskawicz, B.J., Luan, S., 2019. A calmodulin-gated calcium channel links pathogen patterns to plant immunity. Nature 572 (7767): 131–135. https://doi.org/10.1038/s41586-019-1413-y

Tian, Y., Zhao, N., Wang, M., Zhou, W., Guo, J., Han, C., Zhou, C., Wang, W., Wu, S., Tang, W., Fan, M., Bai, M.Y., 2022. Integrated regulation of periclinal cell division by transcriptional module of BZR1-SHR in Arabidopsis roots. New Phytologist 233 (2): 795–808. https://doi.org/10.1111/nph.17824

Tie, R., Zhong, X., Shi, Z., Li, H., Liu, J., Libo, W., 2025. Domain-aligned generative downscaling enhances projections of extreme climate events. https://doi.org/10.48550/arXiv.2508.16396

Tietz, S., Hall, C.C., Cruz, J.A., Kramer, D.M., 2017. NPQ(T): a chlorophyll fluorescence parameter for rapid estimation and imaging of non-photochemical quenching of excitons in photosystem-II-associated antenna complexes. Plant Cell Environ. 40 (8): 1243–1255. https://doi.org/10.1111/pce.12924

Tomiyama, M., Inoue, S. ichiro, Tsuzuki, T., Soda, M., Morimoto, S., Okigaki, Y., Ohishi, T., Mochizuki, N., Takahashi, K., Kinoshita, T., 2014. Mg-chelatase I subunit 1 and Mg-protoporphyrin IX methyltransferase affect the stomatal aperture in Arabidopsis thaliana. J. Plant Res. 127 (4): 553–563. https://doi.org/10.1007/s10265-014-0636-0

Torres, M.A., Dangl, J.L., Jones, J.D.G., 2002. Arabidopsis gp91phox homologues Atrbohd and Atrbohf are required for accumulation of reactive oxygen intermediates in the plant defense response. Proc. Natl. Acad. Sci. U.S.A. 99 (1): 517–522. https://doi.org/10.1073/pnas.012452499

Torres, M.A., Onouchi, H., Hamada, S., Machida, C., Hammond-Kosack, K.E., Jones, J.D.G., 1998. Six Arabidopsis thaliana homologues of the human respiratory burst oxidase

(gp91(phox)). Plant Journal 14 (3): 365–370. https://doi.org/10.1046/j.1365-313X.1998.00136.x

Toyota, M., Spencer, D., Sawai-Toyota, S., Jiaqi, W., Zhang, T., Koo, A.J., Howe, G.A., Gilroy, S., 2018. Glutamate triggers long-distance, calcium-based plant defense signaling. *Science* 361 (6407): 1112-1115. https://doi.org/10.1126/science.aat7744

Trick, M., Long, Y., Meng, J., Bancroft, I., 2009. Single nucleotide polymorphism (SNP) discovery in the polyploid Brassica napus using Solexa transcriptome sequencing. Plant Biotechnol. J. 7 (4): 334–346. https://doi.org/10.1111/j.1467-7652.2008.00396.x

Triozzi, P.M., Brunello, L., Novi, G., Ferri, G., Cardarelli, F., Loreti, E., Perales, M., Perata, P., 2024. Spatiotemporal oxygen dynamics in young leaves reveal cyclic hypoxia in plants. Mol. Plant 17 (3): 377–394. https://doi.org/10.1016/j.molp.2024.01.006

Trujillo, M., Ichimura, K., Casais, C., Shirasu, K., 2008. Negative Regulation of PAMP-Triggered Immunity by an E3 Ubiquitin Ligase Triplet in Arabidopsis. Current Biology 18 (18): 1396–1401. https://doi.org/10.1016/j.cub.2008.07.085

Tsai, K.J., Suen, D.F., Shih, M.C., 2023. Hypoxia response protein HRM1 modulates the activity of mitochondrial electron transport chain in Arabidopsis under hypoxic stress. New Phytologist 239 (4): 1315–1331. https://doi.org/10.1111/nph.19006

Tyagi, A., Ali, S., Mir, R.A., Sharma, S., Arpita, K., Almalki, M.A., Mir, Z.A., 2024. Uncovering the effect of waterlogging stress on plant microbiome and disease development: current knowledge and future perspectives. Front. Plant Sci. 15: 1407789. https://doi.org/10.3389/fpls.2024.1407789

Ülker, B., Shahid Mukhtar, M., Somssich, I.E., 2007. The WRKY70 transcription factor of Arabidopsis influences both the plant senescence and defense signaling pathways. Planta 226 (1): 125–137. https://doi.org/10.1007/s00425-006-0474-y

Umbach, A.L., Fiorani, F., Siedow, J.N., 2005. Characterization of transformed Arabidopsis with altered alternative oxidase levels and analysis of effects on reactive oxygen species in tissue. Plant Physiol. 139 (4): 1806–1820. https://doi.org/10.1104/pp.105.070763

Valeri, M.C., Novi, G., Weits, D.A., Mensuali, A., Perata, P., Loreti, E., 2021. Botrytis cinerea induces local hypoxia in Arabidopsis leaves. New Phytologist 229 (1): 173–185. https://doi.org/10.1111/nph.16513

Van Wilder, V., De Brouwer, V., Loizeau, K., Gambonnet, B., Albrieux, C., Van Der Straeten, D., Lambert, W.E., Douce, R., Block, M.A., Rebeille, F., Ravanel, S., 2009. C1 metabolism and chlorophyll synthesis: The Mg-protoporphyrin IX methyltransferase activity is dependent on the folate status. New Phytologist 182 (1): 137–145. https://doi.org/10.1111/j.1469-8137.2008.02707.x

Vanlerberghe, C.C., Mclntosh, L., 1996. Signals Regulating the Expression of the Nuclear Gene Encoding Alternative Oxidase of Plant Mitochondria'. Plant Physiol 11 (2): 589–595. https://doi.org/10.1104/pp.111.2.589

Velásquez, A.C., Castroverde, C.D.M., He, S.Y., 2018. Plant–Pathogen Warfare under Changing Climate Conditions. Current Biology. 28 (10): R619-R634. https://doi.org/10.1016/j.cub.2018.03.054

Vervuren, P.J.A., Blom, C.W.P.M., De Kroon, H., 2003. Extreme flooding events on the Rhine and the survival and distribution of riparian plant species. Journal of Ecology 91 (1): 135–146. https://doi.org/10.1046/j.1365-2745.2003.00749.x

Vescovi, M., Zaffagnini, M., Festa, M., Trost, P., Lo Schiavo, F., Costa, A., 2013. Nuclear accumulation of cytosolic glyceraldehyde-3-phosphate dehydrogenase in cadmium-stressed Arabidopsis roots. Plant Physiol. 162 (1): 333–346. https://doi.org/10.1104/pp.113.215194

Vicente, J., Mendiondo, G.M., Movahedi, M., Peirats-Llobet, M., Juan, Y. ting, Shen, Y. yen, Dambire, C., Smart, K., Rodriguez, P.L., Charng, Y. yung, Gray, J.E., Holdsworth, M.J., 2017. The Cys-Arg/N-End Rule Pathway Is a General Sensor of Abiotic Stress in Flowering Plants. Current Biology 27 (20): 3183-3190.e4. https://doi.org/10.1016/j.cub.2017.09.006

Vicente, J., Mendiondo, G.M., Pauwels, J., Pastor, V., Izquierdo, Y., Naumann, C., Movahedi, M., Rooney, D., Gibbs, D.J., Smart, K., Bachmair, A., Gray, J.E., Dissmeyer, N., Castresana, C., Ray, R. V., Gevaert, K., Holdsworth, M.J., 2019. Distinct branches of the N-end rule pathway modulate the plant immune response. New Phytologist 221 (2): 988–1000. https://doi.org/10.1111/nph.15387

Vishwakarma, A., Kumari, A., Mur, L.A.J., Gupta, K.J., 2018. A discrete role for alternative oxidase under hypoxia to increase nitric oxide and drive energy production. Free Radic. Biol. Med. 122, 40–51. https://doi.org/10.1016/j.freeradbiomed.2018.03.045

Voesenek, L.A.C.J., Armstrong, W., Bögemann, G.M., McDonald, M.P., Colmer, T.D., 1999. A lack of aerenchyma and high rates of radial oxygen loss from the root base contribute to the waterlogging intolerance of Brassica napus. Aust. J. Plant Physiol. 26 (1): 87–93. https://doi.org/10.1071/PP98086

Wagner, S., Steinbeck, J., Fuchs, P., Lichtenauer, S., Elsässer, M., Schippers, J.H.M., Nietzel, T., Ruberti, C., Van Aken, O., Meyer, A.J., Van Dongen, J.T., Schmidt, R.R., Schwarzländer, M., 2019. Multiparametric real-time sensing of cytosolic physiology links hypoxia responses to mitochondrial electron transport. New Phytologist 224 (4): 1668–1684. https://doi.org/10.1111/nph.16093

Wang, D., Chai, G., Xu, L., Yang, K., Zhuang, Y., Yang, A., Liu, S., Kong, Y., Zhou, G., 2022. Phosphorylation-mediated inactivation of C3H14 by MPK4 enhances bacterial-triggered immunity in Arabidopsis. Plant Physiol. 190 (3): 1941–1959. https://doi.org/10.1093/plphys/kiac300

Wang, D., Wei, L., Liu, T., Ma, J., Huang, K., Guo, H., Huang, Y., Zhang, L., Zhao, J., Tsuda, K., Wang, Y., 2023. Suppression of ETI by PTI priming to balance plant growth and defense through an MPK3/MPK6-WRKYs-PP2Cs module. Mol. Plant 16 (5): 903–918. https://doi.org/10.1016/j.molp.2023.04.004

Wang, F., Chen, Z.H., Liu, X., Colmer, T.D., Shabala, L., Salih, A., Zhou, M., Shabala, S., 2017. Revealing the roles of GORK channels and NADPH oxidase in acclimation to hypoxia in Arabidopsis. J. Exp. Bot. 68 (12): 3191–3204. https://doi.org/10.1093/jxb/erw378

Wang, F.L., Tan, Y.L., Wallrad, L., Du, X.Q., Eickelkamp, A., Wang, Z.F., He, G.F., Rehms, F., Li, Z., Han, J.P., Schmitz-Thom, I., Wu, W.H., Kudla, J., Wang, Y., 2021. A potassium-sensing niche

in Arabidopsis roots orchestrates signaling and adaptation responses to maintain nutrient homeostasis. Dev. Cell 56 (6): 781-794.e6. https://doi.org/10.1016/j.devcel.2021.02.027

Wang, J., Grubb, L.E., Wang, Jiayu, Liang, X., Li, Lin, Gao, C., Ma, M., Feng, F., Li, M., Li, Lei, Zhang, X., Yu, F., Xie, Q., Chen, S., Zipfel, C., Monaghan, J., Zhou, J.M., 2018. A Regulatory Module Controlling Homeostasis of a Plant Immune Kinase. Mol. Cell 69 (3): 493-504.e6. https://doi.org/10.1016/j.molcel.2017.12.026

Wang, P., Du, Y., Zhao, X., Miao, Y., Song, C.P., 2013. The MPK6-ERF6-ROS-responsive cis-acting element7/GCC box complex modulates oxidative gene transcription and the oxidative response in arabidopsis. Plant Physiol. 161 (3): 1392–1408. https://doi.org/10.1104/pp.112.210724

Wang, P., Hsu, C.-C., Du, Y., Zhu, P., Zhao, C., Fu, X., Zhang, C., Sebastian Paez, J., Macho, A.P., Andy Tao, W., Zhu, J.-K., 2019. Mapping proteome-wide targets of protein kinases in plant stress responses. PNAS 117 (6): 3270–3280. https://doi.org/10.1073/pnas.1919901117

Wang, W., Barnaby, J.Y., Tada, Y., Li, H., Tör, M., Caldelari, D., Lee, D.U., Fu, X.D., Dong, X., 2011. Timing of plant immune responses by a central circadian regulator. Nature 470 (7332): 110–115. https://doi.org/10.1038/nature09766

Wang, W., Zhang, Q., Tang, D., Chen, S., Zhong, G., Gao, C., 2024. MITOGEN-ACTIVATED PROTEIN KINASE3 enhances disease resistance of edr1 mutants by phosphorylating MAPKKK5. Plant Physiol. 194 (1): 578–591. https://doi.org/10.1093/plphys/kiad472

Wang, X., Meng, H., Tang, Y., Zhang, Y., He, Y., Zhou, J., Meng, X., 2022. Phosphorylation of an ethylene response factor by MPK3/MPK6 mediates negative feedback regulation of pathogen-induced ethylene biosynthesis in Arabidopsis. Journal of Genetics and Genomics 49 (8): 810–822. https://doi.org/10.1016/j.jgg.2022.04.012

Wang, X., Sun, L., Li, W., Peng, M., Chen, F., Zhang, W., Sun, C., Chen, S., Hua, W., Zhang, J., 2020. Dissecting the genetic mechanisms of waterlogging tolerance in Brassica napus through linkage mapping and a genome-wide association study. Ind. Crops Prod. 147: 112269. https://doi.org/10.1016/j.indcrop.2020.112269

Wang, Y., Cui, X., Yang, B., Xu, S., Wei, X., Zhao, P., Niu, F., Sun, M., Wang, C., Cheng, H., Jiang, Y.Q., 2020. WRKY55 transcription factor positively regulates leaf senescence and the defense response by modulating the transcription of genes implicated in the biosynthesis of reactive oxygen species and salicylic acid in Arabidopsis. Development 147 (16): dev189647. https://doi.org/10.1242/dev.189647

Wang, Y., Schuck, S., Wu, J., Yang, P., Döring, A.C., Zeier, J., Tsuda, K., 2018. A mpk3/6-wrky33-ald1-pipecolic acid regulatory loop contributes to systemic acquired resistance[open]. Plant Cell 30 (10): 2480–2494. https://doi.org/10.1105/tpc.18.00547

Wang, Y., Wu, Y., Zhong, H., Chen, S., Wong, K.B., Xia, Y., 2022. Arabidopsis PUB2 and PUB4 connect signaling components of pattern-triggered immunity. New Phytologist 233 (5): 2249–2265. https://doi.org/10.1111/nph.17922

Wang, Y., Zhang, H., Wang, P., Zhong, H., Liu, W., Zhang, S., Xiong, L., Wu, Y., Xia, Y., 2023. Arabidopsis EXTRA-LARGE G PROTEIN 1 (XLG1) functions together with XLG2 and XLG3 in PAMP-triggered MAPK activation and immunity. J. Integr. Plant Biol. 65 (3): 825–837. https://doi.org/10.1111/jipb.13391

Wang, Z., Fang, H., Chen, Y., Chen, K., Li, G., Gu, S., Tan, X., 2014. Overexpression of BnWRKY33 in oilseed rape enhances resistance to Sclerotinia sclerotiorum. Mol. Plant Pathol. 15 (7): 677–689. https://doi.org/10.1111/mpp.12123

Wang, Z., Gou, X., 2020. Receptor-like protein kinases function upstream of mapks in regulating plant development. Int. J. Mol. Sci. 21 (20): 7638. https://doi.org/10.3390/ijms21207638

Wang, Zuodong, Li, X., Yao, X., Ma, J., Lu, K., An, Y., Sun, Z., Wang, Q., Zhou, M., Qin, L., Zhang, L., Zou, S., Chen, L., Song, C., Dong, H., Zhang, M., Chen, X., 2023. MYB44 regulates PTI by promoting the expression of EIN2 and MPK3/6 in Arabidopsis. Plant Commun. 4 (6): 100628. https://doi.org/10.1016/j.xplc.2023.100628

Wang, Z., Wei, X., Cui, X., Wang, J., Wang, Y., Sun, M., Zhao, P., Yang, B., Wang, Q., Jiang, Y.Q., 2024. The transcription factor WRKY22 modulates ethylene biosynthesis and root development through transactivating the transcription of ACS5 and ACO5 in Arabidopsis. Physiol. Plant. 176 (3): e14371. https://doi.org/10.1111/ppl.14371

Wang, Zhaoqiang, Wei, X., Wang, Y., Sun, M., Zhao, P., Wang, Q., Yang, B., Li, J., Jiang, Y.Q., 2023. WRKY29 transcription factor regulates ethylene biosynthesis and response in arabidopsis. Plant Physiology and Biochemistry 194, 134–145. https://doi.org/10.1016/j.plaphy.2022.11.012

Wany, A., Gupta, A.K., Brotman, Y., Pandey, S., Vishwakarma, A.P., Kumari, A., Singh, P., Pathak, P.K., Igamberdiev, A.U., Gupta, K.J., 2018. Nitric oxide is important for sensing and survival under hypoxia in Arabidopsis. bioRxiv. https://doi.org/10.1101/462218

Ward, J.M., Schroeder, J., 1994. Calcium-Activated K+ Channels and Calcium-Induced Calcium Release by Slow Vacuolar Ion Channels in Guard Cell Vacuoles Implicated in the Control of Stomatal Closure, The Plant Cell. 6 (5): 669–683. https://doi.org/10.1105/tpc.6.5.669

Wdowiak, A., Podgórska, A., Szal, B., 2024. Calcium in plants: an important element of cell physiology and structure, signaling, and stress responses. Acta Physiol. Plant. 46 (12): 108. https://doi.org/10.1007/s11738-024-03733-w

Weits, D.A., Giuntoli, B., Kosmacz, M., Parlanti, S., Hubberten, H.M., Riegler, H., Hoefgen, R., Perata, P., Van Dongen, J.T., Licausi, F., 2014. Plant cysteine oxidases control the oxygen-dependent branch of the N-end-rule pathway. Nat. Commun. 5 (1): 3425. https://doi.org/10.1038/ncomms4425

White, M.D., Kamps, J.J.A.G., East, S., Taylor Kearney, L.J., Flashman, E., 2018. The plant cysteine oxidases from Arabidopsis thaliana are kinetically tailored to act as oxygen sensors. Journal of Biological Chemistry 293 (30): 11786–11795. https://doi.org/10.1074/jbc.RA118.003496

White, M.D., Klecker, M., Hopkinson, R.J., Weits, D.A., Mueller, C., Naumann, C., O'Neill, R., Wickens, J., Yang, J., Brooks-Bartlett, J.C., Garman, E.F., Grossmann, T.N., Dissmeyer, N., Flashman, E., 2017. Plant cysteine oxidases are dioxygenases that directly enable arginyl transferase-catalysed arginylation of N-end rule targets. Nat. Commun. 8 (1): 14690. https://doi.org/10.1038/ncomms14690

Wildermuth, M.C., Dewdney, J., Wu, G., Ausubel, F.M., 2001. Isochorismate synthase is required to synthesize salicylic acid for plant defence. 414 (6863): 562–565. https://doi.org/10.1038/35107108

Winter, C.M., Austin, R.S., Blanvillain-Baufumé, S., Reback, M.A., Monniaux, M., Wu, M.F., Sang, Y., Yamaguchi, A., Yamaguchi, N., Parker, J.E., Parcy, F., Jensen, S.T., Li, H., Wagner, D., 2011. LEAFY Target Genes Reveal Floral Regulatory Logic, cis Motifs, and a Link to Biotic Stimulus Response. Dev. Cell 20 (4): 430–443. https://doi.org/10.1016/j.devcel.2011.03.019

Wollmer, A.C., Pitann, B., Mühling, K.H., 2019. Timing of Waterlogging Is Crucial for the Development of Micronutrient Deficiencies or Toxicities in Winter Wheat and Rapeseed. J. Plant Growth Regul. 38 (3): 824–830. https://doi.org/10.1007/s00344-018-9893-9

Wollmer, A.C., Pitann, B., Mühling, K.H., 2018. Waterlogging events during stem elongation or flowering affect yield of oilseed rape (Brassica napus L.) but not seed quality. J. Agron. Crop Sci. 204 (2): 165–174. https://doi.org/10.1111/jac.12244

Wu, F., Chi, Y., Jiang, Z., Xu, Y., Xie, L., Huang, F., Wan, D., Ni, J., Yuan, F., Wu, X., Zhang, Y., Wang, L., Ye, R., Byeon, B., Wang, W., Zhang, S., Sima, M., Chen, S., Zhu, M., Pei, J., Johnson, D.M., Zhu, S., Cao, X., Pei, C., Zai, Z., Liu, Y., Liu, T., Swift, G.B., Zhang, W., Yu, M., Hu, Z., Siedow, J.N., Chen, X., Pei, Z.M., 2020. Hydrogen peroxide sensor HPCA1 is an LRR receptor kinase in Arabidopsis. Nature 578 (7796): 577–581. https://doi.org/10.1038/s41586-020-2032-3

Wu, J., Zhao, Q., Liu, S., Shahid, M., Lan, L., Cai, G., Zhang, C., Fan, C., Wang, Y., Zhou, Y., 2016. Genome-wide association study identifies new loci for resistance to sclerotinia stem rot in Brassica napus. Front. Plant Sci. 7: 1418. https://doi.org/10.3389/fpls.2016.01418

Wu, L., Yang, H.Q., 2010. CRYPTOCHROME 1 is implicated in promoting R protein-mediated plant resistance to pseudomonas syringae in arabidopsis. Mol. Plant 3 (3): 539–548. https://doi.org/10.1093/mp/ssp107

Wurts, W.A., Durborow, R.M., 1992. Southern Regional Aquaculture Center Interactions of pH, Carbon Dioxide, Alkalinity and Hardness in Fish Ponds. South. Reg. Aquac. Cent. Publ. 464.

Xie, L.J., Chen, Q.F., Chen, M.X., Yu, L.J., Huang, L., Chen, L., Wang, F.Z., Xia, F.N., Zhu, T.R., Wu, J.X., Yin, J., Liao, B., Shi, J., Zhang, J.H., Aharoni, A., Yao, N., Shu, W., Xiao, S., 2015. Unsaturation of Very-Long-Chain Ceramides Protects Plant from Hypoxia-Induced Damages by Modulating Ethylene Signaling in Arabidopsis. PLoS Genet. 11 (3): e1005143. https://doi.org/10.1371/journal.pgen.1005143

Xu, B., Cheng, Y., Zou, X., Zhang, X., 2016. Ethanol content in plants of Brassica napus L. correlated with waterlogging tolerance index and regulated by lactate dehydrogenase and citrate synthase. Acta Physiol. Plant. 38 (3): 1–9. https://doi.org/10.1007/s11738-016-2098-6

Xu, J., Meng, J., Meng, X., Zhao, Y., Liu, J., Sun, T., Liu, Y., Wang, Q., Zhang, S., 2016. Pathogen-responsive MPK3 and MPK6 reprogram the biosynthesis of indole glucosinolates and their derivatives in arabidopsis immunity. Plant Cell 28 (5): 1144–1162. https://doi.org/10.1105/tpc.15.00871

Xu, J., Xie, J., Yan, C., Zou, X., Ren, D., Zhang, S., 2014. A chemical genetic approach demonstrates that MPK3/MPK6 activation and NADPH oxidase-mediated oxidative burst are two independent signaling events in plant immunity. Plant Journal 77 (2): 222–234. https://doi.org/10.1111/tpj.12382

Xu, Le, Pan, R., Shabala, L., Shabala, S., Zhang, W.Y., 2019. Temperature influences waterlogging stress-induced damage in Arabidopsis through the regulation of photosynthesis and hypoxia-related genes. Plant Growth Regul. 89 (2): 143–152. https://doi.org/10.1007/s10725-019-00518-x

Xu, Lahong, Yao, X., Zhang, N., Gong, B.Q., Li, J.F., 2019. Dynamic G protein alpha signaling in Arabidopsis innate immunity. Biochem. Biophys. Res. Commun. 516 (3): 1039–1045. https://doi.org/10.1016/j.bbrc.2017.07.040

Xu, M., Ma, H., Zeng, L., Cheng, Y., Lu, G., Xu, J., Zhang, X., Zou, X., 2015. The effect of waterlogging on yield and seed quality at the early flowering stage in Brassica napus L. Field Crops Res. 180 (15): 238–245. https://doi.org/10.1016/j.fcr.2015.06.007

Yamamoto, Y.Y., Matsui, M., Ang, L.-H., Deng, X.-W., 1998. Role of a COP1 Interactive Protein in Mediating Light-Regulated Gene Expression in Arabidopsis, The Plant Cell. 10 (7): 1083–1094. https://doi.org/10.1105/tpc.10.7.1083

Yang, CY., 2014. Hydrogen peroxide controls transcriptional responses of *ERF73/HRE1* and *ADH1* via modulation of ethylene signaling during hypoxic stress. Planta 239 (4): 877–885. https://doi.org/10.1007/s00425-013-2020-z

Yang, C.Y., 2014. Ethylene and hydrogen peroxide are involved in hypoxia signaling that modulates AtERF73/HRE1 expression. Plant Signal. Behav. 9 (5): 1–3. https://doi.org/10.4161/psb.28583

Yang, C.Y., Hong, C.P., 2015. The NADPH oxidase Rboh D is involved in primary hypoxia signalling and modulates expression of hypoxia-inducible genes under hypoxic stress. Environ. Exp. Bot. 115, 63–72. https://doi.org/10.1016/j.envexpbot.2015.02.008

Yang, C.Y., Hsu, F.C., Li, J.P., Wang, N.N., Shih, M.C., 2011. The AP2/ERF transcription factor AtERF73/HRE1 modulates ethylene responses during hypoxia in Arabidopsis. Plant Physiol. 156 (1): 202–212. https://doi.org/10.1104/pp.111.172486

Yang, C.Y., Huang, Y.C., Ou, S.L., 2017. ERF73/HRE1 is involved in H2O2 production via hypoxia-inducible Rboh gene expression in hypoxia signaling. Protoplasma 254 (4): 1705–1714. https://doi.org/10.1007/s00709-016-1064-x

Yang, H., Mu, J., Chen, L., Feng, J., Hu, J., Li, L., Zhou, J.M., Zuo, J., 2015. S-nitrosylation positively regulates ascorbate peroxidase activity during plant stress responses. Plant Physiol. 167 (4): 1604–1615. https://doi.org/10.1104/pp.114.255216

Yang, L., Ye, C., Zhao, Y., Cheng, X., Wang, Y., Jiang, Y.-Q., Yang, B., 2018. An oilseed rape WRKY-type transcription factor regulates ROS accumulation and leaf senescence in Nicotiana benthamiana and Arabidopsis through modulating transcription of RbohD and RbohF. Planta 247 (6): 1323–1338. https://doi.org/10.1007/s00425-018-2868-z

Yang, L., Zhang, Y., Guan, R., Li, S., Xu, X., Zhang, S., Xu, J., 2020. Co-regulation of indole glucosinolates and camalexin biosynthesis by CPK5/CPK6 and MPK3/MPK6 signaling pathways. J. Integr. Plant Biol. 62 (11): 1780–1796. https://doi.org/10.1111/jipb.12973

Yang, R., Wang, C., Yang, Y., Harrison, M.T., Zhou, M., Liu, K., 2024. Implications of soil waterlogging for crop quality: A meta-analysis. European Journal of Agronomy 161: 127395. https://doi.org/10.1016/j.eja.2024.127395

Yang, Y.-X., Ahammed, G.J., Wu, C., Fan, S.-Y., Zhou, Y.-H., 2015. Crosstalk among Jasmonate, Salicylate and Ethylene Signaling Pathways in Plant Disease and Immune Responses, Current Protein and Peptide Science. 16 (5): 450 – 461. https://doi.org/10.2174/1389203716666150330141638

Yao, Y., He, R.J., Xie, Q.L., Zhao, X. hai, Deng, X. mei, He, J. bo, Song, L., He, J., Marchant, A., Chen, X.Y., Wu, A.M., 2017. ETHYLENE RESPONSE FACTOR 74 (ERF74) plays an essential role in controlling a respiratory burst oxidase homolog D (RbohD)-dependent mechanism in response to different stresses in Arabidopsis. New Phytologist 213 (4): 1667–1681. https://doi.org/10.1111/nph.14278

Yemelyanov, V. V., Shishova, M.F., Chirkova, T. V., Lindberg, S.M., 2011. Anoxia-induced elevation of cytosolic Ca2+ concentration depends on different Ca2+ sources in rice and wheat protoplasts. Planta 234 (2): 271–280. https://doi.org/10.1007/s00425-011-1396-x

Yin, H., Zhang, X., Liu, J., Wang, Y., He, J., Yang, T., Hong, X., Yang, Q., Gong, Z., 2009. Epigenetic regulation, somatic homologous recombination, and abscisic acid signaling are influenced by dna polymerase ε mutation in arabidopsis. Plant Cell 21 (2): 386–402. https://doi.org/10.1105/tpc.108.061549

Yoo, S.D., Cho, Y.H., Tena, G., Xiong, Y., Sheen, J., 2008. Dual control of nuclear EIN3 by bifurcate MAPK cascades in C 2H4 signalling. Nature 451 (7180): 789–795. https://doi.org/10.1038/nature06543

Yoon, G.M., 2015. New insights into the protein turnover regulation in ethylene biosynthesis. Mol. Cells. 38 (7): 597-603. https://doi.org/10.14348/molcells.2015.0152

Yosef Fichman, Ron Mittler, 2021. Integration of electric, calcium, reactive oxygen species and hydraulic signals during rapid systemic signaling in plants. Plant Journal 107 (1): 5–6. https://doi.org/10.1111/tpj.15385

Yoshida, S., Ito, M., Callis, J., Nishida, I., Watanabe, A., 2002. A delayed leaf senescence mutant is defective in arginyl-tRNA:protein arginyltransferase, a component of the N-end rule pathway in Arabidopsis. Plant Journal 32 (1): 129–137. https://doi.org/10.1046/j.1365-313X.2002.01407.x

Yu, M., Lamattina, L., Spoel, S.H., Loake, G.J., 2014. Nitric oxide function in plant biology: A redox cue in deconvolution. New Phytologist 202 (4): 1142-1156. https://doi.org/10.1111/nph.12739

Yu, W.W., Chen, Q.F., Liao, K., Zhou, D.M., Yang, Y.C., He, M., Yu, L.J., Guo, D.Y., Xiao, S., Xie, R.H., Zhou, Y., 2024. The calcium-dependent protein kinase CPK16 regulates hypoxia-induced ROS production by phosphorylating the NADPH oxidase RBOHD in Arabidopsis. Plant Cell 36 (9): 3451–3466. https://doi.org/10.1093/plcell/koae153

Yu, X., Liu, Z., Qin, A., Zhou, Y., Zhao, Z., Yang, J., Hu, M., Liu, H., Liu, Y., Sun, S., Zhang, Y., Jan, M., Bawa, G., Sun, X., 2023. FLS2-RBOHD module regulates changes in the metabolome of Arabidopsis in response to abiotic stress. Plant-Environment Interactions 4 (1): 36–54. https://doi.org/10.1002/pei3.10101

Yu, X., Xu, G., Li, B., de Souza Vespoli, L., Liu, H., Moeder, W., Chen, S., de Oliveira, M.V.V., Ariádina de Souza, S., Shao, W., Rodrigues, B., Ma, Y., Chhajed, S., Xue, S., Berkowitz, G.A., Yoshioka, K., He, P., Shan, L., 2019. The Receptor Kinases BAK1/SERK4 Regulate Ca2+

Channel-Mediated Cellular Homeostasis for Cell Death Containment. Current Biology 29 (22): 3778-3790.e8. https://doi.org/10.1016/j.cub.2019.09.018

Yu, Z., Cao, J., Zhu, S., Zhang, L., Peng, Y., Shi, J., 2020. Exogenous Nitric Oxide Enhances Disease Resistance by Nitrosylation and Inhibition of S-Nitrosoglutathione Reductase in Peach Fruit. Front. Plant Sci. 11: 543. https://doi.org/10.3389/fpls.2020.00543

Yuan, L.B., Dai, Y.S., Xie, L.J., Yu, L.J., Zhou, Y., Lai, Y.X., Yang, Y.C., Xu, L., Chen, Q.F., Xiao, S., 2017. Jasmonate regulates plant responses to postsubmergence reoxygenation through transcriptional activation of antioxidant synthesis. Plant Physiol. 173 (3): 1864–1880. https://doi.org/10.1104/pp.16.01803

Yuan, M., Jiang, Z., Bi, G., Nomura, K., Liu, M., Wang, Y., Cai, B., Zhou, J.M., He, S.Y., Xin, X.F., 2021. Pattern-recognition receptors are required for NLR-mediated plant immunity. Nature 592 (7852): 105–109. https://doi.org/10.1038/s41586-021-03316-6

Yun, B.W., Feechan, A., Yin, M., Saidi, N.B.B., Le Bihan, T., Yu, M., Moore, J.W., Kang, J.G., Kwon, E., Spoel, S.H., Pallas, J.A., Loake, G.J., 2011. S-nitrosylation of NADPH oxidase regulates cell death in plant immunity. Nature 478 (7368): 264–268. https://doi.org/10.1038/nature10427

Zaffagnini, M., Fermani, S., Calvaresi, M., Orrù, R., Iommarini, L., Sparla, F., Falini, G., Bottoni, A., Trost, P., 2016. Tuning Cysteine reactivity and Sulfenic Acid stability by protein microenvironment in Glyceraldehyde-3-Phosphate Dehydrogenases of Arabidopsis thaliana. Antioxidants & Redox Signaling 24 (9): 502-517. https://doi.org/10.1089/ars.2015.6417

Zamani-Noor, N., Jedryczka, M., 2025. Inoculum and inoculation techniques: key steps in studying pathogenicity and resistance to Sclerotinia stem rot in oilseed rape. Front. Plant Sci. 16: 1610049. https://doi.org/10.3389/fpls.2025.1610049

Zandalinas, S.I., Balfagón, D., Arbona, V., Gómez-Cadenas, A., Inupakutika, M.A., Mittler, R., 2016. ABA is required for the accumulation of APX1 and MBF1c during a combination of water deficit and heat stress. J. Exp. Bot. 67 (18): 5381–5390. https://doi.org/10.1093/jxb/erw299

Zandalinas, S.I., Casal, J., Rouached, H., Mittler, R., 2024. Stress combination: from genes to ecosystems. Plant Journal 117 (6): 1639-1641. https://doi.org/10.1111/tpj.16681

Zandalinas, S.I., Fichman, Y., Mittler, R., 2020. Vascular bundles mediate systemic reactive oxygen signaling during light stress. Plant Cell 32 (11): 3425–3435. https://doi.org/10.1105/TPC.20.00453

Zandalinas, S.I., Sengupta, S., Fritschi, F.B., Azad, R.K., Nechushtai, R., Mittler, R., 2021. The impact of multifactorial stress combination on plant growth and survival. New Phytologist 230 (3): 1034–1048. https://doi.org/10.1111/nph.17232

Zhan, N., Wang, C., Chen, L., Yang, H., Feng, J., Gong, X., Ren, B., Wu, R., Mu, J., Li, Y., Liu, Z., Zhou, Y., Peng, J., Wang, K., Huang, X., Xiao, S., Zuo, J., 2018. S-Nitrosylation Targets GSNO Reductase for Selective Autophagy during Hypoxia Responses in Plants. Mol. Cell 71 (1): 142-154.e6. https://doi.org/10.1016/j.molcel.2018.05.024

Zhang, C., Atanasov, K.E., Alcázar, R., 2023. Spermine inhibits PAMP-induced ROS and Ca2+burst and reshapes the transcriptional landscape of PAMP-Triggered immunity in Arabidopsis. J. Exp. Bot. 74 (1): 427–442. https://doi.org/10.1093/jxb/erac411

Zhang, C.X., Kang, X., Bai, Q.W., Li, J.X., Mu, M.T., Ma, X.Y., Hei, S.M., 2025. Gα Protein Mediates High-Concentration CO2-Induced Stomata Closure Through Interaction With Carbonic Anhydrase to Promote Guard Cell Hydrogen Peroxide Production in Arabidopsis. Plant Cell Environ. 48 (9): 6704–6721. https://doi.org/10.1111/pce.15645

Zhang, H., Rundle, C., Winter, N., Miricescu, A., Mooney, B.C., Bachmair, A., Graciet, E., Theodoulou, F.L., 2024. BIG enhances Arg/N-degron pathway-mediated protein degradation to regulate Arabidopsis hypoxia responses and suberin deposition. Plant Cell 36 (9): 3177–3200. https://doi.org/10.1093/plcell/koae117

Zhang, H., Sonnewald, U., 2017. Differences and commonalities of plant responses to single and combined stresses. Plant Journal 90 (5): 839–855. https://doi.org/10.1111/tpj.13557

Zhang, J., Liu, B., Song, Y., Chen, Y., Fu, J., Liu, J., Ma, T., Xi, Z., Liu, H., 2021. Genome-wide (ChIP-seq) identification of target genes regulated by WRKY33 during submergence stress in Arabidopsis. BMC Genom. Data 22 (1): 16. https://doi.org/10.1186/s12863-021-00972-5

Zhang, K., Liu, F., Wang, Z., Zhuo, C., Hu, K., Li, X., Wen, J., Yi, B., Shen, J., Ma, C., Fu, T., Tu, J., 2022. Transcription factor WRKY28 curbs WRKY33-mediated resistance to Sclerotinia sclerotiorum in Brassica napus. Plant Physiol. 190 (4): 2757–2774. https://doi.org/10.1093/plphys/kiac439

Zhang, M., Chiang, Y.H., Toruño, T.Y., Lee, D.H., Ma, M., Liang, X., Lal, N.K., Lemos, M., Lu, Y.J., Ma, S., Liu, J., Day, B., Dinesh-Kumar, S.P., Dehesh, K., Dou, D., Zhou, J.M., Coaker, G., 2018. The MAP4 Kinase SIK1 Ensures Robust Extracellular ROS Burst and Antibacterial Immunity in Plants. Cell Host Microbe 24 (3): 379-391.e5. https://doi.org/10.1016/j.chom.2018.08.007

Zhang, M., Zhang, S., 2022. Mitogen-activated protein kinase cascades in plant signaling. J. Integr. Plant Biol. 64 (2): 301–341. https://doi.org/10.1111/jipb.13215

Zhang, W., Kumar, N., Helwig, J.R., Hoerter, A., Iyer-Pascuzzi, A.S., Umulis, D.M., Pienaar, E., Staiger, C.J., 2025. Local traveling waves of cytosolic calcium elicited by defense signals or wounding are propagated by distinct mechanisms. BioRxiv. https://doi.org/10.1101/2025.01.23.634554

Zhang, Y., Xie, Y., Shi, H., Zhuang, Y., Zheng, Y., Lin, H., Zhou, H., 2023. MYB30 Regulates Submergence Tolerance by Repressing Ethylene Biosynthesis via ACS7 in Arabidopsis. Plant Cell Physiol. 64 (7): 814–825. https://doi.org/10.1093/pcp/pcad041

Zhang, Y., Zhu, H., Zhang, Q., Li, M., Yan, M., Wang, R., Wang, L., Welti, R., Zhang, W., Wang, X., 2009. Phospholipase Dα1 and phosphatidic acid regulate NADPH oxidase activity and production of reactive oxygen species in ABA-mediated stomatal closure in arabidopsis. Plant Cell 21 (8): 2357–2377. https://doi.org/10.1105/tpc.108.062992

Zhao, J., Chen, Q., Zhou, S., Sun, Y., Li, X., Li, Y., 2020. H2Bub1 regulates rbohd-dependent hydrogen peroxide signal pathway in the defense responses to verticillium dahliae toxins. Plant Physiol. 182 (1): 640–657. https://doi.org/10.1104/pp.19.00913

Zhao, X., Ebert, B., Zhang, B., Liu, H., Zhang, Y., Zeng, W., Rautengarten, C., Li, H., Chen, X., Bacic, A., Wang, G., Men, S., Zhou, Y., Heazlewood, J.L., Wu, A.M., 2020. UDP-Api/UDP-Xyl synthases affect plant development by controlling the content of UDP-Api to regulate the RG-II-borate complex. Plant Journal 104 (1): 252–267. https://doi.org/10.1111/tpj.14921

Zhao, Y., Wei, T., Yin, K.Q., Chen, Z., Gu, H., Qu, L.J., Qin, G., 2012. Arabidopsis RAP2.2 plays an important role in plant resistance to Botrytis cinerea and ethylene responses. New Phytologist 195 (2): 450–460. https://doi.org/10.1111/j.1469-8137.2012.04160.x

Zheng, Z., Qamar, S.A., Chen, Z., Mengiste, T., 2006. Arabidopsis WRKY33 transcription factor is required for resistance to necrotrophic fungal pathogens. Plant Journal 48 (4): 592–605. https://doi.org/10.1111/j.1365-313X.2006.02901.x

Zhou, J., Wang, X., He, Y., Sang, T., Wang, P., Dai, S., Zhang, S., Meng, X., 2020. Differential phosphorylation of the transcription factor WRKY33 by the protein kinases CPK5/CPK6 and MPK3/MPK6 cooperatively regulates camalexin biosynthesis in arabidopsis. Plant Cell 32 (8): 2621–2638. https://doi.org/10.1105/tpc.19.00971

Zhou, W., Lin, X., 1995. Field Crops Research Effects of waterlogging at different growth stages on physiological characteristics and seed yield of winter rape (Brassica napus L.). Field Crops Research. 44 (2): 103-110. https://doi.org/10.1016/0378-4290(95)00075-5

Zhou, Y., Tan, W.J., Xie, L.J., Qi, H., Yang, Y.C., Huang, L.P., Lai, Y.X., Tan, Y.F., Zhou, D.M., Yu, L.J., Chen, Q.F., Chye, M.L., Xiao, S., 2020. Polyunsaturated linolenoyl-CoA modulates ERF-VII-mediated hypoxia signaling in Arabidopsis. J. Integr. Plant Biol. 62 (3): 330–348. https://doi.org/10.1111/jipb.12875

Zhou, Y., Zhou, D.M., Yu, W.W., Shi, L.L., Zhang, Y., Lai, Y.X., Huang, L.P., Qi, H., Chen, Q.F., Yao, N., Li, J.F., Xie, L.J., Xiao, S., 2022. Phosphatidic acid modulates MPK3- and MPK6-mediated hypoxia signaling in Arabidopsis. Plant Cell 34 (2): 889–909. https://doi.org/10.1093/plcell/koab289

Zhu, H., Bao, Y., Peng, H., Li, X., Pan, W., Yang, Y., Kuang, Z., Ji, P., Liu, J., Shen, D., Ai, G., Dou, D., 2025. Phosphorylation of PIP2;7 by CPK28 or Phytophthora kinase effectors dampens pattern-triggered immunity in Arabidopsis. Plant Commun. 6 (1): 101135. https://doi.org/10.1016/j.xplc.2024.101135

Zhu, X., Feng, Y., Liang, G., Liu, N., Zhu, J.K., 2013. Aequorin-based luminescence imaging reveals stimulus- and tissue-specific Ca2+ dynamics in arabidopsis plants. Mol. Plant 6 (2): 444–455. https://doi.org/10.1093/mp/sst013

Zhu, Z., An, F., Feng, Y., Li, P., Xue, L., A, M., Jiang, Z., Kim, J.M., To, T.K., Li, W., Zhang, X., Yu, Q., Dong, Z., Chen, W.Q., Seki, M., Zhou, J.M., Guo, H., 2011. Derepression of ethylene-stabilized transcription factors (EIN3/EIL1) mediates jasmonate and ethylene signaling synergy in Arabidopsis. Proc. Natl. Acad. Sci. U.S.A. 108 (30): 12539–12544. https://doi.org/10.1073/pnas.1103959108

Zimmermann, P., Heinlein, C., Orendi, G., Zentgraf, U., 2006. Senescence-specific regulation of catalases in Arabidopsis thaliana (L.) Heynh. Plant Cell Environ. 29 (6): 1049–1060. https://doi.org/10.1111/j.1365-3040.2005.01459.x

Zou, M., Guo, M., Zhou, Z., Wang, B., Pan, Q., Li, Jiajing, Zhou, J.M., Li, Jiejie, 2021. MPK3- and MPK6-mediated VLN3 phosphorylation regulates actin dynamics during stomatal

immunity in Arabidopsis. Nat. Commun. 12 (1): 6474. https://doi.org/10.1038/s41467-021-26827-2

Zou, X., Hu, C., Zeng, L., Cheng, Y., Xu, M., Zhang, X., 2014. A comparison of screening methods to identify waterlogging tolerance in the field in Brassica napus L. during plant ontogeny. PLoS One 9 (3): e89731. https://doi.org/10.1371/journal.pone.0089731

Zou, X., Tan, X., Hu, C., Zeng, L., Lu, G., Fu, G., Cheng, Y., Zhang, X., 2013. The transcriptome of Brassica napus L. roots under waterlogging at the seedling stage. Int. J. Mol. Sci. 14 (2): 2637–2651. https://doi.org/10.3390/ijms14022637

Zou, X.L., Zeng, L., Lu, G.Y., Cheng, Y., Xu, J.S., Zhang, X.K., 2015. Comparison of transcriptomes undergoing waterlogging at the seedling stage between tolerant and sensitive varieties of Brassica napus L. J. Integr. Agric. 14 (9): 1723–1734. https://doi.org/10.1016/S2095-3119(15)61138-8

Zou, Y., Wang, S., Zhou, Y., Bai, J., Huang, G., Liu, X., Zhang, Y., Tang, D., Lu, D., 2018. Transcriptional regulation of the immune receptor FLS2 controls the ontogeny of plant innate immunity. Plant Cell 30 (11): 2779–2794. https://doi.org/10.1105/tpc.18.00297

Zubrycka, A., Dambire, C., Dalle Carbonare, L., Sharma, G., Boeckx, T., Swarup, K., Sturrock, C.J., Atkinson, B.S., Swarup, R., Corbineau, F., Oldham, N.J., Holdsworth, M.J., 2023. ERFVII action and modulation through oxygen-sensing in Arabidopsis thaliana. Nat. Commun. 14 (1): 4665. https://doi.org/10.1038/s41467-023-40366-y

Appendix A

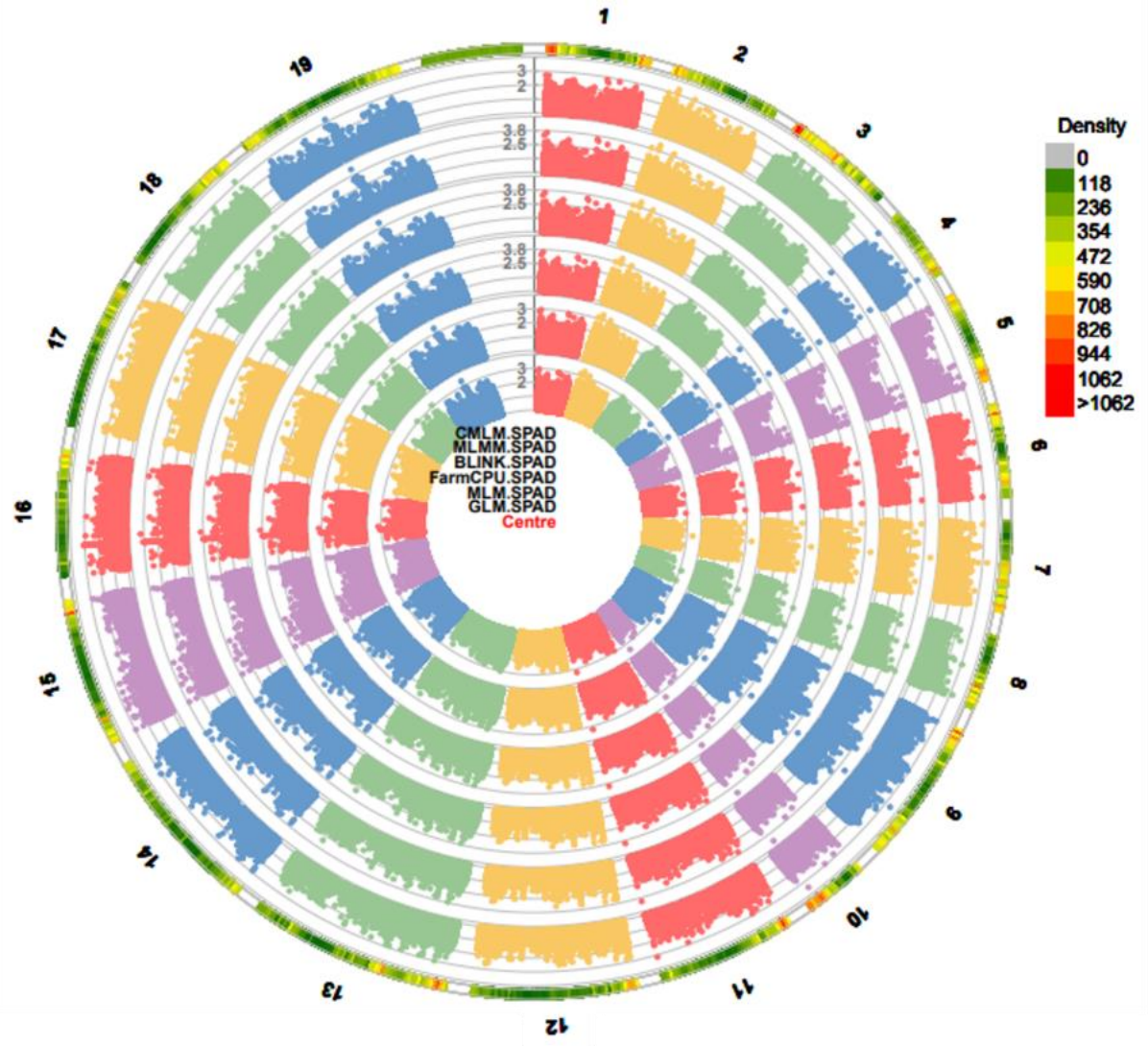

Figure 7.1. SNP markers associated with SPAD performance in waterlogged compared to control conditions. Manhattan plots for each *B. napus* chromosome plotting significance of SNP against its predicted unigene position. Significance (i.e. $-\log_{10}(p) > 6.64$ after Bonferroni-correction) is marked with a blue dashed line.

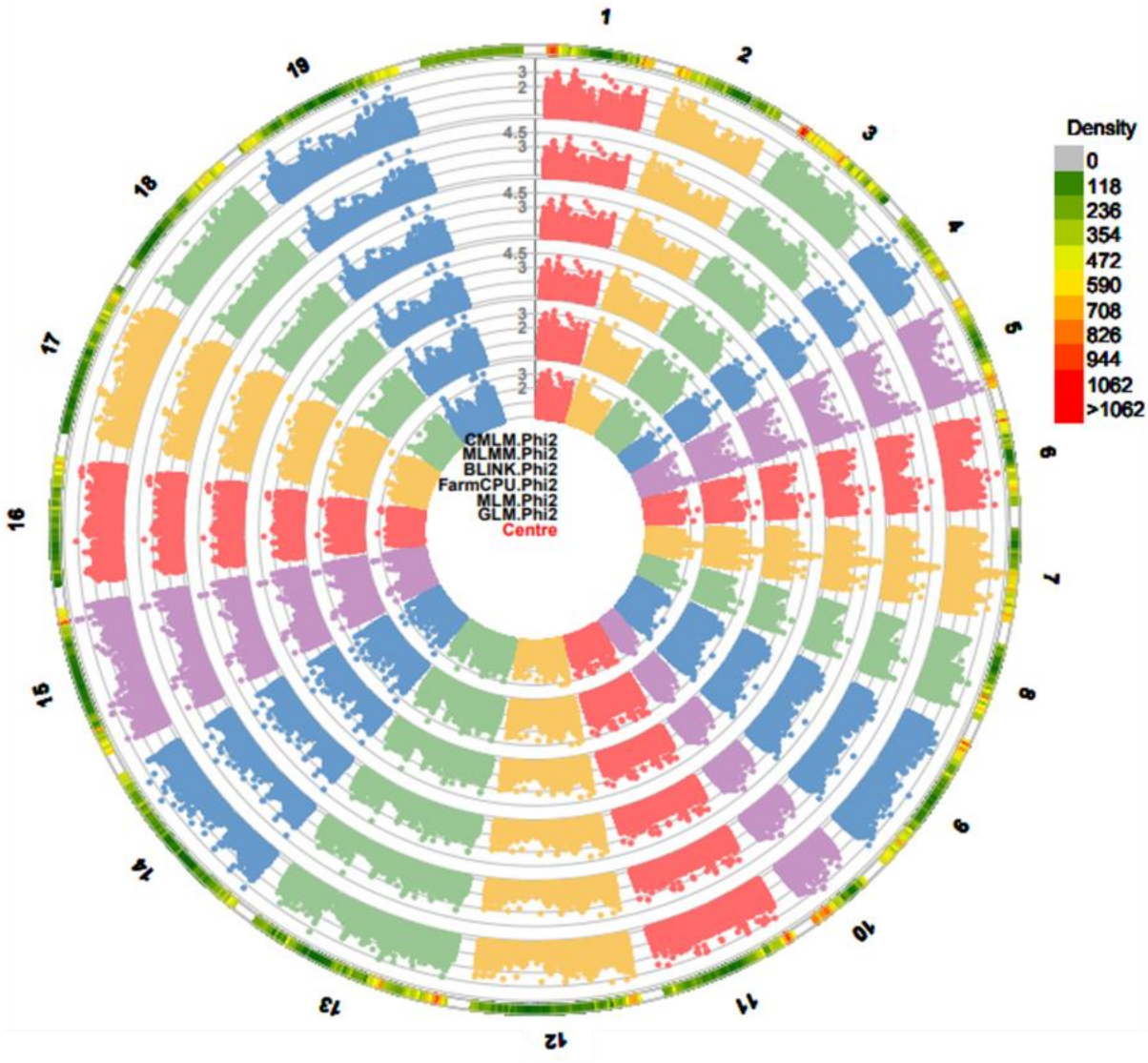

Figure 7.2. SNP markers associated with Phi2 performance in waterlogging compared to control conditions. Manhattan plots for each B. napus chromosome plotting significance of SNP against its predicted unigene position. Significance (a –log10 P value of >7) is marked with a blue dashed line.

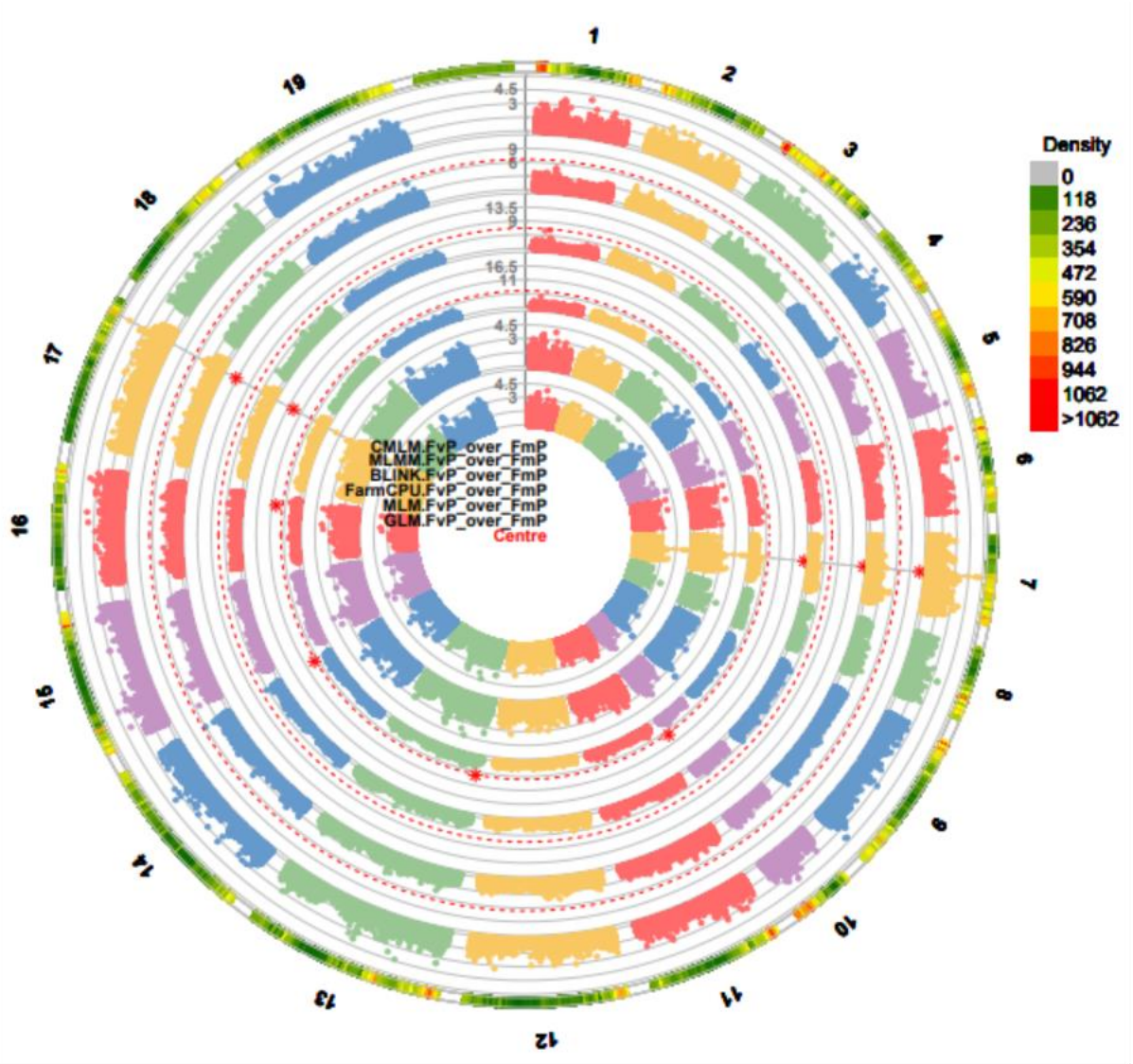

Figure 7.3. SNP markers associated with Fv'/Fm' performance in waterlogging compared to control conditions. Manhattan plots for each *B. napus* chromosome plotting significance of SNP against its predicted unigene position. Red asterisks indicate SNPs identified for each of the models used.

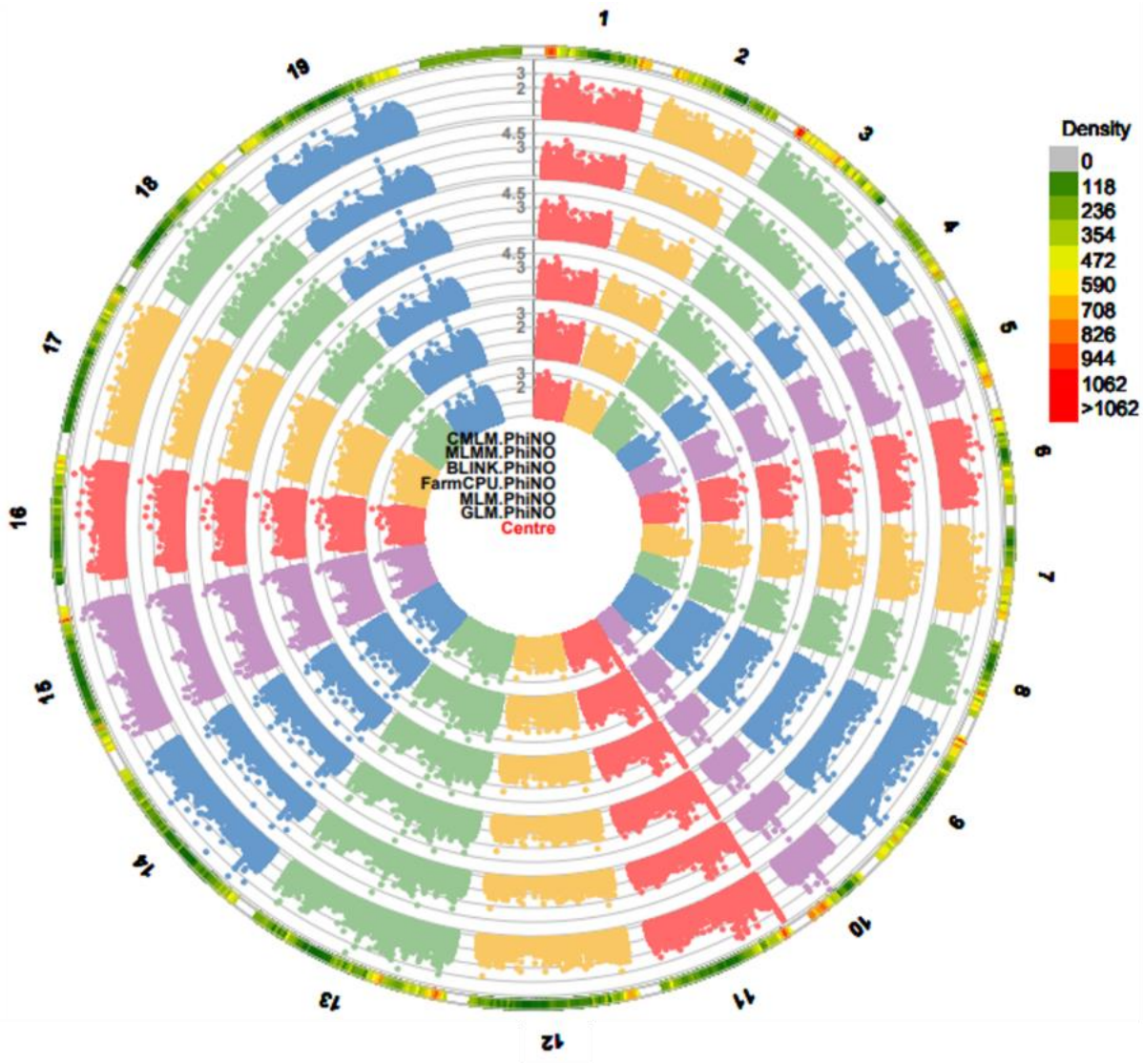

Figure 7.4. SNP markers associated with PhiNO performance in waterlogging compared to control conditions. Manhattan plots for each B. napus chromosome plotting significance of SNP against its predicted unigene position. Significance (a –log10 P value of >7) is marked with a blue dashed line.

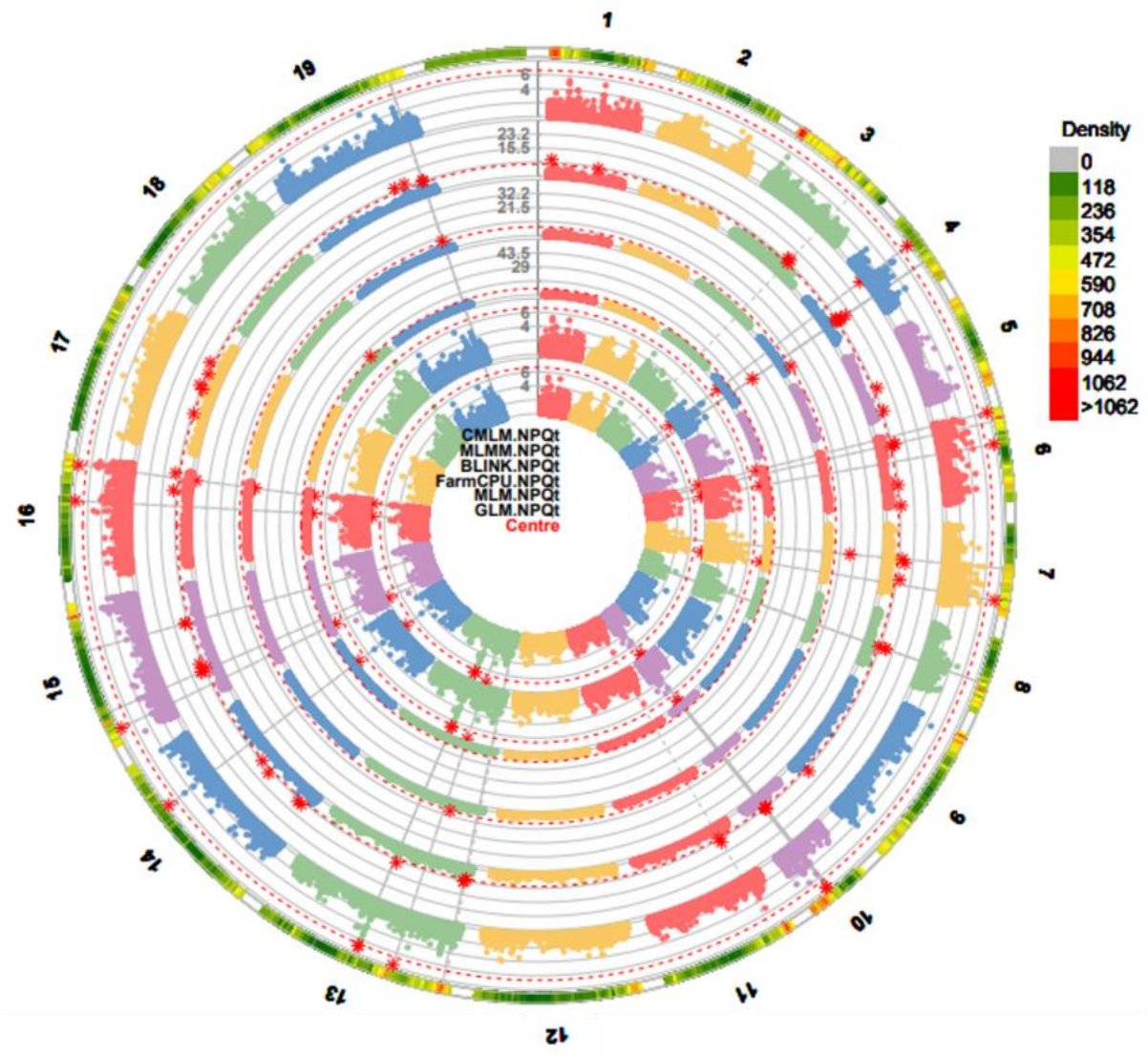

Figure 7.5. SNP markers associated with NPQt performance in waterlogging compared to control conditions. Manhattan plots for each B. napus chromosome plotting significance of SNP against its predicted unigene position. Significance (a –log10 P value of >7) is marked with a blue dashed line.

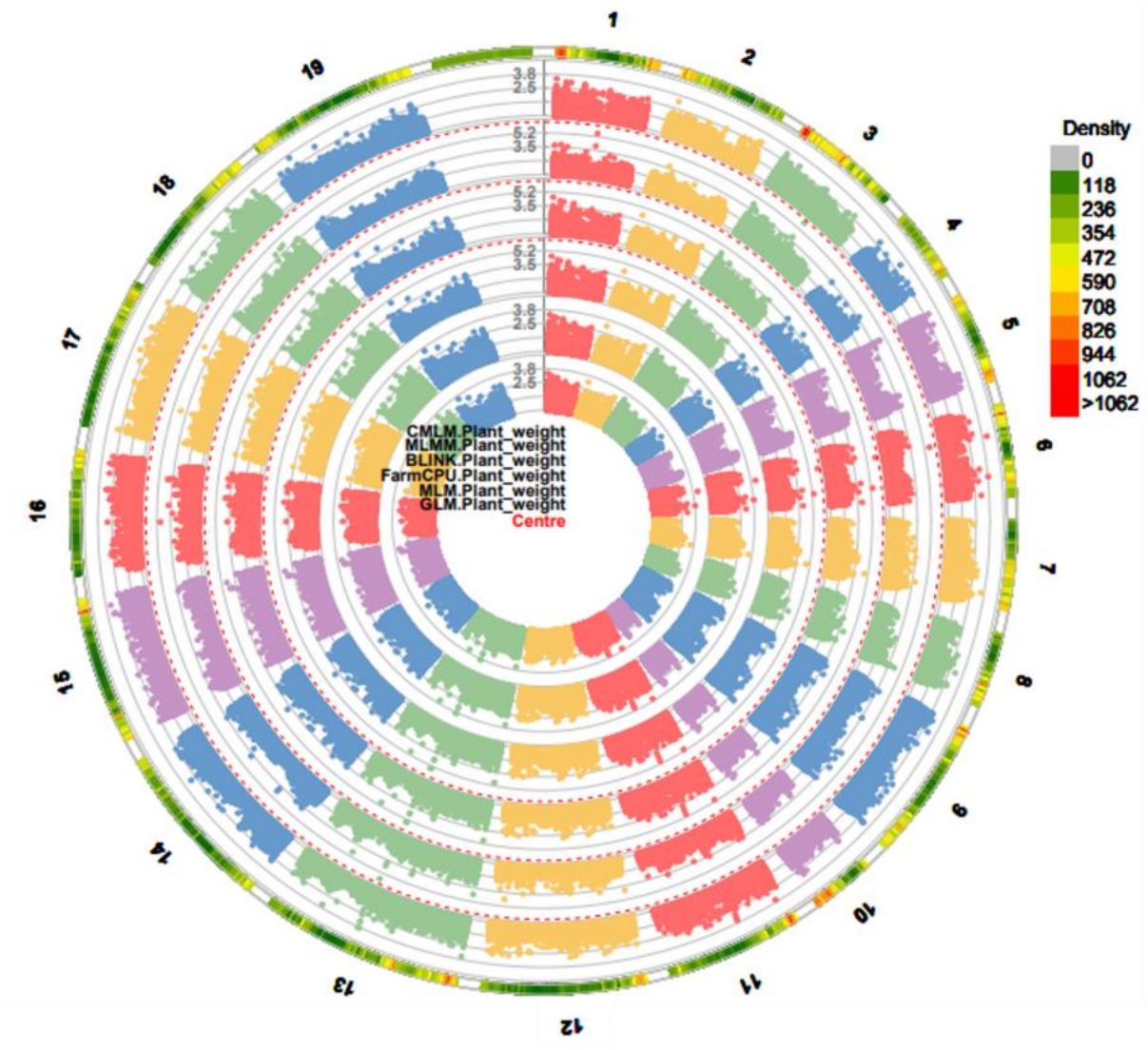

Figure 7.6. SNP markers associated with plant weight performance in waterlogging compared to control conditions. Manhattan plots for each B. napus chromosome plotting significance of SNP against its predicted unigene position. Significance (a –log10 P value of >7) is marked with a blue dashed line.

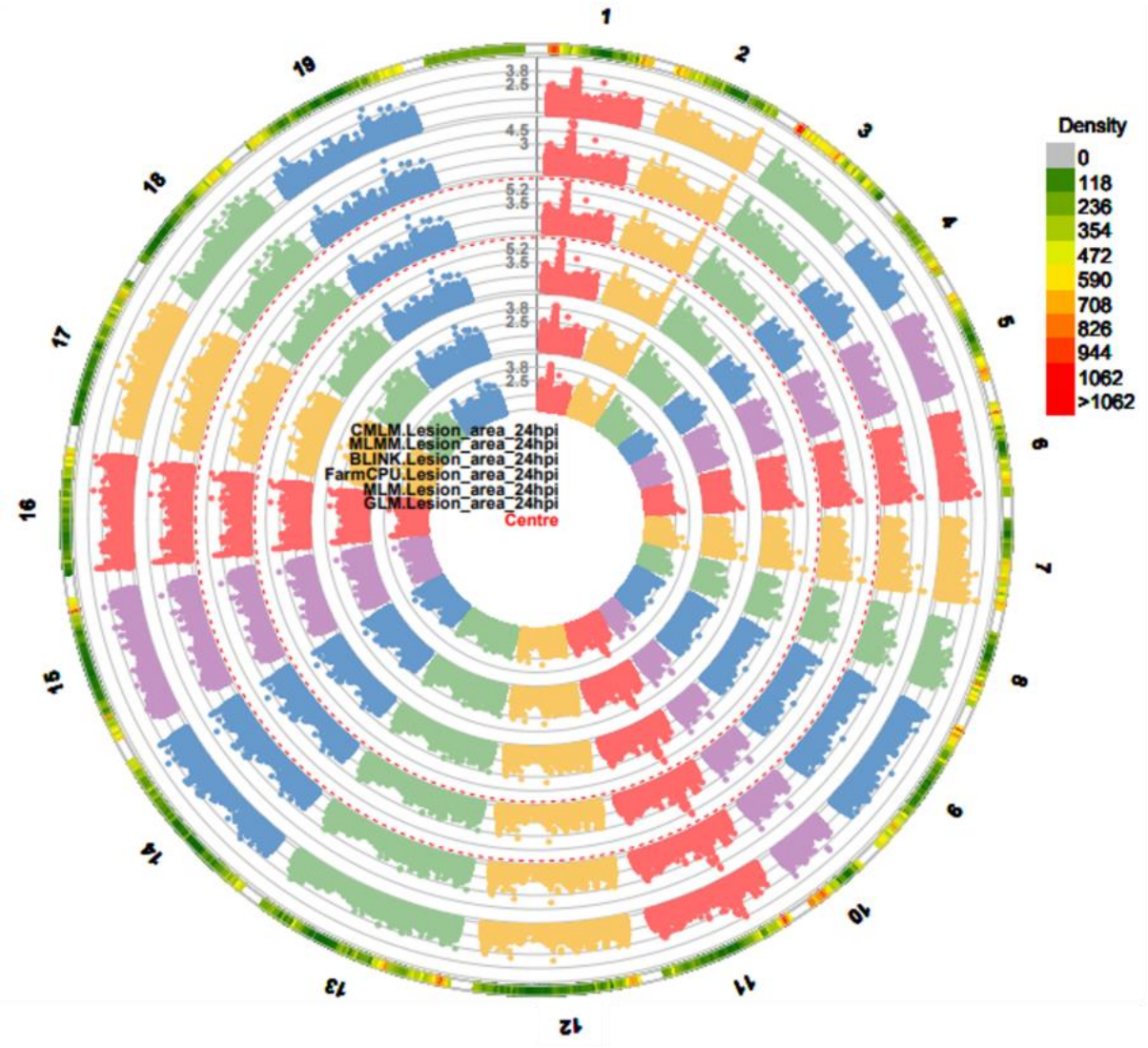

Figure 7.7. SNP markers associated with lesion size caused by S. sclerotinium in plants facing waterlogging prior to pathogen infection compared to plants facing control conditions prior to pathogen infection. Manhattan plots for each B. napus chromosome plotting significance of SNP against its predicted unigene position. Significance (a –log10 P value of >7) is marked with a blue dashed line.

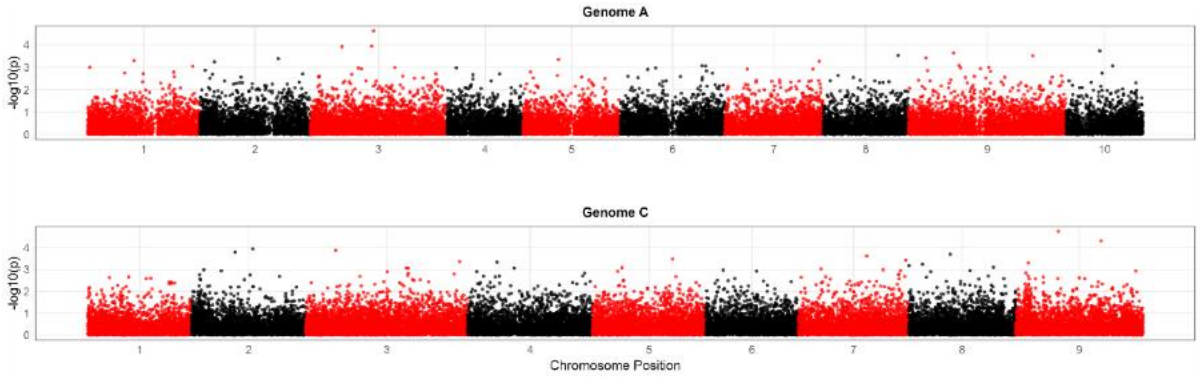

Figure 7.8. Manhattan plots for GEM markers associated with SPAD performance in waterlogged compared to control conditions. Manhattan plots for each *B. napus* chromosome plotting significance of SNP against its predicted unigene position.

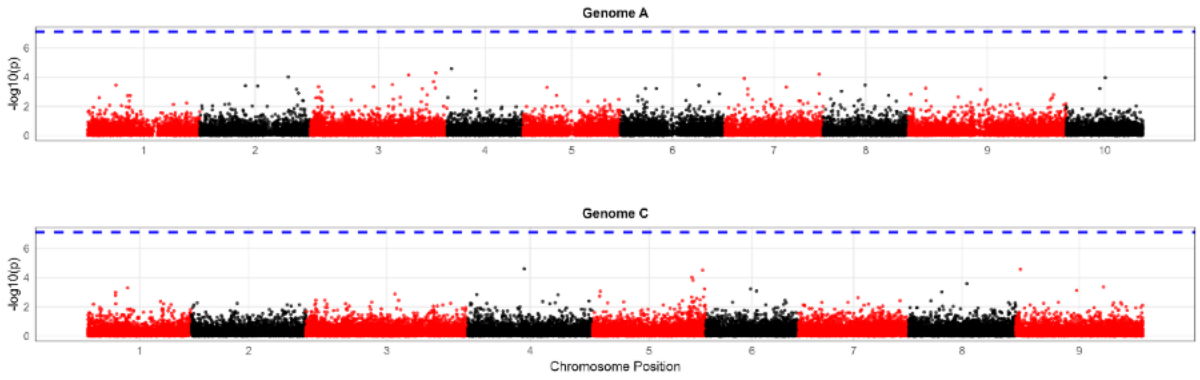

Figure 7.9. GEM markers associated with normalised Fv'/Fm' performance. Manhattan plots for each *B. napus* chromosome plotting significance of SNP against its predicted unigene position. Significance threshold (i.e. $-\log_{10}(p) > 6.64$) is marked with a blue dashed line.

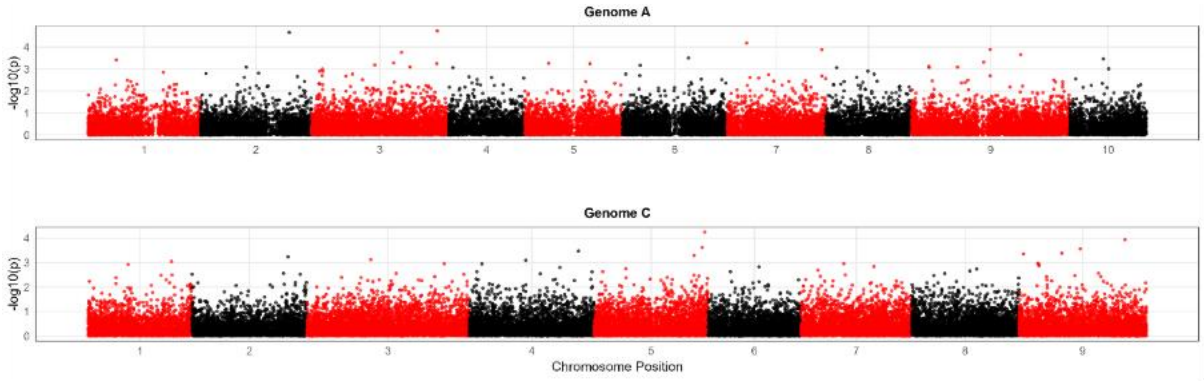

Figure 7.10. GEM markers associated with normalised Phi2 performance. Manhattan plots for each *B. napus* chromosome plotting significance of SNP against its predicted unigene position. Significance threshold (i.e. $-\log_{10}(p) > 6.64$) is marked with a blue dashed line.

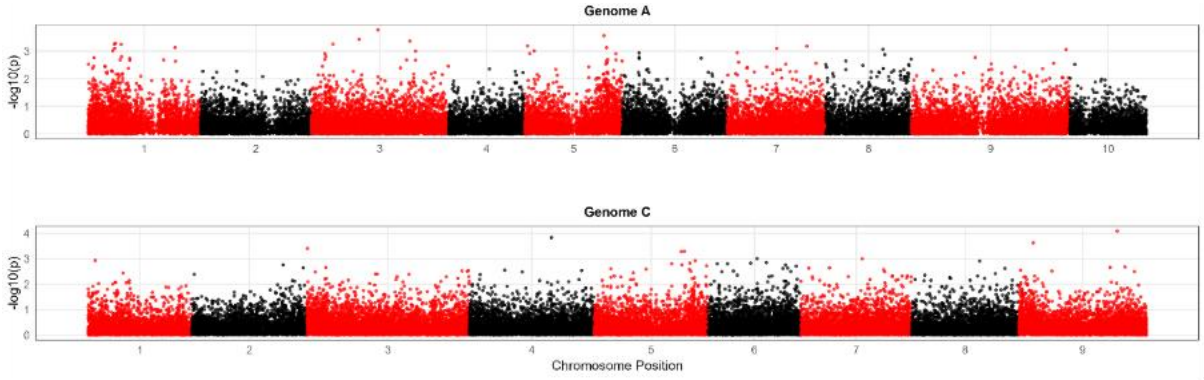

Figure 7.11. GEM markers associated with Phi2 performance in waterlogging compared to control conditions. Manhattan plots for each B. napus chromosome plotting significance of SNP against its predicted unigene position. Significance (a -log10 P value of >7) is marked with a blue dashed line.

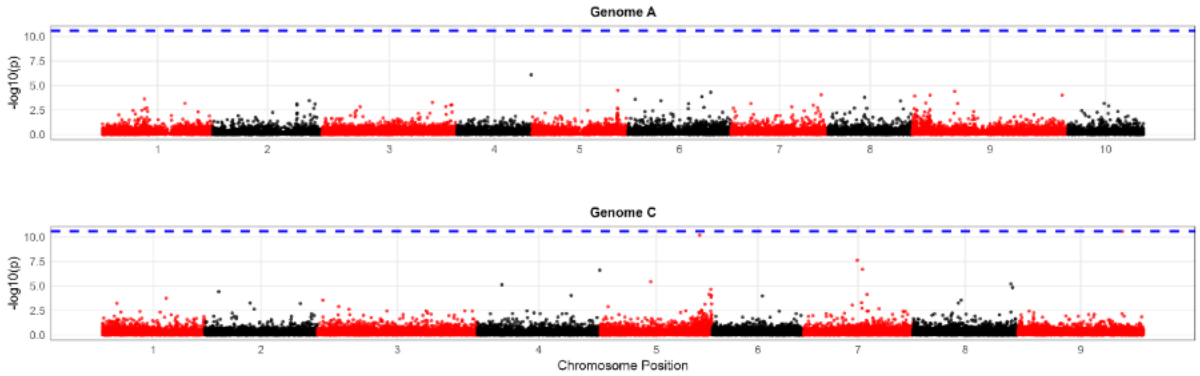

Figure 7.12. GEM markers associated with NPQt performance in waterlogging compared to control conditions. Manhattan plots for each B. napus chromosome plotting significance of SNP against its predicted unigene position. Significance (a -log10 P value of >7) is marked with a blue dashed line.

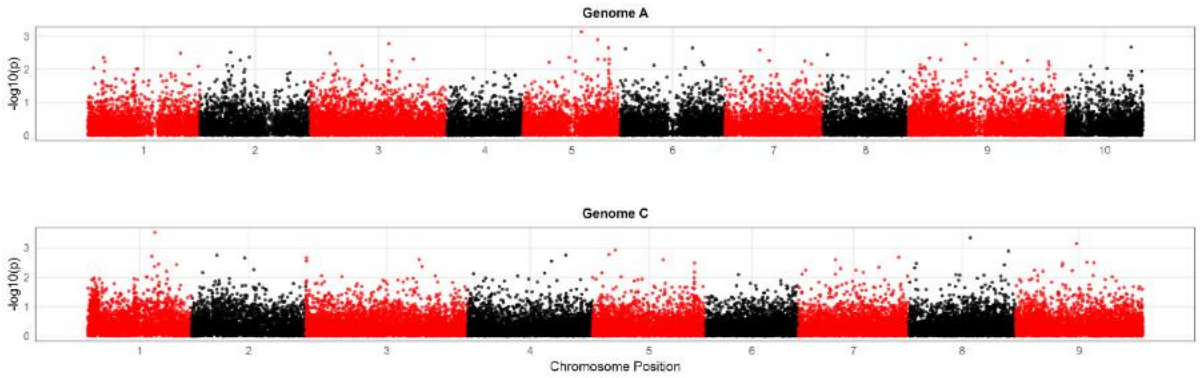

Figure 7.13. GEM markers associated with plant weight performance in waterlogging compared to control conditions. Manhattan plots for each B. napus chromosome plotting significance of SNP against its predicted unigene position. Significance (a -log10 P value of >7) is marked with a blue dashed line.

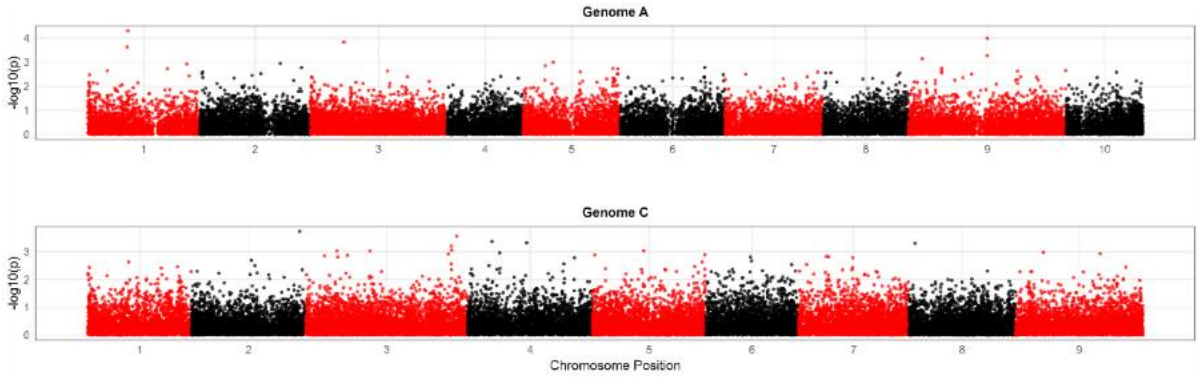

Figure 7.14. GEM markers associated with lesion size caused by S. sclerotinium in plants facing waterlogging prior to pathogen infection compared to plants facing control conditions prior to pathogen infection. Manhattan plots for each B. napus chromosome plotting significance of SNP against its predicted unigene position. Significance (a -log10 P value of >7) is marked with a blue dashed line.